Structural and functional studies of histidine-rich glycoprotein in relation to its roles in angiogenesis and coagulation

Omar Kassaar

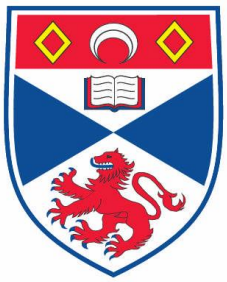

This thesis is submitted in partial fulfilment for the degree of

Doctor of Philosophy

at the University of St Andrews

April 2014

Declarations

I, Omar Kassaar hereby certify that this thesis, which is approximately 40 000 words in length, has been written by me, and that it is the record of work carried out by me, or principally by myself in collaboration with others as acknowledged, and that it has not been submitted in any previous application for a higher degree.

I was admitted as a research student in October, 2010 and as a candidate for the degree of Ph.D. in November, 2011; the higher study for which this is a record was carried out in the University of St Andrews between 2010 and 2014.

Date Signature of candidate

Supervisor's declaration:

I hereby certify that the candidate has fulfilled the conditions of the Resolution and Regulations appropriate for the degree of Ph.D. in the University of St Andrews and that the candidate is qualified to submit this thesis in application for that degree.

Date Signature of supervisor

Permission for publication:

In submitting this thesis to the University of St Andrews I understand that I am giving permission for it to be made available for use in accordance with the regulations of the University Library for the time being in force, subject to any copyright vested in the work not being affected thereby. I also understand that the title and the abstract will be published, and that a copy of the work may be made and supplied to any bona fide library or research worker, that my thesis will be electronically accessible for personal or research use unless exempt by award of an embargo as requested below, and that the library has the right to migrate my thesis into new electronic forms as required to ensure continued access to the thesis. I have obtained any third-party copyright permissions that may be required in order to allow such access and migration, or have requested the appropriate embargo below.

The following is an agreed request by candidate and supervisor regarding the publication of this thesis:

An embargo on both the printed and electronic copy for the same fixed period of two years on the following grounds: publication would be commercially damaging to the researcher, supervisor and the University; publication would preclude further publications.

Date Signature of candidate Signature of supervisor

Abstract

Histidine-rich glycoprotein (HRG) is a plasma protein that regulates key cardiovascular processes such as coagulation, angiogenesis and immune response. The protein consists of six distinct functional domains: two N-terminal domains (N1 and N2), two proline-rich regions (PRR1 and PRR2), a central histidine-rich region (HRR) and a C-terminal domain. The HRR binds Zn^{2+}, which alters the affinity of HRG towards various ligands including the anticoagulant, heparin.

A key aim of this study was to structurally characterise HRG. The 1.93 Å crystal structure of the HRG N2 domain presented here represents the first crystallographic snapshot of the molecule. The N2 domain is cystatin-like and *N*-glycosylated at Asn184. An *S*-glutathionyl adduct was observed at Cys185, providing *in vivo* evidence that release of an anti-angiogenic HRR/PRR fragment is controlled in part by a redox mechanism, representing a novel further role for GSH in regulation of angiogenesis.

Since Zn^{2+} regulates some of the functions of HRG, the dynamics of Zn^{2+} in plasma were investigated using a combination of ITC, ELISA and thrombin assay systems. Zn^{2+} is normally associated with albumin in circulation, but its ability to bind Zn^{2+} is allosterically inhibited upon fatty acids binding to albumin. Elevated plasma fatty acid levels are associated with some disease states. It is proposed that this may alter the proportion of Zn^{2+} bound to HRG, which could in turn activate thrombin to promote coagulation. These studies provide evidence to suggest that Zn^{2+}-dependent activation of HRG (following fatty acid binding to albumin) may play a role in the development of haemostatic complications in susceptible individuals.

Finally, the Zn^{2+} binding ability of albumin was probed in order to locate unidentified sites using recombinant albumin mutants. H9A, H67A, E252A, D256A and H288A mutants all exhibited diminished Zn^{2+} binding ability, indicating that these residues are involved directly or indirectly in Zn^{2+} binding.

Acknowledgments

I would like to thank Dr. Alan Stewart for his ideas, support and supervision from the start to finish of this project. I would also like to thank past and present members of the Stewart group for their help during the project and Dr. Gordon Cramb for generously allowing the use of his chemicals and laboratory equipment.

The protein crystallography carried out here was with the support of Dr. Stephen McMahon and Professor Jim Naismith, and would not have been possible without their help.

Finally, I would like to thank Dr. Claudia Blindauer (University of Warwick) and Dr. Ulrich Schwarz-Linek for their support with isothermal titration calorimetry.

This project was only made possible by funding from the British Heart Foundation.

Contents

List of Figures

List of Tables

Abbreviations

ACB	Albumin-cobalt-binding assay
AFP	α-Fetoprotein
Asn	Asparagine
Asp	Aspartic acid
ATCUN	Amino terminal Cu^{2+} and Ni^{2+} binding motif
BSA	Bovine serum albumin
CD	Circular dichroism
Cys	Cysteine
DTNB	5,5'-dithiobis(2-nitrobenzoic acid)
DTT	Dithiothreitol
EDTA	Ethylenediaminetetraacetic acid
ELISA	Enzyme-linked immunosorbent assay
ESI	Electrospray ionisation
EXAFS	Extended X-ray absorption fine structure
FA 1-5	Fatty acid sites 1-5
GAGs	Glycosoaminoglycans
Gly	Glycine
Glu	Glutamic acid
GSH	Glutathione
HEPES	4-(2-hydroxyethyl)-1-piperazineethanesulfonic acid
HIF	Hypoxia inducible factor
His	Histidine
HSA	Human serum albumin
HRG	Histidine-rich glycoprotein
HRR	Histidine-rich region
IMA	Ischemia-modified albumin
ITC	Isothermal titration calorimetry
LMW	Low molecular weight
MALDI	Matrix-assisted laser desorption/ionisation
MAN	α-D-mannose
MES	2-(N-morpholino)ethanesulfonic acid
MI	Myocardial ischemia
MS	Mass spectrometry
Mol. Eq.	Molar equivalent
N1	N1 domain of histidine-rich glycoprotein
N2	N2 domain of histidine-rich glycoprotein
NAG	N-acetyl glucosamine
NMR	Nuclear magnetic resonance
PEG MME	Polyethylene glycol monomethyl ether
pNPP	para-Nitrophenylphosphate
Pro	Proline
PRR	Proline-rich region
SDS-PAGE	Sodium dodecyl sulfate-polyacrylamide gel electrophoresis
S.E.M	Standard error of mean
Ser	Serine
Tris	Tris(hydroxymethyl)aminomethane
TFA	Trifluoroacetic acid
TOF	Time-of-flight
VEGF	Vascular endothelial growth factor

Chapter 1

Introduction

The cardiovascular system of humans, and other vertebrates, can be simplified to its basic components: the heart muscle, blood vessels and blood itself. Blood is a fluid which had a mystic and poetic role in the history of medicine, until slowly revealing its complex composition and extensive function through the modern age. Blood can be described as a type of connective tissue consisting of 45% formed elements (cells, fragments) and 55% aqueous phase (plasma). The formed element phase gives the blood its structural matter, containing platelets, white blood cells and the haem-porphyrin carrying red blood cells from where the distinctive red colour is observed. Plasma is a pale yellow fluid, acting as the continuous phase of the colloidal suspension and a solvent for water soluble proteins, small molecules, nutrients and ions. The major proteins in plasma include serum albumin, fibrinogen and globulins (Seeley *et al*. 2007).

Albumin

Albumin dominates the proteins which make up the dynamic and diverse plasma proteome, circulating at a concentration of 600 μM (approximately 60% of total plasma protein) and is responsible for maintaining the osmotic pressure of blood since it does not pass easily into tissues (Peters, 1996). The 585 amino acid sequence of albumin leads to a single chain globular protein of 66.5 kDa with a characteristic high solubility due to the abundance of ionic residues affording a high total charge to the structure at physiological pH. This high aqueous solubility allows albumin to indulge in a range of binding and transportation activities involving a broad spectrum of compounds, including metals, fatty acids, haematin, bilirubin and steroidal hormones (Richieri *et al*., 1993; Adams *et al*., 1980; Brodersen, 1982) that have an intrinsic hydrophobicity which would otherwise preclude their high concentrations in plasma.

Albumin undergoes discrete phases of allosteric modulation in response to external conditions and internal effectors. At acidic pH between 2.7 and 4.3, albumin displays increased viscosity and decreased solubility with reduced α-helix content in a conformation described as the fast (F) form. The neutral (N) form occurs between pH 4.3 and 8, in the absence of any binding partners. In the presence of ligands at this pH

range (or at basic pH above 8 without ligands) albumin develops the basic (B) form, losing some α-helix content (Figure 1.1).

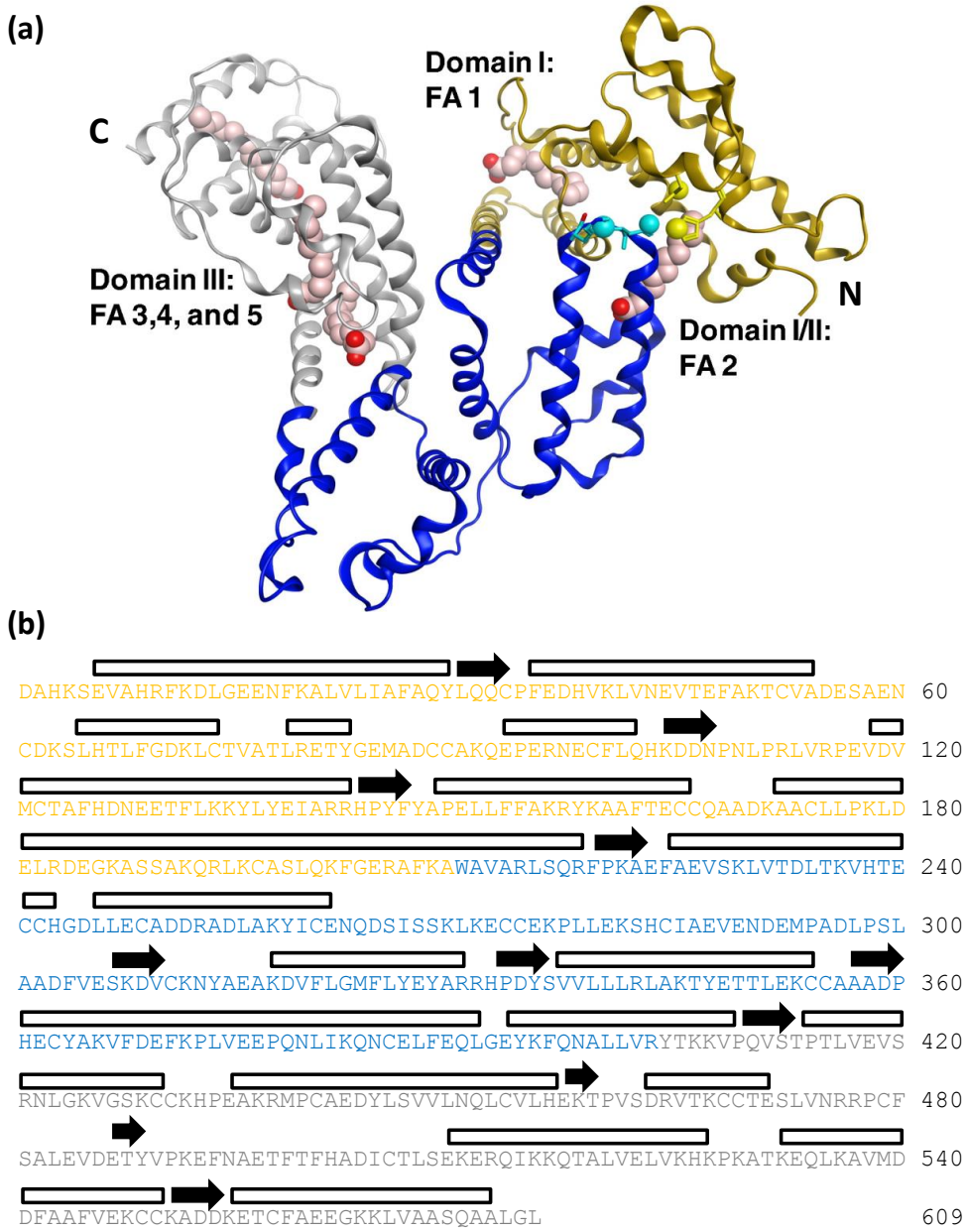

Figure 1.1. (a) Crystal structure of human serum albumin (PDB ID: 1BJ5), showing five fatty acid binding sites (FA 1-5). The fats are shown as pink spheres with their respective carboxyl oxygen atoms in red. Residues forming the major zinc binding site are also shown as spheres where interacting atoms of Asn99 and His67 are coloured yellow, and those of His247 and Asp248 are coloured cyan. The protein peptide backbone is coloured to show the individual domain as labelled (Barnett *et al*., 2013). The N- and C-terminal are labelled. Figure drawn using PyMol by Dr. Claudia Blindauer. (b) Amino acid sequence of human serum albumin, showing the domains (coloured as before) and the secondary structure elements (rectangle: α-helix; arrow: β-sheet).

This flexibility is the key to the extensive binding ability of the albumin molecule and its facility to provide a variety of reversible binding sites. Analysis of the primary structure shows three homologous domains (domain I, II and III respectively), each made up of two separate subdomains (A and B). The flexibility is a corollary of the high α-helix content, inducing a spring-like effect on the structure resulting in controlled contraction and expansion influenced by binding partners. X-ray crystal results show a globular heart-shaped structure; selected significant albumin structures are given in Table 1.1.

Table 1.1. Selected albumin structures, giving PDB codes and highlighting importance.

PDB Code	Year	Authors	Notes
1AO6	1997	Sugio et. al. (1999)	First X-ray crystal structure of HSA
1BJ5	1998	Curry et. Al. (1998)	Structure of HSA with myristic acid
2BXG	2005	Ghuman et. Al. (2005)	HSA complexed with ibuprofen
2I2Z	2006	Yang et. al. (2007)	HSA complexed with asprin
4F5S	2012	Bujacz (2012)	First X-ray crystal structure of bovine albumin. First structure of albumin complexed with a metal (calcium).

Albumin ligand binding: Fatty acids

Plasma free fatty acids are generally dominated by C16 and C18 (long-chain) fatty acids, and these are predominantly mobilised by tightly regulated enzymatic lipolysis from triglyceride stores in adipose tissues (Lafontan and Langin, 2009). Following which, they are then released into the circulation and made available for transport by albumin (van der Vusse, 2009). Transport of fatty acids has a characteristic rapid turnover and a short circulatory half-life of up to 4 minutes (Eaton *et al*., 1969). Although the exact mechanism by which albumin enables the uptake of fatty acids to cells is unknown, the presence of albumin specific receptors on cell surfaces may partake in this process (Schnitzer *et al*., 1992; Schnitzer and Oh, 1994). Dole and Gordon investigated the importance and function of fatty acids in general metabolism (Dole, 1956; Gordon, 1957; Gordon and Cherkes, 1956). Fatty acids are the primary

source of energy for several tissues such as the renal cortex, resting skeletal muscle, myocardium and liver (Coppack *et al*., 1994). Concentration of plasma fatty acids has been shown to be in the region of 250–500 μM as a basal level (Rogiers, 1993) of which most originates from subcutaneous abdominal fat while only a small proportion originates from visceral fatty deposits (Nielsen *et al*., 2004; Karpe *et al*., 2011). An increase in adipose tissue lipolysis is observed when there is an increased demand for energy by the body, hence increasing the bioavailability of fatty acids in the system (Coppack *et al*., 1994). Chronically elevated levels of plasma fatty acid have been clinically associated with certain conditions such as cancer, obesity and diabetes (Richieri *et al*., 1993). They have also been observed as a symptom of analbuminemia (plasma HSA deficiency) (Bartter *et al*., 1961). In obesity, the plasma fatty acid concentration increase is mainly due to the expansion of adipose tissue and a subsequent delay in the clearing process (Boden, 1998). In addition, plasma fatty acid levels in such conditions can lead to further subsequent elevations, since high levels of fatty acids in circulation can inhibit the effects of insulin on lipolysis (Jensen *et al*., 1989).

The fatty acid interaction with albumin has been studied extensively by a variety of complementary biophysical techniques including dialysis (Pedersen *et al*., 1995), ^{13}C NMR (Choi *et al*., 2002; Simard *et al*., 2006) and X-ray crystallography (Curry *et al*., 1998; Bhattacharya *et al*., 2000; Petitpas *et al*., 2001). It is supposed that up to 6 molar equivalents of fatty acid can be bound to albumin under physiological conditions with K_d values ranging between 1.5 and 90 nM (Peters, 1996). Greater than 2 molar equivalents will only bind during conditions of elevated plasma fatty acid levels (Richieri and Kleinfeld, 1995). Figure 1.1 illustrates the heart-shaped form of albumin and shows the binding sites for its main endogenous ligands, fatty acids, distributed across the protein. Human albumin is able to bind up to ten molecules of fatty acids per protein molecule, with the five main sites labelled FA1-5 (Figure 1.1) (Bhattacharya *et al*., 2000). Crystallographic analysis describes precise details of each fatty acid binding site, revealing a considerable divergence of topology (Curry *et al*., 1998; Curry *et al*., 1999). The sites are situated either within individual sub-domains, at the interface between two domains or at the interface of two sub-domains of the same major domain. This assortment of binding sites through otherwise homologous domains leads to varied fatty acid affinity due to the primary intermolecular interactions involved in non-covalent bonding and the heterologous steric interdomain regions. Studies on albumin

mutants have shown that the greatest affinity of fatty acid binding occurs at sites FA2, FA4 and FA5. These sites form narrow tunnels fitting the hydrophobic tail of the fatty acid molecule, with its carboxylate head at the pocket entrance interacting electrostatically with polar or basic groups (Simard *et al*., 2005; Simard *et al*., 2006). Two additional sites of medium affinity, fatty acid sites 1 and 3, share a similar interaction but form shorter flattened slots as the binding cavity. These sites all involve well defined salt bridges between the positively charged protein side chains and negatively charged fatty acid head groups as well hydrogen bonding to stabilise the fatty acid to protein interaction (Curry *et al*., 1998; Bhattacharya *et al*., 2000). The two weakest sites, sites 6 and 7, are located at the protein surface, with relatively poorly defined van der Waals interactions with the hydrophobic fatty acid tail. Most of these binding sites are an intrinsic construct of the protein tertiary structure, but some conformational rearrangement is required for albumin to reach repletion of fatty acids.

The response to fatty acid binding essentially involves the rearrangement of domains I and III relative to domain II *via* rotations around the interdomain helices (Fasano *et al*., 2009). Thus, fatty acid sites 2 and 3 which intersect their respective domains (Figure 1) take the greatest allosteric responsibility when occupied.

Preceding the wealth of crystallographic structural information, binding studies by Sudlow *et al.* showed the presence of two drug binding sites (Sudlow *et al*., 1975; Sudlow *et al*., 1976) located in sub-domains IIA and IIIA respectively (Carter and Ho, 1994). These sites present an attractive opportunity to allow the transport and delivery of drug compounds otherwise affected by adverse solubility in the blood. However, physiology exhibits a complexity prohibiting this simplicity. For example, a drug compound would need to have a measured affinity for albumin allowing reversible binding and favourable pharmacokinetics to reach a desired target. Also, the allosteric spirit of albumin is susceptible to changes in levels of endogenous ligands, which could result in an unanticipated release of drug compound with the potential for intoxication.

Albumin ligand binding: Metals

Having referred so far to examples of organic compounds involved with albumin, it should be noted that this relationship is not exclusive: albumin also binds inorganic species such as transition metal ions, providing a vehicle for their circulatory travels and moderating plasma levels of free species. Essential and toxic cations including Ca^{2+},

Ni^{2+}, Cu^{2+}, Cd^{2+} and Zn^{2+} have been observed to bind to one of at least four metal sites. These metal sites include the generic "Amino terminal Cu^{2+} and Ni^{2+} binding" motif (ATCUN) which is present in many proteins, the main Zn^{2+} binding site known as "site A", a Cd^{2+} binding site known as "site B" which is currently unidentified and the only free thiol group in the structure, Cys34, which can bind heavy metal compounds of Au, Pt and Hg^{2+} (Harford and Sarkar, 1997; Bal *et al*., 1998; Sadler and Viles, 1996; Christodoulou *et al*., 1994; Esposito and Najjar, 2002). This solitary free thiol is redox active, partaking in thiolation and nitrosylation and forming mixed disulphides. Also, Cys34 is involved in the dimerisation of albumin observed *in vitro* (Quinlan *et al*., 2005). Additionally, albumin is known to bind Ca^{2+} and Mg^{2+}. However, it is known that Ca^{2+} (and thus analogously, Mg^{2+}) bind stronger to the B form of albumin but also help cause this conformational change in a synergistic approach (Kragh-Hansen and Vorum, 1993; Peters, 1996). Recently, a crystal structure of bovine albumin complexed with Ca^{2+} was solved, and was the first instance of a metal bound albumin structure (Majorek *et al*., 2012). Figure 1.2 shows a schematic diagram of the HSA molecules, with the features significant in regards to this project highlighted.

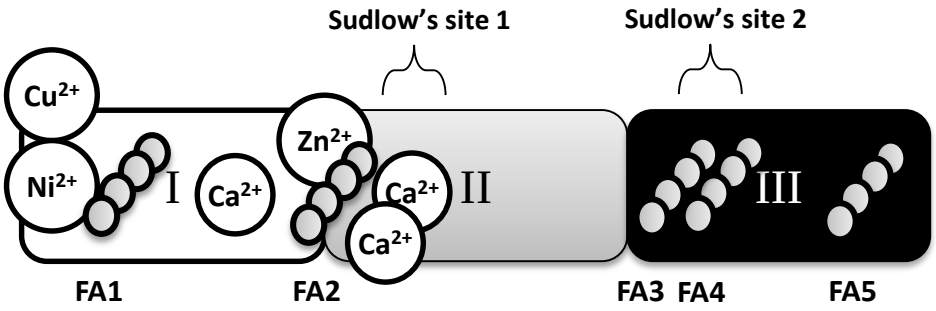

Figure 1.2. Schematic diagram of HSA, showing the domains labelled I, II and II. The positions of five main fatty acid sites (FA1-FA5) are highlighted. The binding positions for Zn^{2+}, Cu^{2+}, Ni^{2+} and Ca^{2+} are shown. The proximity of the major Zn^{2+} binding site (site A) and FA2 can be observed.

Zinc is an essential nutrient, involved in a profuse array of structural, catalytic and cocatalytic functions in enzymes and proteins amounting to 10% of the human proteome (Andreini *et al*., 2006). Zinc was revealed to be an essential nutrient first in the 1930s during an animal study on the effect of dietary zinc intake on the growth and survival of rats and mice (Todd *et al*., 1993). However it took 30 years for the realisation that zinc is also important for human health (Prasad, 1991). The full d^{10} valence shell of Zn^{2+} permits an isotropic ionic environment with regards to ligand

binding, allowing a distortion from strict tetrahedral or trigonal bipyramidal coordination spheres which is commonly observed in Zn^{2+} protein structures (Thorp, 1998). The d^{10} electronic configuration also renders the zinc ion inactive towards redox reactions, indicating a reason for the bias of nature towards using Zn^{2+} in many applications, although this property contributes frustration to the analytical chemist. Numerous studies have attempted to define the interactions between Zn^{2+} and human blood plasma proteins (Himmelhoch *et al*., 1966; Song and Adham, 1979; Dawson *et al*., 1981; Scott and Bradwell, 1983; Chilvers *et al*., 1984; Foote and Delves, 1984; Manley and Gailer, 2009; Malavolta *et al*., 2012), and have led to the agreement that serum albumin is the key Zn^{2+} transporter in plasma (Chesters and Will, 1981). Additionally, albumin is suggested to facilitate the endothelial uptake of zinc (Rowe and Bobilya, 2000).The proposed zinc binding site in albumin is unusual, firstly because it is assumed to adopt the less common trigonal bipyramidal arrangement but also because of the inclusion of asparagine as an oxygen donor. Typical ligands are histidine, cysteine, aspartic acid and glutamic acid. However, structures of zinc binding proteins with the same framework as site A have been solved (Odintsov *et al*., 2004). A standard value for the zinc concentration in normal adult blood plasma is 16.6 ± 6.2 μM (Rukgauer *et al*., 1997). The zinc pool in plasma is subjective to dietary intake, along with a range of other influences. For example, plasma zinc levels decrease during inflammation and infection as part of the acute phase response. The complete rate of turnover of plasma Zn^{2+} is substantial, since the total amount of plasma zinc is replaced around 150 times each day (King, 2011).

A usual means of assessing zinc speciation in plasma involves fractionation into low- and high-molecular weight components (by ultrafiltration) (Foote and Delves, 1988). Recently, several zinc specific fluorescent dyes have been synthesised and used to quantify total and free plasma zinc (Kelly *et al*., 2011). A free Zn^{2+} concentration in the range of 1–3 nM was inferred by studies using the dye ZnAF-2 and confirmed that most of the Zn^{2+} binding capability of plasma is located in the high-molecular weight fraction. Between 75-90% of total Zn^{2+} in plasma is chelated to HSA, and this fraction makes up the majority of the plasma Zn^{2+} pool available for exchange (Chilvers *et al*., 1984; Manley and Gailer, 2009). Total plasma zinc associated with the low-molecular weight fraction was found to be less than 1% (Foote and Delves, 1988), most likely due to the amino acids cysteine and histidine chelating zinc (Giroux and Henkin, 1972). The

remaining 10–20% of plasma zinc is bound tightly to α2-macroglobulin (Parisi and Vallee, 1970) and retinol-binding protein (Chilvers *et al*., 1984), and is unavailable for exchange.The interaction between Zn^{2+} and albumin is thus particularly important within the blood. Perfused rat intestine studies have shown that albumin is responsible for the transport of newly-absorbed Zn^{2+} to the liver (Smith *et al*., 1979).

Nuclear magnetic resonance (NMR) experiments have been used to identify the Zn^{2+} and Cd^{2+} binding sites, using $^{111}Cd^{2+}$ and $^{113}Cd^{2+}$ as a probe for Zn^{2+} in combination with site directed mutagenesis studies. NMR resonances equate to three different sites of chelation for Cd^{2+} and Zn^{2+} with each respective metal having one high affinity binding site, not affected by competition from other metals. Site A appears at 110–150 ppm and site B at 25–30 ppm (Martins and Drakenberg, 1982; Goumakos *et. al*., 1991; Sadler and Viles, 1996).

The characteristic chemical shift of site A pointed to a metal coordination which included 2 or 3 nitrogen donors with additional oxygen donors, while site B is structured around one nitrogen donor and three oxygen donors. Addition of 1 equivalent of Zn^{2+} during the Cd^{2+} NMR experiments blocked the peak relating to site A, but left the site B signal intact, leading to the inference that site A had a stronger affinity for zinc (Martins and Drakenberg, 1982; Goumakos *et. al*., 1991; Sadler and Viles, 1996). Corresponding examination of the structural database revealed conserved residues at the domain I/II interface composed of His67 and Asn99 (domain I) and His247 and Asp249 from domain II. The high affinity zinc binding site has recently been situated, modelled and characterised using NMR, zinc k-edge extended X-ray absorption fine structure (EXAFS) spectroscopy and site-directed mutagenesis (Figure 1.3) (Stewart *et al*., 2003; Blindauer *et al*., 2009).

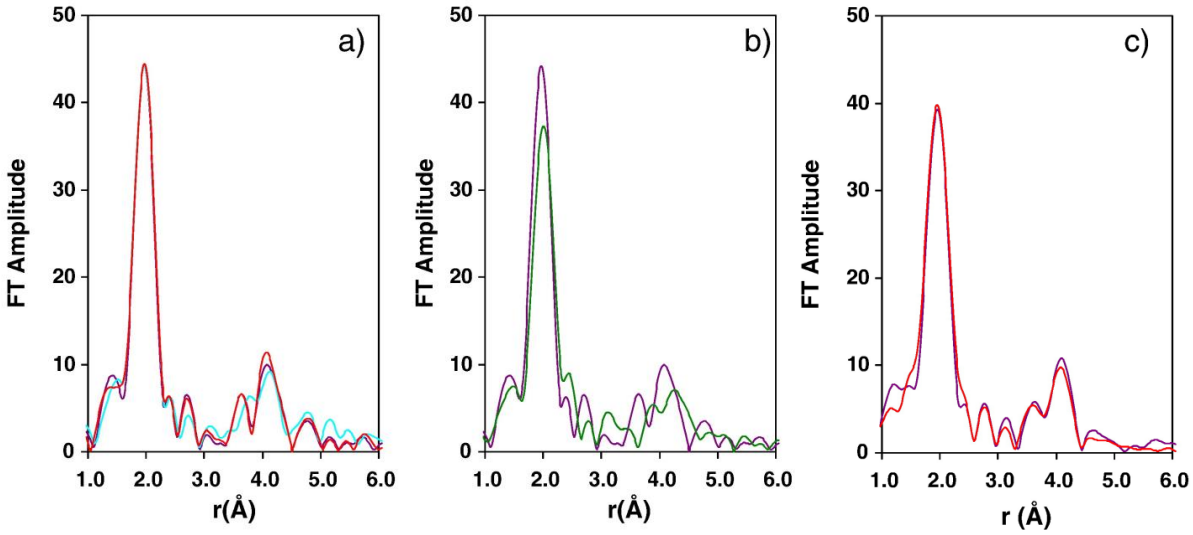

Figure 1.3. Data from Zn k-edge EXAFS experiments for wild-type and mutant albumin-zinc complexes. (a) HSA + 1 molar equivalent Zn^{2+} in purple, HSA + 1 molar equivalent Zn^{2+} + 1 molar equivalent Cd^{2+} in red. HSA + 1 molar equivalent Zn^{2+} + 1 molar equivalent Cd^{2+} + 1 molar equivalent Cu^{2+} in cyan. Under these conditions, Zn^{2+} is thought to occupy site A, Cd^{2+} is thought to occupy site B preferentially, and Cu^{2+} the N-terminal ATCUN site. The excellent agreement of intense peak at ca. 2 Å suggests that in each sample, Zn^{2+} coordinated to the same site. (b) EXAFS spectra for wild-type HSA (purple) and H67A mutant HSA (green), where the H67A mutation is clearly shown to perturb zinc binding to albumin. (c) Comparison of experimental (purple) and modelled (red) data (Blindauer *et al*., 2009).

Site A is fundamentally a five-coordinate interdomain site involving His67 and Asn99 residues from domain I and His247 and Asp249 residues from domain II, plus one non-protein ligand, likely to be a water molecule. The backbone carbonyl oxygen of His247 offers a weak sixth coordination position (Figure 1.4). The molecular model calculated for this proposed site showed a favourable geometry with respect to the apo-albumin structure. Furthermore, this site neighbours fatty acid site 2 and shows structural disruption upon fatty acid binding, correlating with the absence of the characteristic $^{111}Cd^{2+}$ peak in albumin exposed to high fatty acid concentrations (Stewart *et al*., 2003; Lu *et al*., 2008). This leads to a possible physiological implication where extracellular Zn^{2+} concentrations may be influenced by this relation with plasma fatty acid levels.

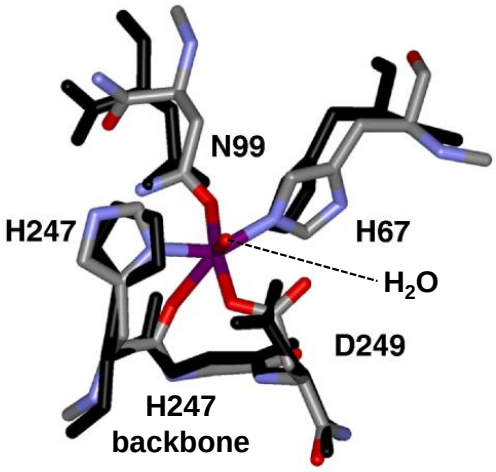

Figure 1.4. Structural overlay of residues forming the main zinc site on albumin from published X-ray structure of unliganded albumin (PDB ID: 1AO6) in black, and EXAFS-refined model in Corey-Pauling-Koltun colouring (Zn ion shown in purple, oxygen in red, nitrogen in blue) (Blindauer *et al*., 2009). Figure drawn using PyMol by Dr. Claudia Blindauer.

In addition to its role in Zn^{2+} binding, Asp249 in HSA has been identified as being involved in the binding of Ca^{2+}, as observed in the crystal structure of bovine serum albumin (Asp248 in domain II of bovine albumin corresponds to Asp249 in human albumin), signifying that an interplay between Zn^{2+} and Ca^{2+} might occur in plasma (Majorek *et al*., 2012). Also, albumin binding Mn^{2+} has been shown to be affected by binding of Zn^{2+}, leading to the conclusion that the high-affinity Zn^{2+} site is also a Mn^{2+} binding site (Fanali *et al*., 2012a). Cisplatin, the anticancer drug, can preclude Zn^{2+} binding to the high-affinity site by crosslinking between the side chains of His67 and His247 (Hu *et al*., 2011). Mutant recombinant human albumins have helped identify the major residues involved in the zinc binding site of HSA and have also been shown to augment or impede the HSA affinity for zinc. By replacing the weak binding side-chain of Asn99 with His or Asp, HSA was shown to have an increased Zn^{2+} affinity (by one order of magnitude at least). In contrast, a decrease in Zn^{2+} affinity is acquired upon mutation of His67 to a non-chelating Ala residue (Blindauer *et al*., 2009). Extended X-ray absorption fine structure studies established that both Asn99His and Asn99Asp mutants bind zinc in a similar 5(+ 1) coordinate ligand site, while the His67Ala mutant data produced an EXAFS fit with one fewer ligand (Figure 1.2). 2D ^{1}H total correlation spectroscopy NMR analysis of the mutants identified the cross-peaks relating to His67 and His247 for wild-type HSA, which enabled monitoring of the effects of different binding partners (metals, fatty acids) on this site.

Albumin ligand binding: Allosteric effects between fatty acids and metals

Based on the X-ray crystal structural data available at the time, identification of the first Zn^{2+}-binding site of HSA (site A) revealed that the site is pre-formed in crystal structures of fatty acid free albumin (i.e. fatty acid binding to albumin disrupts the Zn^{2+}-binding site structure). Fatty acid site 2 (FA2) is the main fatty acid binding site accountable for structural disruption in this location. Being one of the highest affinity fatty acid sites, even at 1:1 albumin:fatty acid ratios, it is considerably occupied.

FA2 is one of the highest affinity sites and becomes significantly occupied at fatty acid:albumin ratios as low as 1:1 (Simard *et al*., 2006). It is a very enclosed site with an almost completely linear binding pocket shaped from subdomains IA, and IIA and IIB (Curry *et al*., 1999). However, FA2 requires a substantial change in protein conformation upon binding fatty acids, since the subdomain pockets which form the sites are observed to be apart by 10 Å in structures of fatty acid free albumin. The change required involves the rotation of the domains (domain I with respect to domain II) (Curry *et al*., 1998; Bhattacharya *et al*., 2000), the procession of which alters the arrangement of the residues involved in Zn^{2+} binding. Essentially, this allosteric modulation means that the normally preformed zinc site is disrupted, once fatty acid binding has occurred at FA2 (Figure 1.5). This phenomenon is observed in all current crystal structures of fatty acid bound albumin, over a fatty acid chain length from C10 to C22 (Bhattacharya *et al*., 2000; Choi *et al*., 2002; Lu *et al*., 2008; Stewart *et al*., 2009). However, the crystal based structural data did not allow for any conclusions to be drawn regarding the dynamics of zinc and fatty acid binding; fatty acid binding to FA2 and zinc binding to site A may be equally exclusive, or fatty acid binding would preclude zinc binding (or *vice versa*).

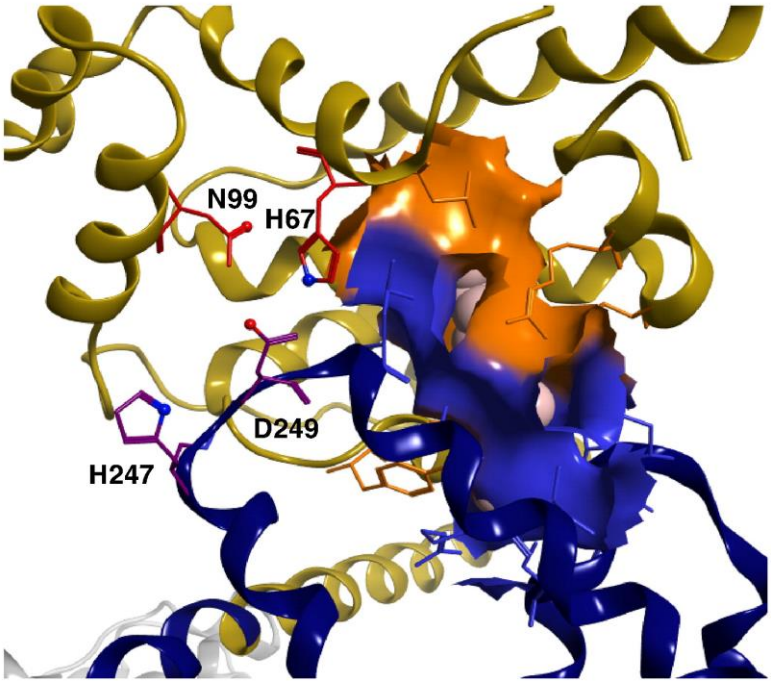

Figure 1.5. Fatty acid binding site FA2 and the major zinc site (site A) residues. The binding pocket for fatty acids in FA2 is formed by residues from both domain I (yellow/orange) and domain II (blue), illustrated as a coloured surface. The carbons of the fatty acid molecule are shown as pink space-filling spheres, and can be seen under the coloured surface. Metal-binding nitrogen and oxygen atoms are also highlighted as spheres. The presence of the fatty acid molecules forces the two His residues apart by > 8 Å, thereby destroying the zinc site. Under apo-conditions, the His residues are separated by approximately 4 Å (Barnett *et al*., 2013). Figure drawn using PyMol by Dr. Claudia Blindauer.

^{113}Cd NMR spectroscopy provided early experimental evidence for the disturbing of metal binding by fatty acids, since the spectra showed significant broadening and a lower intensity in albumin samples isolated from plasma that were not subjected to a de-fatting process (Sadler and Viles, 1996). Later, it was established for recombinant Cd_2HSA that an 8-times excess of octanoate had a significant effect on the ^{111}Cd peak corresponding to site A (although site B was not affected) (Figure 1.6a) (Stewart *et al*., 2003). The Hε1 ^{1}H NMR resonances for His67 and His247 were affected by titrating octanoate into HSA, signifying that octanoate binds close to these residues (Figure 1.6b) (Lu *et al*., 2012a). These experiments also determined that zinc binding to site A was not eliminated by octanoate binding to FA2, since the ^{1}H spectra of Zn–HSA were identical, regardless of the presence and absence of octanoate.

From this, it was unclear if HSA is able to bind Zn^{2+} stronger to site A than octanoate is to FA2 (and therefore causing octanoate displacement), or whether binding of zinc and octanoate could occur simultaneously. Isothermal titration calorimetry (ITC) was used

to address this question by studying the binding of Zn^{2+} and octanoate to bovine serum albumin (BSA) interactively. Both ligands produced identical binding curves regardless of the presence or absence of the other. Incidentally, previous reports had stated that the presence of octanoate in HSA samples prevented it from crystallising isomorphically to all other fatty acid-bound structures (Bhattacharya *et al*., 2000). Thus it was proposed that the short C8 chain of octanoate is not able to provoke the same conformational change that is observed when longer chain fatty acids bind, since it is unable to pin the two interdomain half-sites together. This was in agreement with a structural model describing the simultaneous binding of Zn^{2+} and octanoate (Lu *et al*., 2012a). Concerning the disappearance of peak A in ^{111}Cd NMR spectra of HSA samples with two equivalents of Cd^{2+} induced by octanoate, it is possible that the metal is not displaced but binding of octanoate to one pocket simply affects the dynamics of Cd^{2+} at site A.

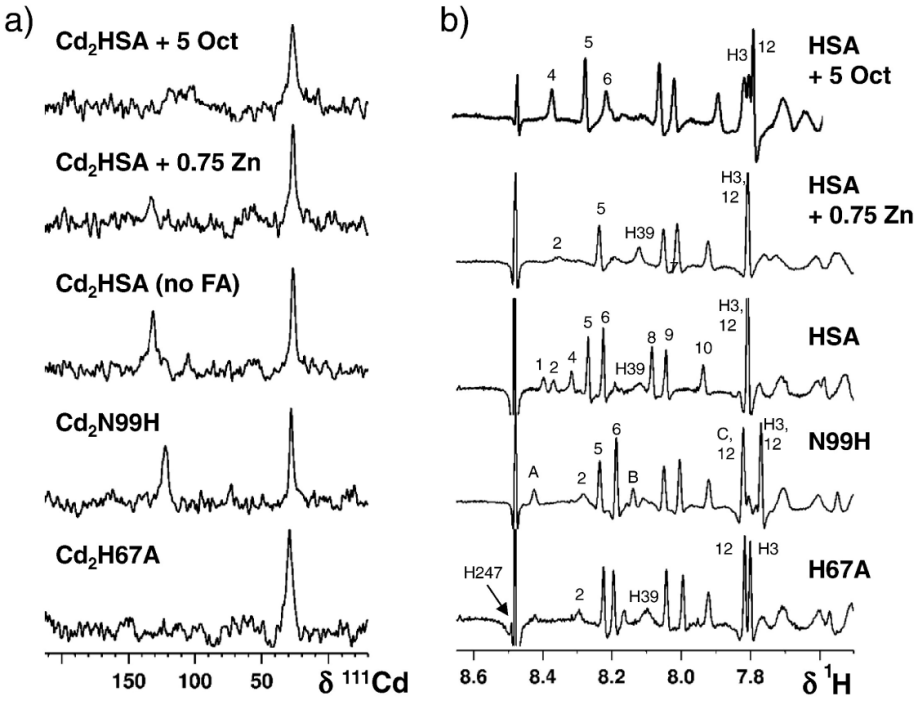

Figure 1.6. NMR experiments on wild-type and mutant albumins. (a) ^{111}Cd NMR spectra conducted under conditions of 1.5 mM Cd_2HSA, 50 mM Tris, 50 mM NaCl at pH 7.4. The centre spectrum shows Cd_2HSA. Both octanoate and Zn^{2+} perturb Cd^{2+} binding to the peak at ca. 130 ppm corresponding to site A. Mutations of zinc-binding residues either eliminate the peak (H67A) or shift it (N99H mutant) (b) Resolution-enhanced ^1H NMR spectroscopy of metal and fatty acid binding to HSA. His Hε1 protons are represented by the sharp peaks. Peaks 1 and 4 have been assigned to residues H67 and H247 respectively, and both are affected by octanoate, Zn^{2+}, and mutations of H67 or N99 (Blindauer *et al*., 2009).

Contrastingly, the competition between Zn^{2+} and myristate (C14) studied by ITC revealed that these ligands influenced the binding of each other to BSA (Figure 1.7a and b).

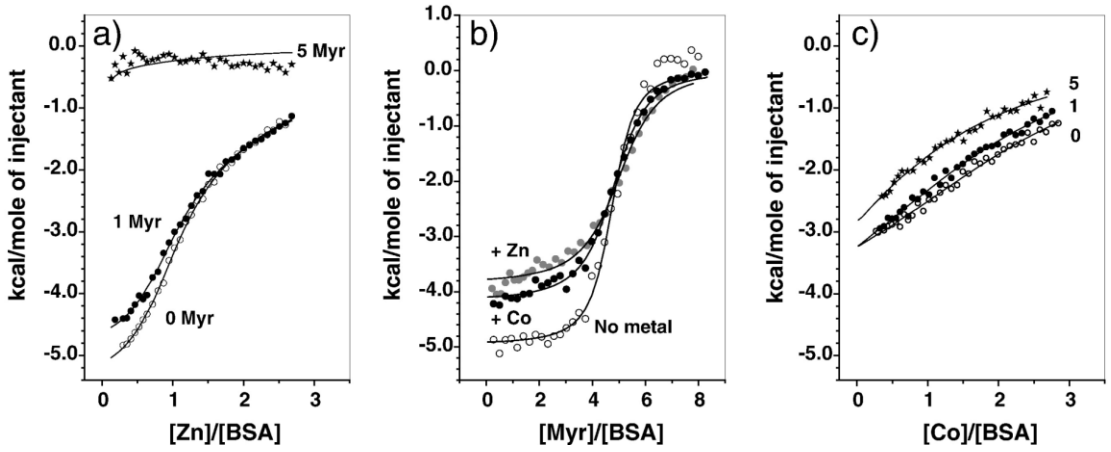

Figure 1.7.Thermodynamic studies between metal and fatty acid binding to HSA by isothermal titration calorimetry. (a) Titration of Zn^{2+} (333 μM) into bovine serum albumin (25 μM) in 50 mM Tris, 50 mM NaCl, pH 7.2 at 298 K, in the presence and absence of myristate. Here, zinc binding to two sites was observed, with apparent binding constants of log K' = 5.67 and 4.15 respectively. Correcting for pH influence and the weak Zn^{2+} chelation by the Tris buffer gave a stoichiometric log K = 7.0 for the strongest site. At high myristate concentrations (5 molar equivalents), no zinc binding could be detected. (b) Titration of bovine serum albumin (12.5 μM) with myristate in the presence and absence of Zn^{2+} or Co^{2+} in H_2O at 298 K. Although no effect on fatty acid binding stoichiometry was observed, there was a reduction in the exothermic strength of the interaction, as it is likely that the binding of a fatty acid molecule to FA2 requires the removal of metal ions in site A and/or B. (c) Cobalt binding to bovine serum albumin was studied under identical conditions to those used for Zn^{2+} binding to allow for direct comparisons to be made. Evidently, Co^{2+} binding is significantly weaker than Zn^{2+} binding, in agreement with Sokolowska *et al*. (2009), but an effect of myristate is still seen. However, in contrast to the effect on Zn^{2+} binding, 5 molar equivalents of myristate did not completely eliminate Co^{2+} binding. This could indicate that either site B is less affected by fatty acids than site A, and/or that Co^{2+} can compensate for the potential loss of sites A and B by binding to the N-terminal ATCUN motif (Blindauer, 2013).

Increasing the myristate concentration significantly decreased the stoichiometry of Zn^{2+}:BSA and the overall affinity of the interaction, while Zn^{2+} did not alter the stoichiometry of myristate binding to BSA, but the binding energetics were observed to be less exothermic. Thus the affinity of albumin for myristate was concluded to be higher than that for Zn^{2+} (Lu *et al*., 2012a), consistent with literature data. The data obtained showed the occupation of two Zn^{2+} sites, which were affected by the myristate concentration. The maximum ratios used (5:1 myristate:BSA) showed complete

inhibition of Zn^{2+} binding at the experimental conditions used. ^{111}Cd NMR experiments using myristate showed an effect on a second metal site. Addition of a 5-fold excess of myristate suppressed the peak corresponding to site A in a similar manner as octanoate. However, unlike with octanoate, the peak corresponding to site B also disappeared upon addition of myristate (Lu *et al*., 2012a). This suggests that myristate binding could have an extra influence on site B, which is propositioned as a candidate for a second Zn^{2+} site. Site B currently remains unidentified, but based on the effects of fatty acids observed in these experiments it is possible that, like site A, it may also be an interdomain site.

Interestingly, the ITC experiments revealed that the zinc binding properties (affinity and capacity) of BSA are affected by levels of myristate as low as 1 molar equivalent. Therefore, the phenomenon of fatty acids modulating the affinity of albumin for Zn^{2+} is likely to occur at all physiological levels, and is not exclusive to extreme experimental conditions. This is given some context by the fact that FA2 is one of the highest affinity fatty acid sites and so its occupation upon binding of the first equivalent of fatty acid is reasonable (Simard *et al*., 2006). The binding of zinc and fatty acids (medium to long chain) to albumin are therefore interactive, as advocated by the examination of X-ray structures. This mechanism might mean that albumin is a link between the distribution and levels of plasma fatty acids, which reflect energy status, and zinc in plasma and nearby tissues.

Physiological implications of modulation of metal binding by fatty acids

There are many links between Zn^{2+} homeostasis and signalling in energy metabolism (Cunnane, 1982; Costarelli *et al*., 2010). Zinc affects concentration and activities of the hormones, glucagon (Hardy *et al*., 2011), leptin (Mantzoros et al., 1998; Chen *et al*., 2000) and insulin (Rutter, 2010). Insulin is essential for sufficient HSA synthesis. In diabetes, patients have a diminished albumin synthesis rate, which may influence fatty acid transport by albumin and cell uptake (Fanali *et al*., 2012b). Leptin, made in adipocytes, controls energy intake and expenditure and it is believed that because of this, Zn^{2+} status has a direct impact on appetite and eating behaviour (Shay and Mangain, 2000). Hyperleptinemia (high levels of leptin) in obesity is coupled with hypozincemia (low levels of plasma zinc) (Oh and Choi, 2004). Similarly, zinc influences the activity of adiponectin (a hormone also secreted by adipocytes) which is

also implicated in fatty acid oxidation and plays a part in insulin resistance (Briggs *et al*., 2012). The oligimerisation and thus activity of both adiponectin and insulin is due to their direct interaction with Zn^{2+}, and so is heavily reliant on available zinc ion levels. Fatty acid synthesis and esterification (lipogenesis) in adipocytes has been shown to be heightened by Zn^{2+} i*n vitro* (Oh and Choi, 2004), and Zn^{2+} is actively taken up into adipocytes during fatty tissue formation (Smidt *et al*., 2011). Increased intracellular Zn^{2+} levels may influence leptin signaling directly *via* inhibition of protein tyrosine phosphatase 1B, which leads to the inhibition of a key enzyme in the leptin and insulin signaling pathways, phosphoinositide 3-kinase (Volpe *et al*., 2007).

Modulation of the albumin affinity for zinc may lead to substantial consequences. One possibility would be that the reduced affinity of fatty acid-bound albumin for zinc alters the speciation of zinc in plasma (i.e. the zinc would bind to alternative proteins). Another possibility could be a change in plasma zinc speciation would affect its uptake by endothelial cells leading to consequent downstream effects.

Albumin influences Zn^{2+} uptake into cells, as described by evidence from several experiments. Albumin affects uptake of zinc by fibroblasts, since it can act as an extracellular ligand for zinc and so buffer the free Zn^{2+} levels (Ackland and McArdle, 1990). For endothelial cells, Zn^{2+} coordinated by albumin can be taken up through endocytosis pathways. Also, the cells have a greater affinity for albumin carrying Zn^{2+} compared to the apoprotein (Gálvez *et al*., 2001). Hence, regardless of the mechanism by which albumin contributes in cellular Zn^{2+} uptake, any modulation of its Zn^{2+} affinity can be expected to impact cellular Zn^{2+} homeostasis. However, it should be noted that other mechanisms of cellular regulation (including the expression of membrane-bound zinc transporters) exist and are significant (Devirgiliis *et al*., 2007).

While zinc levels in plasma are reliably constant, there exist certain conditions where these levels are reduced (King, 2011). Due to the numerous connections between zinc and lipid (and thus energy) metabolism, it is problematic to separate consequences from causes. However, in order to ascertain the credibility of a contribution of fatty acid induced redistribution of Zn^{2+}, clinical or physiological conditions in which both raised plasma fatty acid levels and reduced plasma zinc levels may be encountered are of interest. Conditions where lower plasma zinc levels and increased plasma fatty acid levels were observed together have been reported and include vigorous aerobic exercise

(Volpe *et al*., 2007), obesity, diabetes and cardiovascular disease (Ghayour-Mobarhan *et al*., 2005; Soinio *et al*., 2007; Jansen *et al*., 2012; Boden, 2011).

In cardiovascular disease, conditions leading to reduced energy consumption by the heart could potentially lead to elevations of free fatty acids (at least a temporary increase), since fatty acids provide a large fraction of the energy used by the heart (myocardium in particular). Consequently, it could be that the lower levels of plasma zinc recorded in chronic heart failure (Foster and Samman, 2010) and acute myocardial infarction (Katayama *et al*., 1990; Tan *et al*., 1992; Arnaud *et al*., 1994; Gomez *et al*., 2000) are a direct corollary of the high free fatty acids levels. It is known that levels of zinc in serum are known to fall suddenly in the few hours following a myocardial infarction (MI), with lowest levels detected after 2 or 3 days, subsequently returning slowly to baseline values (Katayama *et al*., 1990). Saliently, the plasma of patients with MI was observed to have a reduced capacity to bind metals, resulting in the development of a clinical test: the albumin-cobalt-binding (ACB) assay (Bar-Or *et al*., 2000).

MI is defined by the heart muscle experiencing a lack of oxygen supply and is a precursory sign for acute myocardial infarction (i.e. heart attack). Bar-Or *et al.* designed the ACB assay (Bar-Or *et al*., 2000) founded on the premise that MI could provoke modifications to albumin molecules in circulation that affect its capability to coordinate to metals. It was established that plasma or serum from MI patients exhibits a considerably lower capacity for Co^{2+} binding, which can be measured rapidly in a colorimetric assay by the reaction of Co^{2+} in excess with the reducing agent, dithiothreitol. Detection of the brown coloured Co^{2+}-dithiothreitol complex is measured at 500 nm to provide the result (Bar-Or *et al*., 2000). The ACB assay has a respectable negative prognostic use and is the only clinical test available for the rapid early assessment of MI. An abormal reading of the ACB allows MI (and hence imminent heart attacks) to be prevented (Collinson and Gaze, 2008; Gaze, 2009; Christenson *et al*., 2001). However, the efficacy of the test has been called into question, since the test is not necessarily specific for this condition (Dominguez-Rodriguez and Abreu-Gonzalez, 2010). Irregular readings relating to low cobalt binding capacity have been observed in cases other than that of ischemia. These include diabetes, obesity (Kaefer *et al*., 2010), cancer, metabolic syndrome, fatty liver infections (Amirtharaj *et al*., 2008),

renal disease, stroke, and even continuous aggressive exercise (Apple *et al*., 2002; Lippi *et al*., 2005).

The ACB assay is thought to detect the biomarker known as "ischemia-modified albumin" (IMA), with the fundamental premise that ischemia causes modifications to the amino-terminal copper and nickel binding (ATCUN) motif. For example, truncation at the N-terminus, a known modification of albumin that occurs due to oxidation (Chan *et al*., 1995). Peptide models of the N-terminus have been used to study the binding of Co^{2+} (Bar-Or *et al*., 2001) but critically N-terminus modifications of albumin from ischemic patients could not be validated (Bhagavan *et al*., 2003; Bar-Or *et al*., 2008). The molecular mechanism behind the lower Co^{2+} affinity has remained obscure. Some studies have suggested that the major sites for Co^{2+} binding are sites A and B, and not the N-terminus (Mothes and Faller, 2007; Sokolowska *et al*., 2009).

Although the N-terminus can in principle bind $Zn^{2+}$and Co^{2+} (Lakusta and Sarkar, 1979), the ATCUN motif generates a square planar geometry which is more suitable to low-spin d^8 and d^9 metal ions such as Ni^{2+} and Cu^{2+}. The d^7 Co^{2+} ion and the d^{10} Zn^{2+} ion are not as attracted to the ATCUN motif site, instead preferring octahedral geometries in general. This introduced the possibility that fatty acids could also influence Co^{2+} binding if site A or B are indeed involved in its coordination (Mothes and Faller, 2007). This direct effect was demonstrated, where high levels of plasma fatty acids affect the cobalt binding capacity of albumin (Amirtharaj *et al*., 2008) and the correlation between plasma fatty acids and IMA was described as "plausible but not causative" (Bhagavan *et al*., 2009). Later, site B was identified as the major Co^{2+} binding site (Sokolowska *et al*., 2009) which had previously been shown to be susceptible to fatty acid binding (Lu *et al*., 2012a).

Based on these clinical observations and *in vitro* studies, it was proposed that IMA was simple regular albumin in the presence of higher fatty acid levels. ITC studies involving the competitive binding of myristate and Co^{2+} (analogous to the Zn^{2+} and myristate studies) established that the presence of myristate did indeed affect Co^{2+} binding (Figure 1.6b and c) (Lu *et al*., 2012b). Interestingly, Co^{2+} binding was less affected by the addition of five molar equivalents of myristate compared to Zn^{2+} binding, where 1.3 molecular equivalents of Co^{2+} were still observed to bind. This effect was attributed to variances in binding affinities of the three sites (site A, site B and a third unknown site

which is possibly the ACTUN motif) for Zn^{2+} and Co^{2+}, and to the different effects that fatty acids induce on each of the three sites. Based on ITC and ^{111}Cd NMR data, site A is impaired to the greatest extent, followed by site B, but no significant negative change is anticipated at the N-terminus, based on structural deliberations. Thus, with site A being the primary site for Zn^{2+} but only a secondary site for Co^{2+}, comprehensive abolition of site A has a major influence on Zn^{2+} binding, but a minor effect on Co^{2+} (which can be compensated by alternate binding of Co^{2+} to the N-terminus). Absorbance readings of a mock ACB test involving physiologically applicable concentrations of BSA and 0–5 molar equivalents of myristate showed an association between the level of fats and the read out from the test (Lu *et al*., 2012b). This was an *in vitro* demonstration that elevated fatty acids in plasma are able to directly influence the results of the ACB assay.

Additionally, since IMA involves non-covalent binding, it explains the quick return to normal IMA levels within hours once the ischemic incident is complete. Since albumin has a long half-life in plasma, any covalent modifications that are formed are not likely to be processed and cleared in such a short time frame, while plasma fatty acids are known to be cleared from the system in a similar frame of time (Eaton *et al*., 1969). Although this is a plausible and likely mechanism, it is important to note that it does not exclude the workings of other mechanisms that are able to influence cobalt binding to albumin, such as acidosis reducing local pH.

The abundance of zinc in the body requires tight homeostatic regulation which is achieved through many mediators and transporters in both intracellular and extracellular environments. As stated earlier, a consequence of fatty acid induced inhibition of zinc binding to albumin could be the alteration of the speciation of zinc in circulation. That is to say, since albumin is the main transporter of zinc in plasma, if the zinc is unable to bind to where it usually would (its binding sites on albumin), the zinc in circulation must be bound to alternate proteins. One such protein is histidine rich glycoprotein (HRG), which is of particular interest since its action is regulated by its coordination of zinc.

Histidine Rich Glycoprotein (HRG)

HRG is a 507 amino acid multidomain protein of an approximate mass of 75 kDa, with six predicted N-linked glycosylation sites, present in the plasma at low micromolar concentrations (Jones *et al*., 2005). The plasma proteome is dominated by the presence of up to 60% HSA, which equates to around 40 mg/ml. HRG can be said to be moderately abundant in plasma since it circulates in the same range as other classic plasma proteins such as IgG, IgA, factor H and the complement proteins in the range of 0.05-0.5 mg/ml (Anderson and Anderson, 2002).

The amino acid sequence of HRG was derived from the nucleotide sequence of its cDNA by Koide *et al*. (1986). The structure of HRG is composed of two N-terminal domains (N1 and N2) evolutionarily related to cystatins, a central eponymous histidine rich region (HRR) with two proline rich regions (PRR1 and PRR2) at either side of the HRR and a C-terminal domain (C) (Jones *et al*., 2005). The distinctive domains are held together by an arrangement of six disulphide bonds, forming the intact protein molecule (Figure 1.8). The domain structure allows for HRG to bind to a multitude of molecules including plasminogen (Lijnen *et al*., 1980), fibrinogen (Leung, 1986), thrombospondin (Leung *et al*., 1984), IgG (Gorgani *et al*., 1997), heparin (Lijnen *et al*., 1983a) and haem (Katagiri *et al*., 1987) as well as cell surface receptors such as Fcγ receptors (Poon *et al*., 2010), heparan sulphate (Jones *et al*., 2004) and platelets (Horne *et al*., 2001). Some of the studies on the binding profile of HRG used recombinant HRG expressed in human embryonic kidney cells (Olsson *et. al*. 2004; Rydengard *et. al*., 2007) or insect cells (Jones *et. al*., 2004). The variety of ligands that HRG displays an affinity for is mirrored in its presence as a regulator of several physiological processes, including immune function, angiogenesis and the coagulation of blood.

HRG binds to heparin, a potent anticoagulant, with a strong affinity thereby regulating the cascade of usual mechanisms. Heparin would normally bind to antithrombin III, forming a heparin-antithrombin III complex that inhibits activated coagulants such as thrombin (Lijnen *et al*., 1983b). The formation of the HRG–heparin complex is enhanced in the presence of Zn^{2+} (Jones *et al*., 2004). The most salient feature of HRG is promoted by its etymology, it contains an unusual prevalence of histidine (and proline) residues each accounting for approximately 13% of the amino acid sequence. The histidine rich region bears an extraordinary repeating amino acid sequence of Gly-

His-His-Pro-His, developing a chain of histidine residues associated with binding metal ions (Figure 1.8).

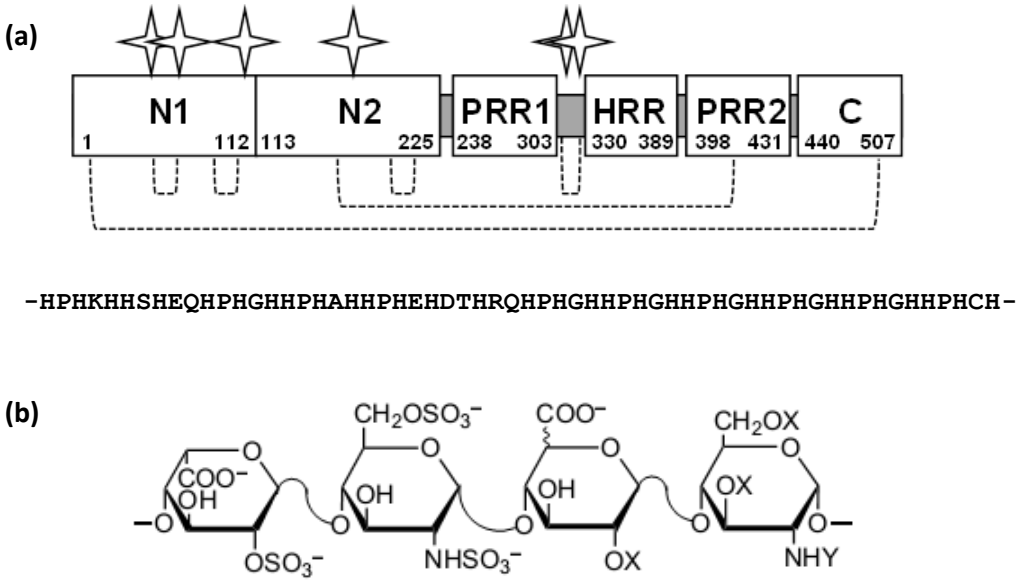

Figure 1.8. (a) The domain structure of the 507 amino acid human HRG represented as blocks, showing the N-terminal domains (N1 and N2), the first proline rich region (PRR1), the histidine-rich region (HRR), the second proline-rich region (PRR2), and the C-terminal domain (C). The dotted lines show the disulphide bridging arrangement through the protein, and the stars represent putative glycosylation sites. The unique repeating amino acid sequence of the HRR is also shown. (b) Chemical structure of the polysaccharide heparin. X = H or SO_3^-, Y = H, SO_3^- or Ac.

Pioneering work by Morgan showed that HRG can bind, Zn^{2+}, Cu^{2+}, Cd^{2+}, Hg^{2+}, Co^{2+} and Ni^{2+} (Morgan, 1981; Morgan and Guthans, 1982). These studies provided fundamental insights into the methods of the protein, revealing that the Zn^{2+} binding is pH dependent, with less binding observed at acidic pH, indicating that protonation of histidine residues reduces affinity. It was also reported that rabbit HRG is able to compete with albumin in respect to Zn^{2+} binding (Morgan, 1981; Morgan and Guthans, 1982). This is an intriguing observation since albumin has a greater affinity for Zn^{2+} (K_d = 30 nM *cf.* K_d = 1-4 µM) (Masuoka, 1993) and circulates at a much higher plasma concentration than HRG (Masuoka *et al*., 1993), but has less known binding sites. These studies demonstrated that that the affinities of the two proteins are relatively close together in relation to Zn^{2+} chelation.

The ability of human HRG to bind up to 10 molar equivalents of Zn^{2+} effectively multiplies the zinc binding site concentration of HRG (Morgan and Guthans, 1982). Therefore, relatively small perturbations could possibly lead to shifts in Zn^{2+}

distribution between albumin and HRG. Additionally, the concentration of Zn^{2+} that is essentially free to move in plasma may reach the levels necessary for Zn^{2+}-dependent HRG complex formation (i.e. activation) during thrombosis, since platelet-derived α-granules release Zn^{2+} at the site of a thrombus (Horne *et al*., 2001). It is supposed that this system may assist in the temporal and spatial regulation of blood clotting (Vu *et al*., 2013).

In individuals suffering from elevated plasma fatty acid levels, it is conceivable that fatty acid-binding to albumin could release exchangeable Zn^{2+} which may consequently enhance the formation of HRG–heparin complexes. Indirect evidence for this includes blood analbuminemia (no serum albumin), which is associated with hypercoagulability (Koot *et al*., 2004). Dietary studies have also shown that platelet aggregation and fibrinolysis can be increased by intake of some fatty acids (Prost-Dvojakovic and Samama, 1973; Kerr *et al*., 1965). Therefore it is possible that this mechanism may contribute to thrombotic symptoms that are clinically associated with conditions such as diabetes, cancer and obesity (Richieri *et al*., 1993). The examination of this relationship between fatty acid binding to albumin, the consequent Zn^{2+}release and possible increased coordination of zinc to HRG forms the premise and hypothesis of this research project.

Albumin, Fatty Acids and Zn^{2+} Dynamics: Activation of HRG and a possible implication in blood coagulation

One reservation regarding the early albumin studies looking at fatty acid and metal binding is to do with the preparation of the albumin samples used in experiments. One study using sheep albumin gave preliminary results showing no metal binding to the protein. It was noted that the albumin preparation did not include a de-fatting step, the inclusion of which resulted in the expected metal binding (Sadler and Viles, 1996). Following on from here, it was postulated that the presence of fatty acids induces an allosteric disruption of the Zn^{2+} binding site, confirmed by crystal structure comparison.

This supposed release of exchangeable Zn^{2+} could switch on a chain of molecular events, where its binding to HRG leads to the formation of anticoagulant inhibiting complexes. High levels of plasma fatty acids are prevalent in conditions such as cancer, diabetes, obesity (Ghayour-Mobarhan *et al*., 2005; Soinio *et al*., 2007; Jansen *et al*., 2012; Boden, 2011) and these conditions also present an increased risk of thrombosis.

With high levels of HRG associated with thrombotic disorders, it is pertinent to propose a potential relation between fatty acids binding to albumin, the subsequent release of Zn^{2+} and the increased coordination of zinc to HRG (Figure 1.9).

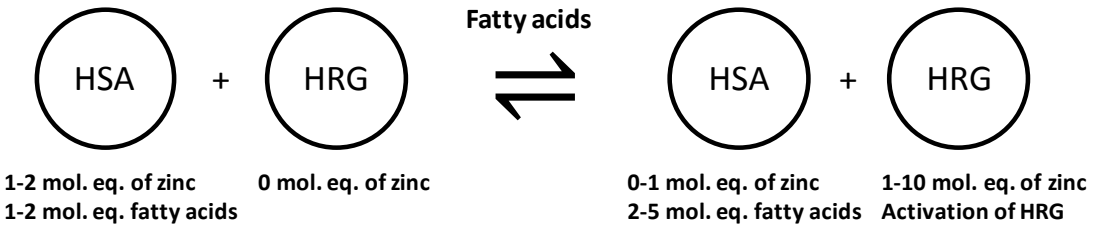

Figure 1.9. Schematic representation of the molecular interactions under investigation. Increasing fatty acid levels may shift the equilibrium towards the right.

Aims

The major hypothesis under investigation during this doctoral research project is to develop an understanding of the regulation of the Zn^{2+} dependent activities of histidine-rich glycoprotein as influenced by fatty acid binding to albumin. Another major aim is to gain better insight into the metal binding properties of albumin. The project is divided into separate chapters with individual aims.

Chapter 2: Experimental techniques

Chapter 3: Structural characterisation of HRG.

Chapter 4: Investigations into Zn^{2+} and heparin binding to HRG and implications for thrombin activation.

Chapter 5: Identification of novel metal binding sites on albumin.

Chapter 6: Conclusions

References

Ackland ML, McArdle HJ. Significance of extracellular zinc-binding ligands in the uptake of zinc by human fibroblasts. *J. Cell. Physiol*. 1990,**145**, 409–413.

Adams PA, Berman MC. Kinetics and mechanism of the interaction between human serum albumin and monomeric haemin, *Biochem J*. 1980, **191**, 95–102.

Amirtharaj GJ, Natarajan SK, Mukhopadhya A, Zachariah UG, Hegde SK, Kurian G, Balasubramanian KA, Ramachandran A. Fatty acids influence binding of cobalt to serum albumin in patients with fatty liver. *Biochim. Biophys. Acta*. 2008, **1782**, 349–354.

Anderson NL, Anderson NG. The human plasma proteome: history, character, and diagnostic prospects. *Mol. Cell. Proteomics*. 2002, **1**, 845-867.

Andreini C, Banci L, Bertini I, Rosato A. Zinc through the Three Domains of Life, *J. Proteome Res*. 2006, **5**(11), 3173–3178.

Apple FS, Quist HE, Otto AP, Matthews WE, Murakami MM. Release characteristics of cardiac biomarkers and ischemia-modified albumin as measured by the albumin cobalt-binding test after a marathon race. *Clinical Chemistry*. 2002, **48**, 1097–1100.

Arnaud J, Faure H, Bourland P, Denis B, Favier AE. Longitudinal changes in serum zinc concentration and distribution after acute myocardial infarction. *Clin. Chim. Acta*. 1994, **230**, 147–156.

Bal W, Christodoulou J, Sadler PJ, Tucker A. Multi-metal binding site of serum albumin, *J. Inorg. Biochem*. 1998, **70**, 33–39.

Bar-Or D, Lau E, Winkler JV. A novel assay for cobalt-albumin binding and its potential as a marker for myocardial ischemia-a preliminary report. *J. Emerg. Med*. 2000, **19**, 311–315.

Bar-Or D, Curtis G, Rao N, Bampos N, Lau E. Characterization of the Co^{2+} and Ni^{2+} binding amino-acid residues of the N-terminus of human albumin: an insight into the mechanism of a new assay for myocardial ischemia. *Eur. J. Biochem.* 2001, **268**, 42–47.

Bar-Or D, Rael LT, Bar-Or R, Slone DS, Mains CW, Rao NK, Curtis CG. The cobalt-albumin binding assay: insights into its mode of action. *Clin. Chim. Acta*. 2008, **387**, 120–127.

Barnett JP, Blindauer CA, Kassaar O, Khazaipoul S, Martin EM, Sadler PJ, Stewart AJ. Allosteric modulation of zinc speciation by fatty acids. Biochim Biophys Acta. 2013, **1830**(12), 5456-5464.

Bartter FC, Steinfeld JL, Waldmann T, Delea CS. Metabolism of infused serum albumin in the hypoproteinemia of gastrointestinal protein loss and in analbuminemia. *Trans. Assoc. Am. Phys*. 1961, **74**, 180–194.

Bhagavan NV, Lai EM, Rios PA, Yang JS, Ortega-Lopez AM, Shinoda H, Honda SAA, Rios CN, Sugiyama CE, Ha CE. Evaluation of human serum albumin cobalt binding assay for the assessment of myocardial ischemia and myocardial infarction. *Clin. Chem*. 2003, **49**, 581–585.

Bhagavan NV, Ha JS, Park JH, Honda SA, Rios CN, Sugiyama C, Fujitani GK, Takeuchi IK, Ha CE. Utility of serum fatty acid concentrations as a marker for acute myocardial infarction and their potential role in the formation of ischemia-modified albumin: a pilot study. *Clin. Chem*. 2009, **55**, 1588–1590.

Bhattacharya AA, Grüne T, Curry S. Crystallographic analysis reveals common modes of binding of medium and long-chain fatty acids to human serum albumin. *J. Mol. Biol*. 2000, **303**, 721–732.

Blindauer CA, Harvey I, Bunyan KE, Stewart AJ, Sleep D, Harrison DJ, Berezenko S, Sadler PJ. Structure, properties, and engineering of the major zinc binding site on human albumin. *J. Biol. Chem*. 2009, **284**, 23116–23124.

Blindauer CA. Lessons on the critical interplay between zinc binding and protein structure and dynamics. *J. Inorg. Biochem*. 2013, **121**, 145–155.

Boden G. Free fatty acids, a link between obesity and insulin resistance. *Front. Biosci*. 1998, **3**, d169–d175.

Boden G. Obesity, insulin resistance and free fatty acids. *Curr. Opin. Endocrinol.Obes*. 2011, **18,** 139–143.

Briggs DB, Giron RM, Schnittker K, Hart MV, Park CK, Hausrath AC, Tsao TS. Zinc enhances adiponectin oligomerization to octadecamers but decreases the rate of disulfide bond formation. *Biometals*. 2012, **25**, 469–486.

Brodersen R. Physical chemistry of bilirubin: binding to macromolecules and membranes., *Bilirubin*, 1982, **1**, 75–123.

Carter DC, Ho JX. Structure of serum albumin, *Adv. Protein Chem*., 1994, **45**, 153-203.

Chan B, Dodsworth N, Woodrow J, Tucker A, Harris R. Site-specific N-terminal auto-degradation of human serum albumin. *Eur. J. Biochem*. 1995, **227**, 524–528.

Chen MD, Song YM, Lin PY. Zinc may be a mediator of leptin production in humans. Life Sci. 2000, **66**, 2143–2149.

Chesters JK, Will M. Zinc transport proteins in plasma. *Br. J. Nutr*. 1981, **45**, 111–118.

Chilvers DC, Dawson JB, Bahreyni-Toosi MH, Hodgkinson A. Identification and determination of copper- and zinc-protein complexes in blood plasma after chromatographic separation on DEAE-Sepharose CL-6B. *Analyst*, 1984, **109**, 871–876.

Choi JK, Ho J, Curry S, Qin D, Bittman R, Hamilton JA. Interactions of very long-chain saturated fatty acids with serum albumin. *J. Lipid Res*. 2002, **43**, 1000–1010.

Christenson RH, Duh SH, Sanhai WR, Wu AHB, Holtman V, Painter P, Branham E, Apple FS, Murakami M, Morris DL. Characteristics of an albumin cobalt binding test for assessment of acute coronary syndrome patients: a multicentre study. *Clin. Chem*. 2001, **47**, 464–470.

Christodoulou J, Sadler PJ, Tucker A. A new structural transition of serum albumin dependent on the state of Cys34: detectionby ^{1}H-NMR spectroscopy. *Eur. J. Biochem*., 1994, **225**, 363–368.

Collinson PO, Gaze DC. Ischaemia-modified albumin: clinical utility and pitfalls in measurement. *J. Clin. Pathol*. 2008, **61**, 1025–1028.

Coppack SW, Jensen MD, Miles JM. In vivo regulation of lipolysis in humans. *J. Lipid Res*. 1994, **35**, 177–193.

Costarelli L, Muti E, Malavolta M, Cipriano C, Giacconi R, Tesei S, Piacenza F, Pierpaoli S, Gasparini N, Faloia E, Tirabassi G, Boscaro M, Polito A, Mauro B, Maiani F, Raguzzini A, Marcellini F, Giuli C, Papa R, Emanuelli M, Lattanzio F, Mocchegiani E. Distinctive modulation of inflammatory and metabolic parameters in relation to zinc nutritional status in adult overweight/obese subjects. *J. Nutr. Biochem*. 2010, **21**, 432–437.

Cunnane SC. Differential regulation of essential fatty-acid metabolism to the prostaglandins. Possible basis for the interaction of zinc and copper in biological systems. *Prog. Lipid Res*. 1982, **21**, 73–90.

Curry S, Brick P, Franks NP. Fatty acid binding to human serum albumin: new insights from crystallographic studies. *Biochim. Biophys. Acta*. 1999, **1441**, 131–140.

Curry S, Mandelkow H, Brick P, Franks N. Crystal structure of human serum albumin complexed with fatty acid reveals an asymmetric distribution of binding sites. *Nat. Struct. Biol*. 1998, **5**, 827–835.

Dawson JB, Bahreyni-Toosi MH, Ellis DJ, Hodgkinson A. Separation of protein-bound copper and zinc in human plasma by means of gel filtration ion exchange chromatography. *Analyst*. 1981, **106**, 153–159.

Devirgiliis C, Zalewski PD, Perozzi G, Murgia C. Zinc fluxes and zinc transporter genes in chronic diseases. *Mutat. Res*. 2007, **622**, 84–93.

Dole VP. A relation between non-esterified fatty acids in plasma and the metabolism of glucose. *J. Clin. Invest*. 1956, **35**, 150–154.

Dominguez-Rodriguez A, Abreu-Gonzalez P. Current role of ischemia-modified albumin in routine clinical practice. *Biomarkers*. 2010, **15**, 655–662.

Eaton RP, Berman M, Steinberg D. Kinetic studies of plasma free fatty acid and triglyceride metabolism in man. *J. Clin. Invest*. 1969, **48**, 1560–1579.

Esposito BP, Najjar R, Interactions of antitumoralplatinum-group metallodrugs with albumin. *Coord. Chem. Rev*. 2002, **232**,137–149.

[a]Fanali G, Cao Y, Ascenzi P, Fasano M. Mn(II) binding to human serum albumin: a 1H-NMR relaxometric study. *J. Inorg. Biochem*. 2012, **117**, 198–203.

[b]Fanali G, di Masi A, Trezza V, Marino M, Fasano M, Ascenzi P. Human serum albumin: from bench to bedside. *Mol. Asp. Med*. 2012, **33**, 209–290.

Fasano M, Curry S, Terreno E, Galliano M, Fanali G, Narciso P, Notari S, Ascenzi P. The Extraordinary Ligand Binding Properties of Human Serum Albumin. *Life*. 2005, **57,** 787-796.

Foote JW, Delves HT. Distribution of zinc amongst human serum globulins determined by gel filtration chromatography-affinity chromatography and atomic-absorption spectrometry. *Analyst*. 1984, **109**, 709–711.

Foote JW, Delves HT. Determination of non-protein-bound zinc in human serum using ultrafiltration and atomic absorption spectrometry with electrothermal atomisation. *Analyst*. 1988, **109**, 709–711.

Foster M, Samman S. Zinc and redox signaling: perturbations associated with cardiovascular disease and diabetes mellitus. *Antioxid. Redox Signal*. 2010, **13**, 1549-1573.

Gálvez M, Moreno JA, Elósegui LM, Escanero JF. Zinc uptake by human erythrocytes with and without serum albumin in the medium. *Biol. Trace Elem. Res*. 2001, **84**, 45-56.

Gaze DC. Ischemia modified albumin: a novel biomarker for the detection of cardiac ischemia. *Drug Metab. Pharmacokinet*. 2009, **24**, 333–341.

Ghayour-Mobarhan M, Taylor A, New SA, Lamb DJ, Ferns GAA. Determinants of serum copper, zinc and selenium in healthy subjects. *Ann. Clin. Biochem*. 2005, **42**, 364-375.

Giroux EL, Henkin RI. Competition for zinc among serum albumin and amino acids. *Biochim. Biophys. Acta*. 1972, **273**, 64–72.

Gomez E, del Diego C, Orden I, Elosegui LM, Borque L, Escanero JF. Longitudinal study of serum copper and zinc levels and their distribution in blood proteins after acute myocardial infarction. *J. Trace Elem. Med. Biol*. 2000, **14**, 65–70.

Gordon Jr RS. Unesterified fatty acid in human blood plasma. II. The transport function of unesterified fatty acid. *J. Clin. Invest*. 1957, **36**, 810–815.

Gordon Jr RS, Cherkes A. Unesterified fatty acid in human blood plasma. *J. Clin. Invest*. 1956, **35**, 206–212.

Gorgani NN, Parish CR, Easterbrook Smith SB, Altin JG. Histidine-rich glycoprotein binds to human IgG and C1q and inhibits the formation of insoluble immune complexes. *Biochemistry*. 1997, **36**, 6653–6662.

Goumakos W, Laussac JP, Sarkar B. Binding of cadmium(II) and zinc(II) to human and dog serum albumins - an equilibrium dialysis and Cd-113-NMR study. *Biochem. Cell Biol.* 1991, **69**, 809–820.

Hardy AB, Serino AS, Wijesekara N, Chimienti F, Wheeler MB. Regulation of glucagon secretion by zinc: lessons from the beta cell-specific Znt8 knockout mouse model. *Diabetes Obes. Metab*. 2011, **13**, 112–117.

Harford C, Sarkar B. Amino terminal Cu(II)- and Ni(II)-binding (ATCUN) motif of proteins and peptides: metal binding, DNA cleavage, and other properties. *Acc. Chem. Res*. 1997, **30**, 123–130.

Himmelhoch SR, Sober HA, Vallee BL, Peterson EA, Fuwa K. Spectrographic and chromatographic resolution of metalloproteins in human serum. *Biochemistry*. 1966, **5**, 2523–2530.

Horne MK, Merryman PK, Cullinane AM. Histidine–proline-rich glycoprotein binding to platelets mediated by tansition metals. *Thromb. Haemost*. 2001, **85**, 890–895.

Hu W, Luo Q, Li X, Wang F, Chen Y, Ma X, Wang J, Lui J, Xiong S, Sadler PJ. The anticancer drug cisplatin can cross-link the interdomain zinc site on human albumin. *Chem. Commun*. 2011, **47**, 6006–6008.

Jansen J, Rosenkranz E, Overbeck S, Warmuth S, Mocchegiani E, Giacconi R, Weiskirchen R, Karges W, Rink L. Disturbed zinc homeostasis in diabetic patients by in vitro and in vivo analysis of insulinomimetic activity of zinc. *J. Nutr. Biochem*. 2012, **23**, 1458–1466.

Jensen MD, Caruso M, Heiling V, Miles JM. Influence of body fat distribution on free fatty acid metabolism in obesity. *J. Clin. Invest*. 1989, **83**, 1168–1173.

Jones AL, Hulett MD, Parish CR. Histidine-rich glycoprotein binds to cell-surface heparan sulfate via its N-terminal domain following Zn2 + chelation. *J. Biol. Chem*. 2004, **279**, 30114–30122.

Jones AL, Hulett MD, Parish CR. Histidine-rich glycoprotein: a novel adaptor protein in plasma that modulates the immune, vascular and coagulation systems. *Immunol. Cell Biol*. 2005, **83**, 106–118.

Kaefer M, Piva SJ, De Carvalho JAM, Da Silva DB, Becker AM, Coelho AC, Duarte M, Moresco RN. Association between ischemia modified albumin, inflammation and hyperglycemia in type 2 diabetes mellitus. *Clin. Biochem*. 2010, **43**, 450–454.

Karpe F, Dickmann JR, Frayn KN. Fatty acids, obesity, and insulin resistance: time for a re-evaluation. *Diabetes*. 2011, **60**, 2441–2449.

Katagiri M, Tsutsui K, Yamano T, Shimonishi Y, Ishibashi F. Interaction of heme with a synthetic peptide mimicking the putative heme-binding site of histidine-rich glycoprotein. *Biochem. Biophys. Res. Commun*. 1987, **149**, 1070–1076.

Katayama T, Honda Y, Yamasaki H, Kitamura S, Okano Y. Serum zinc concentration in acute myocardial infarction. *Angiology*. 1990, **41**, 479–485.

Kelly E, Mathew J, Kohler JE, Blass AL, Soybel DI. Redistribution of labile plasma zinc during mild surgical stress in the rat. *Transl. Res*. 2011, **157**, 139–149.

Kerr JW, MacAulay I, Pirrie R, Bronte-Stewart B. Platelet-aggregation by phospholipids and free fatty acids. *Lancet*. 1965, **285**, 1296–1299.

King JC. Zinc: an essential but elusive nutrient. *Am. J. Clin. Nutr*. 2011, **94**, 679S–684S.

Koide T, Foster D, Yoshitake S, Davie EW. Amino acid sequence of human histidine-rich glycoprotein derived from the nucleotide sequence of its cDNA. *Biochemistry*. 1986, **25**(8), 2220-2225.

Koot BGP, Houwen R, Pot DJ, Nauta J. Congenital analbuminaemia: biochemical and clinical implications. A case report and literature review. *Eur. J. Pediatr*. 2004, **163**, 664-670.

Kragh-Hansen U, Vorum H. Quantitative analyses of the interaction between calcium ions and human serum albumin. *Clinical Chemistry*. 1993, **39**, 202-208.

Lafontan M, Langin D. Lipolysis and lipid mobilization in human adipose tissue. *Prog Lipid Res*. 2009, **48**(5), 275-297.

Lakusta H, Sarkar B. Equilibrium studies of zinc(II) and cobalt(II) binding to tripeptide analogs of the amino terminus of human serum albumin. *J. Inorg. Biochem.* 1979, **11**, 303–315.

Leung LL, Nachman RL, Harpel PC. Complex formation of platelet thrombospondin with histidine-rich glycoprotein. *J. Clin. Invest*. 1984, **73**, 5–12.

Leung LL. Interaction of histidine-rich glycoprotein with fibrinogen and fibrin. *J. Clin. Invest*. 1986, **77**, 1305–1311.

Lijnen HR, Hoylaerts M, Collen D. Isolation and characterization of a human plasma protein with affinity for the lysine binding sites in plasminogen. Role in the regulation of fibrinolysis and identification as histidine-rich glycoprotein. *J. Biol. Chem*. 1980, **255**, 10214–10222.

[a]Lijnen HR, Hoylaerts M, Collen D. Heparin binding properties of human histidine-rich glycoprotein. Mechanism and role in the neutralization of heparin in plasma. *J. Biol. Chem*. 1983, **258**, 3803–3808.

[b]Lijnen HR, Hoylaerts M, Collen D. Neutralization of heparin activity by binding to human histidine-rich glycoprotein. *Thromb Res*. 1983, **29**(4), 443-446.

Lippi G, Brocco G, Salvagno GL, Montagnana M, Dima F, Guidi GC. High-workload endurance training may increase serum ischemia-modified albumin concentrations. *Clin. Chem. Lab. Med*. 2005, **43**, 741–744.

Lu J, Stewart AJ, Sadler PJ, Pinheiro TJT, Blindauer CA, Albumin as a zinc carrier: properties of its high-affinity zinc-binding site. *Biochem. Soc. Trans*. 2008, **36**, 1317-1321.

[a]Lu J, Stewart AJ, Sleep D, Sadler PJ, Pinheiro TJT, Blindauer CA. A molecular mechanism for modulating plasma Zn speciation by fatty acids. *J. Am. Chem. Soc*. 2012, **134**, 1454–1457.

[b]Lu J, Stewart AJ, Sadler PJ, Pinheiro TJT, Blindauer CA. Allosteric inhibition of cobalt binding to albumin by fatty acids: implications for the detection of myocardial ischemia. *J. Med. Chem*. 2012, **55**, 4425–4430.

Malavolta M, Piacenza F, Basso A, Giacconi R, Costarelli L, Pierpaoli S, Mocchegiani E. Speciation of trace elements in human serum by micro anion exchange chromatography coupled with inductively coupled plasma mass spectrometry. *Anal. Biochem*. **421**, (2012), pp. 16–25

Manley SA, Gailer J. Analysis of the plasma metalloproteome by SEC-ICP-AES: bridging proteomics and metabolomics. *Expert. Rev. Proteome*. 2009, **6**, 251–265.

Majorek KA, Porebski PJ, Dayal A, Zimmerman MD, Jablonska K, Stewart AJ, Chruszcz M, Minor W. Structural and immunologic characterization of bovine, horse, and rabbit serum albumins. *Mol. Immunol*. 2012, **52**, 174–182.

Mantzoros CS, Prasad AS, Beck FWJ, Grabowski S, Kaplan J, Adair C, Brewer GJ. Zinc may regulate serum leptin concentrations in humans. *J. Am. Coll. Nutr*. 1998, **17**, 270–275.

Martins EO, Drakenberg T. Cadmium(II), zinc(II), and copper(II) ions binding to bovine serum albumin. A ^{113}Cd NMR study. *Inorg. Chim. Acta*. 1982, 67, 71–74.

Masuoka J, Hegenauer J, van Dyke BR, Saltman P. Intrinsic stoichiometric equilibrium constants for the binding of zinc(II) and copper(II) to the high affinity site of serum albumin. *J. Biol. Chem*. 1993, **268**, 21533–21537.

Morgan WT. Interactions of the histidine-rich glycoprotein of serum with metals. *Biochemistry*. 1981, 20, 1054–1061.

Morgan WT, Guthans SL. The interaction of zinc, nickel and cadmium with serum albumin and histidine-rich glycoprotein assessed by equilibrium dialysis and immunoadsorbent chromatography. *Arch. Biochem. Biophys*. 1982, **218**, 320–328.

Mothes E, Faller P. Evidence that the principal Co(II)-binding site in human serum albumin is not at the N-terminus: implication on the albumin cobalt binding test for detecting myocardial ischemia. *Biochemistry*. 2007, **45**, 2267–2274.

Nielsen S, Guo ZK, Johnson CM, Hensrud DD, Jensen MD. Splanchnic lipolysis in human obesity. *J. Clin. Invest*. 2004, **113**, 1582–1588.

Odintsov SG, Sabala I, Marcyjaniak M, Bochtler M. Latent. LytM at 1.3A resolution. *J. Mol. Biol*. 2004, **335**, 775-85.

Oh YS, Choi CB. Effects of zinc on lipogenesis of bovine intramuscular adipocytes, Asian Australas. *J. Anim. Sci*. 2004, **17**, 1378–1382.

Parisi AF, Vallee BL. Isolation of a zinc α2-macroglobulin from human serum. *Biochemistry*. 1970, **9**, 2421–2426.

Pedersen AO, Mensberg KL, Kragh-Hansen U. Effects of ionic strength and pH on the binding of medium-chain fatty acids to human serum albumin. *Eur. J. Biochem*. 1995, **233**, 395–405.

Petitpas I, Grüne T, Bhattacharya AA, Curry S. Crystal structures of human serum albumin complexed with monounsaturated and polyunsaturated fatty acids. *J. Mol. Biol.* 2001, **314**, 955–960.

Peters Jr T. All about albumin: biochemistry, genetics, and medical applications. New York: Academic Press, 1996.

Poon IK, Hulett MD, Parish CR. Histidine-rich glycoprotein is a novel plasma pattern recognition molecule that recruits IgG to facilitate necrotic cell clearance via FcγRI on phagocytes. *Blood*. 2010, **115**, 2473–2482.

Prasad AS. Discovery of human zinc deficiency and studies in an experimental human model. *Am. J. Clin. Nutr*. 1991, **53**, 403–412.

Prost-Dvojakovic RJ, Samama M. Clot-promoting and platelet-aggregating effects of fatty acids. *Haemostasis*. 1973, **174**, 73–84.

Quinlan GJ, Martin GS, Evans TW. Albumin: Biochemical Properties and Therapeutic Potential, *Hepatology*. 2005, **41**, 1211-1219.

Richieri GV, Anel A, Kleinfeld AM. Interactions of long chain fatty acids and albumin; determination of free fatty acid levels using the fluorescent probe *ADIFAB*, *Biochemistry*. 1993, **32**, 7574–7580.

Richieri GV, Kleinfeld AM. Unbound free fatty acid levels in human serum. *J. Lipid Res*. 1995, **36**, 229–240.

Rogiers V. Long chain nonesterified fatty acid patterns in plasma of healthy children and young adults in relation to age and sex. *J. Lipid Res*. 1981, **22**, 1–6.

Rowe DJ, Bobilya DJ. Albumin facilitates zinc acquisition by endothelial cells, *Proc Soc Exp Biol Med*. 2000, **224**(3), 178-186.

Rukgauer M, Klein J, Kruse-Jarres JD. Reference values for the trace elements copper, manganese, selenium, and zinc in the serum/plasma of children, adolescents, and adults. *J. Trace Elem. Med. Biol*. 1997, **11**, 92–98.

Rutter GA. Think zinc: new roles for zinc in the control of insulin secretion. *Islets*, 2010, 2, 49–50.

Rydengard V, Olsson AK, Morgelin M, Schmidtchen A. Histidine-rich glycoprotein exerts antibacterial activity. *FEBS J.* 2007, **274**(2), 377-389.

Sadler PJ, Viles JH. ^{1}H and ^{113}Cd NMR investigations of Cd^{2+} and Zn^{2+} binding sites on serum albumin: competition with Ca^{2+}, Ni^{2+},Cu^{2+},and Zn^{2+}, *Inorg. Chem*., 1996, **35**, 4490-4496.

Schnitzer JE, Sung A, Horvat SR, Bravo J. Preferential interaction of albumin-binding proteins, gp30 and gp18, with conformationally modified albumins. Presence in many cells and tissues with a possible role in catabolism. *J. Biol. Chem*. 1992, **267**, 24544–24553.

Schnitzer JE, Oh P. Albondin-mediated capillary permeability to albumin. Differential role of receptors in endothelial transcytosis and endocytosis of native and modified albumins. *J. Biol. Chem*. 1994, **269**, 6072–6082.

Scott BJ, Bradwell AR. Identification of the serum binding proteins for iron, zinc, cadmium, nickel, and calcium. *Clin. Chem*. 1983, **29**, 629–633.

Seeley R, Trent S, Tate P. *Anatomy and Physiology*, McGraw-Hill Higher Education, 8th edition, 2007.

Shay NF, Mangian HF. Neurobiology of zinc-influenced eating behaviour. *J. Nutr*. 2000, **130**, 1493S–1499S.

Simard JR, Zunszain PA, Ha CE, Yang JS, Bhagavan NV, Petitpas I, Curry S, Hamilton JA. Locating high-affinity fatty acid-binding sites on albumin by x-ray crystallography and NMR spectroscopy. *Proc. Natl. Acad. Sci. U. S. A.* 2005, **102**, 17958–17963.

Simard JR, Zunszain PA, Hamilton JA, Curry S. Location of high and low affinity fatty acid binding sites on human serum albumin revealed by NMR drug-competition analysis. *J. Mol. Biol*. 2006, **361**, 336–351.

Smidt K, Pedersen SB, Brock B, Schmitz O, Fisker S, Bendix J, Wogensen L, Rungby J. Zinc-transporter genes in human visceral and subcutaneous adipocytes: lean versus obese. *Mol. Cell. Endocrinol*. 2007, 264, 68–73.

Smith KT, Failla ML, Cousins RJ. Identification of albumin as the plasma carrier for zinc absorption by perfused rat intestine. *Biochem. J*. 1979, **184**, 627–633.

Song MK, Adham NF. Determination of native zinc content of alpha-2-macroglobulin in normal, hyperzincemic and hypozincemic sera by sucrose density gradient centrifugation. *Clin. Chim. Acta*., 1979, **99**, 13–21.

Soinio M, Marniemi J, Laakso M, Pyorala K, Lehto S, Ronnemaa T. Serum zinc level and coronary heart disease events in patients with type 2 diabetes. *Diabetes Care.* 2007, **30**, 523–528.

Sokolowska M, Wszelaka-Rylik M, Poznanski J, Bal W. Spectroscopic and thermodynamic determination of three distinct binding sites for Co(II) ions in human serum albumin. *J. Inorg. Biochem*. 2009, **103**, 1005–1013.

Stewart AJ, Blindauer CA, Berezenko S, Sleep D, Sadler PJ. Interdomain zinc site on human albumin. *Proc. Natl. Acad. Sci*. 2003, **100**, 3701–3706.

Stewart AJ, Blindauer CA, Sadler PJ. Plasma fatty acid levels may regulate the Zn2+-dependent activities of histidine-rich glycoprotein. *Biochimie.* 2009, **91**, 1518–1522.

Sudlow G, Birkett DJ, Wade DN. The characterization of two specific drug binding sites on human serum albumin, *Mol Pharmacol*, 1975, **11**, 824–832

Sudlow G, Birkett DJ, Wade DN. Further characterization of specific drug binding sites on human serum albumin, *Mol. Pharmacol*., 1976, **12**, 1052 – 1061

Tan IK, Chua KS, Toh AK. Serum magnesium, copper, and zinc concentrations in acute myocardial infarction. *J. Clin. Lab. Anal*. 1992, **6**, 324–328.

Thorp H. Bioinorganic chemistry and drug design: here comes zinc again. *Chemistry & Biology*, 1998, **5**, 125-127.

Todd WR, Elvehjem CA, Hart EB. Zinc in the nutrition of the rat. *Am. J. Physiol*. 1933, **107**, 146–156.

van der Vusse GJ. Albumin as fatty acid transporter. *Drug Metab Pharmacokinet*. 2009, **24**(4), 300-307.

Volpe SL, Lowe NM, Woodhouse LR, King JC. Effect of maximal exercise on the short-term kinetics of zinc metabolism in sedentary men. *Br. J. Sports Med*. 2007, **41**, 156–161.

Vu TT, Fredenburgh JC, Weitz JI. Zinc: an important co-factor in haemostasis and thrombosis. *Thromb. Haemost*. 2013, **109**(3), 421-430.

Chapter 2

Experimental techniques

Protein purification

One of the simplest and easiest methods for protein purification is immobilised metal affinity chromatography, which was developed in the '70s (Porath *et al*. 1975). This process utilises either a protein's native or engineered affinity for metals (usually Ni^{2+} or Cu^{2+}) immobilised on a matrix. Histidine exhibits the strongest interaction with immobilised metal ions, as electron donor groups on the histidine imidazole ring readily form coordination bonds with the metal. Nickel, copper and zinc can coordinate with donor atoms such as O and S but have a distinct preference for N. Also, the imidazole group of histidine is partially deprotonated at physiological pH (pK_a ~ 6.5). Therefore, provided that the histidine is accessible, it will provide the protein with the ability to bind to these metal ions.

Consecutive histidine residue containing amino acid sequences are proficiently retained during immobilised metal affinity chromatography. The matrix is washed, and the polyhistidine sequences can be eluted simply by either adjusting the imidazole content or the pH of the buffer. Imidazole, due to structural similarity with histidine, provides effective competition for the metal matrix thereby releasing the histidine sequence from binding. Reducing the pH alters the charges of the imidazole group of histidine (making it more positively charged), hence precluding its binding to the positive metal matrix. This understanding and simplicity led to the development of "His-tags" to modify desired proteins for ease of purification (Hochuli *et al.* 1987, 1988), and is now common practise in purification protocols.

The nickel affinity chromatography method was used here to purify HRG either from rabbit serum/plasma or human plasma, by exploiting the histidine-rich nature of HRG and consequent affinity for metal ions. The procedure used was a modified version of established protocols for HRG purifications (Mori *et al*. 2003), which in one simple step affords high yields and high purities.

While this one step procedure was deemed suitable for most experiments, an extra purification step was added prior to protein crystallography experiments. To further

purify and ensure homogeneity, HRG was subjected to size exclusion chromatography (also known as gel filtration). Size exclusion chromatography separates molecules based on their hydrodynamic volume (their sphere of rotation in solution) and has been applied in protein purification for decades. During size exclusion, larger molecules are retained on the column for shorter periods of time than for smaller molecules (which could include salt and other buffer constituents), thus effective separation of a heterogeneous sample can be achieved, once optimal procedures and conditions are developed. This method can also be used to "desalt" or exchange the buffer solution in protein samples. Separation is made possible by pores within the resin that provide a longer pathway through the column for smaller analytes, which can fit through the pore.

Size exclusion columns generally have a low resolution and come in many stationary phase arrangements of different pore sizes and matrix material allowing for the selection of the most appropriate column for specific samples. The state of the protein sample can also affect the retention time of proteins, since hydrophobic and electrostatic interactions occur between the protein and the matrix, which can result in larger peak volumes or lower resolution (Regnier, 1983). The ionic strength of the solution can also influence retention times, where moderate to high salt concentrations subdue electrostatic interactions of proteins with the column matrix (Stulík *et al*. 2003). As with high-performance liquid chromatography, organic solvents like acetonitrile can be used in the buffers to reduce interactions (Welling *et al*. 1985). However, this is a harsh method which can potentially denature the target protein.

Protein Crystallography

Protein crystallography attempts a molecular choreography of the most dynamic and pliable constructs in chemical physiology. Protein molecules display an abstract quality of arranging into structures relating to function while paradoxically being composed of apparent random sequences of amino acids. Crystallography is the most powerful technique available to examine the tertiary and even quaternary structure of proteins. Crystals are achieved by exposing a protein sample of high purity to conditions at the limit of precipitation. In order to establish these, parameters including protein concentration, salt content, precipitant, pH and temperature are varied to establish optimal conditions for crystallisation to occur. Another aspect of importance is the homogeneity of the protein in the sample. It is imperative that the protein molecules are

of the same homogeneity in order to build on one another to form a crystal (Benvenuti and Mangani, 2007).

During the crystallisation process, molecules in solution associate with each other to form a uniform solid phase lattice. This process is encouraged by altering the chemical and physical environment to make the formation of the lattice conformation thermodynamically favourable. The difference between the changes in entropy and enthalpy is the energy released during crystallisation. Due to rotational and translational disorder, the molecule has favourable entropy in solution, but is enclosed by a coordination sphere of water molecules that give the system unfavourable entropy. The surface charge of the protein molecule allows it to hydrogen bond with the water molecules (enthalpically favourable). However, these interactions are altered during crystallisation where hydrogen bonds with some of the water molecules are sacrificed in areas where stronger intramolecular ionic and hydrogen bonds are available, and thus the regular order of the crystal lattice lowers the entropy of the crystalline system. Hydrophobic regions of protein molecules are likely to be hidden by intermolecular interactions, preventing the formation of unfavourable bonds with water molecules. The solution entropy is increased however, by the expulsion of water molecules (Benvenuti and Mangani, 2007).

Varying the conditions described above can be used to control and exploit these energy profiles. For example, the pH determines the charge on the molecule thereby manipulating the interactions of the protein with the solution. Polymeric alcohols such as polyethylene glycol (PEG) quench water molecules away from a crystal lattice, allowing it to pack tighter. Adding counter-ions can protect surface charges and alter the solvent chemical potential. Divalent metals can directly interact with the protein and attenuate lattice contacts. The inclusion of metal ions can also help solve phasing issues further on in the structure resolution process. The physical environment during crystallisation can be changed by several methods including dialysis, controlled evaporation or vapour diffusion (Dessau and Modis, 2011).

A popular vapour diffusion method used routinely for crystallisation is the sitting drop vapour diffusion technique. A mixed drop (between nanoliter and microliter in volume) containing sample, buffer and precipitant reagents is placed on a platform to put it in vapour equilibration with a liquid reservoir well. Initially, the precipitant concentration

in the drop is lower than that in the reservoir (i.e. the water concentration in the drop is higher). Over a period of time water vapour leaves the drop and equilibrates with the reservoir well. Since water is leaving the drop solution, the sample is effectively being concentrated thereby increasing the relative supersaturation of the sample. This is a key step during crystallisation, since the process involves the effort to push the sample through different phases to achieve reproducible crystal growth.

A phase diagram provides an appropriate illustration of the crystallisation process, showing the states which occur during attempted crystallisation. It shows the balance of pivotal parameters such as protein concentration, additives and precipitants in a constant juggle to produce crystals. Phase diagrams are kept in mind during the design and optimisation of crystal experiments (Figure 2.1) (Ataka, 1993; McPherson 1999).

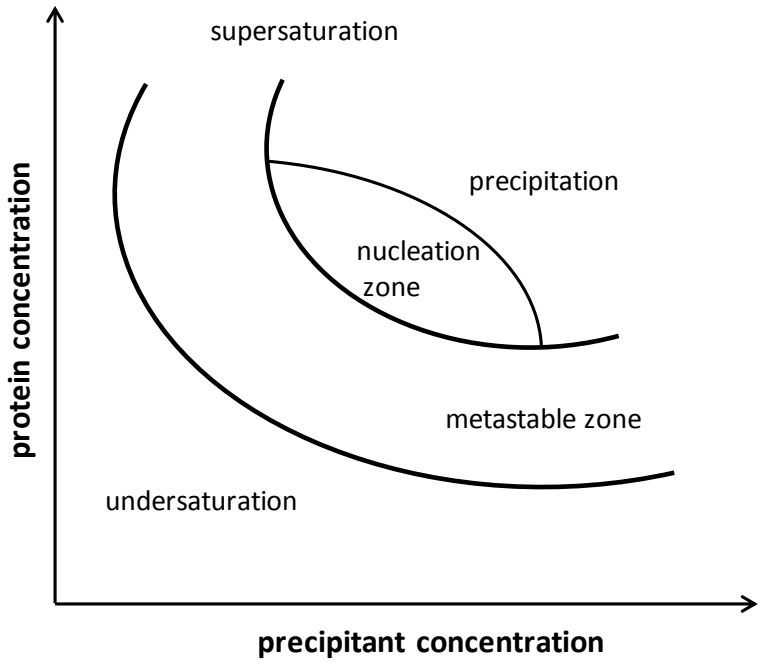

Figure 2.1. Phase diagram for a vapour diffusion crystallisation experiment, showing the four possible zones. The protein sample begins in an undersaturated state but during the evaporation process becomes more concentrated and tends towards the nucleation zone. Once crystals nucleate, the protein concentration in solution drops and the sample sits in the metastable zone, most suitable for crystal growth.

Four zones represent the varying points of saturation where the zone of high supersaturation is likely to induce protein precipitation and a zone of undersaturation where the protein is soluble and stable in solution thus precluding crystal formation. In between these conditions exists a zone of moderate supersaturation, where nucleation

occurs spontaneously. This zone is encouraging for the growth of crystals. But the desired condition rests in the metastable zone of supersaturation, where crystals forming after nucleation are stable and may grow well ordered crystals. Crystallisation ensues in two phases, nucleation followed by growth. Nucleation is a necessary for crystallisation, but requires different conditions than those required for growth. According to the phase diagram, once nucleation has been achieved and spontaneous growth follows, the protein concentration in solution will decrease and the phase will drop down into the metastable zone (Ataka, 1993; McPherson, 1999). Generally, the crystallisation process takes two stages where the first aim is to determine lead conditions for crystallisation of the molecule and secondly to optimise those conditions to produce quality single crystals of at least 10 μm^3 in dimension for X-ray diffraction.

All X-ray diffraction experiments were performed by Dr. Stephen McMahon.

Isothermal Titration Calorimetry (ITC)

One of the main calorimetric techniques applied to investigate protein binding interactions is isothermal titration calorimetry (ITC). ITC measures the heat energy generated during the association of molecules at a constant temperature; once a ligand is titrated into a protein solution the exothermic or endothermic heat is detected. ITC allows for the association constant (K_a, and thus the dissociation constant, K_d), the standard Gibbs free energy change (ΔG), the enthalpy change (ΔH), the entropy change (ΔS) and the stoichiometry (n) of the binding reaction to be determined simultaneously. Additionally, if experiments are performed over a range of different temperatures the heat capacity change (ΔCp) of the binding reaction can be calculated (Chen and Wadso, 1982; Wiseman *et al.*, 1989; Freire *et al.*, 1990). Since most interacting systems are characterised by changes in enthalpy, ITC has vast range of potential applications.

In modern instruments, the calorimeter is based on a cell feedback system which measures the difference in heat effects between the sample cell and a reference cell. A constant power is applied to the reference cell which activates the feedback circuit, in turn regulating the temperature in the sample cell. The baseline signal is the resting power applied to the sample cell. If the reaction between the sample and the titrant is exothermic a decrease in the necessary feedback power is required (since the reaction provides energy to the system), and endothermic reactions require an increased feedback power (since the reaction will take energy out of the system). The reaction

enthalpy for each injection is obtained by integrating the area of the peak formed which deviates away from the resting baseline. Thus the power applied by the calorimeter to keep the system under isothermal conditions is a means of following the interaction. Figure 2.2 shows a schematic representation of an ITC calorimeter (Wiseman *et al*., 1989; Freire *et al*., 1990).

For a typical ITC experiment, the reference cell is filled with water and the sample cell with the sample of interest. The ligand is introduced by an electronically controlled injection syringe which is continuously stirring during an experiment, to allow complete instantaneous mixing in the sample cell after an injection. The mechanical heat provided by the stirring is constant and becomes part of the resting baseline. Setting up ITC binding experiments is very challenging due to the nature of non-covalent binding, where heats are intrinsically small (in the range of 5-10 $kcalmol^{-1}$), and are released during the binding experiment. Additionally, ligand titration produces further heat effects arising from mixing and dilution which are frequently comparable to the binding heat of interest, and so corrections must be made to account for these. The setup of an ITC experiment depends largely on the thermodynamic characteristics (the expected binding affinity and the heat effect) of the system of interest. Thus the appropriate concentration of the protein placed in the cell depends on the binding affinity between the protein and ligand. The shape of the binding curve is dependent on the product of the concentration of macromolecule [M] and the binding constant K_a, which is termed as the dimensionless constant, C.

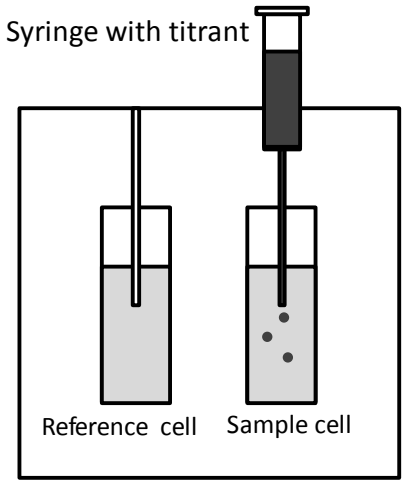

Figure 2.2. Diagram showing the concept behind an isothermal titration calorimeter. The system is kept at a constant temperature, and the power required to sustain this temperature relative to the reference cell is recorded as the titrant is injected into the sample cell.

At high C-values (over 500), the shape of the curve approaches a step function and so becomes insensitive to changes in K_a and thus unsuitable for determining binding constants. At low C-values (less than 10), the binding curve essentially forms a horizontal line which reveals very little experimental information regarding affinity constants. Conditions should be optimised to have a C-value in the range of 10–100 for an accurate and reliable determination of K_a. To measure at these C-values, very strong binding interactions (10^7–10^8 M^{-1}) require low concentrations of the protein. With a lower affinity of the interaction or lower concentrations of the protein, the signal will becomes smaller and reach the detection limit of ITC. Therefore, it is necessary to use high protein concentrations to obtain informative isotherm curves if a low binding affinity is expected or observed. There is no limit in principle to the low binding affinity interactions that can be determined, however in experimental practice there are problems with stability or solubility and often with availability of the precious protein sample in order to optimise conditions such that the C-value range is 10–100. Even at low ligand concentration, only a small percentage of ligand is bound to the protein, making sufficient heat detection difficult and thus problematic to determine ΔH accurately (Bhatnagar and Gordon, 1995).

For high quality isotherms, an appropriate protocol has to be established by optimising parameters such as protein concentration, ligand concentration, the injection volume and the injection spacing. The ligand concentration is usually much higher than the sample concentration since several molar equivalents must be injected to reach saturation. The ITC experiment should be designed to reach or at least approach complete saturation of the binding sites by the end of the experiment. To generate an appropriate number of data points, which will improve data analysis by allowing for better curve fitting, the ligand is added in small quotients. However, this volume should not be so small such that the heat signal is too small to maintain high precision of each injection data point. In the instance of the interaction heat being small, the injection volume can be increased. In cases where the ligand has poor solubility, it is possible to place it in the sample cell and to inject the protein (Bhatnagar and Gordon, 1995).

The time interval in between consecutive injections is an additional significant parameter in obtaining quality data. If the binding association is quick, the calorimeter will be able to equilibrate to baseline in a short time, and so only a few minutes would be sufficient to reach baseline again after injection. However, a slow binding process

will require much longer to reach equilibrium. When running an ITC experiment, it is imperative that the solutions of protein and ligand are pure and at exactly the same pH, buffer composition and salt concentration. To achieve this, the protein and ligand are usually dissolved in the same buffer or dialysed prior to the experiment. This ensures the prevention of spurious heat effects which result from the mixing of different buffer components. Additionally, air bubble formation is to be avoided, and so samples are degassed prior to the experiment. Air bubbles in the sample cell can lead to false signals since they can interfere with the thermal contact of solution and cell wall. Lastly, the heat effect of the first injection is usually too small as a result of diffusion during equilibration of the system. Thus it is common practice to make a small first injection and then subsequently delete the first data point prior to analysis (Bundle and Sigurskjold, 1994).

ITC measures the total heat released or absorbed during a binding interaction which includes the heat contributions from dilution of ligand in the buffer, heat of mixing and possible mixing of buffers of slightly different composition. Before analysing the data for a specific reaction, these effects (particularly the heat of dilution) need to be accounted for by performing control experiments of the injecting ligand into buffer. An alternative option is to ensure that the experiment reaches complete saturation by the end of the titration so that the nonspecific heat effects can be averaged from the final injections. The area under the signal against time curve which is evolved during an ITC experiment represents the total heat absorbed or released by an injection (Figure 2.3). From this raw data, the baseline and dilution heats are subtracted. The data are presented in integral mode as a hyperbolic saturation curve or in differential mode as a sigmoid plot (Sigurskjold *et al.*, 1991; Bundle and Sigurskjold, 1994).

To obtain quantitative information, the data is subjected to non-linear curve fitting. In the simplest case, each protein molecule contains only one type of binding site, all of which display the same intrinsic affinity for the ligand. More complex fitting methods are also used to attempt to describe more complex binding systems, where multiple independent sets of binding sites occur or where cooperative binding sites exist. Using statistical thermodynamic treatment makes it possible to deconvolute a binding isotherm of such complex systems (Perozzo *et al.*, 2004). However, the quality and reliability of the experimental data dictate the success of fitting parameters.

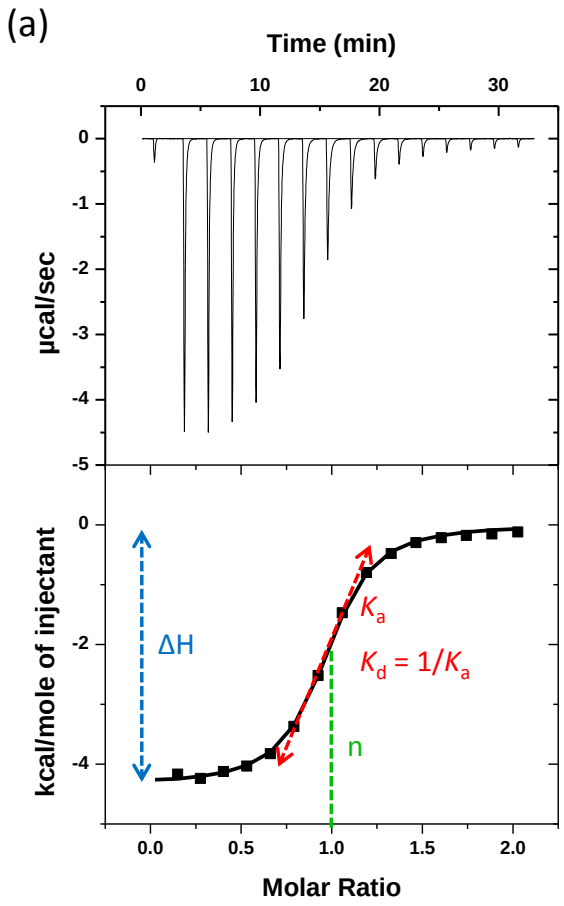

(b) $RT\ln K_d = \Delta G = \Delta H - T\Delta S$

Figure 2.3. (a) An ITC isotherm for EDTA (0.4 mM) titrated with Ca^{2+} (5 mM). The top panel is the raw data showing the heat generated for each injection of Ca^{2+}. The bottom panel is an integration of the raw data peaks showing the energy per mole of reactant, and the non-linear fit can be used to quantify the interaction. In this case, the reaction was exothermic with N= 0.93 and $K_a = 1.35 \times 10^5$ M^{-1}. The important paraeters are highlighted. (b) The thermodynamic equations relating the change in enthalpy (ΔH) and the dissociation constant (K_d) with Gibbs' free energy (ΔG). R is the Gas constant, T is temperature and ΔS the change in entropy.

References

Ataka M. Protein crystal growth: an approach based on phase diagram determination. Phase Transitions. 1993, **45**, 205–219.

Benvenuti M, Mangani S. Crystallization of soluble proteins in vapor diffusion for x-ray crystallography. *Nat Protoc*. 2007, **2**(7), 1633-1651.

Bhatnagar RS, Gordon JI. Thermodynamic studies of myristoyl-CoA:protein N-myristoyltransferase using isothermal titration calorimetry. *Method Enzymol*. 1995, **250**, 467–486.

Bundle DR, Sigurskjold BW. Determination of accurate thermodynamics of binding by titration microcalorimetry. *Method Enzymol*. 1994, **247**, 288–305.

Bragg WL, Bragg WH. The structure of crystals as indicated by their diffraction of X-ray. *Proc Roy Soc London*. 1913, **89**, 248–277.

Chen A, Wadso I. Simultaneous determination of delta G, delta H and delta S by an automatic microcalorimetric titration technique: application to protein ligand binding. *J Biochem Biophys Meth*. 1982, **6**, 307–316.

Dessau MA, Modis Y. Protein crystallization for X-ray crystallography. *J Vis Exp*. 2011, **47**, 2285.

Freire E, Mayorga OL, Straume M. Isothermal titration calorimetry. *Anal Chem*. 1990, **62**, 950A–959A.

Hochuli E, Dobeli H, Schacher A. New metal chelate adsorbent selective for proteins and peptide containing neighbouring histidine residues. *J Chromatogr*. 1987, **411**, 177-184.

Hochuli E, Bannwarth W, Dobeli H, Gentz R, Stuber D. Genetic approach to facilitate purification of recombinant proteins with a novel metal chelate adsorbent. *Bio/Technology*. 1988, **6**, 1321-1325.

Ilari A, Savino C. Protein Structure Determination by X-Ray Crystallography. *Bioinformatics*. 2008, **452**, 63-87.

McPherson A. Crystallization of Biological Macromolecules.1999, Cold Spring Harbor Laboratory Press, Cold Spring Harbor.

Mori S, Takahashi HK, Yamaoka K, Okamoto M, Nishibori M. *Life Sci*. 2003, **73**(1), 93-102.

Perozzo R, Folkers G, Scapozza L. Thermodynamics of protein-ligand interactions: history, presence, and future aspects. *J Recept Signal Transduct Res*. 2004, **24**, 1-52.

Porath J, Carlsson J, Olsson I, Belfrage G. Metal chelate affinity chromatography, a new approach to protein fractionation. *Nature*. 1975, **258**, 598–599.

Regnier FE. High-performance liquid chromatography of biopolymers. *Science*. 1983, **222**, 245–252.

Sigurskjold BW, Altman E, Bundle DR. Sensitive titration microcalorimetric study of the binding of salmonella O-antigenic oligosaccharides by a monoclonal antibody. *Eur J Biochem*. 1991, **197**, 239–246.

Stulík K, Pacáková V, Tichá M. Some potentialities and drawbacks of contemporary size-exclusion chromatography. J Biochem Biophys Methods. 2003, **56**(1-3), 1-13.

Taylor GL. Introduction to phasing. *Acta Crystallogr D Biol Crystallogr*. 2010, **66**(4), 325-338.

Welling GW, Groen G, Slopsema K, Welling-Wester S. Combined size-exclusion and reversed-phase high-performance liquid chromatography of a detergent extract of Sendai virus. *J Chromatogr*. 1985, **326**, 173-178.

Wiseman T, Williston S, Brandts JF, Lin LN. Rapid measurement of binding constants and heats of binding using a new titration calorimeter. *Anal Biochem*. 1989, **179**, 131–137.

Chapter 3

Structural characterisation of HRG

This chapter details the structural investigations into histidine-rich glycoprotein (HRG). As discussed previously, HRG is known to modulate a variety of processes in plasma through its ability to bind to a range of ligands but little is known about how these binding interactions occur and how HRG folds into a 3-dimensional structure (Figure 3.1).

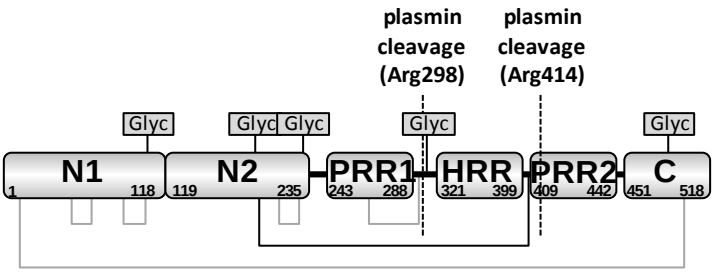

disulfide bonds	predicted glycosylation sites
Cys6 – Cys497	Asn107
Cys60 – Cys71	Asn184
Cys87 – Cys108	Asn232
Cys185 – Cys407	Asn302
Cys199 – Cys222	Asn477
Cys264 – Cys294	

Figure 3.1. Domain structure of rabbit HRG, showing the N1 and N2 domains, the proline-rich regions (PRR1 and PRR2), the histidine-rich region (HRR) and the C-terminal domain (C). The putative glycosylation sites and the cleavage sites for plasmin are also shown. The disulphide bridging arrangement is highlighted by grey lines, with the disulfide bridge between the N2 domain and the HRR/PRR fragment highlighted in bold black (Kassaar *et al*., 2014).

Although the HRG sequence and domains are well conserved across different species, minor variations amongst species exist. Alignment of rabbit HRG with human HRG shows a 64% identity, with 69% similarity (Figure 3.2). The greatest homology occurs at the N-terminal domains, where the respective N2 domains are 68% identical and 93% similar. However, the HRR and PRR regions exhibit a lower degree of homology due to substitution of histidine for proline along the sequence in the rabbit protein. The HRR/PRR region of rabbit HRG is also extended compared to the human protein; human HRG contains 12 tandem repeats of the sequence Gly-His-His-Pro-His, while the rabbit HRG contains 16 repeats (including repeats where a proline substitutes for histidine). The HRR is involved in the binding of metal ions, particularly Zn^{2+}. The binding of Zn^{2+} can modulate the affinity of HRG for its other ligand molecules and thereby regulate the activity of HRG in several processes like coagulation or angiogenesis.

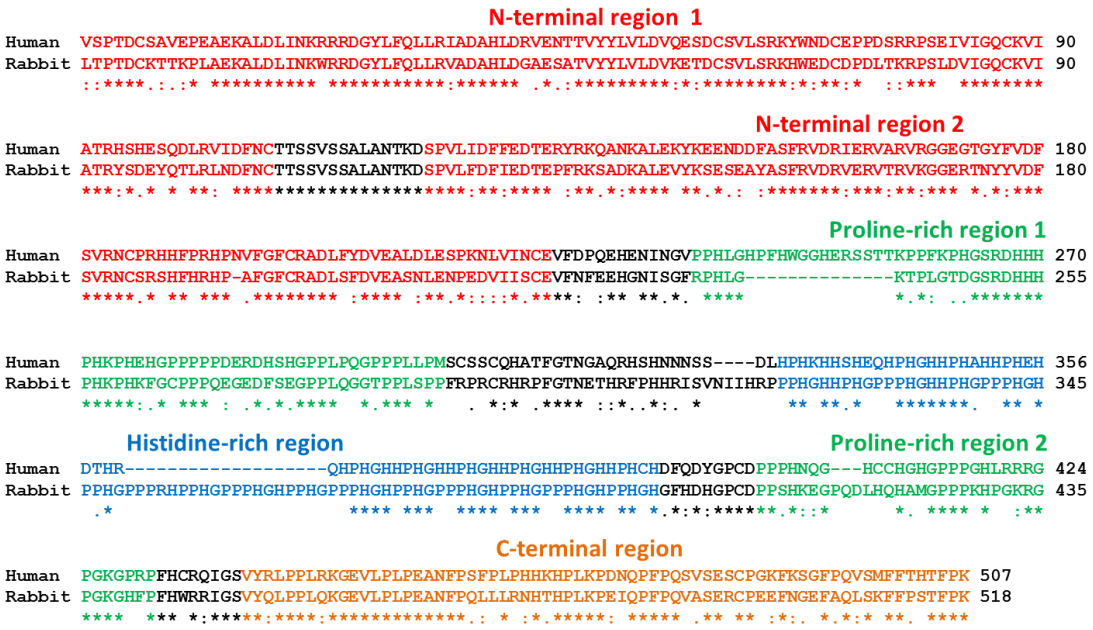

Figure 3.2. Sequence alignment of human HRG (NCBI: P04196) and rabbit HRG (NCBI: Q28640). Domains are labelled and coloured, and the high homology in the N-domains and C-domains can be seen. Rabbit HRG has a longer histidine-rich region.

As described by its etymology, HRG is heavily glycosylated with six putative *N*-linked glycosylation sites. While the histidine- and proline-rich regions are anticipated to be intrinsically disordered due to the peculiar sequence, the remaining N1, N2 and the C-terminal domains are predicted to have ordered structures. In particular, both the N1 and N2 domains are derived from the cystatin superfamily of cysteine protease inhibitors with which they share high sequence homology (Koide and Odani, 1987). Type 1 cystatins (stefins) are characterised by a lack of disulfide bridges, while type 2 cystatins have two conserved disulfide bridges (Barrett *et al*., 1986). These include cystatin B and cystatin C which are suggested to have roles in inhibiting tumour neovascularisation (Chang *et al*., 2009). The homology between the HRG N1 and N2 domain sequences with cystatin proteins has led to the classification of HRG as a type 3 cystatin (in the same class as fetuins and kininogens) (Lee *et al*., 2009). Although HRG has been classified as a cystatin, it does not exhibit cysteine protease inhibitor activity since it is incapable of inhibiting cysteine peptidases of the papain (C1) family (Lee *et al*., 2009).

The N-terminal domains of HRG also share a degree of sequence homology with the N-terminal region of antithrombin. This is understandable when considering that the respective N-terminal domains of both HGR and antithrombin associate with heparin

(Koide *et al*., 1986).This taken together with the fact that both proteins are involved in the regulation of thrombin activity, by competing for heparin with one another (Kluszynski et al., 1997), suggests an evolutionary relationship between the two. The HRG N1 and N2 terminal domains are also involved in interactions with C1q, IgG (Gorgani *et al*., 1997) and FcγRI (Poon *et al*., 2010) to regulate immune function.

HRG controls the formation of blood vessels through both positive and negative mechanisms. The angiogenic activity of HRG is rooted in its high affinity for the angiogenesis inhibitor, thrombospondin, via CLESH motifs within the HRG C-terminal domain (Simantov *et al*., 2001). A similar interaction, but with vasculostatin, is also thought to induce a positive angiogenic mechanism (Klenotic *et al*., 2010). A negative angiogenic effect facilitated by HRG was determined to be due to the HRR in studies using truncated recombinant HRG proteins, peptides based on the HRR and proteolytic fragments (Juarez *et al*., 2002). Inhibition of the proliferation of endothelial cells both *in vitro* and *in vivo* has been observed with HRG after being subjected to partial proteolysis with the plasma protease, plasmin (Juarez *et al*., 2002). This proteolytic regulation by plasmin of HRG is known to be required for some of its physiological functions, where release of a fragment from the intact protein that includes the HRR is necessary. For example, the endotoxin-neutralising and anti-microbial properties of HRG are solely down to the release of the HRR portion and subsequent further degradation (Bosshart and Heinzelmann, 2003; Rydengard *et al*., 2007). Various truncations and fragments of recombinant HRG were examined using fibrosarcoma tumor model mice to investigate the anti-angiogenic properties of HRG (Olsson *et al*., 2004). HRG proteins and fragments containing the HRR reduced vascularisation and tumour growth, while those without the HRR had no effect. This strongly suggests that the histidine rich region is a potent angiogenesis inhibitor. HRGP330 is a 35-amino acid peptide that is based upon a sequence within the HRR and has been described as the minimal sequence with active anti-angiogenic properties *in vitro* and *in vivo* (Dixelius *et al*., 2006; Lee *et al*., 2006). HRGP330 works by disrupting focal adhesion kinase (FAK) and integrin-linked kinase functions, subsequently stopping endothelial cell motility (Bosshart and Heinzelmann, 2003). Taken together, these studies associate HRG in the regulation of angiogenesis through a proteolytically-controlled mechanism which releases the HRR (Borza *et al*., 1996; Poon *et al*., 2009). The precursor to plasmin (plasminogen) is in close association with HRG in circulation, and approximately 50%

of plasminogen is bound to HRG in plasma (Lijnen *et al*., 1980). However due to the presence of a particular conserved disulfide bridge within HRG, proteolysis by plasmin alone is not sufficient to release the HRR. Four intradomain and two interdomain disulfide bridges hold the structure of HRG together. One of the interdomain bonds links the N1 and C-terminal domains, as is observed in the other members of the type 3 cystatin family. Uniquely to HRG, the second interdomain disulphide links the N2 domain to a region in between the HRR and PRR2 domains (Figure 3.1) (Sørensen *et al*., 1993). A peptide corresponding to the HRR/PRR fragment has been identified *in vivo* through mass spectrometric analysis of human tissue samples. However, the mechanism by which the interdomain disulfide is reduced is not understood (Thulin *et al*., 2009).

A key aim here was to structurally characterise HRG using X-ray crystallography, which may help to unravel the binding characteristics of HRG with its binding partners and also provide clues for the *in vivo* functioning of HRG.

Methods

Purification

HRG was purified directly from either rabbit serum (Sigma-Aldrich) or human plasma (TCS Biosciences, Buckingham, UK) using Immobilised Metal Affinity Chromatography (IMAC) by exploiting its intrinsic histidine abundance and subsequent affinity for nickel. Elution was achieved by increasing the imidazole content of the buffer to provide competition for binding sites as imidazole and histidine show structural similarities: both are diazole rings. All purifications were performed using the ÄKTApurifier FPLC system (GE Healthcare, UK).

Serum or plasma was centrifuged (4 000 x g, 30 minutes) and filtered through a 0.45 µm syringe filter (Sartorius, Epsom, UK) to remove any aggregates and large particles. The sample was treated with 5 mM imidazole in keeping with the equilibration buffer (10 mM Tris, 150 mM NaCl, 5 mM imidazole, pH 8). A 5 ml HisTrap nickel column (6% highly cross-linked agarose matrix; GE Healthcare Life Sciences, Little Chalfont, UK) was equilibrated with 5-10 column volumes of the equilibration buffer and sample (50 ml) loaded. The column was washed with equilibration buffer and then with 30% elution buffer (10 mM Tris, 150 mM NaCl, 400 mM imidazole, pH 8). HRG was eluted with a gradient of 60-80% elution buffer. The purified HRG sample was then dialysed to remove any bound metals in a buffer of choice for further experiments, or in 50 mM ammonium carbonate prior to lyophilisation. This protocol was also repeated but using one tablet of SIGMA*FAST*^{TM} (Sigma-Aldrich) protease inhibitor cocktail per 100 ml of serum or plasma.

All protein samples were confirmed to contain no detectable levels of Zn^{2+}, as assessed by the colorimetric Zinc Assay Kit (Sigma-Aldrich).

Protein Concentration Determination

Protein concentration was determined either by direct weighing of samples prior to reconstitution in buffer, or by measuring absorbance at 280 nm. An extinction coefficient of 32150 M^{-1} cm^{-1} was used for rabbit and 26900 M^{-1} cm^{-1} for human HRG.

Sodium dodecyl sulfate-polyacrylamide gel electrophoresis (SDS-PAGE)

Analysis of protein purifications was followed by SDS-PAGE under denatured conditions to determine purities of samples. Samples to be analysed were mixed with NuPAGE LDS Sample Buffer at a typical ratio of 3:1 and loaded onto 4-12% NuPAGE Bis-Tris gels. Electrophoresis was conducted in NuPAGE MES SDS Running Buffer for 45 minutes at 200 V. All electrophoresis materials were supplied from Invitrogen. After the desired separation had been achieved, the gels were either stained with Coomassie Blue. Gels were visualised by staining with Coomassie stain (0.025% Coomassie Brilliant Blue R250, 40% methanol, 10% acetic acid) for 10 minutes, followed by destaining in boiling water. If greater sensitivity was desired, the staining incubation time was increased.

To determine the redox condition of plasma HRG and the effect of the protease action of plasmin, SDS-PAGE analysis followed by Coomassie staining was used to monitor the domain structure of HRG after being subjected to a range of conditions: native non-reduced HRG, native reduced HRG and plasmin-treated reduced HRG. Reduction was achieved with 2.5 mM dithiothreitol (DTT). To further analyse HRR/PRR and achieve sequence information, a band of approximately 25 kDa, putatively thought to correspond to this fragment, was cut and submitted for MS/MS analysis.

Crystallography

Data collection, structure solution and refinement were performed by Dr. Stephen McMahon and Prof. Jim Naismith.

Rabbit HRG was used for crystallisation trials since it is ten times more abundant compared to human HRG. Prior to setting up crystallisation trials, the HRG sample was furthered purified by size exclusion chromatography using an S-200 column (GE Healthcare, Life Sciences) in 10 mM Tris, 150 mM NaCl, pH 8. HRG eluted as a single peak at a molecular weight of ~140 kDa. The sample was subjected to a Pre-Crystallisation Test (Hampton) to determine a suitable concentration for crystallisation screens. HRG was screened for crystallization using two commercial screens, JCSG+

and PACT (Qiagen, Manchester, UK), at a concentration of 16 mg/ml, alongside in-house stochastically designed screens, on an Art Robbins Gryphon crystallization robot by sitting-drop vapor diffusion. Crystals appeared after 4 weeks at room temperature as two visibly distinct crystal morphologies: cubic and rod-shaped. Crystals were grown from 22.5% PEG MME 5000, 100 mM MES and 73 mM potassium sodium tartrate at pH 6.5. The rod-shaped crystals diffracted best and subsequently both native and heavy atom soaked data sets were collected with this morphology of crystal. For phasing, a rod shaped crystal was harvested and soaked for 5 minutes in mother liquor supplemented with 50 mM K_2PtCl_4 before being back-soaked in cryoprotectant (mother liquor with 25% glycerol) and then immediately frozen in liquid nitrogen. Data were collected on Diamond beamline I02 as 1,000 non-overlapping images using a Pilatus 6M detector. Later, a high-resolution native data set was collected on Diamond beamline I04-1 from a different crystal. All data were processed with xia2 (Winter *et al*., 2013). The data obtained from these crystals were analysed using PHENIX. Using both anomalous and isomorphous difference, Autosol identified two Pt sites in spacegroup $P3_121$ with a figure of merit of 0.18 at 3.1 Å. Density modification and extension to 2.9 Å using Autobuild gave a preliminary model of 107 residues and an R-factor of 30%. This model was rebuilt using COOT by manual inspection and with new data extended to 1.93 Å. The final structure was deposited in the RCSB Protein Databank (PDB code: 4CCV).

Protein Deglycosylation

It was anticipated that the extent of glycosylation on HRG would seriously hinder and even preclude the formation of crystals. For this reason, an endeavour to establish a viable protocol for deglycosylation was investigated. Sugar chains of the heavily glycosylated HRG were removed using a Protein Deglycosylation Mix (NEB). The mixture contained PNGase F (500 units/µl), *O*-glycosidase (40,000 units/µl), neuraminidase (50 units/µl), β1-4 galactosidase (8 units/µl) and β-*N*-acetylglucosaminidase (4 units/µl). A range of conditions were attempted in order to optimise the deglycosylation, the extent of which was analysed using mass spectrometry. Essentially, the protein sample was incubated with the Deglycosylation Enzyme Mix at 37 °C. Various concentrations of sample and enzymes, for a range of incubation times and in a native or denatured state were tested. Samples were denatured

by boiling for 10 minutes in the presence of SDS.

Mass spectrometry (MS)

Mass spectrometry was performed by Dr Catherine Botting.

To determine the intact mass of plasma/serum purified HRG, protein samples (20 µL, 1 mg/mL) were desalted on-line through a MassPrep On-Line Desalting Cartridge 2.1 x 10 mm (eluting at 50 µL/min) with an increasing acetonitrile concentration (98 % H_2O, 2 % acetonitrile, 1 % formic acid to 98 % acetonitrile, 2 % H_2O, 1 % formic acid) and delivered to a Waters LCT electrospray ionisation mass spectrometer. The molecular mass of the protein was obtained from an envelope of multiply charged signals which were deconvoluted using MaxEnt1 software. The mass spectrometer had previously been calibrated using myoglobin.

For sequence analysis, the protein sample was analysed by SDS-PAGE as described above and the gel band was excised and cut into 1 mm^3 cubes. These were subjected to a ProGest Investigator in-gel digestion robot (Genomic Solutions, Ann Arbor, MI). The gel cubes were digested with trypsin at 37 °C or thermolysin at 55 °C after being destained by washing with acetonitrile and subjected to reduction and alkylation. The peptides were extracted with 10% formic acid and the solution (0.5 µl) applied to the Matrix-assisted laser desorption/ionisation (MALDI) target along with alpha-cyano-4-hydroxycinnamic acid matrix (10 mg/ml in 50:50 0.1% TFA:acetonitrile, 0.5 µl) and allowed to dry.

Trypsin was used as is standard in this type of peptide identification. However, since trypsin cleaves after arginine or lysine residues, thermolysin was used in instances where the identification of the HRR was required (because of the lack of arginine and lysine residues in the HRR domain).

MALDI MS was acquired using a 4800 MALDI TOF/TOF Analyzer (AB Sciex, Foster City, CA) equipped with a 355 nm Nd:YAG laser and calibrated using a peptide mixture. In positive MS mode, the spot was initially analysed between 800 and 4000 m/z, by averaging 1000 laser spots. Up to 15 of the most intense peptides were selected

for MS/MS analysis and acquired to a maximum of 3000 laser shots or until the accumulated spectrum reached a S/N ratio of 35. All MS/MS data were acquired using a collision energy of 1 keV. ProteinPilot 4.1 Paragon algorithm (AB Sciex) was used to analyse the MS/MS data, searching against an internal database to which the HRG sequence had been added, with no enzyme digestion parameters selected and modification of cysteines by carbamidomethyl selected.

Free thiol concentration determination using Ellman's reagent

The rabbit plasma or serum samples were diluted 1:50, while the HRG from plasma or serum was reconstituted in PBS to 1 mg/ml, pH 7.2, and thiol determination was carried out using 5,5'-dithiobis(2-nitrobenzoic acid) (DTNB). 5 µl of a 20 mM DTNB solution was added to 100 µl of sample. Absorbance was recorded at 405 nm and a thiol concentration calculated using a coefficient of 17 780 M^{-1} cm^{-1} (Ellman, 1958).

Plasmin Digest

Digests of 1 mg/ml samples of HRG with 1 unit of plasmin were performed for 30 minutes at 37 °C in 20 mM potassium phosphate, 150 mM sodium chloride at pH 7.5. Samples were reduced with the addition of 2 mM dithiothreitol (DTT).

Results and Discussion

Characterisation of HRG

HRG was purified directly from serum or plasma with a simple one-step protocol, taking advantage of its natural abundance of histidine by using a nickel column This resulted in high yields (> 80%) and high purity of protein (> 95%) as assessed by SDS-PAGE. Figure 3.3 shows an SDS-PAGE gel following purification of HRG. As judged by comparison with the molecular weight markers (Bioline) the mass of rabbit HRG is approximately 75 kDa. The band lanes 1 and 2 at approximately 140 kDa and is a HRG dimer.

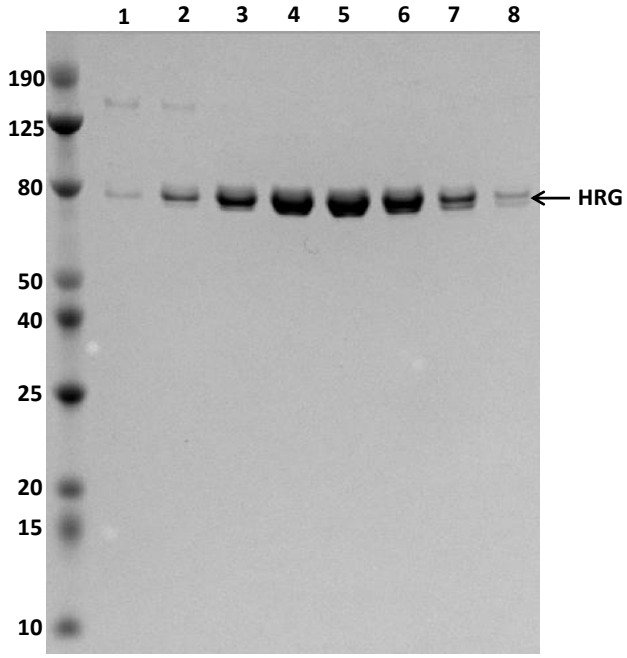

Figure 3.3. SDS-PAGE analysis (following Coomassie stain) of rabbit HRG following nickel affinity and gel filtration purification steps. HRG can be seen in lanes 1 to 8. The sample pooled from lanes 3-7 was used for crystallisation trials.

The relative purity of the sample preparations was assessed using the gel imaging software (ImageLab) by comparing the relative intensities of visible bands. Typical working samples were > 95% HRG. To confirm the protein identity, gel bands were

excised and submitted for sequence analysis. The mass spectrometry results for sequence analysis are shown in Figure 3.4. The rabbit HRG sample achieved coverage of 41.2% with 45 significant peptides while the human HRG was covered to 25.5% with 12 significant peptides.

a

LTPTDCKTTKPLAEKALDLINKWR**RDGYLFQLLRVADAHLDGAESATVYYLVLD**
VKETDCSVLSRKHWEDCDPDLTKRPSLDVIGQCKVIATR**YSDEYQTLR**LNDFN**C**
TTSSVSSALANTKDSPVLFDFIEDTEPFRKSADKALEVYK**SESEAYASFR**VDRV
ERVTRVKGGER**TNYYVDFSVR**NCSRSHFHRHPNAFGFCRADLSFDVEASNLENP
EDVIISCEVFNFEEHGNISGFRPH**LGKTPLGTDGSR**DHHHPHKPHKFGCPPPQE
GEDFSEGPPSQGGTPPLSPPSGPRCRHRPFGTNETHRFPHHRNFSEHHPHGPPP
HGHHPHGPPPHGHHPHGPPPHGHPPHGPPPHGHPPHGPPPHGHPPHGPPPHGHP
PHGPPPHGHPPHGPPPHGHPPHGPPPHGHPPHGHGFHDHGPCDPPSHK**EGPQDL**
HQHGHGPPPKHPGKRGPGK**GHFPFHWRRIGSVYQLPPLQKGEVLPLPEANFPSF**
SLRNHTHPLKPEIQPFPQVASERCPEEFNGEFAQLSKFFPSTFPK

b

VSPTDCSAVEPEAEKALDLINKRRR**DGYLFQLLR**IADAHLDRVENTTVYYLVLD
VQESDCSVLSR**KYWNDCEPPDSR**RPSEIVIGQCKVIATRHSHESQDLRVIDFNC
TTSSVSSALANTK**DSPVLIDFFEDTER**YRKQANKALEK**YKEENDDFASFR**VDRI
ERVAR**VRGGEGTGYFVDFSVR**NCPRHHFPR**HPNVFGFCRADLFYDVEALDLESP**
KNLVINCEVFDPQEHENINGVPPHLGHPFHWGGHERSSTTKPPFKPHGSRDHHH
PHKPHEHGPPPPPDERDHSHGPPLPQGPPPLLPMSCSSCQHATFGTNGAQRHSH
NNNSSDLHPHKHHSHEQHPHGHHPHAHHPHEHDTHRQHPHGHHPHGHHPHGHHP
HGHHPHGHHPHCHDFQDYGPCDPPPHNQGHCCHGHGPPPGHLRRRGPGK**GPRPF**
HCRQIGSVYRLPPLRKGEVLPLPEANFPSFPLPHHK**HPLKPDNQPFPQSVSESC**
PGKFK**SGFPQVSMFFTHTFPK**

Figure 3.4. Sequence analysis for identification of (a) rabbit HRG and (b) human HRG. Significant peptide fragments are highlighted in green.

To show that there is no difference in HRG purified from serum or plasma and to determine whether the process of plasma developing to serum may have redox influences on activity at Cys185, free thiol concentrations were measured to represent the redox state in plasma and serum from rabbits. The free thiol concentration of plasma was determined to be 250 µM, significantly greater than that of serum, 208 µM (Figure 3.5A). Additionally, HRG samples prepared from either serum or plasma were characterised and compared. Both preparations, serum and plasma HRG, had the same free thiol content (0.7 mol thiol/mol HRG; Figure 3.5B). The samples were also subjected to analysis by mass spectrometry and showed the same molecular mass profile (Figure 3.5C) and thus molecular composition. This provides definitive proof that preparing HRG from serum did not affect the redox state of the protein and the

glutathione related conclusions that can be drawn from structural data are also applicable to plasma HRG. The predicted mass of rabbit HRG based on sequence is 58 015.9 kDa, which is significantly lower than the mass of 72 179.9 kDa observed in ESI-mass spectrometry. This discrepancy is explained by the heavy glycosyation of the HRG molecule, account for the 14 kDa difference in mass.

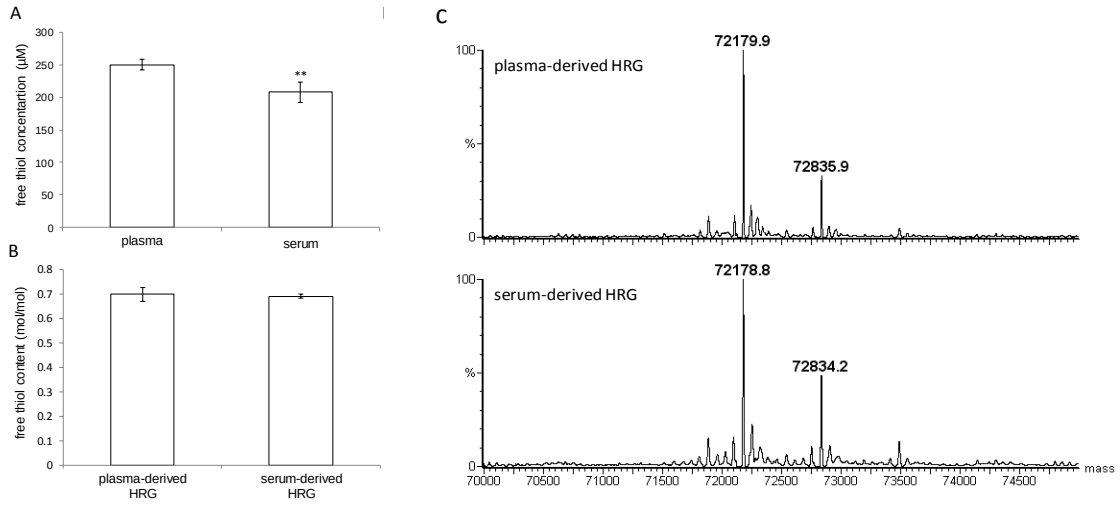

Figure 3.5. Free thiol measurements of rabbit plasma, serum and HRG samples and mass spectrometric analysis of HRG purified from either rabbit serum or plasma. (A) The free thiol concentrations in rabbit plasma and serum were found to be different and were calculated to be 250 µM and 208 µM, respectively. (B) The free thiol contents of HRG preparations from both rabbit plasma and serum were very similar at ~0.7 mol/mol, with this likely to correspond to the reduced form of Cys407. Error bars indicate standard deviation. Statistical analyses were performed using a T-test (** indicates $p<0.01$; n=3). (C) ESI mass spectra of rabbit HRG purified from plasma and serum showing the samples to be almost identical in composition. One major form of HRG can be observed, which in each sample has essentially the same molecular mass (72 179 Da). A minor form can also be observed (72 835 Da), which likely corresponds to alternative glycosylation of the protein.

Crystallography and Structure of HRG

Prior to setting up crystallisation trials, the HRG sample was subjected to further purification by gel filtration to ensure maximum sample homogeneity. HRG eluted from the gel filtration column in line with a 140 kDa standard, which would suggest that it exists as a dimer, at least in the buffer solution. The precipitation rate of the pre-crystallisation tests indicated a HRG concentration of 16 mg/ml as a starting point. Crystallisation screens set up at room temperature showed several incidents of salt precipitation and a few of protein precipitation, indicating promising conditions. After 4 weeks, rod-shaped crystals appeared and later cubic crystals formed independently in

22.5% PEG MME 5000, 100 mM MES and 73 mM potassium sodium tartrate at pH 6.5.

The rod-shaped crystals diffracted best and were prioritised. The rod-shaped crystals grew from 21.3% PEG MME 5000, 30 mM potassium sodium tartrate, 100 mM MES at pH 6.5, which is from a stochastically designed in house crystal screen. Reproducible highly diffracting rod-shaped crystals were yielded from expanded trials of this condition after four weeks. Crystals with a cubic morphology were also identified (Appendix A1.5-A1.8), but only diffracted to 5.2 Å with an average unit cell (a,b,c) of 87.8, 87.8 and 87.8 Å with angles (α, β, γ) of 90, 90 and 90° (space group: F23). The rod-shaped crystals diffracted to 1.93 Å with an average unit cell (a,b,c) of 77.1, 77.1 and 69.2 Å with angles (α, β, γ) of 90, 90 and 120° (space group: P 3_1 2 1).

The heavy glycosylation and intrinsic disorder of HRG have limited structural studies to date. The first step towards 3D characterisation of HRG at the molecular level is given here. In this study, crystallisation was attempted using purified intact HRG, producing crystals of the N2 domain which required 4 weeks to appear. This suggests that the relatively long crystallisation period may be due to the slow degradation process of whole HRG to release the N2 domain over this period of time and to allow the domain to arrange into a crystal. Flexible linker regions between the distinct domains of HRG would be very susceptible to cleavage either *in vivo* before purification, or even by co-purified contaminating proteases from serum. Further evidence for a co-purified protease causing the cleavage of the HRG molecules was observed during crystallisation protocols which included protease inhibitors. These experiments failed to yield crystals, despite all other conditions remaining the same.

It was revealed that these crystals were formed by the HRG N2 domain and thus the structure of the N2 domain of rabbit HRG was solved to a resolution of 1.93 Å (Kassaar *et al*., 2014). One complete N2 domain was contained in the structure of 115 amino acids from Ser123 to Arg237. Although the asymmetric unit contains a single due to the symmetry of the crystal, a dimeric arrangement of the domain exists within the unit cell (Figure 3.6).

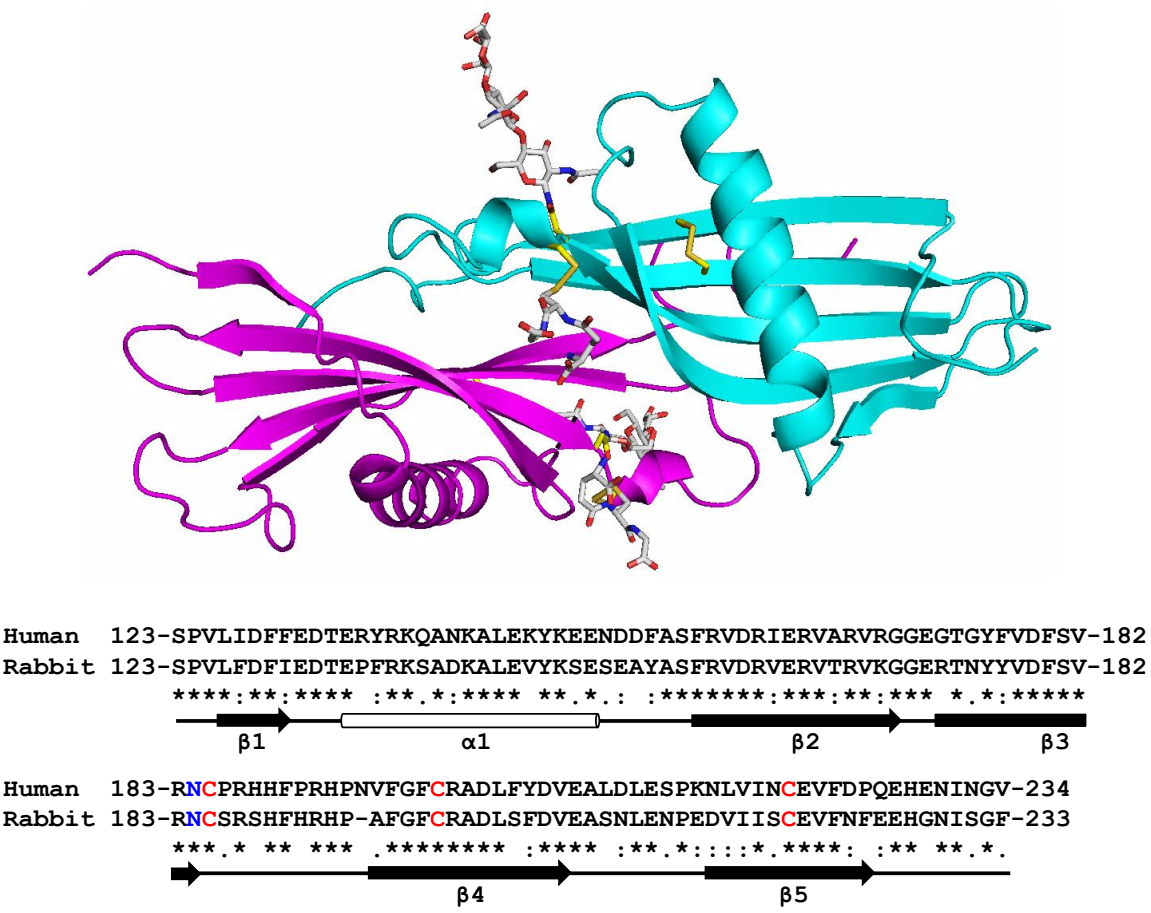

Figure 3.6. Crystal structure of the HRG N2 domain. The structure obtained was in a dimeric arrangement of the N2 domain composed of 2 identical chains, A (cyan) and B (magenta). The sequence alignment of human and rabbit N2 domains is shown with secondary structure elements emphasised as follows: α-helix (cylinder) and the β-sheets (arrows). The N-glycosylated Asn184 residue is shown in blue and the conserved cysteine residues within the N2 domain are shown in red (Kassaar *et al*., 2014). Figure was drawn using PyMol by Prof. Jim Naismith.

Since the rabbit and human HRG proteins share 64% sequence identity and 69% sequence similarity and the respective domain sequences of human and rabbit HRG N2 are highly homologous (68% identity, 93% similarity), it can therefore be stated with confidence that these share the same folding pattern. The N2 domain sequence is also homologous with the cystatin family and HRG itself is classified as a type 3 cystatin. Conformation of this is provided by the structure showing the N2 domain possessing a cystatin-like fold consisting of a five-turn α-helix (Figure 3.7A) with a five-stranded anti-parallel β-sheet wrapped around it. The fold starts from a short β1 (Leu126 – Phe129) and follows through to an α-helix (Glu134 – Glu150) of five-turns with β2 (Phe157 – Lys169), β3 (Thr174 – Asn184), β4 (Ala195 – Phe205) and β5 (Glu216 – Asn226) wrapping and twisting around the central α-helix. Interestingly, the electron

density maps show the surprising presence of an S-glutathionyl adduct at Cys185 and also one site of glycosylation on the heavily glycosylated HRG at the conserved Asn184 residue. Two N-acetyl glucosamine molecules (NAG1 and NAG2) and one α-D-mannose molecule (MAN3) can be modelled at each N-linked glycan chain.

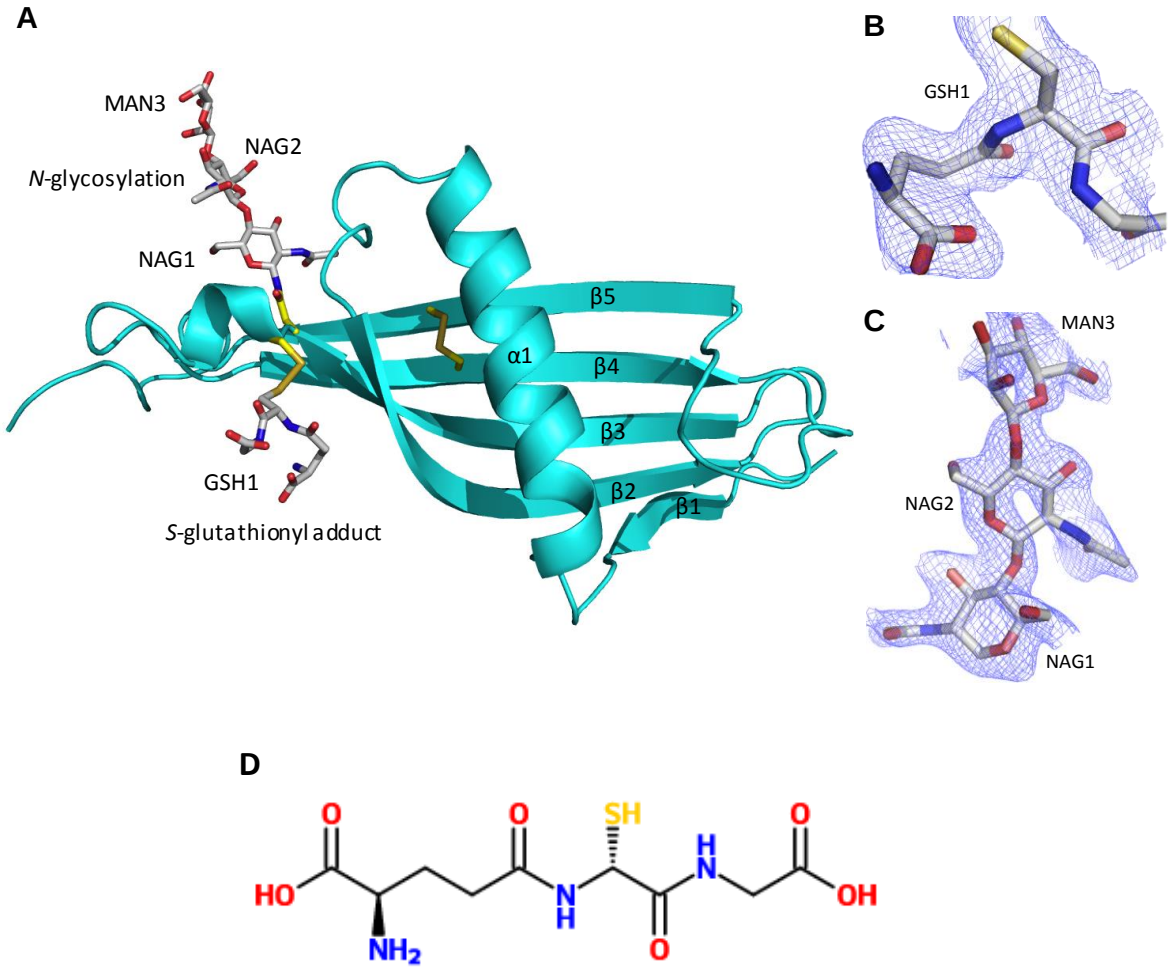

Figure 3.7. The HRG N2 domain shown in closer detail, emphasising its cystatin-like fold. (A) Chain A (from Figure 2.5) is shown illustrating the 5 β-strands (β1- β5) twisting around the α-helix (α1). The internal disulfide bridge can be observed connecting β4 and β5 (yellow cylinders). The glycosylation at Asn184 and the *S*-glutathionyl adduct at Cys185 are also shown as labelled. (B) F_o-F_c electron density map showing the *S*-glutathionyl adduct (GSH1) bound to Cys185 as a mixed disulfide. (C) F_o-F_c electron density map for the first 3 sugars, NAG1, NAG2, and MAN3, of the carbohydrate chain linked to Asn184. The F_o-F_c maps (blue chicken wire contoured at 1s, carve radius 1.6 Å) were calculated from a model which has never contained NAG, MAN, or glutathione (GSH) (Kassaar *et al.*, 2014). Figure was drawn using PyMol by Prof. Jim Naismith. (D) Chemical structure of glutathione.

Both N1 and N2, the N-domains of HRG, based on their sequence homology to cystatin proteins are predicted to possess a cystatin-like fold (Lee *et al.*, 2009). The N2 domain

crystal structure confirms that the N2 domain of rabbit HRG does indeed have a fold composed of an anti-parallel five-stranded β-sheet twisting around a five-turn α-helix that is characteristic of cystatin-like structures. Although the structure obtained here was that derived from rabbit HRG, the findings are also valid to the human protein due to the high degree of homology between human and rabbit HRG sequences (Figure 3.2). In addition to this structure being the first of HRG, it is also the first of a type 3 cystatin protein, even though several structures of other cystatin proteins have been solved. As mentioned previously, despite being part of the cystatin family, HRG does not exhibit any protease inhibitory activity (Lee *et al*., 2009). The crystal structures of pig cystatin A (Jenko *et al*., 2003), chicken egg white cystatin (Bode *et al*., 1988) and human cystatin B complexed with the protease papain (Stubbs *et al*., 1990) reveal the cystatin N-terminus and two loops called L1 (between β2 and β3) and L2 (between β3 and β4) to be important for their protease inhibitory activity. This wedge shaped segment docks into the active site opening of cysteine proteases. By looking at the structure of HRG, in the N2 domain the corresponding L2 loop is extended by six amino acids, which would preclude binding to papain-like proteases. This would provide an explanation for the lack of inhibitory activity of HRG.

The two N-terminal domains of HRG also share sequence homology with the antithrombin III heparin binding region (Jones *et al*., 2004; Koide *et al*., 1986). The α-helix of the cystatin-like fold in the HRG N2 domain could mimic the antithrombin heparin binding site which is composed of positively charged helical regions. A heparin molecule has been observed binding by hydrogen bonds using its carboxylates and sulfates to the D-helix (residues Arg129 and Lys125), to the A-helix (residues Arg46 and Arg47), to the P-helix (residues Lys114 and Glu113) and to Lys11 and Arg13 at the antithrombin III N-terminal (Jin *et al*., 1997). Helical regions are also found in other proteins that bind to heparin, for example the protease nexin-1. The structure of nexin-1 shows two monomers that bind heparin in between two helical segments with each monomer providing one helix (corresponding to helix D in each), and binding to heparin through lysine residues (Li and Huntington, 2012). HRG could potentially reflect this binding mechanism, where a heparin-binding site could form between the helix of the two cystatin-like domains, N1 and N2, which also contain lysine residues.

The HRG N2 structure provides evidence that the N2 domains of HRG are likely to contribute to the formation of HRG dimers *in vivo*. Although it must be acknowledged

that the protein concentration necessary for crystallisation was much greater than plasma levels. This could force domains to crystallise in unnatural conformations. It is also possible that other domains in solution could disturb the arrangement of the N2 domains observed in the crystal. However, if the N2 domain does in fact contribute to HRG dimerization, it would be a significant advance in our understanding of the protein molecule. The PISA server (www.ebi.ac.uk) was used to assess the biological relevance of the dimer arrangement which predicts, by analysing the inter-chain interactions, if these are likely to be stable in solution. The arrangement was identified as stable by the analysis (maximum probability, significance = 1) and this arrangement buries 1,659 $Å^2$. This suggests that the observed relative conformation of the N2 domains in the crystal structure is highly likely to be representative of their structure in the solution phase. Additionally, the purification protocol provided evidence for HRG existing as a dimer in solution since it eluted at 140 kDa from the gel filtration column. This dimerisation of HRG might be a necessary requirement for the protein to form binding sites for some of its ligands. In this arrangement the cysteine-glutathionyl adducts are on the same face of the dimer which could allow interdomain disulfides to cross over between molecules.

However, other domain combinations forming a heparin site (or sites) are possible, especially as the protein exists as a dimer under native conditions.

Glycosylation of HRG

HRG is heavily glycosylated with around 13 kDa of its monomeric 72 kDa total mass corresponding to glycan chains and the structure given here confirms Asn184 as one of the *N*-linked glycosylation sites (Figure 3.7A and C). Although the structure only shows the beginning of the chain with three sugars, crystals subjected to deglycosylation with a mixture of deglycosylation enzymes (PNGase F, *O*-glycosidase, neuraminidase, β1-4 galactosidase and β-*N*-acetylglucosaminidase) were analysed by SDS-PAGE, confirming that the electron density maps only show a small extent of the complete glycosylation state of the N2 (Figure 3.8A). Asn232 is annotated in the UniProt database (UniProt code: Q28640) as another potential glycosylation within this domain. However, there was no detectable glycosylation observed at this site in the structure.

In anticipation of difficulty with crystallography due to the inherent characteristics of HRG, prior to obtaining HRG crystals, experiments to investigate deglycosylation of the protein were conducted using a mix of *N*- and *O*-glycosidases. Heavily glycosylated

proteins are notoriously difficult to crystallise due to the heterogeneity and flexibility of the glycan chains. The deglycosylation of rabbit HRG with the enzyme mix over four hours is shown in Figure 3.8B.

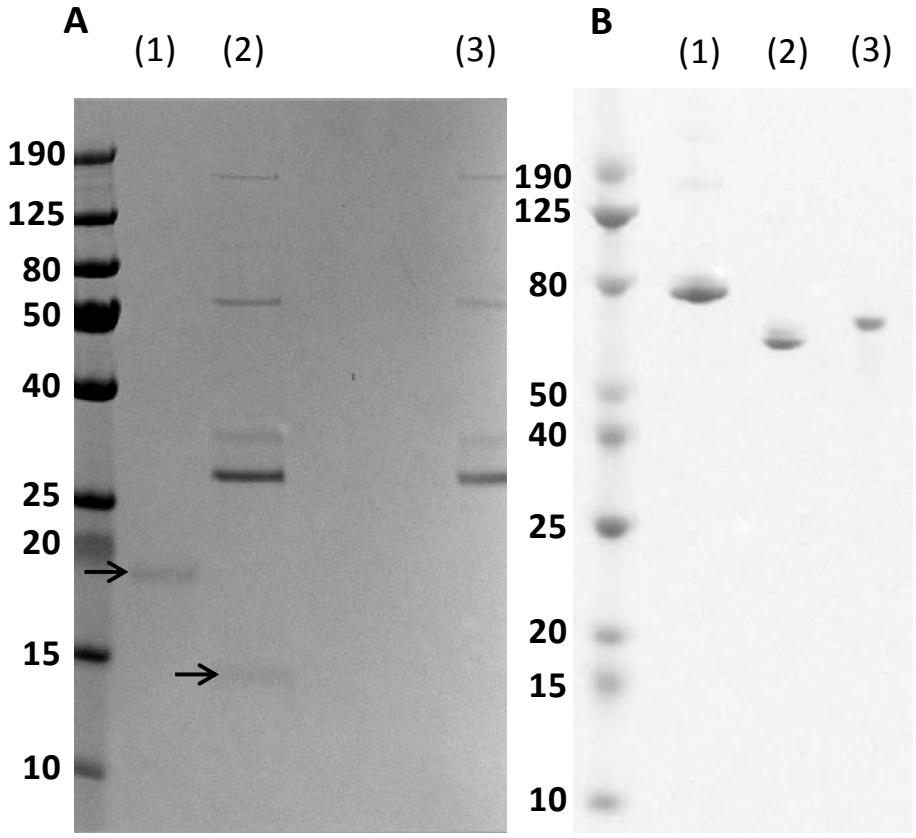

Figure 3.8. SDS-PAGE analysis of (A) N2 domain crystals and (B) HRG having undergone deglycosylation. (A1) N2 domain crystals without deglycosylation, highlighted with an arrow. (A2) N2 domain crystals after deglycosylation, highlighted with an arrow. (A3) The enzyme mix used to achieve deglycosylation. (B1) The untreated control HRG sample. (B2) Deglycosylation of HRG under native conditions. (B3) Deglycosylation of HRG under denatured conditions. Molecular weight markers are given in kDa.

The deglycosylation was conducted under native and denatured conditions. In theory, by denaturing the protein, the enzymes would have full access to the glycosylation sites thereby removing the full quotient of carbohydrate. This would cause degradation of the protein and loss of structure and function for subsequent experiments. Native conditions are gentler to the protein but could obstruct access to glycosylation sites. To determine a more accurate mass, samples were submitted for mass spectrometry analysis (Figure 3.9).

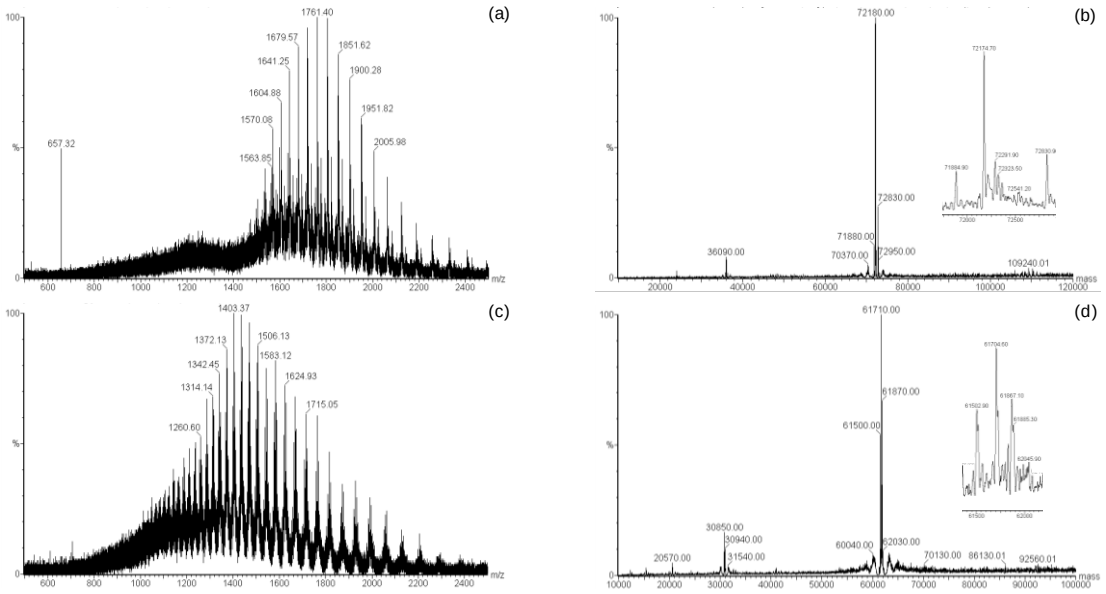

Figure 3.9. ESI mass spectrum of (a) native, untreated rabbit HRG with (b) its calculated mass and (c) deglycosylated rabbit HRG with (d) its calculated mass. Insets show data processed to 0.1 Da for the main peaks. This was a reaction of 1 mg of HRG with 2 µl of enzyme mix for 4 hours.

Comparison of the native HRG mass spectrum with the deglycosylated HRG mass spectrum (Figure 3.9 a and c) reveals that the native HRG protein had a lower charge state distribution. The deglycosylated sample was protonated to a greater extent. This could potentially be explained by the presence of the carbohydrate chains in the glycosylated sample providing a structural barrier towards protonation. It could also be due to their influence on the conformation of HRG. It would be interesting to compare the structural dynamics of native and deglycosylated HRG to investigate whether the carbohydrate chains are able to induce allosteric modulation of the tertiary structure of the protein. The calculated mass of native rabbit HRG (Figure 3.9b) was 72.18 kDa which compares with the observed mass on SDS-PAGE (ca. 75 kDa). The deglycosylated mass was 61.71 kDa, meaning that 10.47 kDa worth of carbohydrate had been removed. The peptide sequence mass of rabbit HRG is 58.5 kDa which means that 3.21 kDa of carbohydrate remained attached. It also appears that the deglycosylation process infracts the homogeneity of the native sample. Figure 3.9b shows one clear central peak of a tentative purity of 70-80%, and also shows two smaller peaks which might be due to different glycosylation states of the native protein. The deglycosylated sample (Figure 3.9d) shows a distinct decrease in homogeneity, most likely indicative of varying extents of deglycosylation. The nature of mass spectrometry does not lend

itself to quantitative analysis, but a comparison of peak intensity can allow for a relative estimation to be made.

Attempts were made to completely deglycosylate rabbit HRG, 100 µg of HRG was incubated with 5 µl of the enzyme mix at 37 °C for 14 hours. Figure 3.10 shows the mass spectra for this reaction.

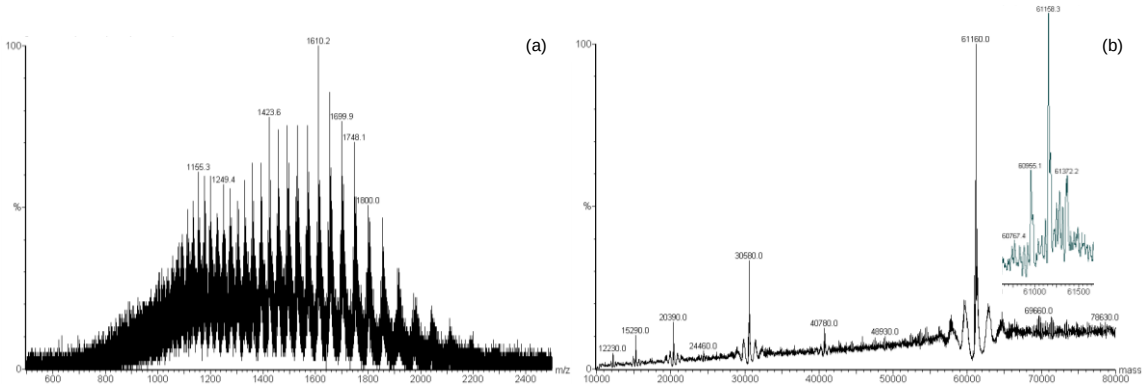

Figure 3.10. ESI mass spectrum of (a) deglycosylated rabbit HRG and (b) its calculated mass. The inset shows data processed to 0.1 Da for the main peaks. This was a reaction of 100 µg of HRG with 5 µl of enzyme mix for 14 hours.

By using less HRG and a higher enzyme concentration, a more optimal deglycosylation procedure was achieved and resulted in a mass of 61.16 kDa. As before, three discrete peaks were observed centred on a mass that was 550 Da less than the previous experiment. The homogeneity of this deglycosylation was slightly greater relative to the previous experiment, but the considerable increase in ratio of enzymes to HRG did not yield a parallel increase in the extent of deglycosylation. These experiments showed that, although complete deglycosylation of HRG is not possible using these simple procedures, a substantial portion of the glycan chains can be removed by the deglycosylation enzymes and provides an important future avenue to explore for the possible crystallization and structure resolution of full-length HRG. Table 3.1 summarises the mass spectrometry data.

Table 3.1. Summary of mass spectrometry, comparing the predicted mass of rHRG with native and deglycosylated rHRG samples.

Sample	Predicted HRG	Native HRG	Deglycosylated HRG
Mass (kDa)	58 015.9	72 180.0	61 710.0 - 61 160.0

S-glutathionyl adduct at Cys185 of HRG

Significantly at Cys185, a *S*-glutathionyl adduct is observed, providing direct *in vivo* evidence of a redox-regulated mechanism for the release of the anti-angiogenic HRR/PRR region (Figure 3.7B). This suggests that the Cys185-Cys407 disulfide bridge is reduced by glutathione (GSH) in plasma at its Cys185 end leading to the mixed disulfide observed. This reaction would free the HRR domain from the N2 domain, which are otherwise connected by the conserved cysteine residues which form the interdomain disulfide bridge.

In an effort to identify the HRR/PRR fragment, purified rabbit HRG was left untreated, reduced with DTT or reduced and exposed to the enzyme plasmin. The samples were then assessed by SDS-PAGE (Figure 3.11A). The resulting pattern on the gel shows interesting features when comparing the appearance of the protein across the range of experimental conditions. The native protein appears essentially as a single band under non-reducing conditions, as would be expected from a sample not exposed to exogenous plasmin. Although a fraction of the protein is subject to cleavage by plasmin in circulation, the disulfide bridges hold the protein together (particularly the Cys185-Cys407 bond). When the HRG sample is reduced by DTT, the bulk of the protein sample appears unchanged, but a band of ~25 kDa can be seen to be released. To identify this band, it was excised from the gel, and reduced, alkylated and digested with thermolysin. The digested peptides were analysed by MALDI MS and MS/MS (Figure 3.11B). Peptide fragments were identified, confirming the identity of the band as the HRR/PRR fragment. A peptide containing Cys407 was amongst the identified fragments. Cys407 forms a disulfide bridge with Cys185 in the N2 domain of the non-reduced protein. The HRR/PRR release following treatment of purified HRG with DTT can be explained by *in vivo* plasmin activity occurring prior to purification. When HRG was treated with both plasmin and reducing agent, the protein was cleaved into several constituent parts as indicated by the band pattern on the gel, which included an intense band corresponding to the HRR/PRR fragment.

GSH is known to be implicated in angiogenesis through post-translational modification of proteins. For example, tyrosine phosphatase provides a negative regulation of angiogenesis upon its *S*-glutathionylation via inhibition of vascular endothelial growth factor (VEGF)-regulated focal adhesion kinase activation (Abdelsaid and El-Remessy,

2012). GSH is involved in regulating the induction of hypoxia inducible factor 1 (HIF-1), which controls the expression of angiogenic genes, including VEGF (Forsythe *et al.*, 1996). In squamous cell carcinoma cells, GSH has been found to reduce HIF-1 binding and HIF-1-dependent promoter activity in a dose-dependent manner. Also, it has been shown that by quenching reactive oxygen species, GSH can prohibit ischemia-induced lung angiogenesis (Tajima *et al.*, 2009).

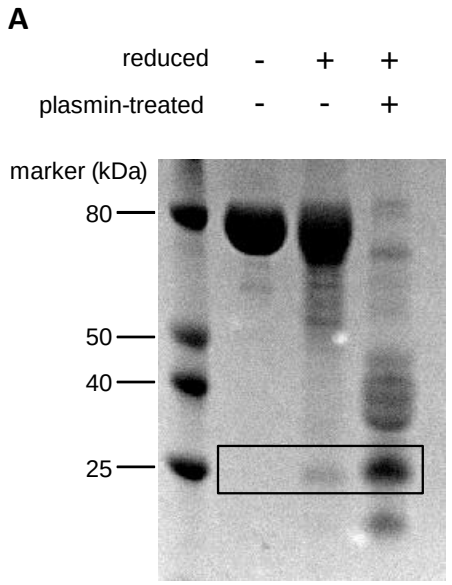

Figure 3.11. HRR/PRR fragment release in rabbit HRG. (A) SDS-PAGE investigation of rabbit HRG under conditions with or without plasmin and the reducing agent dithiothreitol, as assigned by positive and negative symbols. The box highlights the HRR/PRR band and is only observed under reducing conditions. (B) MS/MS analysis of the excised HRR/PRR gel band. Peptide sequences giving a confidence of 99% are in red, and those with a 74% confidence in italics. NCBI accession number:XP_002716393 (Kassaar *et al.*, 2014).

For the GSH-mediated activation of HRG to affect angiogenesis by releasing the anti-angiogenic HRR/PRR fragment, plasmin facilitated cleavage of the HRG backbone is also required. The fact that appropriate quantities of GSH reduced HRG were present in the protein sample to allow N2 domain crystals to form, may suggest that reduction occurs first and not proteolysis, however this offers not an absolute answer but only a clue. Further evidence that a fraction of the protein is first cleaved by plasmin in plasma was the detection of the HRR/PRR fragment in HRG samples in the presence of a reducing agent during SDS-PAGE analysis (i.e. the HRG had already been subjected to plasmin proteolysis *in vivo*, but required the reduction of the Cys185-Cys409 bond to accomplish the release of the HRR/PRR; Figure 3.12). Addition of plasmin to the

sample increased the quantity of the HRR/PRR fragment by further degrading the protein.

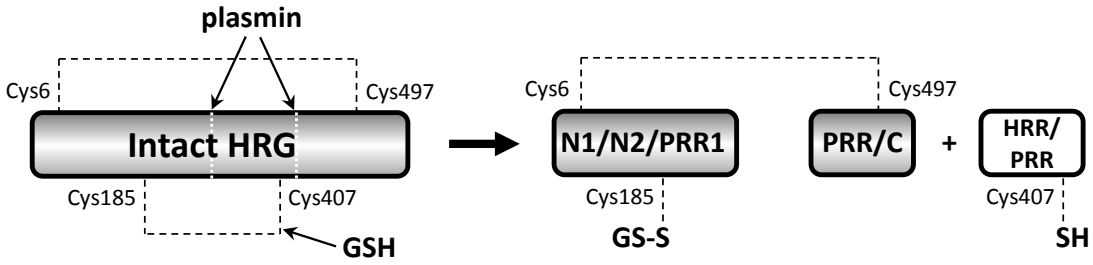

Figure 3.12. Schematic diagram representing the mechanism of release of the HRR/PRR fragment following both plasmin cleavage and reduction of the Cys185-Cys407 bond of HRG by GSH. The second interdomain disulfide bond between Cys6-Cys497 stays intact, holding the remainder of the protein together (Kassaar *et al*., 2014).

HRG shares a close relationship with plasminogen (the precursor to plasmin) in the circulation, and it has been established that HRG can assist activation of plasminogen to plasmin by forming a complex between glycosoaminoglycans (GAGs) and plasminogen at cell surfaces (Jones *et al*., 2004b). Cleavage of HRG by plasmin has been revealed to decrease its capacity to bind heparan sulfate on cell surfaces (Poon *et al*., 2009). One idea suggests that a negative feedback loop exists, where plasmin-mediated cleavage of HRG could limit additional activation of plasminogen by decreasing the quantity of intact HRG that can proficiently bind plasminogen to cell associated GAGs (Poon *et al*., 2009). Release of the HRR/PRR fragment from HRG could consequently act to disrupt the angiogenic affects attributed to activated plasminogen through the anti-angiogenic action of the HRR (Oh *et al*., 2003). Plasminogen promotes vascular remodelling in a genetic study in knock-out mice, via mechanisms that are both dependent and independent on fibrinogen (Drew *et al*., 2000). Reducing levels of intact HRG could conceivably hinder its ability to promote angiogenesis through its binding of thrombospondin, since there would be less whole HRG available for this interaction. Hence, it is possible that the plasmin regulated degradation of HRG along with the release of the HRR/PRR region would simultaneously regulate angiogenesis negatively through the actions of independent mechanisms.

To conclude this chapter on the structural studies of HRG, the crystal structure solved here provides the first insight to the molecular arrangement of HRG. The N2 domain is folded in a cystatin-like manner and is *N*-glycosylated at Asn184. In addition, the *S*-

glutathionyl adduct observed at Cys185 gives potential *in vivo* evidence that the anti-angiogenic HRR/PRR fragment release is controlled in part by a redox mechanism, representing a new role for GSH in regulation of angiogenesis.

References

Abdelsaid MA, El-Remessy AB. *S*-glutathionylation of LMW-PTP regulates VEGFmediated FAK activation and endothelial cell migration. *J Cell Sci.* 2012, **125**(20), 4751-4760.

Barrett A.J., Fritz H., Grubb A, Isemura S, Järvinen M, Katunuma N, Machleidt W, Müller-Esterl W, Sasaki M, Turk V. Nomenclature and classification of the proteins homologous with the cysteine-protease inhibitor chicken cystatin. *Biochem J.* 1986, **236**(1), 312.

Bode W, Engh R, Musil D, Thiele U, Huber R, Karshikov A, Brzin J, Kos J, Turk V. The 2.0 A X-ray crystal structure of chicken egg white cystatin and its possible mode of interaction with cysteine proteinases. *EMBO J*. 1988, **7**(8), 2593-2599.

Borza DB, Tatum FM, Morgan WT. Domain structure and conformation of histidineproline-rich glycoprotein. *Biochemistry*. 1996, **35**(6), 1925-1934.

Bosshart H, Heinzelmann M. Endotoxin-neutralizing effects of histidine-rich peptides. *FEBS Lett.* 2003, **553**(1-2), 135-140.

Chang S.-H., Kanasaki K., Gocheva V, Blum G, Harper J, Moses MA, Shih SC, Nagy JA, Joyce J, Bogyo M, Kalluri R, Dvorak HF. VEGF-A induces angiogenesis by perturbing the cathepsin-cysteine protease inhibitor balance in venules, causing basement membrane degradation and mother vessel formation. *Cancer Res.* 2009, **69**(10), 4537-4544.

Dixelius J, Olsson AK, Thulin A, Lee C, Johansson I, Claesson-Welsh L. Minimal active domain and mechanism of action of the angiogenesis inhibitor histidine-rich glycoprotein. *Cancer Res*. 2006, **66**(4), 2089-2097.

Drew AF, Tucker HL, Kombrinck KW, Simon DI, Bugge TH, Degen JL. Plasminogen is a critical determinant of vascular remodeling in mice. *Circ Res.* 2000, **87**(2), 133-139.

Ellman GL. A colorimetric method for determining low concentrations of mercaptans. *Arch Biochem Biophys*. 1958, **74**(2), 443-450.

Forsythe JA, Jiang BH, Iyer NV, Agani F, Leung SW, Koos RD, Semenza GL. Activation of vascular endothelial growth factor gene transcription by hypoxia-inducible factor 1. *Mol Cell Biol.* 1996, **16**(9), 4604-4613.

Gorgani NN, Parish CR, Easterbrook-Smith SB, Altin JG. Histidine-rich glycoprotein binds to human IgG and C1q and inhibits the formation of insoluble immune complexes. *Biochemistry*. 1997, **36**(22), 6653-6662.

Jenko S, Dolenc I, Guncar G, Dobersek A, Podobnik M, Turk D. Crystal structure of Stefin A in complex with cathepsin H: N-terminal residues of inhibitors can adapt to the active sites of endo- and exopeptidases. *J Mol Biol*. 2003, **326**(3), 875-885.

Jin L, Abrahams JP, Skinner R, Petitou M, Pike RN, Carrell RW. The anticoagulant activation of antithrombin by heparin. *Proc Natl Acad Sci USA*. 1997, **94**(26), 14683-14688.

[a]Jones AL, Hulett MD, Parish CR. Histidine-rich glycoprotein binds to cell-surface heparan sulfate via its N-terminal domain following Zn2+ chelation. *J Biol Chem*. 2004, **279**(29), 30114-30122.

[b]Jones AL, Hulett MD, Altin JG, Hogg P, Parish CR. Plasminogen is tethered with high affinity to the cell surface by the plasma protein, histidine-rich glycoprotein. *J Biol Chem.* 2004, **279**(37), 38267-38276.

Jones AL, Hulett MD, Parish CR. Histidine-rich glycoprotein: a novel adaptor protein in plasma that modulates the immune, vascular and coagulation systems, *Immunol. Cell Biol*., 2005, **83**, 106–118.

Juarez JC, Guan X, Shipulina NV, Plunkett ML, Parry GC, Shaw DE, Zhang JC, Rabbani SA, McCrae KR, Mazar AP, Morgan WT, Doñate F. Histidine-proline-rich glycoprotein has potent antiangiogenic activity mediated through the histidine-proline-rich domain. *Cancer Res.* 2002, **62**(18), 5344-5350.

Kassaar O, McMahon SA, Thompson R, Botting CH, Naismith JH, Stewart AJ. Crystal structure of histidine-rich glycoprotein N2 domain reveals redox activity at an

interdomain disulfide bridge: implications for angiogenic regulation. Blood. 2014, **123**(12), 1948-1955.

Klenotic PA, Huang P, Palomo J, Kaur B, Van Meir EG, Vogelbaum MA, Febbraio M, Gladson CL, Silverstein RL. Histidine-rich glycoprotein modulates the antiangiogenic effects of vasculostatin. *Am J Pathol*. 2010, **176**(4), 2039-2050.

Kluszynski BA, Kim C, Faulk WP. Zinc as a cofactor for heparin neutralization by histidine-rich glycoprotein. *J Biol Chem*. 1997, **272**(21), 13541-13547.

Koide T, Odani S. Histidine-rich glycoprotein is evolutionarily related to the cystatin superfamily. Presence of two cystatin domains in the N-terminal region. *FEBS Lett*. 1987, **216**(1), 17-21.

Koide T, Foster D, Yoshitake S, Davie EW. Amino acid sequence of human histidine-rich glycoprotein derived from the nucleotide sequence of its cDNA. *Biochemistry*. 1986, **25**(8), 2220-2225.

Lee C, Bongcam-Rudloff E, Sollner C, Jahnen-Dechent W, Claesson-Welsh L. Type 3 cystatins; fetuins, kininogen and histidine-rich glycoprotein. *Front Biosci*. 2009, **14**, 2911- 2922.

Lee C, Dixelius J, Thulin A, Kawamura H, Claesson-Welsh L, Olsson AK. Signal transduction in endothelial cells by the angiogenesis inhibitor histidine-rich glycoprotein targets focal adhesions. *Exp Cell Res*. 2006, **312**(13), 2547-2556.

Leung LL. Interaction of histidine-rich glycoprotein with fibrinogen and fibrin. *J Clin Invest*. 1986, **77**(4), 1305-1311.

Li W, Huntington JA. Crystal structures of protease nexin-1 in complex with heparin and thrombin suggest a 2-step recognition mechanism. *Blood*. 2012, **120**(2), 459-467.

Lijnen HR, Hoylaerts M, Collen D. Heparin binding properties of human histidine-rich glycoprotein. Mechanism and role in the neutralization of heparin in plasma. *J Biol Chem*. 1983, **258**(6), 3803-3808

Lijnen HR, Hoylaerts M, Collen D. Isolation and characterization of a human plasma protein with affinity for the lysine binding sites in plasminogen. Role in the regulation

of fibrinolysis and identification as histidine-rich glycoprotein. *J Biol Chem*. 1980; **255**(21), 10214-10222.

Morgan WT. Interactions of the Histidine-Rich Glycoprotein of Serum with Metals. *Biochemistry*. 1981, **20**, 1054-1061.

Mori S, Takahashi HK, Yamaoka K, Okamoto M, Nishibori M. *Life Sci*. 2003, **73**(1), 93-102.

Oh CW, Hoover-Plow J, Plow EF. The role of plasminogen in angiogenesis *in vivo*. *J Thromb Haemost.* 2003, **1**(8), 1683-1687.

Olsson AK, Larsson H, Dixelius J, Johansson I, Lee C, Oellig C, Björk I, Claesson-Welsh L. A fragment of histidine-rich glycoprotein is a potent inhibitor of tumor vascularization. *Cancer Res*. 2004, **64**(2), 599-605.

Poon IK, Hulett MD, Parish CR. Histidine-rich glycoprotein is a novel plasma pattern recognition molecule that recruits IgG to facilitate necrotic cell clearance via FcgammaRI on phagocytes. *Blood*. 2010, **115**(12), 2473-2482.

Poon IK, Olsson AK, Hulett MD, Parish CR. Regulation of histidine-rich glycoprotein (HRG) function via plasmin-mediated proteolytic cleavage. *Biochem J*. 2009, **424**(1), 27-37.

Rydengard V, Olsson AK, Morgelin M, Schmidtchen A. Histidine-rich glycoprotein exerts antibacterial activity. *FEBS J.* 2007, **274**(2), 377-389.

Simantov R, Febbraio M, Crombie R, Asch AS, Nachman RL, Silverstein RL. Histidinerich glycoprotein inhibits the antiangiogenic effect of thrombospondin-1. *J Clin Invest*. 2001, **107**(1), 45-52.

Sørensen CB, Krogh-Pedersen H, Petersen TE. Determination of the disulphide bridge arrangement of bovine histidine-rich glycoprotein. *FEBS Lett*. 1993, **328**(3), 285-290.

Stubbs MT, Laber B, Bode W, Huber R, Jerala R, Lenarcic B, Turk V. The refined 2.4 A X-ray crystal structure of recombinant human stefin B in complex with the cysteine proteinase papain: a novel type of proteinase inhibitor interaction. *EMBO J*. 1990, **9**(6), 1939-1947.

Tajima M, Kurashima Y, Sugiyama K, Ogura T, Sakagami H. The redox state of glutathione regulates the hypoxic induction of HIF-1. *Eur J Pharmacol*. 2009, **606**(1-3), 45-49.

Thulin A, Ringvall M, Dimberg A, Kårehed K, Väisänen T, Väisänen MR, Hamad O, Wang J, Bjerkvig R, Nilsson B, Pihlajaniemi T, Akerud H, Pietras K, Jahnen-Dechent W, Siegbahn A, Olsson AK. Activated platelets provide a functional microenvironment for the antiangiogenic fragment of histidine-rich glycoprotein. *Mol Cancer Res*. 2009, **7**(11), 1792-1802.

Winter G, Lobley CM, Prince SM. Decision making in xia2. *Acta Crystallogr D Biol Crystallogr*. 2013, **69**(7), 1260-1273.

Chapter 4

Investigations into Zn^{2+} and heparin binding to HRG and implications for thrombin activation.

This chapter aims to investigate the mechanisms by which histidine-rich glycoprotein (HRG) is activated by zinc and its subsequent processes in the blood, such as coagulation. HRG is a 65 kDa single chain plasma protein, synthesized in the liver and present in the circulation of mammals and birds (Hulett and Parish, 2000; Jones *et al*., 2005). The protein is moderately abundant in the blood, circulating at a concentration of 1.5–2.0 μM (Corrigan *et al*., 1990). HRG interacts with numerous molecules and is involved in the formation of multi-protein complexes that regulate coagulation, immune complex clearance, cell proliferation, cell adhesion and angiogenesis (Jones *et al*., 2005). It has also been suggested that HRG can bind to receptors on the surface of a variety of cell types, including immune cells (Saigo *et al*., 1989). In clinical practice, high HRG levels are associated with thrombotic disorders such as thrombophilia and blood vessel occlusion (Engesser *et al*., 1987; Castaman *et al*., 1993; Kuhli *et al*., 2003). A part for HRG in blood clotting may include cell-cell interactions involving macrophages and platelets (Leung, 1986). Structurally, HRG contains two cystatin-like N-terminal domains (Kassaar *et al*., 2014), a histidine-rich region (HRR), two proline-rich regions (PRR1 and PRR2) and a C-terminal domain (Koide *et al*., 1986).

Uniquely, the HRR comprises of sequential pentapeptide repeat sequences of Gly-His-His-Pro-His and has the ability to bind to ten Zn^{2+} ions (K_d = 1–4 μM) through coordination to the imidazole nitrogen atoms of the many histidine residues (Morgan, 1978). This coordination of zinc ions is integral to the working of HRG by regulating its affinity for the various ligands it binds to, such as directly increasing its affinity for heparin (Borza and Morgan, 1998; Mori *et al*., 2003; Jones *et al*., 2004a), IgG (Gorgani *et al*., 1999) and tropomyosin (Guan *et al*., 2004), while inhibiting the interaction between HRG and the complement protein C1q (Gorgani *et al*., 1997). Additionally, HRG is able to interact independently of Zn^{2+}-binding with other functional partners. These include thrombospondin (Walz *et al*., 1987) and plasminogen (Jones *et al*., 2004b), through interactions with the N- and C-terminal domains of HRG. Importantly, this Zn^{2+}-binding increases the affinity of HRG towards the natural anticoagulants

heparin and heparan sulfate, which in turn neutralises these anticoagulants' inhibition of antithrombin III activity (Mori *et al*., 2003; Jones *et al*., 2004a). Thus Zn^{2+}-binding to HRG provides a potential means of regulating haemostatic function. Despite this, the Zn^{2+}-binding properties of HRG and how exactly Zn^{2+} influences HRG-heparin interactions remain to be fully understood.

Exchangeable zinc in plasma is regulated by albumin and can be affected by fatty acids

Normally, the majority of the 20 μM Zn^{2+} in the blood is bound to human serum albumin (HSA) (Sarkar, 1989) and not HRG (Guthans and Morgan, 1982). HSA is a 66 kDa plasma protein which is composed of three homologous domains (domains I–III) (Sugio *et al*., 1999). HSA binds Zn^{2+} with greater affinity than HRG and is much more abundant in circulation (Masuoka *et al* 1993). Despite this, it is possible that certain conditions exist where the free Zn^{2+} plasma concentration can reach levels required for HRG-complexes that are Zn^{2+}-dependent to form, for example, the release of Zn^{2+} from platelet-derived α-granules (Gorgani *et al*., 1999; Jones *et al*., 2004a), especially since HRG is also released by platelets. However, this would only raise the local Zn^{2+} concentration (e.g. at the surface of platelets), and may not be significant to cause a systemic shift where the levels of Zn^{2+} released would be adequate to activate HRG in the presence of HSA.

One of the main roles of HSA in circulation is to handle Zn^{2+} and other metals ions in order to protect blood cells and the endothelial cells from conditions that would otherwise be toxic. Hence, HSA acts as a chelating agent, tightly regulating the levels of free metal ions to sustain a viable level. Studies on rat WRL-68 cells have shown this protective property *in vitro*, where HSA reduced the toxicity of Zn^{2+} (Blindauer *et al*., 2009). Additionally, an increase in HSA binding to Zn^{2+} is a cause of familial hyperzincemia (Failla *et al*., 1982). HSA is also involved in the transport of Zn^{2+} to cells and tissues. HSA is involved in Zn^{2+} uptake by endothelial cells (Rowe and Bobilya, 2000) and erythrocytes (Gálvez *et al*., 2001) and has been observed to transport freshly absorbed Zn^{2+} in portal blood direct from the intestine to the liver (Smith *et al*., 1979). Recently, the major Zn^{2+} binding site of HSA was discovered using ^{111}Cd-NMR in combination with site-directed mutagenesis (Stewart *et al*., 2003; Lu *et al*., 2008). This site (site A) is localised at the interface of domains I and II, and is composed of N-

donating His67 and His247 residues, O-donating Asn99 and Asp249 residues and a water molecule or Cl^- as a final coordinating ligand. These residues are highly conserved across all mammalian albumin sequences. Previous NMR data supported these findings since it was expected that that the major Zn^{2+} site on HSA consisted mainly of N- and O-ligands (Goumakos *et al*., 1991; Sadler and Viles, 1996).

HSA is the primary fatty acid transport protein in the circulation and binds fatty acids of various chain-lengths at 5 high-affinity sites (termed FA1-5) and several lower affinity sites. An investigation into zinc and cadmium binding to sheep serum albumin surprisingly appeared to show no detectable metal binding to this protein, despite the sheep sequence containing all four of the residues required. Interestingly, it was remarked that the sample preparation was purified directly from sheep plasma and had not been subjected to a defatting protocol. Hence, it was suggested that the observed lack of metal binding in these experiments may have been due to an allosteric effect caused by fatty acid binding to the albumin. Subsequent removal of fatty acids from the sheep albumin samples resulted in a restored metal binding profile at this site (Sadler and Viles, 1996).

X-ray crystal structure comparisons of free and fatty acid-bound HSA (He and Carter, 1992; Curry *et al*., 1998; Sugio *et al*., 1999; Bhattacharya *et al*., 2000a; Bhattacharya *et al*., 2000b; Petitpas *et al*., 2001) showed that the Zn^{2+} site is disrupted by fatty acids, which disengage the domain II residues (His247 and Asp249) with respect to the domain I residues (His67 and Asn99) as shown in Figure 4.1. This structural change is arbitrated by association of the fatty acid molecule to the FA2 binding site which lays in between domains I and II of HSA. Normal physiological conditions allow for HSA to carry 1-2 molecules of fatty acid at other separate fatty acid binding sites. However, when fatty acid concentrations increase above base levels, they are able to coordinate with this site, thereby reducing the affinity of HSA for Zn^{2+}. Significant disruption of the Zn^{2+} site (and so Zn^{2+} binding to HSA) necessitates the binding of 3-5 molecules of fatty acid per molecule of HSA. A recent study examining the binding of myristic acid (C14) to bovine albumin by isothermal titration calorimetry revealed that even the presence of 1 molar equivalent of myristic acid was able to slightly disturb the regular ability of albumin to bind Zn^{2+} and 4 to 5 molar equivalents were able to completely suppress Zn^{2+} binding at this site (Lu *et al*., 2008).

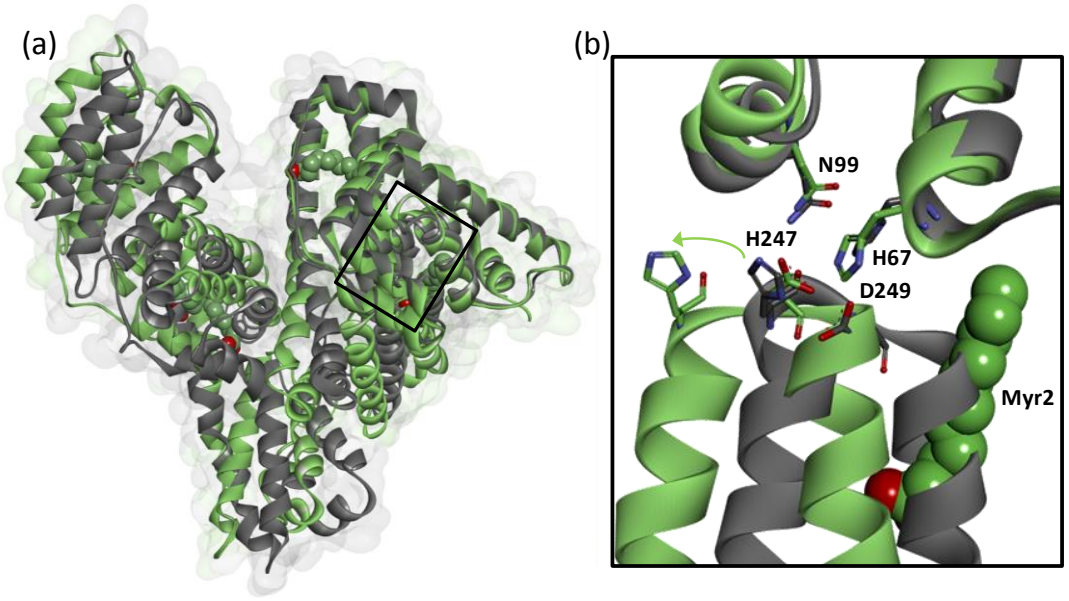

Figure 4.1. The fatty-acid/Zn^{2+} switch on serum albumin. (a) Overlay of crystal structures of human serum albumin with (grey; PDB: 1BK5) and without myristic acid bound (green; PDB: 1AO6) showing the location of the major Zn^{2+}-binding site. (b) Close-up showing the movement of Zn^{2+}-co-ordinating residues His247 and Asp249 relative to His67 and Asn99 between the two structures. Figure drawn using PyMol by Dr. Claudia Blindauer.

Fatty acids could switch zinc speciation and activate HRG

Fatty acids are absorbed into the blood stream through different mechanisms based on the carbon chain length. Medium and short chain fatty acids are directly absorbed into circulation after dietary intake (Jørgensen *et al*., 2001) and are transported through the circulatory system by HSA, to their intended target site, while long chain fatty acids are released into circulation from lipoproteins and adipocytes. Under normal physiological conditions the basal plasma concentration of free fatty acid is between 250-500 µM at rest (<1 molar equivalent, compared to HSA). However, free fatty acid levels are dynamic and rise following meals and during periods of exercise, but the majority remain bound to HSA, since the albumin molecule has a large number of fatty acid binding sites; HSA is able to bind up to 10 fatty acid molecules *in vitro* (Bhattacharya *et al*., 2000a). The most abundant serum fatty acids associated with HSA are palmitic acid (C16), stearic acid (C18) and oleic acid (C18) (Jørgensen *et al*., 2001). Chronically raised free fatty acid levels are associated with various conditions such as obesity (Björntorp *et al*., 1969; Koutsari and Jensen, 2006), diabetes (Reaven *et al*., 1988), fatty liver disease (Donnelly *et al*., 2005), cancer (Charles *et al*., 2001) and are observed as a symptom of plasma HSA deficiency (analbuminemia) (Bartter *et al*., 1961). In obese

individuals, plasma concentrations of free fatty acids at rest are often 2-3 times higher (Koutsari and Jensen, 2006), and in some cancer patients are 4-6 times higher than controls (Kleinfeld and Okada, 2005). These conditions are also associated with an increased risk of thrombotic complications (Connolly and Khorana, 2009; Previtali *et al*., 2011). For example, thromboembolism (caused by obstructive blood clots) is the second leading cause of death associated with malignancy (Connolly and Khorana, 2009).

From current understanding of the Zn^{2+} binding properties of HSA and HRG, it is clear that either continuous or temporary enhanced plasma fatty acid concentrations could prospectively increase the fraction of plasma Zn^{2+} associated with HRG. The reduced Zn^{2+} binding competition from HSA could allow an adequate proportion of Zn^{2+} to switch from its usual speciation (being bound to HSA) to being coordinated to HRG. This could then lead to activation of HRG with respect to some of its binding partners, triggering its actions (such as coagulation). It is likely that HRG and fat-loaded HSA would have comparable affinities for Zn^{2+}, so under these conditions, HRG could bind as much as 5% of plasma Zn^{2+}. This is just speculation, and the percentage would perhaps be even higher (at the surface of platelets following granule release, for example) but would also be contingent on the concentrations of Zn^{2+}-binding proteins and molecules (such as histidine). These observations led us to hypothesize that under conditions where free fatty acid levels are elevated, Zn^{2+} displaced from HSA could bind to HRG, enhancing its interaction with heparin/heparan sulfate and induce a pro-coagulatory effect (Stewart *et al*., 2009). If so, this would constitute a novel targetable mechanism by which thrombotic complications arise in high-risk individuals.

High HRG levels have clinically been associated with thrombotic disorders including blood vessel occlusion (Kuhli *et al*., 2003), and thrombophilia (Engesser *et al*., 1987). This is significant when taking the possible switch of Zn^{2+} speciation into consideration. If fatty acid binding to HSA can increase the Zn^{2+} concentration associated with HRG, this increase in Zn^{2+} activated HRG could consequently cause thrombotic disorders, or at least enhance the possibility of thrombosis occurring. The key mechanism under investigation here is the regulation of the coagulation protease, thrombin, which forms an inactive ternary complex with its binding partners: antithrombin and heparin.

The coagulation cascade and thrombin

The coagulation mechanism which acts to help prevent infection and the loss of blood in mammals and other higher organisms following injury is often described by two pathways, known as the contact activation (intrinsic) pathway and tissue factor (extrinsic) pathway. These mechanisms converge at the final common pathway (Figure 4.2).

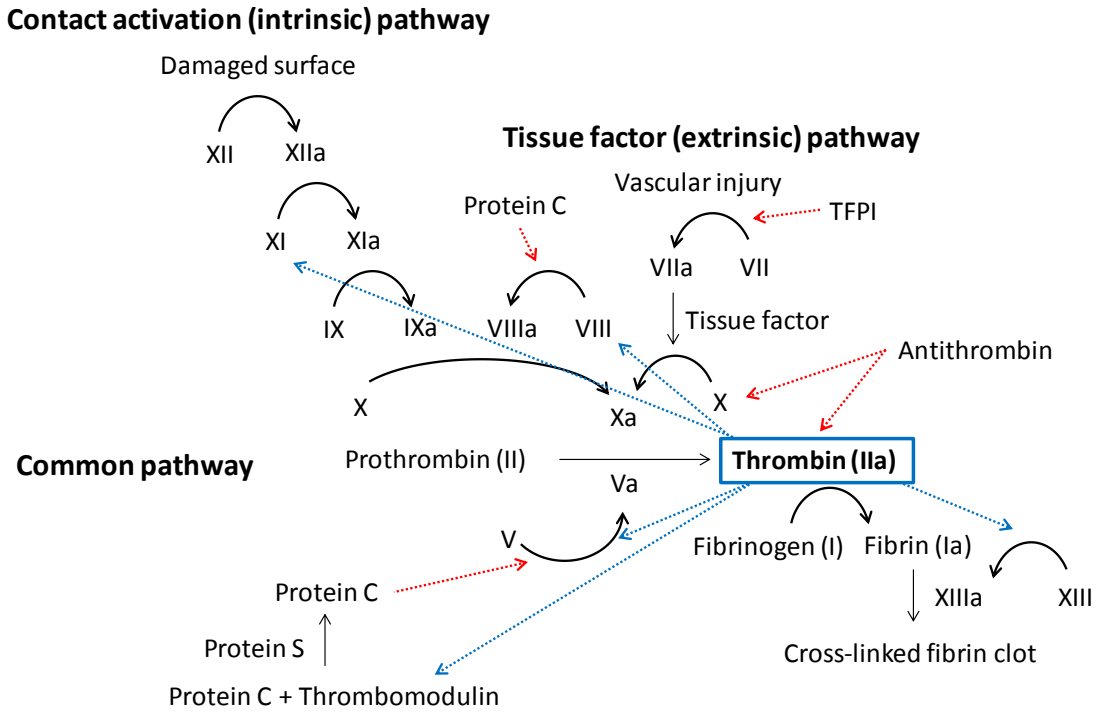

Figure 4.2. Schematic diagram of the coagulation cascade showing the contact activation, tissue factor and common pathways. Factors are shown as their Roman numerals; TFPI is tissue factor pathway inhibitor. The blue arrows show the additional functions of thrombin behind its primary function of fibrinogen conversion to fibrin, highlighting the central role it plays in the process. It can be seen how thrombin is involved in both pro- and anti-coagulant roles and is involved in self-regulation. The red arrows show points of inhibition.

Before these cascades come in to play, platelets become activated and adhere to the injury site. These platelets will then aggregate and form a plug to reduce or stop the loss of blood temporarily. Activation of platelets releases several proteins that increase and accelerate platelet plug formation, and also begin the tissue repair process. The agent, von Willebrand factor, forms a bridge between the subendothelium layer and the activated platelets, thus playing an important role in platelet adhesion (Ruggeri and Zimmerman, 1987). Similarly, fibrinogen forms a bridge between adjacent activated

platelets (Savage and Ruggeri, 1991), leading to aggregation and plug formation. These reactions make negatively charged phospholipids available on the surface of the damaged cell membranes or activated platelets, thereby setting the scene for the coagulation cascade and its terminal insoluble fibrin clot formation which strengthens the platelet plug.

In the intrinsic pathway, fibrin formation is a consequence of a series of stepwise reactions involving plasma proteins circulating in an inactive or precursor form. These zymogens are activated by proteolysis and converted to serine proteases. Many of these calcium dependent reactions occur at activated platelets, which provide the phospholipids. The intrinsic pathway has an important role in regulating the growth and maintenance of fibrin formation, but the extrinsic pathway is the primary and critical mechanism in the formation of a fibrin clot.

The extrinsic pathway is also known as the tissue factor pathway since it requires tissue factor, located in the tissue adventitia, which only comes in contact with blood after vascular injury (Maynard *et al*., 1975, Maynard *et al* 1977; Wilcox *et al*., 1989). Tissue factor apoprotein is a membrane glycoprotein that is tightly associated with phospholipids (Broze *et al*., 1985; Guha *et al*., 1986) and has a high affinity for factor VII (Broze, 1982; Bach *et al*., 1986; Sakai *et al*., 1989). At the point of injury, a complex between the two proteins is formed in the presence of calcium which facilitates the conversion of factor VII to the active factor VIIa by proteolysis (Rao and Rapaport, 1988; Sakai *et al*., 1989) by trace levels of a plasma protease in circulation (such as thrombin) (Masys *et al*., 1982; Wildgoose and Kisiel, 1989; Pedersen *et al*., 1989). The tissue factor-factor VIIa complex then activates factor X to factor Xa. This generated factor Xa forms a complex with factor Va in the presence of calcium and phospholipids (Tracy *et al*., 1981). This complex converts prothrombin to thrombin, which is the final and most critical protease generated in the coagulation cascade since it is the only factor capable of cleaving fibrinogen to create a fibrin clot. Fibrin is formed by the proteolysis of a peptide bond in each of the fibrinogen chains. This releases four fibrino-peptide monomers, which then polymerise to form the insoluble fibrin clot (Laudano and Doolittle, 1980).

Thrombin is the integral enzyme in blood coagulation because of its exclusive ability to cleave fibrinogen to fibrin; it contributes to the “thrombin burst” feedback mechanisms

and stabilises clots. Any deviation from regular functioning can cause grave effects. Without adequate thrombin generation, haemorrhage can occur since stable blood clots cannot form. Equally, unregulated thrombin activity can lead to thrombosis in instances where clots disseminate away from the site of tissue damage.

Thrombin is a serine protease and is a member of the chymotrypsin family. It has a structure and catalytic function like the prototypic protease chymotrypsin, and works in a similar manner to trypsin. The multiple functions of thrombin are balanced by its specificity for the particular substrate. Since thrombin has lost the Gla and kringle domains of its zymogen prothrombin, all substrate recognition occurs at the catalytic domain. Thrombin is composed of two polypeptide chains (A and B) which are linked covalently by a disulfide bridge. The A chain is only 36 amino acid residues long and has no documented functional roles. The B chain is 259 amino acid residues, and composes the entrance to the active site (Bode *et al*., 1992). The active site cleft is a canyon at the centre of the protein. Because of the homology between thrombin and trypsin, thrombin also cleaves preferentially at Arg residues of the substrate, but selectively at specific Arg sites using auxiliary interactions from two exosites at distinct locations from the active site.

Exosite I contains hydrophobic regions and several charged residues on its surface, providing electrostatic navigation and positioning to fibrinogen during its approach to the thrombin active site. This epitope extends from exosite I to the active site (Mosesson *et al*., 2001). Similar epitopes are employed by thrombin to interact with the natural inhibitor hirudin (Rydel *et al*., 1991), fibrin (Ayala *et al*., 2001) and thrombomodulin (Pineda *et al*. 2002). Exosite II is positioned opposite to exosite I and features numerous charged residues, but no hydrophobic regions. The charged residues enable interactions with anionic heparin and other glycosaminoglycans (GAGs) (Sheehan and Sadler, 1994). GAGs are highly sulfated polysaccharide molecules of various chain lengths that festoon the proteoglycans in vascular and extravascular spaces. Heparin is a highly sulfated GAG produced by mast cells and is a potent anticoagulant used in clinical practice. The thrombin binding site for heparin is localised at exosite II (Sheehan and Sadler, 1994; Gan *et al*., 1994; Ye *et al*., 1994; Tsiang *et al*., 1997), and a high-resolution crystal structure shows thrombin binding a heparin octa-saccharide (Carter *et al*., 2005) via a non-specific electrostatic interaction (Olson *et al*., 1991). GAGs are used by thrombin to regulate its interactions with other proteins, including antithrombin,

which is the basis for heparin's role as an anticoagulant. Antithrombin is a serpin which forms a ternary complex with heparin and thrombin, irreversibly inhibiting thrombin activity (Olson and Chuang, 2002). Antithrombin is one of only two specific thrombin inhibitors in circulation (with heparin cofactor II being the other, which also requires the presence of GAGs), and its important inhibition effects are demonstrated in cases of antithrombin deficiency where patients have an increased incidence of thrombosis (van Boven and Lane, 1997), and in knockout mouse models where embryonic mortality was observed (Ishiguro *et al*., 2000). Antithrombin recognises a unique pentasaccharide sequence of heparin (which has a random distribution along the polysaccharide chains) with high affinity that causes a global conformational change through a hinge motion. This conformational change has been shown to be important in the action of antithrombin on factor Xa, but is not the mechanism behind its thrombin inactivation. For this, the heparin chain provides a template on which inhibitor and protease interact, where the high-affinity sites of the heparin chain are occupied by antithrombin while thrombin translates along the chain until encountering the inhibitor (Li *et al*., 2004).

Both unfractionated heparin, which is a mixture of polysaccharide chains ranging from 3 to 30 kDa, and for low molecular weight heparins (less than 8 kDa) can bind to antithrombin. However, for heparin to catalyse antithrombin inhibition of thrombin, a specific ternary complex between the three parties needs to form which requires the pentasaccharide containing heparin chains to be at least 18 saccharide units long. This complex inactivates thrombin activity by factor of greater than 1000. Thrombin binds heparin through an interaction at its exosite II, stabilising the thrombin-antithrombin complex by sharing the same heparin chain (Stone SR and Le Bonniec, 1997). In addition to this, a crystal structure of the ternary complex (Li *et al*., 2004) revealed a close direct contact interface between the thrombin and antithrombin molecules.

Taking all this information together, we hypothesise that HRG activated by Zn^{2+}, the dynamics of which have been affected by increased fatty acid binding to HSA, could allow for HRG to effectively compete for heparin against antithrombin and reduce thrombin inhibition leading to enhanced thrombosis (Figure 4.3). Since clinical conditions which are associated with high levels of plasma fatty acids also are known to show an increased incidence of thrombosis, this novel molecular mechanism could provide an explanation for this observation and also potentially improve the efficacy of heparin anticoagulation treatments. To help prove this hypothesis, studies on HRG

binding to zinc, heparin and both zinc and heparin were conducted using isothermal titration calorimetry and enzyme-linked immunosorbent assays. Similar isothermal titration calorimetry studies on HSA binding to zinc under a range of fatty acid conditions were also performed and an *in vitro* thrombin activity assay was developed to assess the veracity of the proposed mechanism.

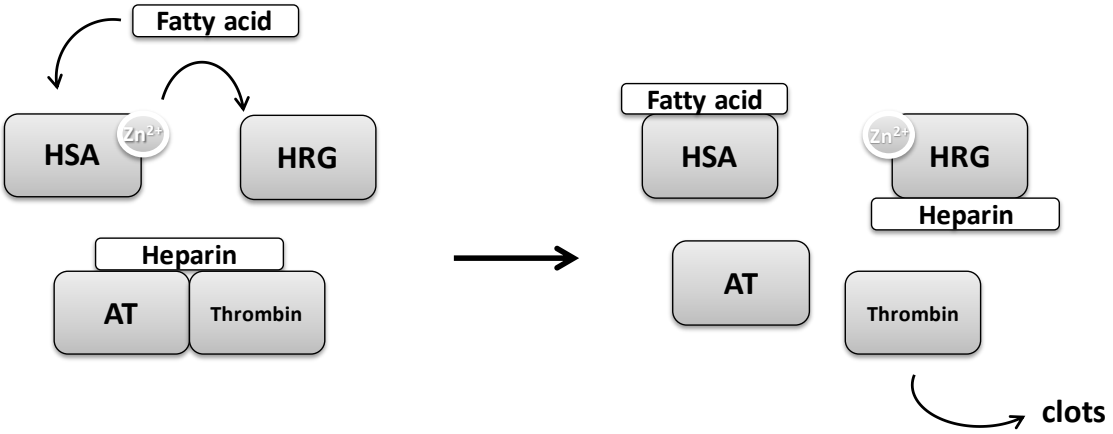

Figure 4.3. A schematic representation of the hypothesis proposed in text. Allosteric modulation of albumin (HSA) can switch the Zn^{2+} dynamics towards histidine-rich glycoprotein (HRG). This activation of HRG makes it more effective in competition for heparin against antithrombin (AT), thereby breaking or preventing the inhibitory ternary complex between AT, heparin and thrombin. This process would free the thrombin to proceed in coagulation.

Methods

Purification

Purification was performed as described earlier (see Chapter 3).

Sodium dodecyl sulfate-polyacrylamide gel electrophoresis (SDS-PAGE)

SDS-PAGE was performed as described earlier (see Chapter 3).

Protein Concentration Determination

Protein concentration was determined as before (see Chapter 3).

Isothermal titration Calorimetry (ITC)

ITC experiments were carried out using a VP-ITC instrument (MicroCal) in 50 mM tris, 140 mM NaCl, pH 7.4, at 25 °C. Titration reagents (zinc, heparin) were added to the reaction buffer and the pH adjusted to 7.4 to match the buffer. Solutions were degassed at 22 ºC for 15 minutes prior to running the experiment. Typical titrations performed were one 2 µl injection over 4 s followed by up to 55 injections of 5 µl over 10 s with an adequate interval of 240 s between injections to allow complete equilibration. The stirring speed was 307 rpm. Heats of dilution were accounted for with blank titrations performed by injecting ligand solution into reaction buffer and subtracting the averaged heat of dilution from the main experiment. Alternatively, in cases of saturated binding blank titrations were omitted where the averaged residual signal of the last injections was used to determine the heat of dilution. Raw data were processed using MicroCal Origin software and data fitted using the same software. Protein concentrations were determined either by using absorbance at 280 nm or by weighing out lyophilised sample. Specific experimental reaction conditions are given in each figure legend.

ITC experiments with low molecular weight heparin were performed on an iTC_{200} (GE Healthcare Life Sciences, Little Chalfont, UK) and were typically of 19 injections of 2 µl with 120 s intervals. Stirring speed was 750 rpm. Consecutive data sets were combined using ConCat32 software.

Raw data for the ITC experiments presented here can be found in Appendix 2.

Enzyme-linked immunosorbent assay (ELISA)

An ELISA experimental set-up was devised to investigate the interaction between HRG and heparin compounds. Undefined heparin (Acros Organics) or low-molecular weight heparin (Iduron, Manchester, UK) were coated overnight at room temperature onto a heparin-binding plate (Iduron) at a concentration of 25 μg/ml in 50 mM HEPES, 150 mM NaCl, 0.2% Tween 20 at pH 7.4 with or without $ZnCl_2$. The wells were washed using the same buffer, and then blocked with the same buffer supplemented with 0.2% gelatin from fish skin (Sigma-Aldrich) for 1 hour at 37°C. Human HRG was incubated for 2 hours over a range of concentrations (0–3 μM) at 37°C. Binding was detected with primary rabbit anti-HRG (Sigma-Aldrich) followed by alkaline phosphatase linked anti-rabbit antibody (Sigma-Aldrich) and observed with a pNPP substrate (Sigma-Aldrich) at 405 nm.

Thrombin assay

To investigate the proposed mechanism of thrombin activation via Zn^{2+}-dependent modulation of HRG functioning by plasma fatty acids, an *in vitro* assay system was established containing all constituents of the proposed pathway at physiological concentrations. Serum albumin (600 μM, purchased from Sigma-Aldrich) was pre-loaded with fatty acid by incubating with lauric acid (0, 1.5 or 3 mM) for 1 hour at 37 °C in 50 mM HEPES, 150 mM NaCl at pH 7.4 and $ZnCl_2$ (20 μM). HRG (1.5 μM), heparin (0.5 U/ml), antithrombin (2 μM) and thrombin (0.5 nM) were mixed with the albumin sample and allowed to equilibrate for 1 hour at 37 °C. S-2238 (100 μM), the thrombin substrate, was then added to the reaction which was detected after 20 minutes at 380 nm using a Fluostar Optima. Final concentrations are shown in parenthesis; experiments were performed in triplicate.

Results and discussion

Purification of HRG

HRG samples were purified from human plasma or rabbit serum. Rabbit HRG was used in initial experiments since a greater yield of protein was afforded and rabbit serum was more readily available. The purification protocol involved one step on a nickel affinity matrix and resulted in yields of > 80% and high purity (> 95%) as assessed by SDS-PAGE (Figure 4.4). Protein identity was confirmed by mass spectrometry.

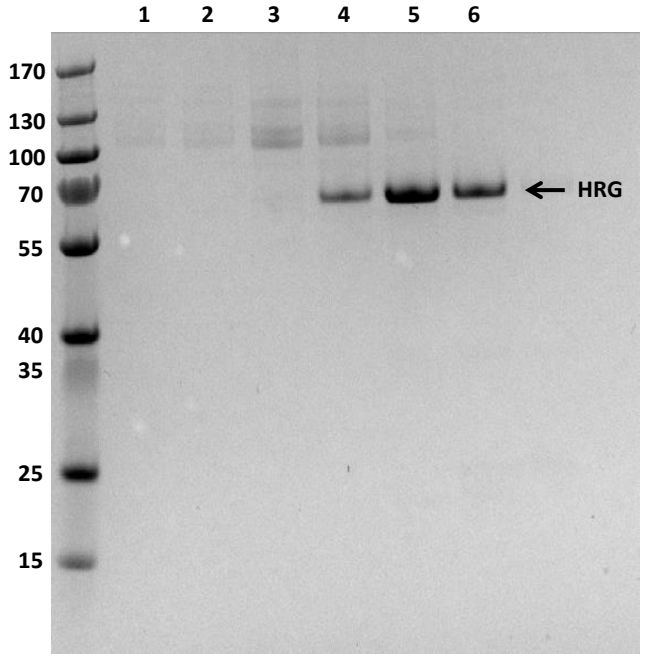

Figure 4.4. SDS-PAGE analysis of the one step nickel affinity purification of human HRG from plasma, stained with coomassie. Molecular weight markers are shown in kDa. HRGcan be seen in lanes 4 to 6. The purity of all samples was assessed to be at least greater than 95%, and samples of this quality were used in experiments. Rabbit HRG was purified as before (Chapter 3, Figure 2.4).

The mass spectrometry analysis was shown earlier (Chapter 3, Figure 3.4), as was the sequence homology between human and rabbit HRG (Chapter 3, Figure 3.2). Although the proteins share a high sequence homology, the greatest variance between their respective sequences is observed in the HRR and PRR2 domains. This region of HRG is involved in Zn^{2+} and heparin binding, so any difference observed between human and rabbit HRG with these interactions could be accounted for by keeping the sequence variance in mind.

Zinc binding studies with HRG

The Zn^{2+}-binding properties of hHRG (human) and rHRG (rabbit) were studied using ITC. Both hHRG and rHRG exhibited almost identical binding profiles, revealing an exothermic binding process between HRG and Zn^{2+} (Figure 4.5).

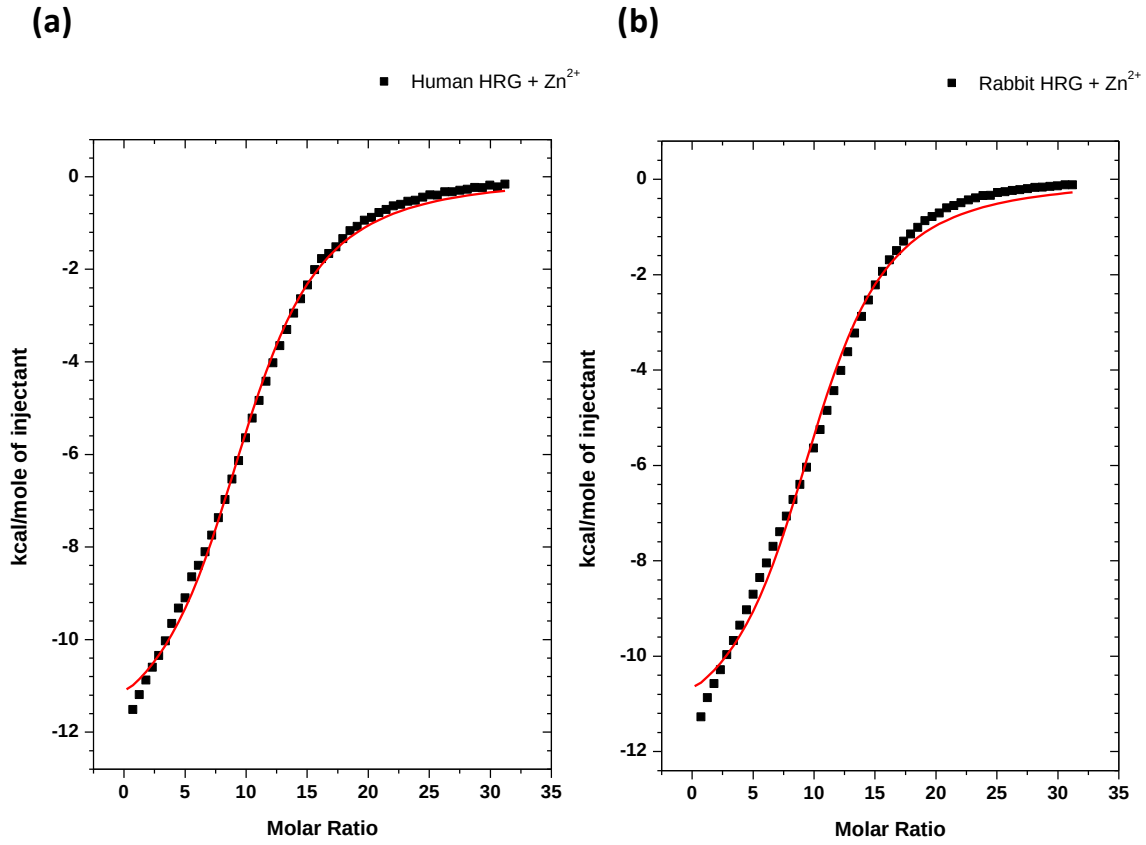

Figure 4.5. ITC data for Zn^{2+} binding to (a) human HRG and (b) rabbit HRG. 55 injections of 5 µl of 150 µM $ZnCl_2$ were delivered to HRG (10 µM in buffer containing 50 mM Tris, 140 mM NaCl at pH 7.4) over 10 s with an adequate interval (240 s) between injections to allow complete equilibration. Raw data can be found in appendix A2.1 and A2.3.

Previous studies on the metal binding properties of HRG have utilised rHRG since rabbit plasma contains almost ten times more of the protein. Thus the hHRG Zn^{2+}-binding characteristics provided here are the first attempts to quantitatively and qualitatively interpret this binding. The ITC data determined that hHRG is capable of binding 10 molar equivalents (N=10.3) of Zn^{2+}, with an average K_a of 8.1×10^4 ($\pm$ 4.0×10^3) M^{-1} (Figure 4.5a). The rHRG ITC data show that the rabbit protein is also able to bind 10 molar equivalents (N=10.4) of Zn^{2+}, in keeping with previously reported data (Morgan, 1981), but had a lower affinity with an average K_a of 4.4×10^4 ($\pm$ 3.3×10^3) M^{-1} (Figure 4.5b). The lower affinity of rHRG for Zn^{2+} when compared with hHRG

could potentially help explain why the former is more abundant in rabbit plasma, than the latter is in human plasma. In addition to this, although both proteins share a high homology, the greatest difference in their sequence comes at the respective HRR and PRR2 domains where the rabbit sequence is elongated (Chapter 3, Figure 3.2).

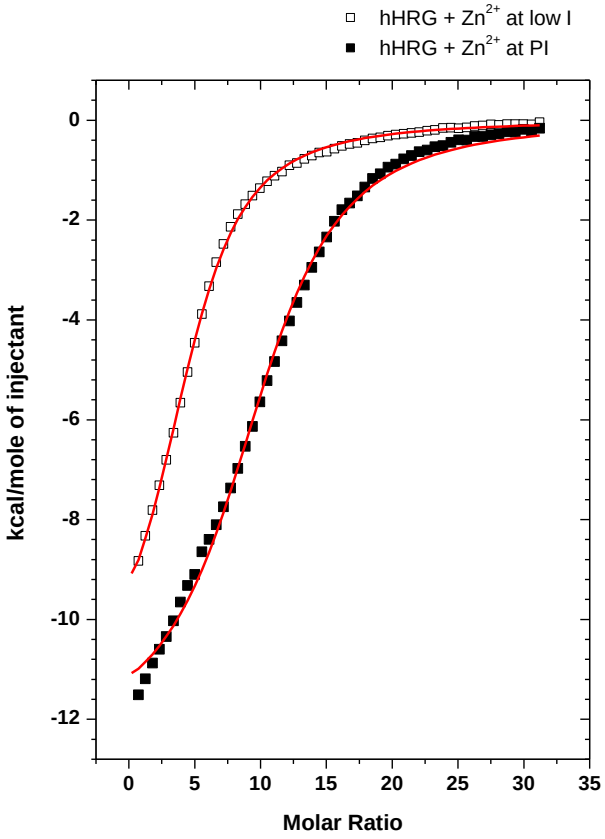

Figure 4.6. ITC data for Zn^{2+} binding to human HRG in physiological ionic strength (PI) and low ionic strength (low I) buffers. 55 injections of 5 µl of 150 µM $ZnCl_2$ were delivered to samples of 10 µM HRG in buffer containing 50 mM Tris, 140 mM NaCl at pH 7.4 (white squares) or 50 mM Tris, 50 mM NaCl at pH 7.4 (Black squares) over 10 s with an adequate interval (240 s) between injections to allow complete equilibration. Raw data can be found in appendix A2.2.

Interestingly, when the ITC experiment was performed under conditions of lower ionic strength (the previous experiments were conducted at physiological ionic strength), hHRG was shown to bind only 5 molar equivalents of Zn^{2+}, with a K_a of 3.6×10^4 ($\pm$ 2.4 $\times 10^3$) M^{-1} (Figure 4.6). This suggests that salt ions are involved in the binding of Zn^{2+} either as a direct ligand for the Zn^{2+} ion or by playing a role in forming binding sites through salt bridges. Intriguingly, EXAFS studies on HRG led the researchers to postulate a Zn^{2+} binding site to be composed of three histidine ligands and one heavier

ligand which was proposed to be a cysteine sulfur atom (Mangani *et al*., 2003). However, they admitted that the EXAFS analysis did not allow for the differentiation between a sulfur or chloride ion. The data presented here conducted at different ionic strengths would support the latter, since at the lower ionic strength (i.e. lower Cl^- levels) significantly attenuated the ability of hHRG to bind Zn^{2+}. If a cysteine sulfur was indeed involved in the Zn^{2+} binding, it would have appeared as a distinct region on the ITC isotherm. The ITC data shows all 10 sites are identical, but since most cysteine residues of HRG are involved in disulphide bridging, it would not be possible for all 10 sites to contain a cysteine residue. Although Cl^- is a weak Zn^{2+} binding ligand, there is evidence that it can form part of a Zn^{2+} binding site (Smith *et al*., 1996; Hymowitz *et al*., 1999).

Heparin binding studies on HRG

A similar approach using ITC was used to examine the effect of Zn^{2+} on the heparin binding properties of hHRG. Unfractionated heparin (molecular weight range 3-30 kDa) was injected into samples of hHRG at different concentrations of $ZnCl_2$ (Figure 4.7).

The presence of $ZnCl_2$ had a marked effect upon the mechanism by which human HRG bound heparin. In the absence of Zn^{2+} the interaction between heparin and HRG is endothermic. Upon the presence of 1 µM Zn^{2+}, an exothermic mode of binding appears observable at the start of the isotherm, which becomes more pronounced at 5 µM. This suggests that heparin binds HRG via different modes, whereby the exothermic mode occurs before the endothermic mode and is enhanced by Zn^{2+} binding to HRG. These modes could arise from heparin binding to different regions of the HRG molecule. HRG is known to have N-terminal sequence homology with the antithrombin heparin binding site which could provide one binding mode, and the HRR (which would become positively charged upon binding Zn^{2+}, thereby enhancing any effect) could provide another region of binding for the negatively charged heparin. It was possible to fit curves to the endothermic data collected in the absence and presence of 1 µM $ZnCl_2$, but not to the most complex isotherm observed at 5 µM. The resultant curves suggested that the endothermic mode most probably corresponds to a single heparin site. The calculated K_a for this mode was 3.27×10^6 ($\pm$ 2.5×10^5) M^{-1} with no $ZnCl_2$ and 3.95×10^6 ($\pm$ 5.2×10^5) M^{-1} in the presence of 1 µM $ZnCl_2$. However, the "real" affinities are likely to be higher as this analysis does not take into account binding via the exothermic mode.

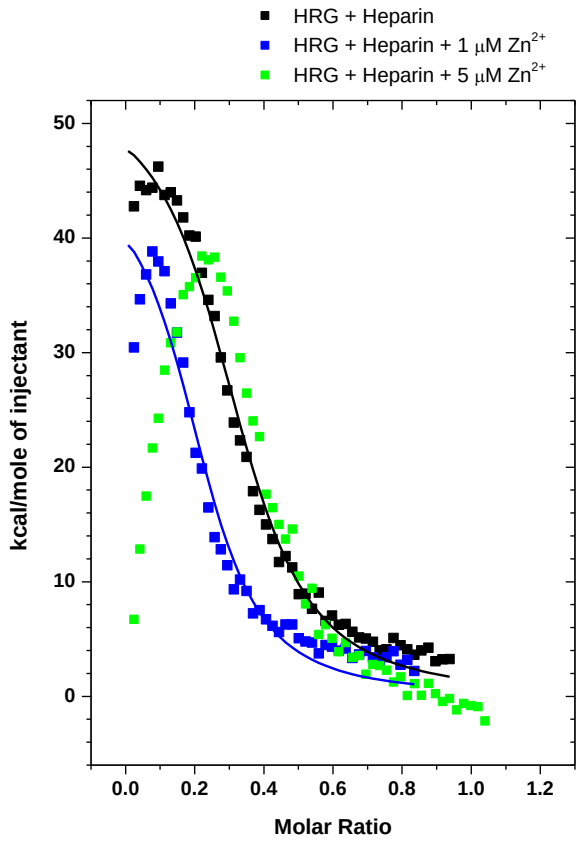

Figure 4.7. Effect of Zn^{2+} on heparin binding to human HRG. Here 45 injections of 5 µl of 50 µM heparin (average mol. wt. assumed to be 15 kDa) was delivered to samples of HRG (10 µM in buffer containing 50 mM Tris, 50 mM NaCl and 0, 1 and 5 µM $ZnCl_2$ at pH 7.4) over 10 s with an adequate interval (240 s) between injections. Zn^{2+} was included in the buffer at concentrations of 0, 1 and 5 µM. Raw data can be found in appendix A2.4-2.6.

It was also observed that there is a difference in the stoichiometry of heparin binding to HRG in the presence of 1 µM Zn^{2+} (as illustrated by a shift in the curve to the left) compared with the data without Zn^{2+} or with 5 µM Zn^{2+}. This correlates with a previous study which revealed that complexes of 1 heparin:1 HRG and of 1 heparin:2 HRG can form with formation of the 1:2 complex enhanced by the presence of Zn^{2+} (Burch *et al.*, 1997). Since we used unfractionated heparin in this instance, it was not possible to assign an accurate molecular mass to the titrant solution (an average mass of 15 kDa was used), and so the x-axis on Figure 4.7 is to a large degree arbitrary. But, if we use the molar ratio of 0.4 observed in these experiments to represent the 1:1 complex (which is the calculated N value for both the without Zn^{2+} and 5 µM Zn^{2+} data sets), then the molar ratio of 0.2 (which is the calculated N value for the 1 µM Zn^{2+} data set) can be taken to represent the 1:2 complex. The data here suggests that higher

concentrations of Zn^{2+} (5 µM) preclude the formation of the 1:2 complex, which will enhance the proportion of heparin bound to HRG. However, this interaction is complex and becomes even more convoluted if experiments at higher Zn^{2+} levels are attempted (Appendix A2.7). The complexity is a corollary of the molecules involved, since HRG is likely able to bind heparin at different regions, and heparin molecules themselves are heterogeneous (existing in varying chain lengths) which interact differently with HRG depending on length. For example, heparin chains of 10 kDa do not form the 1 heparin:2 HRG complex (Burch et al., 1997). It should be stated that the heparin ITC experiments were conducted at an ionic strength lower than physiological for qualitative and aesthetic reasons. Experiments performed at physiological ionic strength showed the same pattern and trends observed here (Appendix A2.8).

Since quantitative information from the ITC data was problematic to obtain due to the mix of endothermic and exothermic interactions observed, and ELISA protocols were established to calculate the affinities involved in this interaction (Figure 4.8).

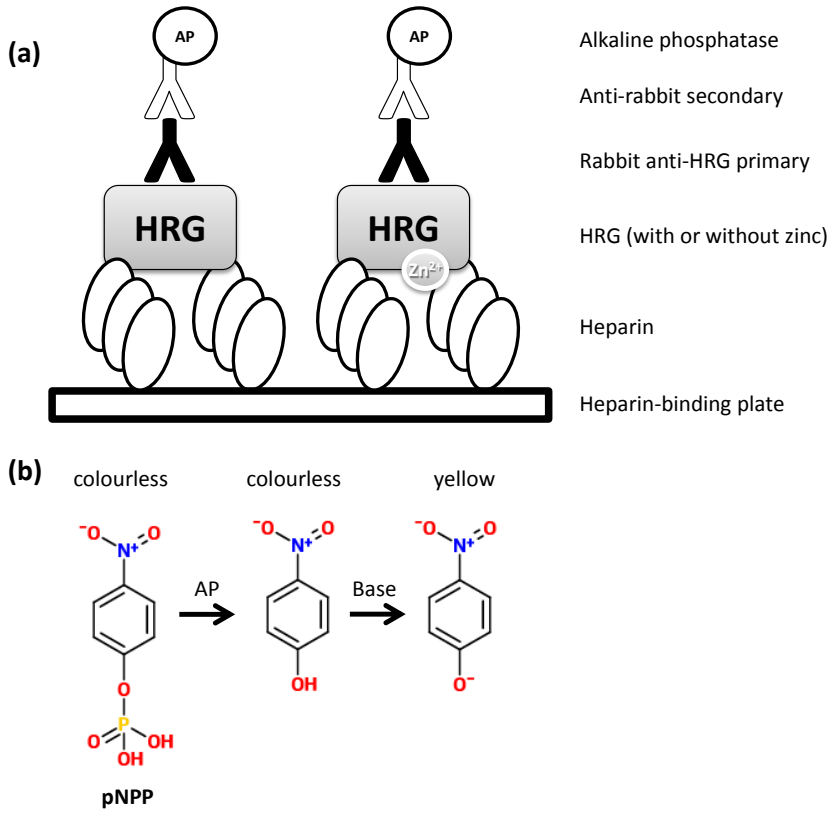

Figure 4.8. (a) Schematic representation of the ELISA set up. (b) The substrate para-Nitrophenylphosphate (pNPP) cleaved by alkaline phosphatase (AP), to produce a yellow coloured compound under basic conditions.

In addition, low molecular weight (LMW) heparin was included in these studies to provide further insights into the mechanistics of heparin binding to HRG under the influence of Zn^{2+}. In these experiments plates were coated with unfractionated heparin (3-30 kDa) and human HRG solutions containing different concentrations of $ZnCl_2$ were added. After washing, binding was detected through the use of a specific rabbit anti-HRG antibody and an alkaline phosphatase-linked anti-rabbit secondary antibody. The alkaline phosphatase cleaves the substrate para-Nitrophenylphosphate (pNPP) to produce a yellow compound.

In each case HRG bound heparin in a concentration-specific manner (Figure 4.9a). In the absence of Zn^{2+}, the average K_d value was 32.9 nM (much stronger than the affinity calculated from the ITC data). However the affinity was significantly higher in the presence of Zn^{2+}, with similar binding profiles observed at all concentrations investigated. In these cases the average K_d values were calculated to be 5.1 nM, 6.2 nM and 8.2 nM in the presence of 1 µM, 5 µM and 20 µM $ZnCl_2$, respectively. The maximum level of binding was similar in all cases suggesting that the independent binding modes observed in the ITC experiments are likely to be mutually exclusive (i.e. coordination of Zn^{2+} does not create additional heparin-binding sites). These data suggest that even relatively small changes in the speciation of plasma Zn^{2+} are likely to affect the heparin-binding properties of HRG and its haemostatic functions. Antithrombin has a high affinity for heparin with a K_d in the region of 10-36 nM (Olson *et al*., 1992), and also binds a fraction of heparin (termed low affinity heparin) with a K_d of 19 µM (Streusand *et al*., 1995). Taking these numbers into account with the data obtained here (showing that HRG binds heparin with a K_d of 32.9 nM in the absence of Zn^{2+} and 5.1-8.2 nM in the presence of Zn^{2+}) it is apparent that HRG is an important competitor for heparin against antithrombin even under normal conditions; but is a more significant and stronger competitor in the presence of Zn^{2+}.

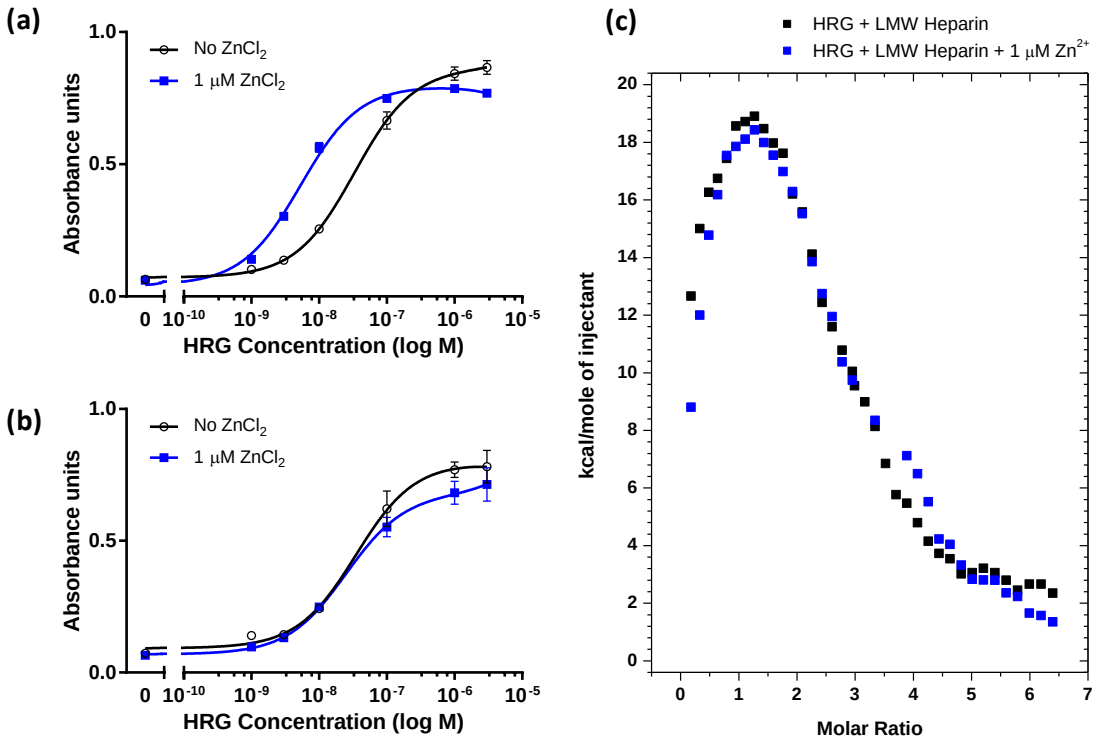

Figure 4.9. Effect of Zn^{2+} on (a) unfractionated heparin (ranging from 3-30 kDa) and (b) low molecular weight heparin (6850 Da) binding to human HRG examined by ELISA. Heparin (25 µg/ml) was coated overnight onto a heparin-binding plate in 50 mM HEPES, 150 mM NaCl, 0.2% Tween 20 and 0, 1, 5 or 20 µM $ZnCl_2$ at pH 7.4 in triplicate. The reaction was washed using the same buffer, then blocked with the same buffer containing 0.2% gelatin. Human HRG was then added over a range of concentrations (0–3 µM) and incubated for 2 hours. Detection was with primary rabbit anti-HRG followed by alkaline phosphatase linked anti-rabbit antibody and observed with a pNPP substrate at 405 nm. (c) ITC experiments performed using low molecular weight heparin (6850 Da). 2µl injections of 150µM low molecular weight heparin was delivered to samples of 10 µM HRG in 50 mM Tris, 50 mM NaCl at pH 7.4. Buffers contained either 0 or 1 µM $ZnCl_2$. Data from consecutive experiments were combined using ConCat32 software. Raw data can be found in appendix A2.9-2.10.

The complementary LMW heparin ELISA experiments (Figure 4.9b) showed that Zn^{2+} had no influence on the ability of HRG to bind to the LMW heparin chain, where the K_d values were ~30 nM for both without Zn^{2+} and with 1 µM Zn^{2+} (Figure 4.9b). To supplement the ELISA data, ITC experiments using the same LMW heparin were conducted (Figure 4.9c) and confirmed that Zn^{2+} has no effect on the affinity or stoichiometry of the HRG interaction with LMW heparin.

By taking the data presented here and by combining it with what is already known about the HRG-heparin interaction, such as both the N1N2 domain and the HRR can

independently bind heparin (Jones *et al*., 2004a; Vanwildemeersch *et al*., 2006), a schematic representing the sophisticated interaction can be developed (Figure 4.10). HRG can initially bind heparin via its N1N2 domain which is then enhanced upon the chelation of Zn^{2+} by the HRR. At higher concentrations of Zn^{2+}, repulsion effects between the dimers force them apart and into the 1:1 complex. This could explain why increasing the Zn^{2+} levels in the ELISA experiments did not show a parallel in increasing the HRG affinity for heparin. It could also explain why HRG binding to LMW heparin is not enhanced by Zn^{2+}, since there is not enough template surface (i.e. heparin chain length) for this augmentation effect to work.

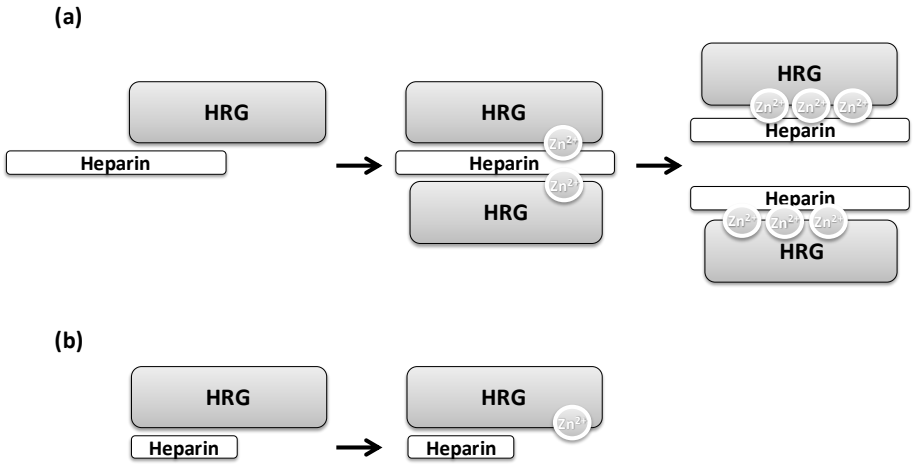

Figure 4.10. Schematic showing a possible mechanism behind the interaction between HRG and heparin and the effect of Zn^{2+}. (a) First, a heparin molecule tethers to HRG at either its N1N2 or HRR domains. The binding of Zn^{2+} by HRG pulls the longer chain heparin into position (perhaps overlapping both regions involved in heparin binding) and facilitates the formation of the 1:2 heparin:HRG complex. As the Zn^{2+} levels increase, repulsion between the HRG molecules cause the return to the 1:1 complex. (b) Low molecular weight heparin is able to bind in the same initial manner. However, due to its shorter length, is unable to provide the template required to feel the effects of Zn^{2+} activated HRG.

However, this is stated with caution since the data here still does not fully decipher the binding mechanism. To do this, a further project would need to be undertaken which used isolated N1N2 and HRR domains (either recombinant or otherwise) to conduct heparin binding ITC studies. This would allow the binding mechanism to be broken down to respective exothermic and endothermic constituents and show how Zn^{2+} activates the HRR in this specific case, leading to the subsequent building up of the mechanism from the bottom up.

These data are significant since heparin is used in clinical practice as an anticoagulant, although there are some complications with its use (particularly for unfractionated heparin). Unfractionated heparin is plagued by a narrow therapeutic window and an unpredictable dose-response profile as well as other problems including the inability to promote inhibition of fibrin-bound thrombin and platelet-bound factor Xa and the potential to trigger heparin-induced thrombocytopenia. LMW heparins have a more predictable dose-response profile, but are still unable to inhibit fibrin-bound thrombin and platelet-bound factor Xa (Weitz, 1997; Hirsh *et al*., 2001). The fact that HRG is enhanced in its affinity for unfractionated heparin and not LMW heparin (by the influence of Zn^{2+}) could help explain the poor clinical predictability of the former compared to the latter. In cases where individuals have altered Zn^{2+} dynamics from normal (e.g. higher plasma fatty acids), a patient receiving unfractionated heparin treatment would show a dose-response profile differing from the expected due to the fact that HRG is able to compete and bind for the heparin molecules against the intended target, antithrombin.

Thrombin activation by HRG following fatty acid induced Zn^{2+} release

Previous studies have demonstrated that fatty acid binding to bovine serum albumin triggers changes in its ability to bind Zn^{2+} to alter the speciation of this metal in plasma (Lu *et al*., 2012). Here, similar experiments were conducted, but used human albumin in place of bovine albumin to examine whether the same process occurs with the human protein. ITC experiments were performed with HSA (50 µM), loaded with increasing molar equivalents of myristic acid (0-250 µM myristic acid, corresponding to 0-5 molar equivalents respectively) being titrated with $ZnCl_2$ (1.5 mM). Myristic acid was used since it balances solubility issues with still being able to bind HSA in a manner which closely matches that of the more physiologically relevant stearic acid and palmitic acid (Curry *et al*., 1998) albeit slightly weaker (Spector, 1975). Figure 4.11 shows the resulting isotherms, where a trend in decreasing stoichiometry and a likely lowering of the affinity of HSA for Zn^{2+} are observed when myristic acid concentration increases. These salient features of the data confirm that as the level of fat associated with HSA progressively increases, its high affinity Zn^{2+} site is destructed as was observed in the BSA experiments.

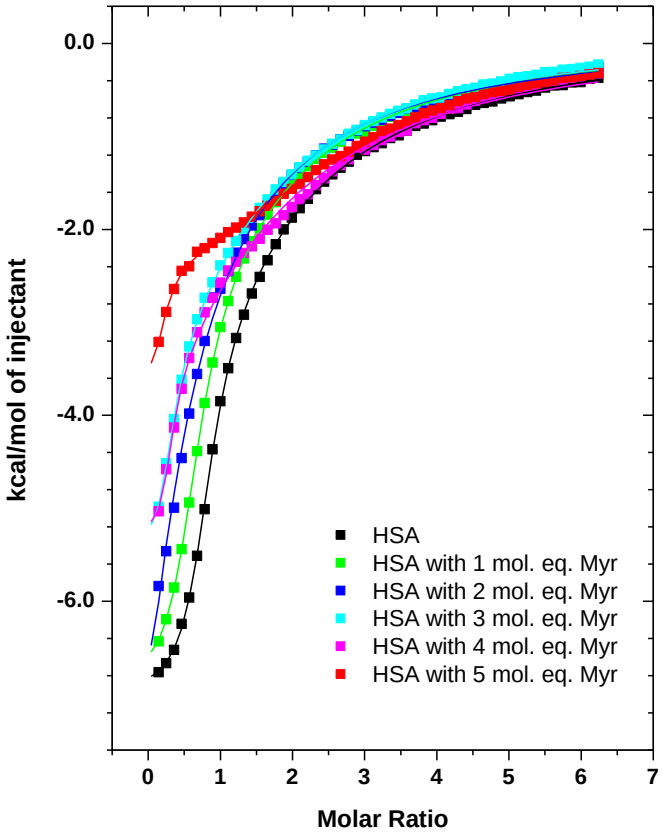

Figure 4.11. ITC experiments showing the interaction between HSA and Zn^{2+} under a range of myristic acid concentrations (0-5 molar equivalents). 50 µM HSA was loaded with the desired amount of myristic acid for 2 hours at 37 °C. The HSA sample was then titrated with 5 µl injections of a 1.5 mM $ZnCl_2$ solution for 55 injections. Experiments were conducted in buffer containing 50 mM Tris, 140 mM NaCl at pH 7.4. Raw data can be found in appendix A2.11-2.16.

The ITC data highlights the complexity of this system where two or three binding sites for one ligand and up to ten binding sites for another exist, making complete fitting of the curves difficult. However, tentative and simplified fitting approaches were taken in an attempt to relatively quantify the process. A sequential binding site model was used to fit two sites to obtain reliable quantitative data for the main Zn^{2+} site (K_a= 1.35 × 10^5 ± 2.5 × 10^4 M^{-1}, ΔH= -8166 $kJmole^{-1}$). These values were then used to fit a two site model to obtain a stoichiometry for the interaction as it progresses through increasing myristic acid levels. The stoichiometry data showed the main Zn^{2+} site disappear as observed in Figure 4.10. N decreased from N=0.95, 0.74, 0.55, 0.37, 0.35 to 0.09 as the myristic acid level increased. From these data, it is clear that the high affinity Zn^{2+} site disappears by 5 molar equivalent of myristic acid but it is uncertain what happens to the other sites. This level of fatty acid (which would equate to around 3 mM *in vivo*) is

observed in the clinical conditions described earlier. Also, it is likely that longer chain fatty acids, which would be more abundant *in vivo*, would induce this allosteric effect on HSA at concentrations lower than observed for myristic acid in these studies. A summary of the ITC data is presented in Table 4.1.

Table 4.1. Summary of the ITC data for selected interactions, showing the K_d where appropriate and the stoichiometry (N). IS is ionic strength; mol. eq. is molar equivalent.

Interaction	K_d (μM)	N
hHRG-Zn^{2+}	12.4	10.3 (± 0.1)
rHRG-Zn^{2+}	22.8	10.4 (± 0.1)
hHRG-Zn^{2+} at low IS	27.8	4.9 (± 0.01)
HSA-Zn^{2+} (Site A)	7.4	0.95 (± 0.01)
HSA-Zn^{2+} (Site A) + 1 mol. eq. Myr	-	0.74 (± 0.01)
HSA-Zn^{2+} (Site A) + 2 mol. eq. Myr	-	0.55 (± 0.01)
HSA-Zn^{2+} (Site A) + 3 mol. eq. Myr	-	0.37 (± 0.02)
HSA-Zn^{2+} (Site A) + 4 mol. eq. Myr	-	0.35 (± 0.02)
HSA-Zn^{2+} (Site A) + 5 mol. eq. Myr	-	0.09 (± 0.01)

Having clearly established that the fatty acid induced allosteric modulation of HSA severely hinders its native ability to bind Zn^{2+}, an approach was established to determine whether this would be likely to impact upon HRG function. An *in vitro* assay was developed based upon HRG's ability to neutralise heparin and inhibit thrombin (Fu and Horn, 2003). This system uses a colorimetric thrombin substrate (S2238), together

with thrombin, antithrombin III, heparin, human HRG, HSA, Zn^{2+} and different concentrations of lauric acid (C12). The reaction scheme is shown in Figure 4.3. The assay conditions were optimised to be as close to physiological as possible (concentrations of Zn^{2+}, serum albumin, HRG, antithrombin and thrombin were all within the normal physiological range). Due to complications arising from attempting to dissolve fatty acids at millimolar levels in aqueous buffers, lauric acid was chosen because of its more favourable solubility, but with the stipulation that any effects observed are likely to be increased in conditions where longer chain fats are present (e.g. *in vivo*), since they bind stronger to HSA and would disrupt the Zn^{2+} easier due to their increased chain length (Curry *et al*., 1998).

In this assay system, increasing concentrations of lauric were found to augment thrombin activity, with the highest activity observed in the presence of 3 mM lauric acid, which equates to 5 molar equivalents relative to HSA (Figure 4.12).

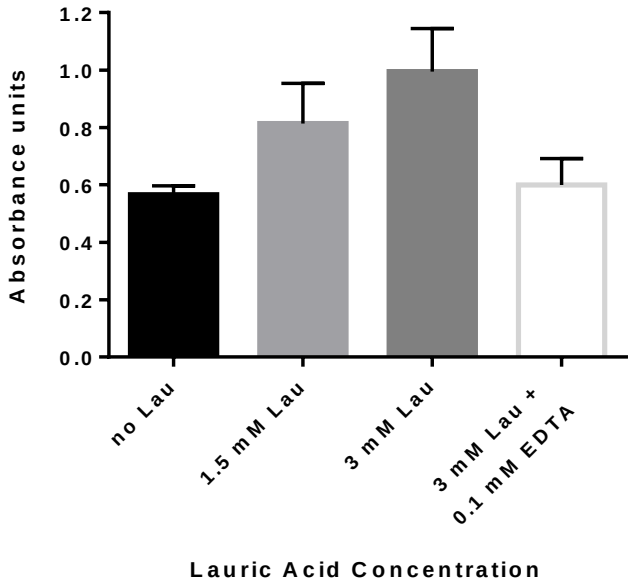

Figure 4.12. Examination of the fatty acid/Zn^{2+} switch and modulation of HRG functioning in the context of thrombin activation. Experiments were performed in triplicate. Data are representative of multiple experiments. Error bars presented are S.E.M. Statistical analysis performed was a two-tailed T-test. Serum albumin (600 μM) was pre-loaded with fatty acid by incubating with lauric acid (0, 1.5 or 3 mM) for 1 hour at 37 °C in 50 mM HEPES, 150 mM NaCl at pH 7.4 with $ZnCl_2$ (20 μM). HRG (1.5 μM), heparin (0.2 U/ml), antithrombin III (2 μM) and thrombin (0.5 nM) were mixed with the albumin sample and allowed to equilibriate for 1 hour at 37 °C. The thrombin substrate S-2238 was then added to the reaction and the reaction was detected after 20 minutes at 380 nm. Final concentrations are shown in parenthesis.

In this case the increase in activity was statistically significant (p=0.0376). The prothrombotic effect of the fatty acid was reversed by the including 0.1 mM EDTA to the system, confidently suggesting that Zn^{2+} is central to this phenomenon.

The concentrations of fatty acid used in this experiment reflect free fatty acid levels observed in certain pathological conditions (such as obesity, diabetes and cancer). It is important to note that other Zn^{2+}-binding molecules are present in the circulation (and absent from this simplified experimental system) that could bind at least some of the Zn^{2+} displaced from serum albumin. The relative abundance of HRG in plasma (low micromolar levels) and its affinity toward Zn^{2+} would suggest that it would be likely to bind a significant proportion of this. Furthermore, it is clear from our experiments that only a small proportion of the Zn^{2+} bound to serum albumin would need to be displaced (and bind HRG) to have a pronounced effect upon the affinity of HRG toward heparin. HRG has been shown to neutralise heparin at Zn^{2+} concentrations as low as 1.25 µM (Kluszynski *et al*., 1997), which is consistent with the enhanced binding between HRG and heparin observed in the study here. Conversely, it should also be noted that other factors (such as factor X) are absent from this system, which would usually also be under inhibition by antithrombin. That is to say, in this assay antithrombin solely inhibits thrombin since its other targets are unavailable, thereby effectively increasing the proportion of antithrombin associated with thrombin than would normally occur *in vivo*. It is also conceivable that some of the HRG, having been activated by Zn^{2+} in this manner, would modulate the other processes in which it is known to be involved through enhanced binding to its partners and so not all of it would be involved in the process described here. Despite the limitations that are obviously intrinsic to such a simplified system, the assay proved that activation of HRG by Zn^{2+} can occur under conditions of elevated fatty acid levels. The HRG in this system was then enhanced in its ability to compete for heparin against antithrombin, which led to increased thrombin activity.

Thus, the data presented here support the hypothesis that elevations in plasma fatty acid levels will negatively influence haemostatic function through changes in Zn^{2+} speciation and contribute to thrombotic pathologies in some individuals. Interestingly, recent clinical trials examining whether the chelation agent, EDTA, offered therapeutic benefit to patients with a history of heart disease found that a subgroup of patients who also had diabetes (and presumably elevated plasma fatty acid levels) benefited from the

treatment (Lamas *et al*., 2013; Escolar *et al*., 2014). The molecular basis for this effect remains unknown, but it is likely that the EDTA would chelate plasma Zn^{2+}, prevent its binding to HRG and return thrombin activity to normal levels.

The results of this study are compelling and provide further evidence to suggest that Zn^{2+}-dependent activation of HRG (following fatty acid binding to HSA) may play a role in the development of haemostatic complications in some individuals. Given that this mechanism would likely be targetable with existing therapeutics (such as chelation agents and heparins), it requires further investigation.

References

Ayala YM, Cantwell AM, Rose T, Bush LA, Arosio D, Di Cera E. Molecular mapping of thrombin-receptor interactions. *Proteins*. 2001, **45**, 107-116.

Bach R, Gentry R, Nemerson Y. Factor VII binding to tissue factor in reconstituted phospholipid vesicles: induction of cooperativity by phosphatidylserine. *Biochemistry*. 1986, **25**(14), 4007-4020.

Bartter FC, Steinfeld JL, Waldmann T, Delea CS. Metabolism of infused serum albumin in the hypoproteinemia of gastrointestinal protein loss and in analbuminemia. *Trans. Assoc. Am. Physicians*. 1961, **74**, 180–194.

[a]Bhattacharya AA, Grüne T, Curry S. Crystallographic analysis reveals common modes of binding of medium and long-chain fatty acids to human serum albumin. *J. Mol. Biol*. 2000, **303**, 721–732.

[b]Bhattacharya AA, Curry S, Franks NP. Binding of the general anesthetics propofol and halothane to human serum albumin. High resolution crystal structures. *J. Biol. Chem*. 2000, **275**, 38731–38738.

Björntorp P, Bergman H, Varnauskas E. Plasma free fatty acid turnover rate in obesity. *Acta Med Scand*. 1969, **185**(4), 351-356.

Blindauer CA, Harvey I, Bunyan KE, Stewart AJ, Sleep D, Harrison DJ, Berezenko S, Sadler PJ. Structure, properties, and engineering of the major zinc binding site on human albumin. *J. Biol. Chem*. 2009, **284**, 23116–23124.

Bode W, Turk D, Karshikov A. The refined 1.9-A X-ray crystal structure of D-Phe-Pro-Arg chloromethylketone- inhibited human α-thrombin: structure analysis, overall structure, electrostatic properties, detailed active-site geometry, and structure-function relationships. *Protein Sci*. 1992, **1**, 426-471.

Borza DB, Morgan WT. Histidine-proline-rich glycoprotein as a plasma pH sensor. Modulation of its interaction with glycosaminoglycans by pH and metals. *J. Biol. Chem*. 1998, **273**, 5493–5499.

Broze GJ Jr. Binding of human factor VII and VIIa to monocytes. *J Clin Invest*. 1982, **70**(3), 526-535.

Broze GJ Jr, Leykam JE, Schwartz BD, Miletich JP. Purification of human brain tissue factor. *J Biol Chem*. 1985, **260**(20), 10917-10920.

Burch MK, Blackburn MN, Morgan WT. Further characterization of the interaction of histidine-rich glycoprotein with heparin: evidence for the binding of two molecules of histidine-rich glycoprotein by high molecular weight heparin and for the involvement of histidine residues in heparin binding. *Biochemistry*. 1987, **26**, 7477-7482.

Carter WJ, Cama E, Huntington JA. Crystal structure of thrombin bound to heparin. *J Biol Chem*. 2005, **280**, 2745–2749.

Castaman G, Ruggeri M, Burei F, Rodeghiero F. High levels of histidine-rich glycoprotein and thrombotic diathesis. *Thromb. Res*. 1993, **69**, 297–305.

Charles MA, Fontbonne A, Thibult N, Claude JR, Warnet JM, Rosselin G, Ducimetière P, Eschwège E. High plasma nonesterified fatty acids are predictive of cancer mortality but not of coronary heart disease mortality: results from the Paris Prospective Study. *Am J Epidemiol*. 2001, **153**(3), 292-298.

Connolly GC, Khorana AA. Risk stratification for cancer-associated venous thromboembolism. *Best Pract Res Clin Haematol*. 2009, **22**(1), 35-47.

Corrigan JJ, Jeter MA, Bruck D, Feinberg WM. Histidine-rich glycoprotein levels in children: the effect of age. *Thromb. Res*. 1990, **59**, 681–686.

Curry S, Mandelkow H, Brick P, Franks N. Crystal structure of human serum albumin complexed with fatty acid reveals an asymmetric distribution of binding sites. *Nat. Struct. Biol*. 1998, **5**, 827–835.

Donnelly KL, Smith CI, Schwarzenberg SJ, Jessurun J, Boldt MD, Parks EJ. Sources of fatty acids stored in liver and secreted via lipoproteins in patients with nonalcoholic fatty liver disease. *J Clin Invest*. 2005, **115**(5), 1343-1351.

Engesser L, Kluft C, Briet E, Brommer EJ. Familial elevation of plasma histidine-rich glycoprotein in a family with thrombophilia. *Br. J. Haematol*. 1987, **67**, 355–358.

Escolar E, Lamas GA, Mark DB, Boineau R, Goertz C, Rosenberg Y, Nahin RL, Ouyang P, Rozema T, Magaziner A, Nahas R, Lewis EF, Lindblad L, Lee KL. The effect of an EDTA-based chelation regimen on patients with diabetes mellitus and prior myocardial infarction in the Trial to Assess Chelation Therapy (TACT). *Circ Cardiovasc Qual Outcomes*. 2014, **7**(1),15-24.

Failla ML, van de Veerdonk M, Morgan WT, Smith Jr. JC. Characterization of zinc-binding proteins of plasma in familial hyperzincemia. *J. Lab. Clin. Med*. 1982, **100**, 943–952.

Fu CL, Horn III MK. Histidine-rich glycoprotein plus zinc to neutralize heparin. *J Lab Clin Med*. 2002, **139**(4), 211-217.

Gálvez M, Moreno JA, Elósegui LM, Escanero JF. Zinc uptake by human erythrocytes with and without serum albumin in the medium. *Biol. Trace Elem. Res*. 2001, **84**, 45-56.

Gan ZR, Li Y, Chen Z, Lewis SD, Shafer JA. Identification of basic amino acid residues in thrombin essential for heparin-catalyzed inactivation by antithrombin III. *J Biol Chem*. 1994, **269**, 1301–1305.

Gorgani NN, Parish CR, Easterbrook-Smith SB, Altin JG. Histidine-rich glycoprotein binds to human IgG and C1q and inhibits the formation of insoluble immune complexes. *Biochemistry*, 1997, **36**, 6653–6662.

Gorgani NN, Parish CR, Altin JG. Differential binding of histidine-rich glycoprotein (HRG) to human IgG subclasses and IgG molecules containing kappa and lambda light chains. *J. Biol. Chem*. 1999, **274**, 29633–29640.

Goumakos W, Laussac JP, Sarkar B. Binding of cadmium(II) and zinc(II) to human and dog serum albumins - an equilibrium dialysis and Cd-113-NMR study. *Biochem. Cell Biol*. 1991, **69**, 809–820.

Guan X, Juarez JC, Qi X, Shipulina NV, Shaw DE, Morgan WT, McCrae KR, Mazar AP, Doñate F. Histidine-proline rich glycoprotein (HPRG) binds and transduces anti-angiogenic signals through cell surface tropomyosin on endothelial cells. *Thromb. Haemost*. 2004, **92**, 403–412.

Guha A, Bach R, Konigsberg W, Nemerson Y. Affinity purification of human tissue factor: interaction of factor VII and tissue factor in detergent micelles. *Proc Natl Acad Sci*. 1986, **83**(2), 299-302.

Guthans SL, Morgan WT. The interaction of zinc, nickel and cadmium with serum albumin and histidine-rich glycoprotein assessed by equilibrium dialysis and immunoadsorbent chromatography. *Arch. Biochem. Biophys*. 1982, **218**, 320–328.

He XM, Carter DC. Atomic structure and chemistry of human serum albumin. *Nature*, 1992, **358**, 209–215.

Hirsh J, Warkentin TE, Shaughnessy SG, Anand SS, Halperin JL, Raschke R, Granger C, Ohman EM, Dalen JE. Heparin and low-molecular-weight heparin: mechanisms of action, pharmacokinetics, dosing, monitoring, efficacy, and safety. *Chest*. 2001, **119**(1 Suppl), 64S-94S.

Hulett MD, Parish CR. Murine histidine-rich glycoprotein: cloning characterization and cellular origin. *Immunol. Cell Biol*. 2000, **78**, 280–287.

Hymowitz SG, Christinger HW, Fuh G, Ultsch M, O'Connell M, Kelley RF, Ashkenazi A, de Vos AM. Triggering cell death: the crystal structure of Apo2L/TRAIL in a complex with death receptor 5. *Mol Cell*. 1999, **4**, 563-571.

Ishiguro K, Kojima T, Kadomatsu K, Nakayama Y, Takagi A, Suzuki M, Takeda N, Ito M, Yamamoto K, Matsushita T, Kusugami K, Muramatsu T, Saito H. Complete antithrombin deficiency in mice results in embryonic lethality. *J Clin Invest*. 2000, **106**, 873-878.

[a]Jones AL, Hulett MD, Parish CR. Histidine-rich glycoprotein binds to cell-surface heparan sulfate via its N-terminal domain following Zn^{2+} chelation. *J. Biol. Chem*. 2004, **279**, 30114–30122.

[b]Jones AL, Hulett MD, Altin JG, Hogg P, Parish CR. Plasminogen is tethered with high affinity to the cell surface by the plasma protein, histidine-rice glycoprotein. *J. Biol. Chem*. 2004, **279**, 38267–38276.

Jones AL, Hulett MD, Parish CR. Histidine-rich glycoprotein: a novel adaptor protein in plasma that modulates the immune, vascular and coagulation systems. *Immunol. Cell Biol*. 2005, **83**, 106–118.

Jørgensen JR, Fitch MD, Mortensen PB, Fleming SE. In vivo absorption of medium-chain fatty acids by the rat colon exceeds that of short-chain fatty acids. *Gastroenterology*. 2001, **120**, 1152–1161.

Kassaar O, McMahon SA, Thompson R, Botting CH, Naismith JH, Stewart AJ. Crystal structure of histidine-rich glycoprotein N2 domain reveals redox activity at an interdomain disulfide bridge: implications for angiogenic regulation. Blood. 2014, **123**(12), 1948-1955.

Kleinfeld AM, Okada C. Free fatty acid release from human breast cancer tissue inhibits cytotoxic T-lymphocyte-mediated killing. *J Lipid Res*. 2005, **46**(9), 1983-1890.

Kluszynski BA, Kim C, Faulk WP. Zinc as a cofactor for heparin neutralization by histidine-rich glycoprotein. *J Biol Chem*. 1997, **272**(21), 13541-13547.

Koide T, Foster D, Yoshitake S, Davie EW. Amino acid sequence of human histidine-rich glycoprotein derived from the nucleotide sequence of its cDNA. *Biochemistry*, 1986, **25**, 2220–2225.

Koutsari C, Jensen MD. Thematic review series: patient-oriented research. Free fatty acid metabolism in human obesity. *J Lipid Res*. 2006, **47**(8), 1643-1650.

Kuhli C, Scharrer I, Koch F, Hattenbach LO. Recurrent retinal vein occlusion in a patient with increased plasma levels of histidine-rich glycoprotein. *Am. J. Opthamol*. 2003, **135**, 232–234.

Lamas GA, Goertz C, Boineau R, Mark DB, Rozema T, Nahin RL, Lindblad L, Lewis EF, Drisko J, Lee KL. Effect of disodium EDTA chelation regimen on cardiovascular events in patients with previous myocardial infarction: the TACT randomized trial. *J. Am. Med. Assoc*. 2013, **309**, 1241-1250.

Laudano AP, Doolittle RF. Studies on synthetic peptides that bind to fibrinogen and prevent fibrin polymerization. Structural requirements, number of binding sites, and species differences. *Biochemistry*. 1980, **19**(5), 1013-1019.

Leung LL. Interaction of histidine-rich glycoprotein with fibrinogen and fibrin. *J. Clin. Invest*. 1986, **77**, 1305–1311.

Li W, Johnson DJ, Esmon CT, Huntington JA. Structure of the antithrombin-thrombin-heparin ternary complex reveals the antithrombotic mechanism of heparin. *Nat Struct Mol Biol*. 2004, **11**, 857–862.

Lu J, Stewart AJ, Sadler PJ, Pinheiro TJT, Blindauer CA, Albumin as a zinc carrier: properties of its high-affinity zinc-binding site. *Biochem. Soc. Trans*. 2008, **36**, 1317-1321.

Mangani S, Meyer-Klaucke W, Moir AJ, Ranieri-Raggi M, Martini D, Raggi A. Characterization of the zinc-binding site of the histidine-proline-rich glycoprotein associated with rabbit skeletal muscle AMP deaminase. *J Biol Chem*. 2003, **278**(5), 3176-3184.

Masuoka J, Hegenauer J, Van Dyke BR, Saltman P. Intrinsic stoichiometric equilibrium constants for the binding of zinc(II) and copper(II) to the high affinity site of serum albumin. *J. Biol. Chem*. 1993, **268**, 21533–21537.

Masys DR, Bajaj SP, Rapaport SI. Activation of human factor VII by activated factors IX and X. *Blood*. 1982, **60**(5), 1143-1150.

Maynard JR, Heckman CA, Pitlick FA, Nemerson Y. Association of tissue factor activity with the surface of cultured cells. *J Clin Invest*. 1975, **55**(4), 814-824.

Morgan WT. Human serum histidine-rich glycoprotein. I. Interactions with heme, metal ions and organic ligands. *Biochim. Biophys. Acta*. 1978, **535**, 319–333.

Morgan WT. Interactions of the Histidine-Rich Glycoprotein of Serum with Metals. *Biochemistry*. 1981, **20**, 1054-1061.

Mori S, Shinohata R, Renbutsu M, Takahashi HK, Fang YI, Yamaoka K, Okamoto M, Yamamoto I, Nishibori M. Histidine-rich glycoprotein plus zinc reverses growth inhibition of vascular smooth muscle cells by heparin. *Cell Tissue Res*. 2003, **312**, 353–359.

Mosesson MW, Siebenlist KR, Meh DA. The structure and biological features of fibrinogen and fibrin. *Ann N Y Acad Sci*. 2001, **936**, 11-30.

Olson ST, Halvorson HR, Bjork I. Quantitative characterization of the thrombin-heparin interaction. Discrimination between specific and nonspecific binding models. *J Biol Chem*. 1991, **266**, 6342–6352.

Olson ST, Björk I, Sheffer R, Craig PA, Shore JD, Choay J. Role of the antithrombin-binding pentasaccharide in heparin acceleration of antithrombin-proteinase reactions. Resolution of the antithrombin conformational change contribution to heparin rate enhancement. *J Biol Chem*. 1992, **267**(18), 12528-12538.

Olson ST, Chuang YJ. Heparin activates antithrombin anticoagulant function by generating new interaction sites (exosites) for blood clotting proteinases. *Trends Cardiovasc Med*. 2002, **12**, 331-338.

Pedersen AH, Lund-Hansen T, Bisgaard-Frantzen H, Olsen F, Petersen LC. Autoactivation of human recombinant coagulation factor VII. *Biochemistry*. 1989, **28**(24), 9331-9336.

Petitpas I, Grüne T, Bhattacharya AA, Curry S. Crystal structures of human serum albumin complexed with monounsaturated and polyunsaturated fatty acids. J. Mol. Biol., 314 (2001), pp. 955–960.

Pineda AO, Cantwell AM, Bush LA, Rose T, Di Cera E. The thrombin epitope recognizing thrombomodulin is a highly cooperative hot spot in exosite I. *J Biol Chem*. 2002, **277**, 32015-32019

Previtali E, Bucciarelli P, Passamonti SM, Martinelli I. Risk factors for venous and arterial thrombosis. *Blood Transfus*. 2011, **9**(2), 120-138.

Reaven GM, Hollenbeck C, Jeng CY, Wu MS, Chen YD. Measurement of plasma glucose, free fatty acid, lactate, and insulin for 24 h in patients with NIDDM. *Diabetes*. 1988, **37**(8), 1020-1024.

Rao LV, Rapaport SI. Activation of factor VII bound to tissue factor: a key early step in the tissue factor pathway of blood coagulation. *Proc Natl Acad Sci*. 1988, **85**(18), 6687-6691.

Rowe DJ, Bobilya DJ. Albumin facilitates zinc acquisition by endothelial cells, *Proc Soc Exp Biol Med*., 2000, **224**(3), 178-186

Ruggeri ZM, Zimmerman TS. von Willebrand factor and von Willebrand disease. *Blood*. 1987, **70**(4), 895-904.

Sadler PJ, Viles JH. ^{1}H and ^{113}Cd NMR investigations of Cd^{2+} and Zn^{2+} binding sites on serum albumin: competition with Ca^{2+}, Ni^{2+},Cu^{2+},and Zn^{2+}, *Inorg. Chem*. 1996, **35**, 4490-4496.

Spector AA. Fatty acid binding to plasma albumin. *J Lipid Res*. 1975, **16**(3), 165-179.

Rydel TJ, Tulinsky A, Bode W, Huber R. Refined structure of the hirudin-thrombin complex. *J Mol Biol*. 1991 **221**, 583-601.

Saigo K, Shatsky M, Levitt LJ, Leung LLK. Interaction of histidine-rich glycoprotein with human T lymphocytes. *J. Biol. Chem*. 1989, **264**, 8249–8253.

Sakai T, Lund-Hansen T, Paborsky L, Pedersen AH, Kisiel W. Binding of human factors VII and VIIa to a human bladder carcinoma cell line (J82). Implications for the initiation of the extrinsic pathway of blood coagulation. *J Biol Chem*. 1989, **264**(17), 9980-9988.

Sarkar B. Metal-protein interactions in transport, accumulation, and excretion of metals. *Biol. Trace Elem. Res*. 1989, **21**, 137–144.

Savage B, Ruggeri ZM. Selective recognition of adhesive sites in surface-bound fibrinogen by glycoprotein IIb-IIIa on nonactivated platelets. *J Biol Chem*. 1991, **266**(17), 11227-11233.

Sheehan JP, Sadler JE. Molecular mapping of the heparin-binding exosite of thrombin. *Proc Natl Acad Sci*. 1994, **91**, 5518-5522.

Smith KT, Failla ML, Cousins RJ. Identification of albumin as the plasma carrier for zinc absorption by perfused rat intestine. *Biochem. J*. 1979, **184**, 627–633.

Smith GD, Ciszak E, Pangborn W. A novel complex of a phenolic derivative with insulin: structural features related to the T-R transition. *Protein Sci*. 1996, **5**, 1502-1511.

Stewart AJ, Blindauer CA, Berezenko S, Sleep D, Sadler PJ. Interdomain zinc site on human albumin. *Proc. Natl. Acad. Sci*. 2003, **100**, 3701–3706.

Stewart AJ, Blindauer CA, Sadler PJ. Plasma fatty acid levels may regulate the Zn^{2+}-dependent activities of histidine-rich glycoprotein. *Biochimie*. 2009, **91**(11-12), 1518-1522.

Stone SR, Le Bonniec BF. Inhibitory mechanism of serpins. Identification of steps involving the active-site serine residue of the protease. *J Mol Biol*. 1997, **265**, 344–362.

Streusand VJ, Björk I, Gettins PG, Petitou M, Olson ST. Mechanism of acceleration of antithrombin-proteinase reactions by low affinity heparin. Role of the antithrombin binding pentasaccharide in heparin rate enhancement. *J Biol Chem*. 1995, **270**(16), 9043-9051.

Sugio S, Kashima A, Mochizuki S, Noda M, Kobayashi K. Crystal structure of human serum albumin at 2.5 Å resolution. *Protein Eng*. 1999, **12**, 439–446.

Tracy PB, Nesheim ME, Mann KG. Coordinate binding of factor Va and factor Xa to the unstimulated platelet. *J Biol Chem*. 1981, **256**(2), 743-751.

Tsiang M, Jain AK, Gibbs CS. Functional requirements for inhibition of thrombin by antithrombin III in the presence and absence of heparin. *J Biol Chem*. 1997, **272**, 12024–12029.

van Boven HH, Lane DA. Antithrombin and its inherited deficiency states. *Semin Hematol*. 1997, **34**, 188-204.

Vanwildemeersch M, Olsson AK, Gottfridsson E, Claesson-Welsh L, Lindahl U, Spillmann D. The anti-angiogenic His/Pro-rich fragment of histidine-rich glycoprotein binds to endothelial cell heparan sulfate in a Zn^{2+}-dependent manner. *J Biol Chem*. 2006, **281**, 10298-10304.

Walz DA, Bacon-Baguley T, Kendra-Franzak S, DePoli P. Binding of thrombospondin to immobilized ligands: specific interaction with fibrinogen, plasminogen, histidine-rich glycoprotein, and fibronectin. Semin. *Thromb. Hemost*. 1987, **13**, 317–325.

Weitz JI. Low-molecular-weight heparins. *N Engl J Med*. 1997, **337**(10), 688-698.

Wilcox JN, Smith KM, Schwartz SM, Gordon D. Localization of tissue factor in the normal vessel wall and in the atherosclerotic plaque. *Proc. Natl. Acad. Sci*. 1989, **86**(8), 2839-2843.

Wildgoose P, Kisiel W. Activation of human factor VII by factors IXa and Xa on human bladder carcinoma cells. *Blood*. 1989, **73**(7), 1888-1895.

Ye J, Rezaie AR, Esmon CT. Glycosaminoglycan contributions to both protein C activation and thrombin inhibition involve a common arginine-rich site in thrombin that includes residues arginine 93, 97, and 101. *J. Biol. Chem.* 1994, **269**, 17965–17970.

Chapter 5

Identification of novel metal binding sites on albumin

This chapter aims to look closer at the metal binding properties of human serum albumin (HSA), by attempting to locate the secondary Zn^{2+} binding site. Typically, HSA will complex approximately 80% of all plasma zinc (Foote and Delves, 1984), making it the major zinc binding protein in plasma (Cousins, 1986). HSA has been shown to modulate zinc uptake into cells endothelial cells (Pattison and Cousins, 1986; Gálvez *et al*., 2001), via a receptor-mediated endocytosis pathway (Rowe and Bobilya, 2000). Additionally, cases of familial hyperzincaemia seem to be a consequence of increased zinc binding to HSA (Failla *et al*., 1982).

In addition to Zn^{2+}, HSA has been shown to bind an assortment of essential and toxic metal ions, including Ca^{2+}, Cd^{2+}, Co^{2+}, Cu^{2+} and Ni^{2+} (Giroux and Schoun, 1981; Martins and Drakenberg, 1982; Goumakos *et al*., 1991; Vidal *et al*., 1992; Masuoka *et al*., 1993; Masuoka and Saltman, 1994; Sadler and Viles, 1996; Ohyoshi *et al*., 1999; Zhang and Wilcox, 2002). Despite a lack of detailed structural information regarding metal coordination to HSA, seven different sites have been described: the N-terminal copper and nickel-binding (ATCUN) motif at the N-terminus which is the primary site for Cu^{2+} and Ni^{2+} (Harford and Sarkar, 1997); site A, the primary Zn^{2+}-binding site that also binds other divalent metal ions (Bal *et al*., 1998); site B, the unknown site which displays a high affinity towards Cd^{2+}, but is likely to be a secondary Zn^{2+} site (Giroux and Schoun, 1981; Goumakos *et al*., 1991; Sadler and Viles, 1996); and the free thiol group at Cys34 which binds heavier soft ions such as Au^{2+} (Christodoulou *et al*., 1994) and Pt^{2+} (Esposito and Najjar, 2002). Lastly, Ca^{2+} is known to be transported by HSA in the plasma (Kragh-Hansen and Vorum, 1993), and a recent crystal structure of bovine albumin co-crystallised with Ca^{2+} revealed the presence of three binding sites (Majorek *et al*., 2012).

N-terminal copper and nickel-binding (ATCUN) motif

The ATCUN motif is characterised by a histidine residue at position three of an amino acid chain, as observed for most serum albumins and other metal binding proteins (Harford and Sarkar, 1997). This binding site is especially suitable for metal ions that

have a desire for square-planar or tetragonal coordination spheres, and provides four coordinating nitrogen ligands, including the imidazole nitrogen of His3, the N-terminal amino group and two deprotonated backbone amide nitrogens. The ATCUN motif has been shown to have a very high affinity for Cu^{2+}, with a dissociation constant in the picomolar region (Rózga *et al*., 2007), and a low micromolar dissociation constant for Ni^{2+} (Sokołowska *et al*., 2002). This high affinity for Cu^{2+} makes HSA one of the largest pools of Cu^{2+} in plasma after ceruloplasmin, even though only 2% of the ATCUN site is populated with Cu^{2+} (Linder and Hazegh-Azam, 1996). Theoretically, because of the residues involved in forming the ATCUN site, it could also bind other metals such as Zn^{2+}, Cd^{2+} and Co^{2+} but this has not been observed experimentally. The Co^{2+} binding is a current controversial topic (Bar-Or *et al*., 2001, 2008; Mothes and Faller, 2007), as was discussed in Chapter 1.

Site A

The term "site A" originates from $^{111/113}Cd^{2+}$ NMR experiments where the addition of $^{111/113}Cd^{2+}$ to HSA resulted in two peaks in the NMR spectra; one with a chemical shift of around 130 ppm (site A) and the other with a chemical shift of around 30 ppm (site B) (Martins and Drakenberg, 1982; Goumakos *et al*., 1991; Sadler and Viles, 1996). $^{111/113}Cd^{2+}$ NMR provides details regarding the binding environment of the metal ion (Oz *et al*., 1998), and in this case showed two nitrogen donors and two oxygen donors were likely to be involved in the binding site. Inspecting the published X-ray crystal structures of HSA showed that two histidine ligands in close proximity to potential oxygen donors are only found in the region involving His67 and His247. Site directed mutagenesis of His67 to alanine had a major effect on site A, strongly suggesting that His67 may indeed be involved in metal binding to this site (Stewart *et al*., 2003). Site A is located at the domains I and II interface, where domain I provides His67 and Asn99 from, and domain II provides His247 and Asp249. In all X-ray structures of fatty acid free HSA, this site appears essentially preformed. A fifth ligand has been suggested as a water molecule, which can be replaced by Cl^- at higher chloride concentrations (Stewart *et al*., 2003). Site A is the preferred site for Zn^{2+} and one of two for Cd^{2+} (Martins and Drakenberg, 1982; Goumakos *et al*., 1991; Blindauer *et al*., 2009), although binding of Cd^{2+} to this site in HSA is not likely to be relevant under normal physiological conditions. Other metals such as Cu^{2+} and Ni^{2+} have also been shown to bind to this site (Sadler and Viles, 1996; Bal *et al*., 1998).

Site B

The location of site B is as yet unidentified. In NMR studies it correspond to a $^{111/113}Cd^{2+}$ peak with a chemical shift of about 30 ppm, indicating the involvement of not more than one nitrogen donor (Martins and Drakenberg, 1982; Goumakos *et al*., 1991; Sadler and Viles, 1996; Oz *et al*., 1998). Mutant studies involving His39 showed no difference in the Cd^{2+} NMR spectrum (Stewart *et al*., 2003), meaning it is unlikely that this residue forms part of the site. Site B has a lower affinity for Zn^{2+} compared with site A, and could be the primary site for Mn^{2+} ions (Fanali *et al*., 2012).

Cys34

HSA in plasma exists as a heterogeneous mixture due to the existence of Cys34. HSA contains 35 cysteine residues, of which 34 are involved in the 17 disulfide bridges that interconnect α-helices and maintain the tertiary structure of the molecule (Peters, 1985). Cys34 in HSA contains the only free thiol group and this can undergo oxidation reactions *in vivo*. Thus, Cys34 is reactive towards glutathione or cysteine (Sogami *et al*., 1986), is involved in disulphide dimerisation of HSA molecules and can be nitrosylated (Stamler *et al*., 1992). The HSA molecules which preserve the free thiol form of Cys34 can bind metal ions at this position. It is most likely that this site is specific for metal ions that can bind to the protein effectively through a single bond such as the heavier Au^{2+} and Pt^{2+} ions (Isab and Shaw, 1990; Ivanov *et al*., 1998).

Ca^{2+} binding sites

Recently, a structure of bovine albumin was solved with Ca^{2+} bound to the molecule (Majorek *et al*., 2012). This was the first structure of bovine serum albumin and the first albumin structure with a metal ion bound. Although the interaction between albumin and Ca^{2+} is relatively weak with a dissociation constant in the high micromolar range (Kragh-Hansen and Vorum, 1993), around 45% of the 2.4 mM of Ca^{2+} circulating in plasma is coordinated to albumin (Peters, 1995). Additionally it has been suggested that albumin mirrors this binding with Mg^{2+}. Approximately 45% of the 1.2 mM Mg^{2+} is also bound to albumin. This would suggest that there are three sites for these ions, as was observed in the Ca^{2+} bound crystal structure.

All three Ca^{2+} binding sites are found in domain I (Figure 5.1). The first site involves residues Glu6, Glu243, Asp248 and Glu251. The second site involves residues Asp13,

Asp254 and Asp258. The third site includes Ser109 and Asp111. Water molecules provided additional ligands in all cases.

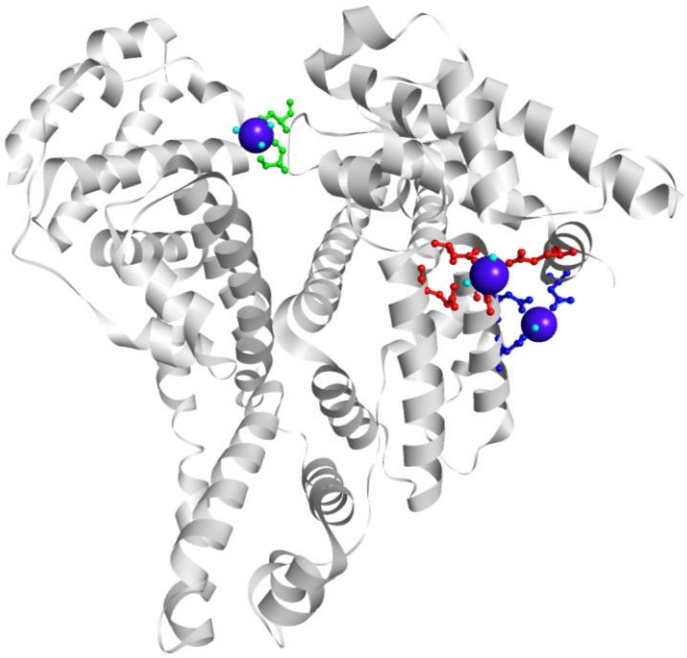

Figure 5.1. Crystal structure of bovine serum albumin complexed with three Ca^{2+} ions (PDB code: 3V03). Site one is highlighted with the residues in red (Glu6, Glu243, Asp248 and Glu251), site two is highlighted in blue (Asp13, Asp254 and Asp258) and site 3 in green (Ser109 and Asp111). Ca^{2+} ions are coloured purple and water molecules are coloured cyan. The peptide backbone is highlighted grey. Figure drawn using Accelrys.

Locating metal binding sites on HSA

The study here aims to locate site B and any other metal binding sites on HSA by site directed mutagenesis and use of isothermal titration calorimetry to monitor binding energetics between HSA and metals. Figure 5.2 shows putative sites for metal binding based on identified clusters of nitrogen and oxygen donating amino acids within close proximity of each other.

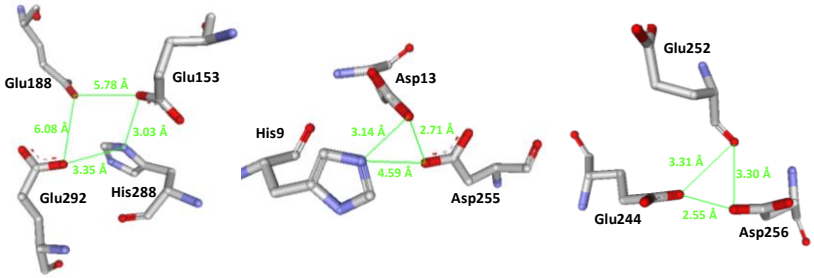

Figure 5.2. Putative novel metal binding sites on HSA (PDB file: 1AO6). Figure drawn using Accelrys.

To probe this experimentally, a eukaryotic recombinant system was developed using the yeast *K. lactis* to express and secrete the proteins of interest. HSA mutants H9A and H288A were constructed to determine additional putative Zn^{2+} binding sites, since they would require the presence of nitrogen donors (most probably histidine). E252, D255A and D256A mutants were constructed to probe Zn^{2+} binding to HSA (the numbering of residues differs by one between human and bovine albumin). The position of each of these residues in the HSA molecule is shown in Figure 5.3.

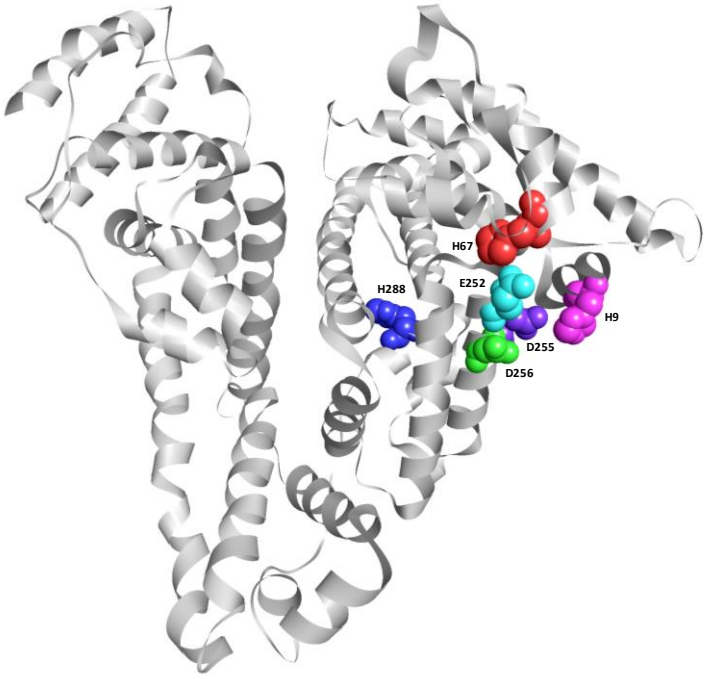

Figure 5.3. Crystal structure of human serum albumin (PDB code: 1AO6), showing the positions of the amino acid residues which were mutated to alanine in this study. The peptide backbone is highlighted grey. Figure drawn using Accelrys.

α-Fetoprotein (AFP)

AFP is the main protein of foetal plasma (Bergstrand and Czar, 1956; Ruoslahti and Seppälä, 1972) and shares 39.4% sequence identity with HSA. AFP is produced by the liver and exists at concentrations ranging between 1–10 mg/ml in the foetus, but it decreases sharply down to trace amounts after birth and is replaced by HSA as the major component of plasma (Bergstrand and Czar, 1956; Ruoslahti and Seppälä, 1972; Deutsch, 1991). It has been observed that the changes in serum AFP levels during pregnancy can lead to the development of several embryonic disorders including Down's syndrome and spina bifida (Seppälä and Ruoslahti, 1973; Brock *et al.*, 1975;

Seppälä, 1975; Ruoslahti, 1979; Deutsch, 1991) and an increase in AFP level in adult plasma correlates with the occurrence of pathological conditions such as hepatocellular carcinoma and several others (Abelev, 1971; Okuda *et al*., 1975; Yoshiki *et al*., 1976). This correlation allows the clinician to use AFP as a diagnostic marker in these cases. The assumed function of AFP is that of a transporter molecule, essentially mimicking the role of HSA (in adult serum) during foetal development. It has been observed that AFP interacts with fatty acids (Parmelee *et al*., 1978; Hsia *et al*., 1980), where each molecule of AFP can contain two or three molecules of polyunsaturated fatty acids, having a high affinity for arachidonic (C20:4) and docosahexaenic (C22:6) acids (Parmelee *et al*., 1978; Nagai *et al*., 1982). AFP also binds Cu^{2+} and Ni^{2+} ions (Aoyagi *et al*., 1978) and has a high affinity for bilirubin (Ruoslahti *et al*., 1979). However, there is a significant functional divergence between AFP and HSA. HSA is known to bind many more ligands, but it usually shows a dissociation constant for these in the low micromolar range, whereas AFP shows stronger binding to its ligands (with dissociation constants in the nanomolar range) (Deutsch, 1991). Additionally, unlike HSA, for which the transport and storage of ligands represents the major function, AFP participates in other physiological processes, such as immune suppression (Yachnin, 1983). AFP has also been stated to play a role in the sexual differentiation of the foetal brain, based on its ability to bind estrogens (Soloff *et al*., 1972; Uriel *et al*., 1972; Nishi *et al*., 1991), thereby protecting the development from the masculinising effects of the hormone. However, only rat and mouse AFP have been shown to bind estradiol and the specific estradiol binding region on the rat and mouse variants is absent in human AFP (Nishi *et al*., 1991).

The homology between AFP and HSA has led to the understanding that AFP will be similar in structure to that of the much studied HSA molecule, but detailed studies on AFP have yet to be conducted. Thus, AFP has been suggested to be composed of three domains and due to 15 disulfide bridges, also takes the ‘heart-shape’ formation as observed in albumins (Barker, 1988). However, the relationship between structure and function of AFP is thought to be more complex than that which has been characterised for HSA. HSA is known to go through strict structural changes in response to pH changes that are fully reversible and non-reliant on ligand binding (Peters, 1996). In the case of AFP, samples purified from the same source but by different methods show a heterogeneity which it has been proposed is due to the stripping of natural ligands

during preparation processes which can ultimately lead to irreversible denaturation of the protein (Uversky *et al*., 1997a; Tomashevski *et al*., 1998).

Hence it is thought that ligands may play a role in maintaining the rigid spatial structure of AFP. It has been suggested that AFP represents a 'molten globule' conformation in its ligand-free form. This means that it will possess compact native secondary structure, but without a unique three-dimensional tertiary structure (Uversky *et al*., 1997b). This semi-rigid molten globule model preserves the main features of the native folding pattern, while allowing for much greater internal rotations, which could bestow the protein molecule with the ideal qualities necessary for living in a cell due to the range of conditions that are encountered. A rigid native protein molecule undergoing a structural transformation into a molten globule state is associated with a substantial increase in flexibility which could prove to be a functional mechanism (i.e. for the release of hydrophobic ligands) (Narizhneva and Uversky, 1997). This molten globule state (or ligand-free) AFP has been postulated to be a functional form of AFP, with regards to its immunomodulating effects.

The immunosuppressive ability of AFP observed *in vitro* is known to be susceptible to variations (Lester *et al*., 1977) and depends on the origin and purification procedure (Lester *et al*., 1977; Yachnin and Lester, 1977; Goeken and Thompson, 1977). Also, it has been observed that AFP purified from serum is capable of immunosuppression, but the source serum (containing the same AFP levels) does not possess the same capability (Yachnin, 1983). Also, the immune-suppression strength of AFP preparations is higher when cord serum is subjected to acidic conditions during ion-exchange protocols (Goeken and Thompson, 1977), which would provide conditions inducing protein denaturation (Uversky *et al*., 1995).

The study here aims to develop a viable expression and purification system for recombinant AFP, which includes the proper conformation of AFP, to be used in fundamental binding studies and potential structural characterisation.

Methods

Materials

Image clones containing full length human serum albumin (HSA) and human α-fetoprotein (AFP) coding sequences was purchased from Source Lifesciences. All primers used during cloning reactions were purchased from Eurofins MWG Operon and are described in Appendix A3.1. *K. lactis* Protein Expression Kit (New England Biolabs, USA) was used to engineer recombinant proteins.

Expression using *Kluyveromyces lactis* and the pKLAC2 plasmid

Recombinant protein expression of wild type-HSA (wtHSA) and the albumin mutants H9A, H67A, E252A, D255A, D256A and H288A, as well as AFP, was attempted using the *K. lactis* Protein Expression Kit (NEB, E1000) which included the *K. lactis* strain GG799 and the plasmid pKLAC2. The pKLAC2 plasmid contains a LAC4 promoter, LAC4 transcription terminator and encodes β-lactamase (Ap^R) as well as the pMB1 origin (ori) to allow for propagation in *E. coli*. The plasmid also contains the *K. lactis* α-mating factor secretion leader sequence (α-MF) which can be used if desired to allow the protein to be secreted into the growth media. To provide a means of selection, the yeast ADH1 promoter drives expression of an acetamidase marker gene, which allows selection to be performed on a carbon based medium where the only nitrogen source is acetamide. The plasmid can be digested with SacII or BstXI to create a linear DNA fragment capable of integrating into the native LAC4 promoter region of the *K. lactis* genome.

Construction of expression vectors

HSA coding sequences were amplified using the Expand Long Template PCR kit with buffer system 1 (Roche) and cloned into pKLAC2 (Figure 5.4) using XhoI/NotI restriction sites. The primers used in this, and all following experiments, are shown in Appendix A3.1. Vector and insert DNA (1 µg) were digested with NotI (20 units) and XhoI (20 units) at 37 °C for 2 hours. The reaction also contained BSA (100 µg/ml), NEBuffer 3 and was made up to 50 µl with ddH_2O. Cloning reactions were completed by ligation of the inserts in to the restriction enzyme treated plasmid at a ratio of

approximately 2.5:1, using T4 DNA ligase (6 units) in reaction buffer (5 µl) at 16 °C overnight.

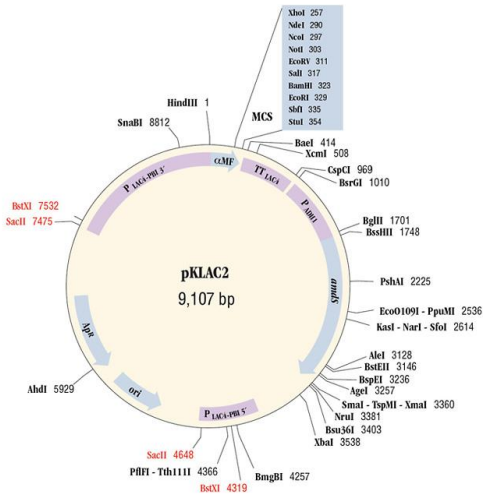

Figure 5.4. The *K. lactis* integrative expression vector pKLAC2. The multiple cloning site (MCS) is the location of gene insertion, which is within the same translational reading frame as the α-mating factor (α-MF) native *K. lactis* leader sequence. *K. lactis* expression is initiated by the $P_{LAC4\text{-}PBI}$ promoter. The promoter ADH1 drives the expression of an acetamidase gene (amdS), allowing for the selection of colonies on acetamide medium. ORI is the origin of replication.

Site Directed Mutagenesis of Albumin

Point mutations within the coding sequence of human albumin (corresponding to putative metal sites in the expressed protein) were generated via a PCR-based method using the Quikchange kit (Stratgene), however VELOCITY DNA Polymerase enzyme (Bioline) was used instead of the Pfu Turbo enzyme (which is usually used as part of the kit). Reactions were set up using the primers shown in Appendix A3.1 (125 ng each), 2 mM dNTP mix, HSA-pKLAC2 template DNA (25 ng), reaction buffer, Quick Solution and polymerase enzyme (2.5 units). The final volume of each reaction was made up to 50 µl with ddH_20. The DNA was sequenced commercially to confirm integration of correct mutations and to show no additional *de novo* mutations occurred (DNA Sequencing & Services, Dundee) using the primers shown in Appendix A3.1.

Media

Liquid cultures of the yeast strain were grown in YPGal medium (1% yeast extract, 2% Bacto™ Peptone, 2% galactose) or YPGlu (1% yeast extract, 2% Bacto™ Peptone, 2% glucose). Solid yeast carbon-based media (YCB) with 5 mM acetamide (New England

Biolabs, B9017S) was used to grow colonies under selective conditions. *K. lactis* cells were grown to an OD_{600} > 30 (typically 4-5 days) in YPGal unless otherwise stated.

Transformation of *K. lactis* GG799 cells

Linearisation of pKLAC2 must precede the integrative transformation of *K. lactis* GG799 cells. This is required to allow integration of the desired gene into the *K. lactis* genome at the LAC4 locus. Plasmid DNA (pKLAC2) containing the coding sequences of HSA (wildtype or mutants) or AFP (2 µg) were digested with SacII (20 units) in 1X NEBuffer 4 (50 µl) at 37 °C for 2 hours. This gives rise to two fragements, one containing the expression cassette and the other containing the remainder of the pKLAC2 plasmid. It was not necessary to purify the digested fragment as only the expression cassette has the ability to integrate within the *K. lactis* genome. However, agarose gel electrophoresis was conducted to confirm the digestion, yielding the expression fragment at >10 kb and the remaining pKLAC2 DNA at 2.8 kb. Following this, the DNA was desalted using SOPE resin (EdgeBio).

Chemical transformation of *K. lactis* GG799 cells was achieved by incubating the linearised DNA (up to 1 µg in less than 15 µl) with the chemically competent *K. lactis* GG799 cells mixed with NEB Yeast Transformation reagent (620 µl) at 30 °C for 30 minutes. After incubation, the cell mixture was heat shocked at 37 °C for 1 hour. The cells were washed and resuspended in YPGlu (1 ml), transferred to a sterile culture tube and incubated with shaking at 30 °C for 4 hours. The cell mixture was resuspended in sterile PBS (1 ml). A dilution of the transformed cells (10 µl in 50 µl sterile H_2O) were spread onto YCB agar plates containing acetamide (5 mM) for selection of correctly integrated colonies. Colonies were picked and spotted onto fresh plates for further use.

Identification of integrated cells

Colonies containing the integrated albumin sequence were confirmed by PCR amplification of the yeast genomic DNA with integration primers 1 and 2 (singly integrated copies) or integration primers 2 and 3 (multiple integrated copies). Reactions were composed of the required primers (5 µl each), dNTP mix (0.2 mM), Green Go Taq® Flexi buffer (10 µl), $MgCl_2$ (2 mM), the yeast DNA (up to 1 µg) and Go Taq® DNA Polymerase (1.25 units). The volume was made up to 50 µl with ddH_2O.

The PCR reaction followed from isolating the yeast genomic DNA using a Yeast DNA Extraction Kit (Thermo) from single colonies grown on YCB agar plates containing acetamide (5 mM). A 1 mm^2 fraction of the colony was suspended in Y-PER (20 µl) to form a homogeneous mixture and incubated at 65 °C for 10 minutes. The cells were centrifuged (13 000 x g, 5 minutes) and resuspended in DNA Releasing Reagent A (16 µl) and DNA Releasing Reagent B (16 µl). The homogeneous mixture was then incubated at 65 °C for 10 minutes. Protein Removal Reagent (8 µl) was added into the mixture and inverted several times. The mixture was centrifuged (13 000 × g for 5 minutes) and the supernatant transferred to a new tube. Isopropyl alcohol (24 µl) and glycogen (1 µl) were added to precipitate the genomic DNA and to make the pellet visible; the mixture was inverted and then centrifuged (13 000 × g for 10 minutes). The supernatant was removed and the DNA pellet washed with 70% ethanol, before resuspension in sterile ddH_2O (5 µl).

Fermentation of yeast

Yeast colonies containing the desired insert were grown overnight in YPGlu medium at 30 °C, with shaking at 200 rpm, prior to fermentation. The starter culture was used to inoculate 3 L of YPGal media in a Fermac 231 fermenter (Electrolab, UK), which had been saturated with O_2. The fermenter culture was left to grow for 3 days within a pH range of 4.5 to 5.5, with stirring at 350 rpm. Cells were removed from the culture by centrifugation at 8,000 rpm for 45 minutes. The 3 L supernatant was concentrated using a PES membrane filter with a molecular weight cut-off of 30 kDa (Sartorius, UK).

Sodium dodecyl sulfate-polyacrylamide gel electrophoresis (SDS-PAGE)

SDS-PAGE was performed as described before (see Chapter 3).

After the desired separation had been achieved, the gels were stained either stained with coomassie, or were immediately transferred for Western Analysis. In the case of staining, gels were visualised by staining with coomassie solution (0.025% Coomassie Brilliant Blue R250, 40% methanol, 10% acetic acid) for 10 minutes, followed by destaining in boiling water.

Immunoblotting Western analysis

All blot module components (Invitrogen) were immersed in NuPAGE Transfer Buffer (Invitrogen) with methanol (20%) before arranging the apparatus. The PVDF membrane was soaked in methanol for 5 minutes, followed by water for 5 minutes. The module was arranged from the anode with: sponge pads/filter paper/gel/membrane/filter paper/sponge pads. The blot module was filled with transfer buffer and the transfer was conducted for 1 hour at 30 V.

Upon completion of the transfer, the blot module was disassembled and the membrane washed with methanol, then water. The membrane was blocked overnight at 4 °C in Tris-buffered saline (TBS) with 5% skimmed milk. The membrane was quickly rinsed and the incubation with the primary antibody was started. Recombinant albumin and its mutants were detected using an anti-HSA antibody raised in rabbit (Sigma, A0433), at 1:1000 dilutions in TBS + 1% skimmed milk and 0.5% Tween 20 for 1.5 hours at room temperature. The primary antibody was washed off with three washes of TBS containing 0.2% Tween 20 of 15 minutes each.

The membrane was incubated with alkaline phosphatase conjugated anti-rabbit secondary antibody (Sigma, A9919) at a dilution of 1:10,000 in TBS containing 5% skimmed milk and 0.5% Tween 20 for 1.5 hours at room temperature. After this time, the membrane was washed three times with TBS containing 0.2% Tween as before, followed by one wash with TBS then one wash with ultrapure water. Protein bands on the membrane were visualised using Western Blue reagent (Promega).

Purification

Recombinant HSA was purified using a HiTrap Blue HP column (GE Healthcare, UK), followed by size exclusion chromatography using a HiLoad Superdex-75 column (GE Healthcare, UK). All preparations were performed on an AKTA Purifier (GE Healthcare, UK). The HSA sample was equilibrated to 20 mM potassium phosphate at pH 7 and bound to the HiTrap Blue HP column, which had previously been equilibrated in the same buffer. After washing with this buffer, elution was achieved by applying 20 mM potassium phosphate, 1.5 M KCl at pH 7 over a gradient. Fractions containing recombinant HSA were pooled and further purified on a HiLoad Superdex-75 column,

which had been equilibrated in a desired buffer (typically 50 mM Tris, 140 mM NaCl at pH 7.4).

Recombinant AFP was purified using a HiTrap chelating column (GE Healthcare, UK) which was charged with copper sulfate. Binding of AFP was achieved using 20 mM sodium phosphate, 1 M NaCl at pH 7.2. After washing in the same buffer, elution was achieved by a one-step introduction of 20 mM sodium phosphate, 1 M NH_4Cl at pH 7.2. The NH_4Cl provides weak competitive binding to the column which is enough to displace AFP. Fractions containing recombinant AFP were pooled and further purified on a HiLoad Superdex-75 column, which had been equilibrated in the experimental buffer of choice.

Protein Concentration Determination

Protein concentration was determined as before (see Chapter 3). An extinction coefficient of 34445 M^{-1} cm^{-1} was used for HSA and 32830 M^{-1} cm^{-1} for AFP.

Isothermal Titration Calorimetry (ITC)

ITC experiments were carried out using either a VP-ITC instrument (MicroCal, USA) or iTC_{200} (GE Healthcare, UK) in 50 mM Tris, 140 mM NaCl, pH 7.4, at 25 °C. The titration ligand was added to the reaction buffer and the pH adjusted to 7.4 to match the buffer of the protein. Specific concentrations used in experiments are given in figure legends. The titration of estradiol into AFP included 1% DMSO in the buffer to facilitate estradiol dissolution. Solutions were degassed at 22 ºC for 15 minutes prior to running the experiment. Typical titrations on the VP-ITC performed were one 2 µl injection over 4 s followed by up to 55 injections of 5 µl over 10 s with an adequate interval of 240 s between injections to allow complete equilibration. The stirring speed was 307 rpm. Typical titrations on the iTC_{200} were an initial injection of 0.4 µl over 0.8 s followed by 18 injections of 2 µl over 4 s with an interval of 120 s between injections. Heats of dilution were accounted for with blank titrations performed by injecting ligand solution into reaction buffer and subtracting the averaged heat of dilution from the main experiment. Alternatively, in cases of saturated binding, blank titrations were omitted where the averaged residual signal of the last injections was used to determine the heat of dilution. Raw data were processed using MicroCal Origin software and data were

fitted using the same software. Raw data for the ITC experiments presented here can be found in Appendix 3. Plasma HSA was obtained from Sigma-Aldrich.

Results and discussion

Expression of recombinant albumin in *K. lactis*

To understand the metal binding properties of albumin, mutant albumins were expressed in *K. lactis* and investigated using ITC. Expression of HSA mutants was detected by Western analysis. Figure 5.5a shows analysis of the H288A mutant as an example of expression. All recombinant albumins (wtHSA, H9A, H67A, E252A, D255A, D256A and H288A) were subjected to the same protocol.

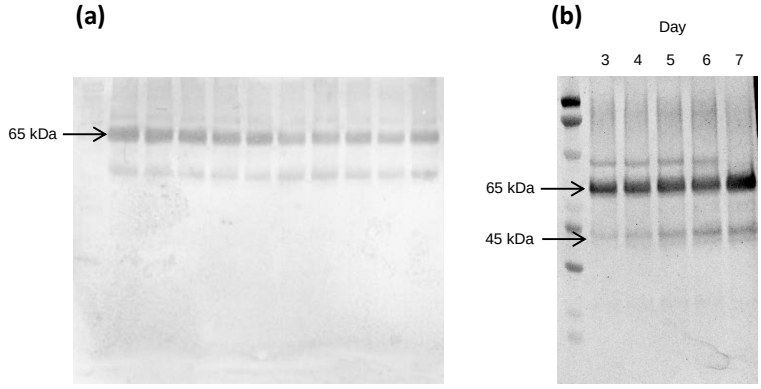

Figure 5.5. (a) Western analysis of the human albumin mutant H228A showing a major band at 65 kDa from 10 random *K. lactis* colonies. (b) Western analysis of the HSA mutant H288A from 3-7 days growth of *K. lactis*.

Ten *K. lactis* colonies were grown in 10 ml liquid cultures to evaluate expression levels. All yeast colonies showed a distinct band at 65 kDa relating to HSA. Coinciding with the mature H288A band is a band at around 45 kDa which was postulated to represent a digested fragment. *K. lactis* are known to secrete proteases and have membrane bound proteases which could interact with any secreted protein in the growth medium. Sleep *et. al.* (1990) made a similar observation in their work comparing the expression of HSA from *S. cerevisiae* using different secretion leader sequences. They found that the α-MF (the secretion signal used in our work) produced a truncated fragment of HSA for secretion and ruled out any degradation possibilities, but were unable to determine an exact cellular cause for its appearance. This pattern was reproducible for all recombinant HSA constructs. Before transforming the competent *K. lactis* cells, the DNA was sequenced to confirm the presence of the mutation. The Western analysis confirms the expression of recombinant HSA, and no *de novo* mutations were present.

In an effort to optimise HSA mutant secretion and purification, the H288A mutant expression was monitored over a period of 7 days in order to determine if there was a maximum level of expression over time (Figure 5.5b). The main band at 65 kDa shows very little alteration from 3 to 7 days. The truncated fragment at around 45 kDa displays a steady increase in secretion during the growth period. It was concluded that no significant advantage could be had by growing the yeast strains longer than 4-5 days.

With regards to recombinant AFP, since at the time we had no anti-AFP antibody, *K. lactis* colonies containing AFP were not subjected to Western analysis; instead they were subjected to purification and subsequent analysis by mass spectrometry.

Purification of recombinant HSA and AFP

Recombinant HSA was purified from culture medium using a HiTrap Blue column. This column contains the ligand Cibracon Blue F3G-A, which is known to bind albumin (Altintaş and Denizli, 2006). Following this, size exclusion chromatography was used to polish the sample (Figure 5.6). Typical protein yields were 1 mg/ml for shake flask cultures, and up to 20 mg for 3 L fermenter culture. The first step of the procedure provided a protein sample typically of 90% purity, which was then improved to >99% pure following the size exclusion step. All recombinant HSA constructs were isolated to this level of purity and used for experimental studies.

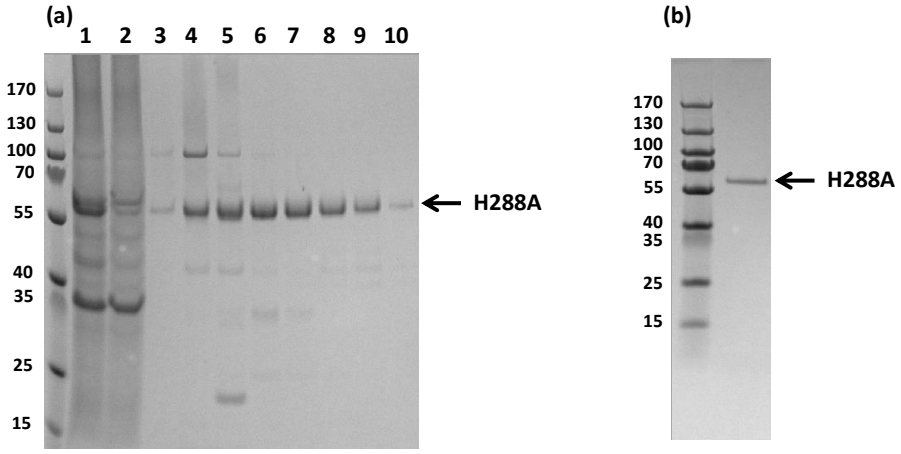

Figure 5.6. Example preparation of the recombinant HSA mutant H288A from *K. Lactis*. (a) SDS-PAGE analysis following the first step of purification on a HiTrap Blue column. Lane 1: media sample, lane 2: flow through from column, lanes 3-10: eluted HSA protein (b) SDS-PAGE analysis following the final size exclusion step, to yield a protein sample of a suitable quality for experimental work. Gels were visualised using Coomassie blue stain.

Recombinant AFP was purified using a Cu^{2+}-column, exploiting the natural affinity AFP has for Cu^{2+}. This step afforded two bands that eluted under the same conditions, which were then separated by size exclusion chromatography to yield a 99% pure AFP sample (Figure 5.7). The gel band was identified as AFP using mass spectrometry.

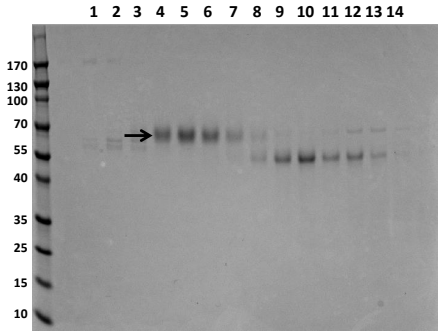

Figure 5.7. Preparation of recombinant AFP from *K. Lactis*. SDS-PAGE analysis of an AFP sample (marked with an arrow) can be seen in lanes 4-7 following Cu^{2+} affinity and size exclusion chromatography. Lanes corresponding to AFP were pooled and used for experimental studies. Gel was visualised using coomassie stain.

The structural integrity of AFP was determined by circular dichroism (CD), since there is a note of controversy regarding AFP preparations (Leong and Middelberg, 2006). Figure 5.8 shows the near-UV spectrum of AFP, which conforms to the shape previously reported indicating that the protein as expressed by *K. Lactis* is in at correctly folded conformation (Leong and Middelberg, 2006).

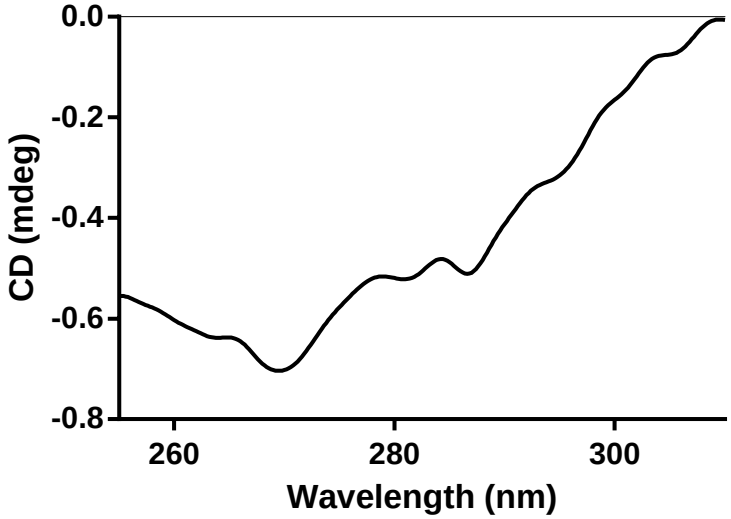

Figure 5.8. Near-UV CD spectra of recombinant AFP. Peaks in this region confirm the protein is in a native folded conformation.

Zn^{2+} binding studies on recombinant HSA mutants

The first step of these studies involved establishing that the properties of the recombinant HSA were comparable to that of native plasma-derived HSA, since although in theory they are the same protein, being derived from different sources could potentially affect binding abilities. To do this, both plasma HSA and recombinant wtHSA were subjected to identical ITC experiments with Zn^{2+} titrations (Figure 5.9).

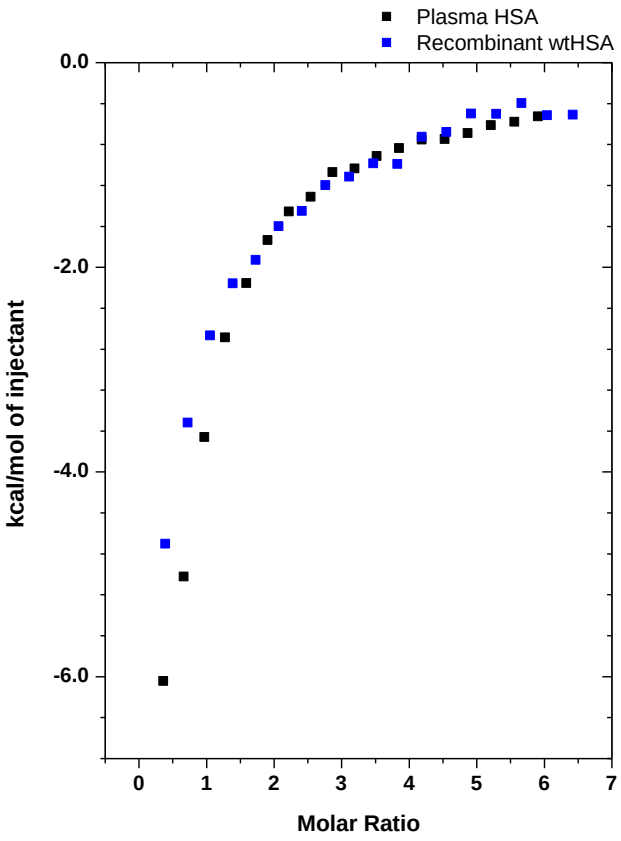

Figure 5.9. Comparison of the Zn^{2+} binding ability of recombinant and plasma derived HSA studied by ITC. 50 µM plasma HSA and 46 µM wtHSA were titrated with 1.5 mM $ZnCl_2$. The binding pattern is very similar with only minor deviances, most notably with the energies of the first few injections.

The ITC data prove that there is essentially no significant difference in the Zn^{2+} binding ability between wtHSA and plasma HSA, since they both show a similar binding profile. However, wtHSA shows lower exothermic energy released for the first 3-4 injections which could be representative of minor differences between the two samples. The wtHSA is supposed to be a more homogeneous sample since each protein molecule is theoretically subjected to the same processes during expression. Plasma HSA on the

other hand will have been circulating through the plasma prior to purification and so would have been subject to various *in vivo* processes that would lead to heterogeneity (e.g. oxidation at Cys34 by different species).

Having established that the recombinant expression system was able to express reliable HSA proteins, all mutants were included in ITC experiments with Zn^{2+} to determine qualitative Zn^{2+} binding profiles of the mutant HSAs (Figure 5.10).

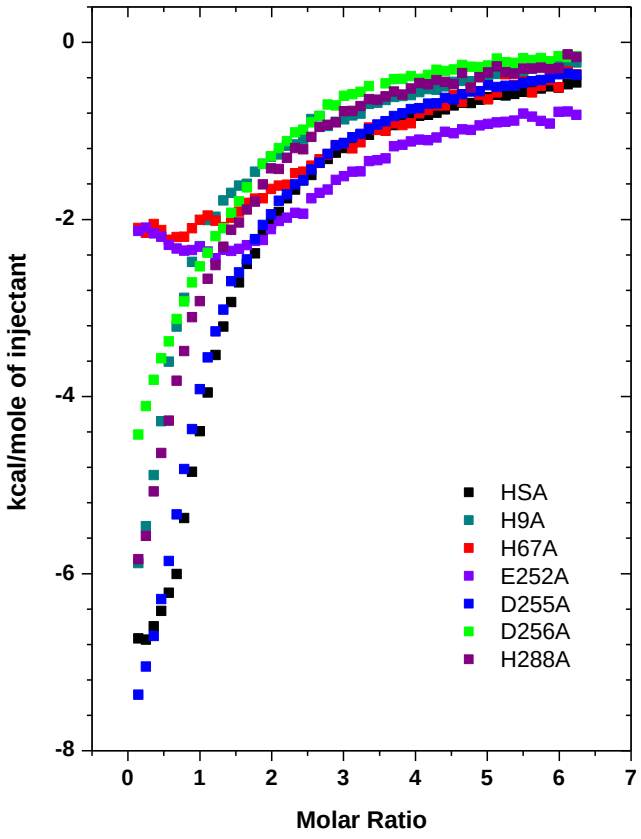

Figure 5.10. ITC data comparing the Zn^{2+} binding ability of the six HSA mutants against plasma HSA. As expected the H67A mutant shows the loss of the high affinity Zn^{2+} binding site (site A), as does the E252A mutant. H9A, D256A and H288A showed a variance in Zn^{2+} binding from plasma HSA which would suggest that these residues are involved in forming the weaker Zn^{2+} sites in some way. D255A had no effect on Zn^{2+} binding. All experiments were performed with 50 µM HSA samples and 1.5 mM $ZnCl_2$, except for H288A which used 25 µM protein and 0.75 mM $ZnCl_2$. Raw data can be found in appendix A3.2-3.7.

The first feature of note is that the D255A mutant shows a virtually identical Zn^{2+} binding profile to that of HSA, meaning that this residue is not involved in any Zn^{2+} binding. Conversely, H67A, which is one residue from site A (Stewart *et al*., 2003),

shows significant disruption of the Zn^{2+} binding ability if HSA, as would be expected. E252A (violet) also shows a profile similar to that of H67A, suggesting that this residue is either involved in directly in Zn^{2+} binding, or allosteric effects caused by mutation of glutamic acid to alanine disrupt a metal binding site (likely to be site A, based on the comparable ITC data between H67A and E252A). This is understandable since the Glu252 residue is only 3.5 Å away from the site A residue Asp249. However, any proposals made regarding the E252A binding profile should be taken with caution as this was the only mutant HSA that was not reproduced due to time constraints. However, the binding profiles of each of the others were reproducible and so can be considered as reliable accounts of their respective Zn^{2+} binding abilities, but E252A would need to be reproduced before any reliable assessment is made. The remaining mutants: H9A, D256A and H288A all showed a significant degree of reduced Zn^{2+} binding compared to HSA, suggesting that these residues are involved in the weaker Zn^{2+} binding sites and could be the location of site B.

These observations can be understood in context with the crystal structure of HSA. His9 would be in close proximity to metal binding residues His3 and Asp13 which could form part of the metal binding site in this position. His288 has nearby neighbours in Glu154 and His157 which would be able to bind metals and together form part of a binding site. In the case of D256A, it is difficult to determine any obvious partner residues that could form a site for Zn^{2+} binding, but looking at the structure of bovine albumin with Ca^{2+} (Figure 5.1), it can be seen that Asp256 is directly next to Ca^{2+} binding residues. Hence, any mutation of this residue could produce allosteric effects which alter metal binding properties of the HSA molecule, which could explain the Zn^{2+} binding profile of the D256A mutant.

Although the ITC data alone does not allow for definitive determination of the weaker Zn^{2+} binding sites, it does indicate whether residues may be involved. The novel histidine mutants (H9A and H288A) showed decreased Zn^{2+} binding ability. Since histidine residues are expected in Zn^{2+} binding, and the fact that both His9 and His288 are in close proximity to other histidine residues (His3 and His157 respectively), it is highly likely that these form the remaining two of the three Zn^{2+} sites that HSA is thought to have (Lu *et al*., 2008). As discussed previously in Chapter 3, the non-linear curve fitting for this interaction (HSA to Zn^{2+}) is complex and proves difficult to achieve a complete quantitative picture of the process. This is compounded by the fact

that the different mutants show different binding profiles and so the same fitting protocol could not be used for each making quantitative comparisons even more problematic. For these reasons, the ITC data in this instance was used purely as a qualitative measure of observing the Zn^{2+} binding differences between the mutants expressed.

Binding of Zn^{2+} and estradiol to AFP

The Zn^{2+} binding ability of AFP was monitored by ITC (Figure 5.11). AFP was shown to have a similar Zn^{2+} binding profile to HSA as studied by ITC. That is, AFP has one high affinity Zn^{2+} site and one (or possibly two) lower Zn^{2+} binding regions. As with the HSA and Zn^{2+} titrations, non-linear curve fitting for AFP and Zn^{2+} was not conclusive, although a low to mid-micromolar dissociation constant was consistently calculated. The data here shows less Zn^{2+} binding to AFP, and at a lower affinity, than previous studies which were conducted using different methods (Wu *et al*., 1987; Permyakov *et al*., 2002).

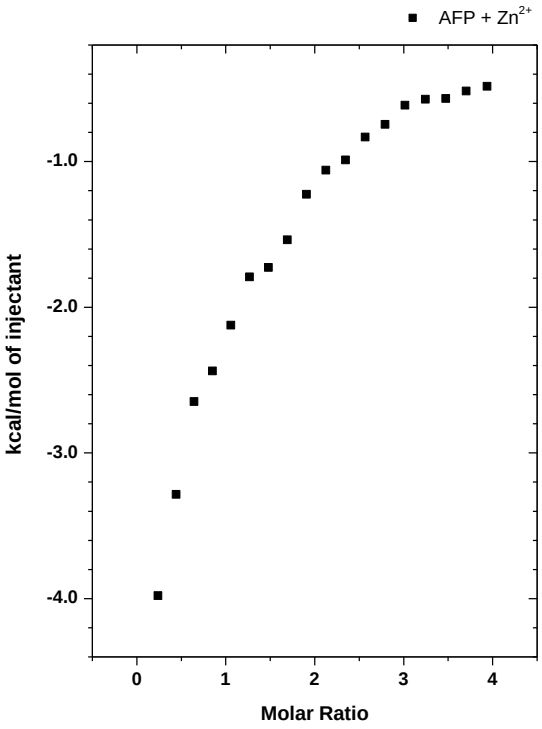

Figure 5.11. ITC data showing the binding of Zn^{2+} into AFP. 25 µM AFP was titrated with 0.75 mM $ZnCl_2$. The shape of the curve is similar to that observed for HSA, albeit with slightly lower affinity and stoichiometry. Raw data can be found in appendix A3.8.

It should be noted that AFP and HSA are likely to display a cooperative binding ability towards Zn^{2+}. So, if the initial binding of Zn^{2+} to the protein is able to induce further binding to the weaker sites within the molecule, the mixture of the sample in the ITC cell becomes heterogeneous (i.e. "protein-Zn^{2+}" is a different species from "apo-protein"). These two species will then compete for the additional Zn^{2+} titrations against each other, affecting the appearance of binding isotherm. This highlights the complexity of these systems and helps explain why simple fitting is not possible using these methods.

Having established that the expressed AFP is able to bind Zn^{2+}, a study on estradiol binding to AFP was conducted (Figure 5.12). The estrogen binding ability of AFP has received considerable attention due to its potential role in reproductive development. Female AFP knockout mice have been shown to be infertile as estradiol can masculinise the female foetus, if no protection is provided by AFP (Brock *et al*., 2012). However, only rat and mouse AFP have been observed binding estradiol, whereas human AFP is unable to, and so the role of AFP in reproductive development in humans is still uncertain.

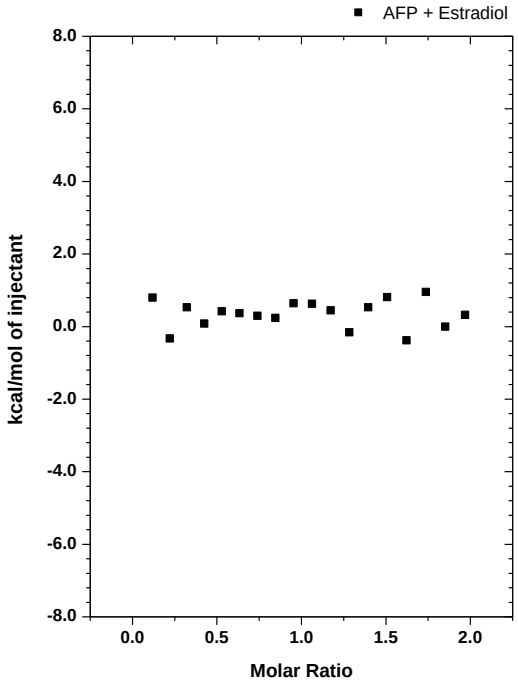

Figure 5.12. ITC data of AFP being titrated with estradiol. 25 µM AFP was titrated with 250 µM estradiol. The experiment showed no binding of estradiol to AFP, which is in line with literature observations. Raw data can be found in appendix A3.9.

The ITC data here confirmed that AFP lacks the ability to bind estradiol, in keeping with literature. These observations here support the fact that AFP expressed in *K. Lactis* is a viable means of preparing this protein for various studies, since the preliminary experiments done here are in line with literature data. It would be interesting in future studies to investigate the structure-function relationship of AFP, particularly with respect to its ligand binding. For example, AFP may need to be in a specific conformation (e.g. molten globule) for binding of estradiol to be observed. The study conducted here made no attempt to alter the structural state of AFP due to time constraints. However, if the molten globule form of AFP could represent a structural regulation of the molecule functions, there may be very different binding observations under this state. Additionally, native ligands (e.g. fatty acids) may first be required to bind to AFP, in order to induce cooperative binding of further ligands to the protein molecule. All these factors have to be taken into account and investigated, and could provide a reason for differences observed between studies.

In conclusion, this project was able to develop a recombinant expression and purification system for both HSA and AFP, yielding natively folded proteins of a high purity. The mutants H9A and H288A were identified as being likely candidates for the additional unknown Zn^{2+} binding sites on HSA, while E252A and D256A were also shown to have alter the ability of HSA to bind Zn^{2+}, although it is not known whether these are direct effects. The expressed AFP showed an ability to bind Zn^{2+}, but did not bind estradiol, suggesting that this expression system is able to produce AFP which conforms to literature observations and thus is ready for use in further studies on the binding properties of AFP and also for structural characterisation by X-ray crystallography.

References

Abelev GI. α-Fetoprotein in ontogenesis and its association with malignant tumors. *Adv. Cancer Res*. 1971, **14**, 295–358.

Altintaş EB, Denizli A. Efficient removal of albumin from human serum by monosize dye-affinity beads. *J Chromatogr B Analyt Technol Biomed Life Sci*. 2006, **832,** 216-223.

Aoyagi Y, Ikenaka T, Ichida F. Copper(II)-binding ability of human alpha-fetoprotein. *Cancer Res*. 1978, **38**, 3483–3486.

Bal W, Christodoulou J, Sadler PJ, Tucker A. Multi-metal binding site of serum albumin, *J. Inorg. Biochem*. 1998, **70**, 33–39.

Bar-Or D, Curtis G, Rao N, Bampos N, Lau E. Characterization of the Co^{2+} and Ni^{2+} binding amino-acid residues of the N-terminus of human albumin: an insight into the mechanism of a new assay for myocardial ischemia. *Eur. J. Biochem.* 2001, **268**, 42–47.

Bar-Or D, Rael LT, Bar-Or R, Slone DS, Mains CW, Rao NK, Curtis CG. The cobalt-albumin binding assay: insights into its mode of action. *Clin. Chim. Acta*. 2008, **387**, 120–127.

Barker ME. Evolution of alpha-fetoprotein: sequence comparisons among AFP species and with albumin species. *Tumor Biol*. 1988, **9**, 123–136.

Bergstrand CG, Czar B. Demonstration of a new protein fraction in serum from the human fetus. Scand. *J. Clin. Lab. Invest*. 1956, **8**, 174.

Blindauer CA, Harvey I, Bunyan KE, Stewart AJ, Sleep D, Harrison DJ, Berezenko S, Sadler PJ. Structure, properties, and engineering of the major zinc binding site on human albumin. *J. Biol. Chem*. 2009, **284**, 23116–23124.

Brock DJ, Scrimgeour JB, Nelson MM. Amniotic fluid alphafetoprotein measurements in the early prenatal diagnosis of central nervous system disorders. *Clin. Genet*. 1975, **7**, 163–169.

Brock O, Keller M, Douhard Q, Bakker J. Female mice deficient in alpha-fetoprotein show female-typical neural responses to conspecific-derived pheromones. *PLoS One*. 2012, **7**, e39204.

Christodoulou J, Sadler PJ, Tucker A. A new structural transition of serum albumin dependent on the state of Cys34: detectionby ^{1}H-NMR spectroscopy. *Eur. J. Biochem.*, 1994, **225**, 363–368.

Colussi PA, Taron CH. Kluyveromyces lactis LAC4 promoter variants that lack function in bacteria but retain full function in K. lactis. *Appl. Environ. Microbiol*. 2005, **71**, 7092-7098.

Cousins RJ. Toward a molecular understanding of zinc metabolism. *Clin. Physiol. Biochem*. 1986, **4**, 20–30.

Deutsch HF. Chemistry and biology of α-fetoprotein. *Adv. Cancer Res*. 1991, 56, 253–312.

Esposito BP, Najjar R. Interactions of antitumoral platinum-group metallodrugs with albumin. *Coord. Chem. Rev*. 2002, **232**, 137–149.

Failla ML, van de Veerdonk M, Morgan WT, Smith Jr JC. Characterization of zinc-binding proteins of plasma in familial hyperzincemia. *J. Lab. Clin. Med*. 1982, **100**, 943–952.

Fanali G, Cao Y, Ascenzi P, Fasano M. Mn(II) binding to human serum albumin: a 1H-NMR relaxometric study. *J. Inorg. Biochem*. 2012, **117**, 198–203.

Foote JW, Delves HT. Albumin bound and α2-macroglobulin bound zinc concentrations in the sera of healthy adults. *J. Clin. Pathol*. 1984, **37**, 1050–1054.

Gálvez M, Moreno JA, Elósegui LM, Escanero JF. Zinc uptake by human erythrocytes with and without serum albumins in the medium. *Biol. Trace Elem. Res*. 2001, **84**, 45–56.

Giroux E, Schoun J. Copper and zinc ion binding by bovine, dog, and rat serum albumins. *J. Inorg. Biochem*. 1981, **14**, 359–362.

Goeken NE, Thompson JS. Conditions affecting the immunosuppressive properties of human α-fetoprotein. *J. Immunol*. 1977, **119**, 139–142.

Goumakos W, Laussac JP, Sarkar B. Binding of cadmium(II) and zinc(II) to human and dog serum albumins - an equilibrium dialysis and Cd-113-NMR study. *Biochem. Cell Biol.* 1991, **69**, 809–820.

Harford C, Sarkar B. Amino terminal Cu(II)- and Ni(II)-binding (ATCUN) motif of proteins and peptides: metal binding, DNA cleavage, and other properties. *Acc. Chem. Res*. 1997, **30**, 123–130.

Hsia JC, Er JS, Tan CT, Ester T, Ruoslahti E. α-Fetoprotein binding specificity for arachidonate, bilirubin, docosahexaenoate, and palmitate. A spin label study. *J. Biol. Chem*. 1980, **255**, 4224–4227.

Isab AA, Shaw 3rd CF. Synthesis of thionato(triethylphosphine) gold(I) complexes:analogues of "auranofin," an antiarthritic drug. *J. Inorg. Biochem*. 1990, **38**, 95-100.

Ivanov AI, Christodoulou J, Parkinson JA, Barnham KJ, Tucker A, Woodrow J, Sadler PJ. Cisplatin binding sites on human albumin. *J. Biol. Chem*. 1998, **273**, 14721-14730.

Kragh-Hansen U, Vorum H. Quantitative analyses of the interaction between calcium ions and human serum albumin. *Clinical Chemistry*. 1993, **39**, 202-208.

Lester EP, Miller JB, Yachnin S. A postsynthetic modification of human alpha-fetoprotein controls its immunosuppressive potency. *Proc. Natl. Acad. Sci. USA*. 1977, **73**, 4645–4648.

Leong SS, Middelberg AP. The refolding of different alpha-fetoprotein variants. *Protein Sci*. 2006, **15**, 2040-2050.

Linder MC, Hazegh-Azam M. Copper biochemistry and molecular biology. *Am. J. Clin. Nutr*. 1996, **63**, 797S–811S.

Lu J, Stewart AJ, Sadler PJ, Pinheiro TJT, Blindauer CA, Albumin as a zinc carrier: properties of its high-affinity zinc-binding site. *Biochem. Soc. Trans*. 2008, **36**, 1317-1321.

Majorek KA, Porebski PJ, Dayal A, Zimmerman MD, Jablonska K, Stewart AJ, Chruszcz M, Minor W. Structural and immunologic characterization of bovine, horse, and rabbit serum albumins. *Mol. Immunol*. 2012, **52**, 174-182.

Martins EO, Drakenberg T. Cadmium(II), zinc(II), and copper(II) ions binding to bovine serum albumin. A 113Cd NMR study. *Inorg. Chim. Acta*. 1982, **67**,71–74.

Masuoka J, Hegenauer J, Van Dyke BR, Saltman P. Intrinsic stoichiometric equilibrium constants for the binding of zinc(II) and copper(II) to the high affinity site of serum albumin. *J. Biol. Chem*. 1993, **268**, 21533–21537.

Masuoka J, Saltman P. Zinc(II) and copper(II) binding to serum albumin: a comparative study of dog, bovine, and human albumin. *J. Biol. Chem.* 1994, **269**, 25557–25561.

Mothes E, Faller P. Evidence that the principal Co(II)-binding site in human serum albumin is not at the N-terminus: implication on the albumin cobalt binding test for detecting myocardial ischemia. *Biochemistry*. 2007, **45**, 2267–2274.

Nagai M, Becker JD, Deutsch HF. The fatty acid levels of rat alpha-fetoprotein derived from fetuses, pregnancy and hepatoma sera. *Oncodev. Biol. Med*. 1982, **3**, 343–350.

Narizhneva NV, Uversky VN. Human α-fetoprotein is in the molten globule state under conditions modeling protein environment near the membrane surface. *Protein Pept. Lett*. 1997, **4**, 243–249.

Nishi S, Matsue H, Yoshida H, Yamamoto R, Sakai M. Localization of the estrogen-binding site of alpha-fetoprotein in the chimeric human-rat proteins. *Proc. Natl. Acad. Sci. USA*. 1991, **88**, 3102–3105.

Ohyoshi E, Hamada Y, Nakata K, Kohata S. The interaction between human and bovine serum albumin and zinc studied by a competitive spectrophotometry. *J. Inorg. Biochem*. 1999, **75**, 213–218.

Okuda K, Kotoda K, Obata H, Hayashi N, Hisamitsu T. Clinical observations during a relatively early stage of hepatocellular carcinoma, with special reference to serum alpha-fetoprotein levels. *Gastroenterology*. 1975, **69**, 226–234.

Oz G, Pountney DL, Armitage IM. NMR spectroscopic studies of I = 1/2 metal ions in biological systems. *Biochem Cell Biol*. 1998, **76**, 223-234.

Parmelee DC, Evenson MA, Deutsch HF. The presence of fatty acids in human alpha-fetoprotein. *J. Biol. Chem*. 1978, **253**, 2114–2119.

Pattison SE, Cousins RJ. Zinc uptake and metabolism by hepatocytes. *Fed. Proc*. 1986. **45**, 2805–2809.

Permyakov SE, Oberg KA, Cherskaya AM, Shavlovsky MM, Permyakov EA, Uversky VN. Human alpha-fetoprotein as a Zn(2+)-binding protein. Tight cation binding is not accompanied by global changes in protein structure and stability. *Biochim Biophys Acta*. 2002, **1586**, 1-10.

Peters Jr T. Serum albumin. *Adv. Protein Chem*. 1985, **37**,161–245.

Peters Jr T. All about albumin: biochemistry, genetics, and medical applications. New York: Academic Press, 1996.

Rowe DJ, Bobilya DJ. Albumin facilitates zinc acquisition by endothelial cells, *Proc. Soc. Exp. Biol. Med*. 2000, **224**(3), 178-186.

Rózga M, Sokołowska M, Protas AM, Bal W. Human serum albumin coordinates Cu(II) at its N-terminal binding site with one picomolar affinity. *J. Biol. Inorg. Chem*. 2007, **12**, 913–918.

Sadler PJ, Viles JH. ^{1}H and ^{113}Cd NMR investigations of Cd^{2+} and Zn^{2+} binding sites on serum albumin: competition with Ca^{2+}, Ni^{2+},Cu^{2+},and Zn^{2+}, *Inorg. Chem*., 1996, **35**, 4490-4496.

Ruoslahti E, Seppälä M. α-Foetoprotein in normal human serum. *Nature*, 1972, **235,** 161–162.

Ruoslahti E. alpha-Fetoprotein in cancer and fetal development. *Adv. Cancer Res*. 1979, **29**, 275–346.

Ruoslahti E, Ester T, Seppälä M. Binding of bilirubin by bovine and human alpha-fetoprotein. *Biochim. Biophys. Acta*. 1979, **578**, 511–519.

Seppälä M, Ruoslahti E. Alpha fetoprotein: physiology and pathology during pregnancy and application to antenatal diagnosis. *J. Perinat. Med*. 1973, **1**, 104–113.

Seppälä M. Fetal pathophysiology of human alpha-fetoprotein. *Ann. New York Acad. Sci*. 1975, **259**, 59–73.

Sleep D, Belfield GP, Goodey AR. The secretion of human serum albumin from the yeast Saccharomyces cerevisiae using five different leader sequences. *Biotechnology*. 1990, **8**, 42-46.

Sogami M, Era S, Nagaoka S, Kuwata K, Kida K, Miura K. HPLC-studies on Nonmercapt–Mercapt conversion of human serum albumin. *Int. J. Pept. Protein Res*. 1985, **25**, 398–402.

Sokołowska M, Krężel A, Dyba M, Szewczuk Z, Bal W. Short peptides are not reliable models of thermodynamic and kinetic properties of the N-terminal metal binding site in serum albumin. *Eur. J. Biochem*. 2002, **269**, 1323–1331.

Soloff MS, Swartz SK, Pearlmutter F, Kithier K. Binding of 17-beta-estradiol by variants of alpha-fetoprotein in rat amniotic fluid. *Biochim. Biophys. Acta*, 1972, **427**, 644–651.

Stamler JS, Jaraki O, Osborne J, Simon DI, Keaney J, Vita J, Singel D, Valeri CR, Loscalzo J. Nitric oxide circulates in mammalian plasma primarily as an S-nitroso adduct of serum albumin. *Proc. Natl. Acad. Sci. U. S. A*. 1992, **89**, 7674–7677.

Stewart AJ, Blindauer CA, Berezenko S, Sleep D, Sadler PJ. Interdomain zinc site on human albumin. *Proc. Natl. Acad. Sci*. 2003, **100**, 3701–3706.

Tomashevski AY, Narizhneva NV, Melnik TN, Uversky VN. α-Fetoprotein structure depends on the protein purification procedure: further evidence on the structure-forming role of the ligands. *Protein Pept. Lett*. 1998, **5**, 295–301.

Uriel J, de Nechaud B, Dupiers M. Estrogen-binding properties of rat, mouse and man fetospecific serum proteins. Demonstration by immuno-autoradiographic methods. *Biochem. Biophys. Res. Commun*. 1972, **46,** 1175–1180.

[a]Uversky VN, Narizhneva NV, Ivanova TV, Tomashevski AY. Rigidity of human α-fetoprotein structure is under the ligand control. *Biochemistry*. 1997, **44**, 13638–13645.

[b]Uversky VN, Narizhneva NV, Ivanova TV, Kirkitadze MD, Tomashevski AY. Ligand-free form of human a-fetoprotein: evidence for the molten globule state. *FEBS Lett*. 1997, **410**, 280–284.

Uversky VN, MKirkitadze MD, Narizhneva NV, Potekhin SA, Tomashevski AY. Structural properties of α-fetoprotein from human cord serum the protein molecule at low pH possesses all the properties of the molten globule. *FEBS Lett*. 1995, **364**, 165–167.

Vidal JC, Cepria G, Castillo JR. Models for studying the binding capacity of albumin to zinc by stripping voltammetry. *Anal. Chim. Acta*. 1992, **259**, 129–138.

Wu JT, Monir-Vaghefi SM, Clayton F. Human alpha-fetoprotein and albumin: differences in zinc binding. *Clin Physiol Biochem*. 1987, **5**, 85-94.

Yachnin S, Lester E. Inhibition of human lymphocyte transformation by human alpha-foetoprotein (HAFP); comparison of foetal and hepatoma HAFP and kinetic studies of in vitro immunosuppression. *Clin. Exp. Immunol*. 1977, **26**, 484–490.

Yachnin S. The immunosuppressive properties of α-fetoprotein: A brief overview. *Ann. New York Acad. Sci*. 1983, **417**, 105–107.

Yoshiki T, Itoh T, Shirai T, Noro T, Tomino Y, HamaJima TI. Primary intracranial yolk sac tumor immunofluorescent demonstration of alpha-fetoprotein synthesis. *Cancer*. 1976, **37**, 2343–2348.

Zhang Y, Wilcox DE. Thermodynamic and spectroscopic study of Cu(II) and Ni(II) binding to bovine serum albumin. *J. Biol. Inorg. Chem*. 2002, **7**, 327–337.

Chapter 6

Conclusions

This project started with ambitious aims and strong directives. HRG was to be structurally characterised and a functional link between plasma fatty acid levels and increased thrombosis through activation of HRG by Zn^{2+} was to be established. Until recently, structural information relating to HRG had come only from sequence analysis and spectroscopic studies. The study here published the X-ray crystal structure of the N2 domain of rabbit HRG. This structure showed the domain has a cystatin-like fold, is N-glycosylated at Asn184, *S*-glutathionylated at Cys185 and is likely to contribute to dimerisation (through interaction with another N2 domain). The observation of the glutathione adduct at Cys185 provided potential *in vivo* evidence that the release of the anti-angiogenic HRR/PRR fragment is controlled in part by a redox mechanism.

The major transporter of Zn^{2+} and fatty acids in plasma is HSA. The Zn^{2+} binding site on HSA had previously been identified, which is also concurrent with one of the fatty acid binding sites. Using ITC experiments to examine the binding of Zn^{2+} to HSA under a range of fatty acid concetrations, this study has revealed that pathophysiological concentrations of free fatty acids (up to 5 molar equivalents) significantly perturb the ability of albumin to bind Zn^{2+}, due to disruption of the main Zn^{2+}-binding site.

From what is currently known regarding the Zn^{2+} binding properties of HRG and HSA, it is clear that either transient or sustained elevation of plasma fatty acid levels would be likely to increase the proportion of plasma Zn^{2+} associated with HRG. Reduced competition from HSA due to the presence of fatty acids could allow a sufficient proportion of Zn^{2+} to bind HRG, activating HRG and triggering association to heparin. This led us to study the the Zn^{2+} binding properties of HRG and the ability of Zn^{2+} to influence HRG-heparin interactions by ITC and ELISA.

The ITC experiments revealed human HRG has 10 Zn^{2+} binding sites with an average K_d of 12.4 μM. The effect of Zn^{2+} on heparin binding by human HRG was also assessed using ITC. Heparins of molecular weight range 3-30 kDa were injected into samples of human HRG that contained different concentrations of Zn^{2+}. Zn^{2+} had a marked effect upon the mechanism by which human HRG bound heparin. In the absence of Zn^{2+} the

interaction between the first few injections of heparin and HRG was exothermic. This initial exothermic form of heparin binding is more pronounced as the concentration of Zn^{2+} is raised to 5 μM. This reveals that heparin binds HRG via different "modes", whereby the exothermic mode of binding occurs with higher affinity than the endothermic mode and is enhanced by Zn^{2+}. It was possible to fit curves to the endothermic data collected in the absence and presence of 1 μM Zn^{2+}. These fits suggest that the endothermic mode most likely corresponds to a single heparin site. However, the "real" affinities are likely to be higher as this analysis does not take into account binding via the exothermic mode. Interestingly a difference in the stoichiometry of heparin binding to HRG in the presence of 1 μM compared with the data without Zn^{2+} or with 5 μM was observed, suggesting that a mixture of 1:1 or 1:2 heparin:HRG complexes exist in solution. Our study suggests that higher concentrations of Zn^{2+} (5 μM) inhibit formation of the 1:2 complex, which will enhance the proportion of heparin bound to HRG.

The effect of Zn^{2+} on human HRG-heparin interactions was further explored through the use of an ELISA-based assay. In each case HRG bound heparin in a concentration-dependent manner. In the absence of Zn^{2+}, HRG bound with an average K_d= 32.9 nM. However the affinity was higher in the presence of 1 μM Zn^{2+} (ca. K_d= 5.1 nM). The ELISA assay was repeated using a low molecular weight heparin fraction, 6,850 Da in size. Zn^{2+} had no effect upon the ability of HRG to bind 6,850 Da heparin (in each case K_d was ~30 nM). The contrast between heparins of different mass ranges is interesting given that heparins of different sizes are used clinically as anti-thrombotic agents.

An *in vitro* assay to study Zn^{2+}-dependent effects upon of the coagulation pathway involving HRG, thrombin, antithrombin and apo- and fatty acid-loaded albumins was also developed. The assay conditions were optimised to be as close to physiological as possible (concentrations of Zn^{2+}, serum albumin, HRG, antithrombin and thrombin were all within the normal physiological range). Lauric acid was chosen as a medium/long-chain fatty acid with a relatively high solubility in aqueous solutions. In this assay system increasing concentrations of lauric acid were found to augment thrombin activity, with the highest activity observed in the presence of 3 mM lauric acid. The prothrombotic effect of the fatty acid was reversed by the introduction of 0.1 mM EDTA to the system, suggesting that Zn^{2+} is involved. If a role for free fatt acids in increasing the risk of thrombotic complications (via modulation of free/exchangeable

Zn^{2+} levels) is confirmed, then chelation therapy could be seen as a viable preventative treatment in certain individuals.

To drive this research onwards from the fundamental studies conducted so far, several salient aims appear appropriate. The only 3D-structural information that currently exists for HRG is the N2 domain structure that was presented here. In order to gain structural insight into the organisation of individual domains, interactions with other molecules (including heparins) and the molecular basis for Zn^{2+}-binding to the HRR, full length and individual domains of human HRG (including HRR, N1/N2 together and C2 domains) should be subjected to crystallisation trials. Full length HRG could be purified from human plasma. Where applicable, co-cystallisation could be attempted with Zn^{2+} and other binding partners. These include homogenous preparations of different heparins.

With the anticipated difficulty in growing suitable crystals of a large protein such as HRG, some complementary approaches should also be adopted. Trials to crystallise the full length protein following a partial protease (trypsin) step may be carried out. Proteases preferentially process proteins at disordered regions, removing these regions can greatly increase the potential to form ordered crystals suitable for diffraction studies. Enzymatic removal of polysaccharide chains using commercially available enzymes may aid formation suitable crystals as can chemical modification (reductive methylation). Any future work should also attempt to establish a recombinant system for the expression of full length and truncated versions of HRG.

To further understand how HRG and heparins interact and the influence of Zn^{2+} in this process, the established approaches of ITC and ELISA can be used to examine binding of heparins of different chain lengths to full length plasma-purified human HRG and recombinant domains (particularly N1/N2 and the HRR, which are known interaction sites) in the presence and absence of Zn^{2+}. This will not only confirm that these domains are responsible for heparin-binding but give clues as to how the Zn^{2+} enhances the high affinity mode of binding. More specifically, it will tell us whether the domains act independently or in concert (following Zn^{2+}-binding) to elicit the high-affinity mode of binding.

Functional assays designed to ascertain the ability of human HRG to neutralise different heparins and the role of Zn^{2+} in this process, could be developed. A thrombin assay

(utilising physiological levels of albumin HRG, antithrombin, heparin, thrombin and the chromogenic thrombin specific substrate S2238) as an *in vivo* platform to examine the effect of Zn^{2+} displacement from serum albumin by free fatty acids has already been developed. Using pathophysiological concentrations of free fatty acids and heparins of different sizes the influence free fatty acid mediated changes in free/exchangeable Zn^{2+} has on the ability of HRG to neutralise heparins of different molecular weights could be examined. The complexity of this assay could be increased by developing a system to detect the thrombin activity in plasma samples. These samples could be spiked with increasing fatty acids, and any detectable increase in thrombin activity could be related to the mechanism detailed.

As a side project, to investigate the metal binding properties of HSA, recombinant mutants were made in an attempt to identify binding sites. H9A, H67A, E252A, D255A, D256A and H288A mutants were engineered. Based on ITC binding profiles between Zn^{2+} and the respective mutants, H9 and H288 were identified as being possible residues involved in the unknown Zn^{2+} binding sites on HSA. E252 and D256 appear to effect the ability of HSA to bind Zn^{2+}, although these effects could be through indirect means. Recombinant AFP was also expressed and purified during this project, and preliminary studies on its Zn^{2+} and estradiol binding abilities suggest that the *K. lactis* expression system used is able to produce viable, fully-folded AFP.

With regards to identifying new metal binding sites on HSA, towards the end of the project our collaborators were able to co-crystallise HSA with Zn^{2+}. The functional data presented here will compliment the solution of the HSA-Zn^{2+} structure. The future direction of the project on AFP could follow the same trajectory as used for the studies on HRG and HSA here. The binding properties of AFP could be studied with ITC using a variety of ligands including metals, fatty acids or hormones. Since there is no structure of AFP currently available, any project involving AFP should make crystallisation trials with the ultimate aim of structure solution a main priority.

Appendix 1

The supporting material provided in this section relates to Chapter 2, the structural characterisation of HRG. This includes images of the crystals, diffraction patterns and X-ray crystallography data tables.

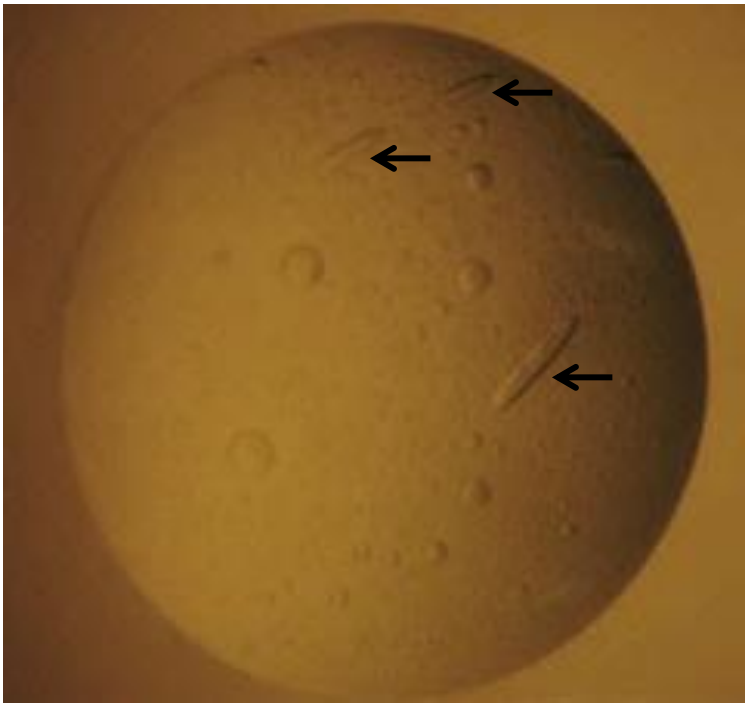

A1.1. Photograph of a drop containing HRG N2 domain crystals. 3 crystals are shown with arrows.

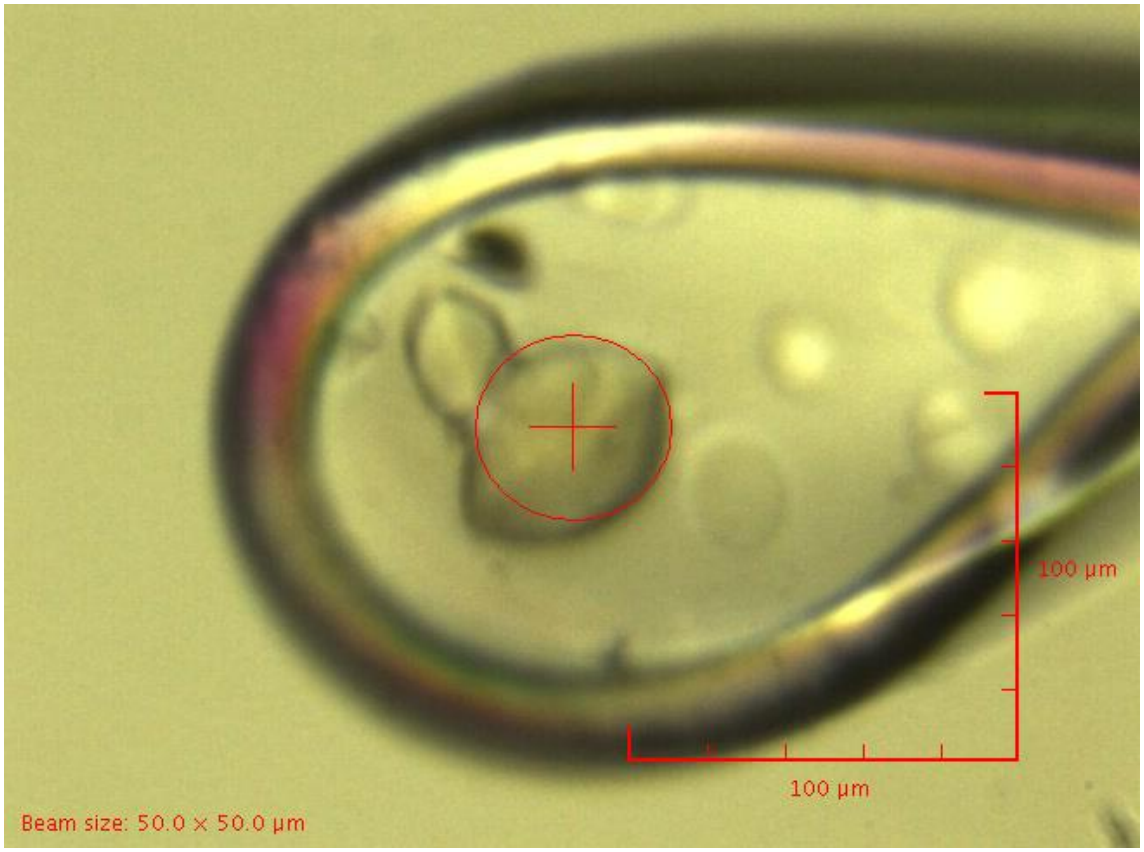

A1.2. Photograph of the HRG crystal used to collect data.

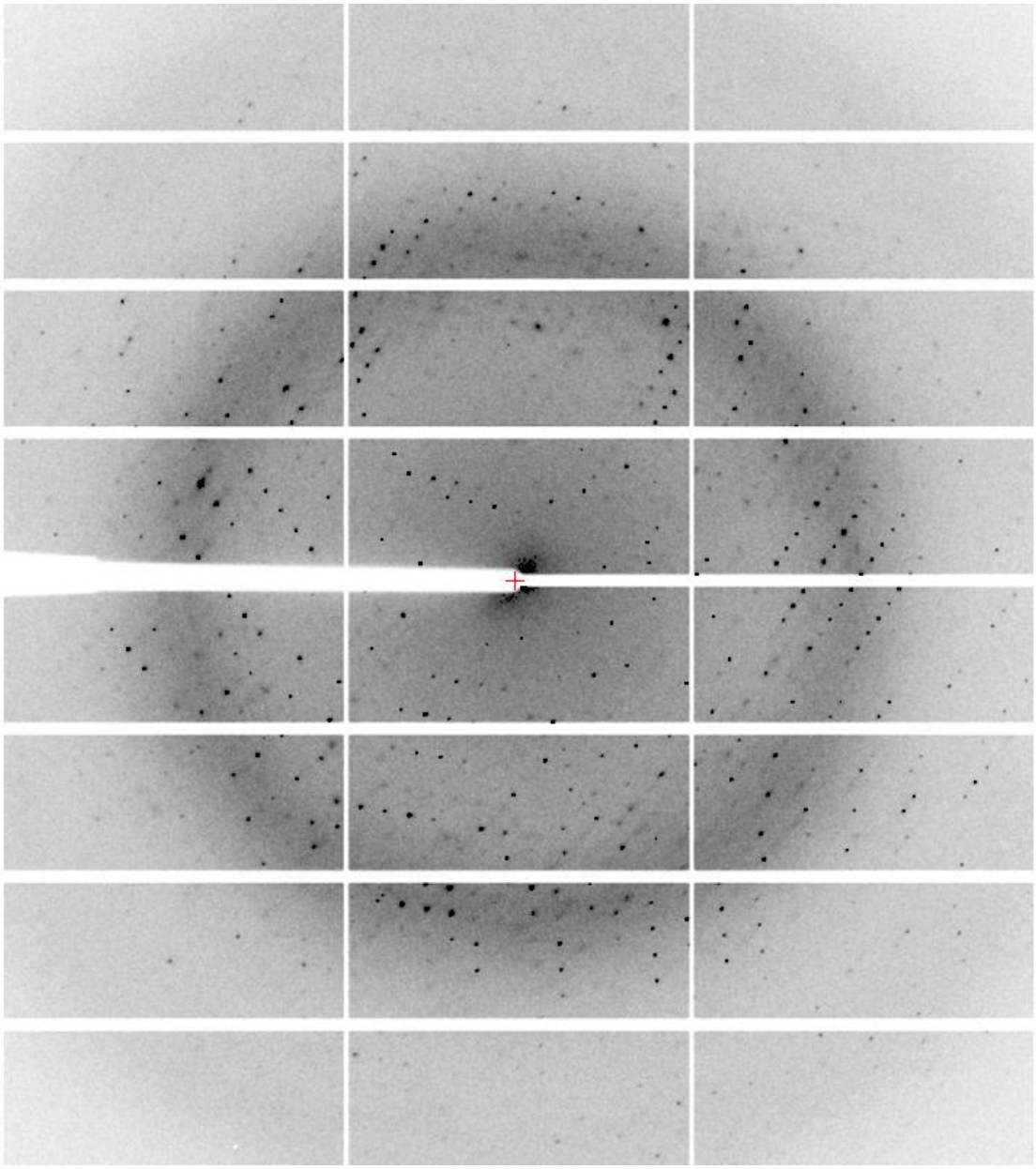

A1.3. Diffraction pattern obtained from the rod-shaped crystal.

Data Collection	**K_2PtCl_4-soaked**	**Native**
Beamline	Diamond I02	Diamond I04-1
Wavelength (Å)	0.97	0.92
Space group	P 3_1 2 1	P 3_1 2 1
Cell dimensions (c), (°)	77.6, 77.6, 69.2	77.1, 77.1, 69.2
	90, 90, 120	90, 90, 120
Resolution (Å)	69.2 – 2.91	34.7 – 1.93
(high resolution)	(2.99 – 2.91)	(2.00 – 1.93)
R_{merge}	10.0 (92.3)	5.1 (33.0)
I / σ (I)	29.2 (5.2)	11.3 (2.1)
Completeness (%)	99.5 (99.2)	93.7 (69.2)
Average redundancy	26.9 (28.6)	4.1 (2.7)
V_m ($Å^3$ / Da)	4.3	4.2
Solvent (%)	71.4	70.9
Refinement		
Unique reflections		17163
R_{work} / R_{free}		0.18 / 0.22
Geometric deviations		
Bonds ($Å^3$) / Angles (°)		0.017 / 2.02
No. atoms		1104
Protein		952
Water		75
Sugar		39
Glutathione		20
Glycerol		18

B factors (Å)	
Protein	41
Water	51.8
Sugar	69.6
Glutathione	63.6
Glycerol	74.3
Ramachandran	
Allowed / disallowed (%)	100 / 0
Molprobity score / centile	3.52 / 100
PDB code	4CCV

* Values in parenthesis refer to the highest resolution shell

A1.4. Crystallographic data collection and structure refinement statistics for the rod-shaped crystal.

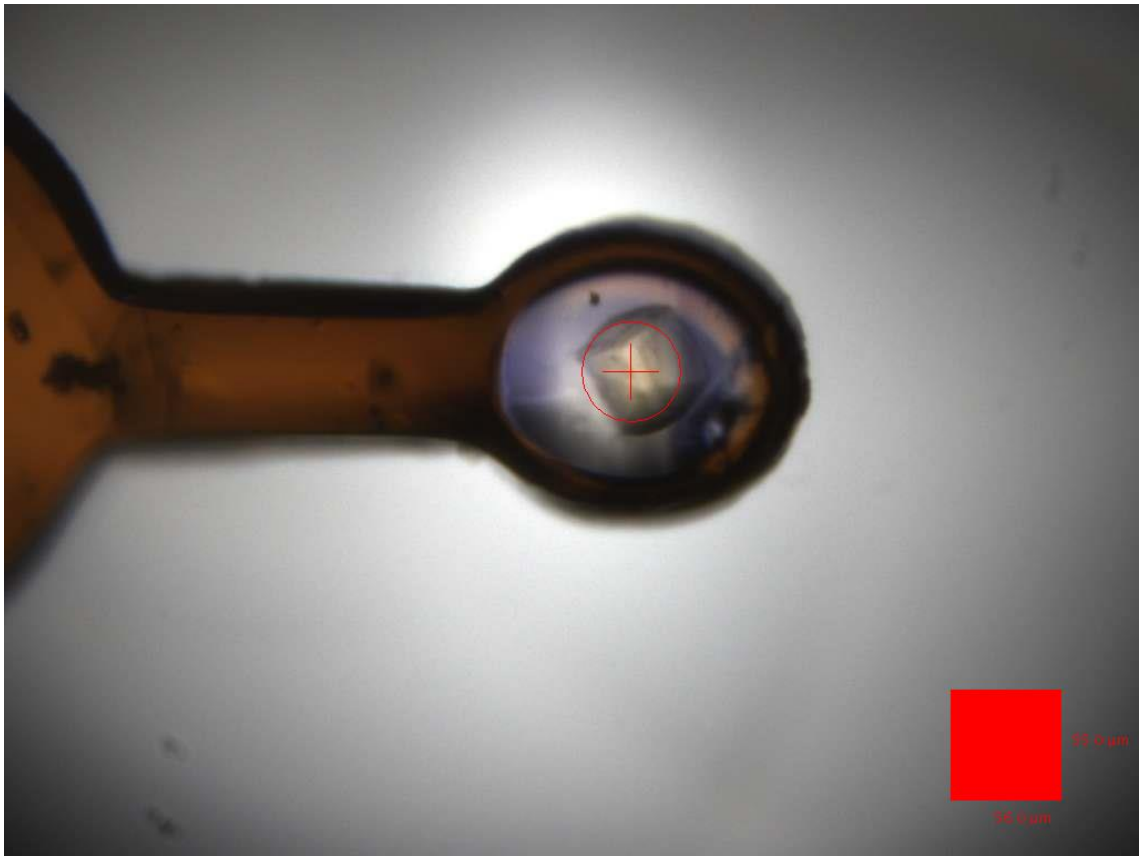

A1.5. Photograph of a cubic HRG crystal used to collect data.

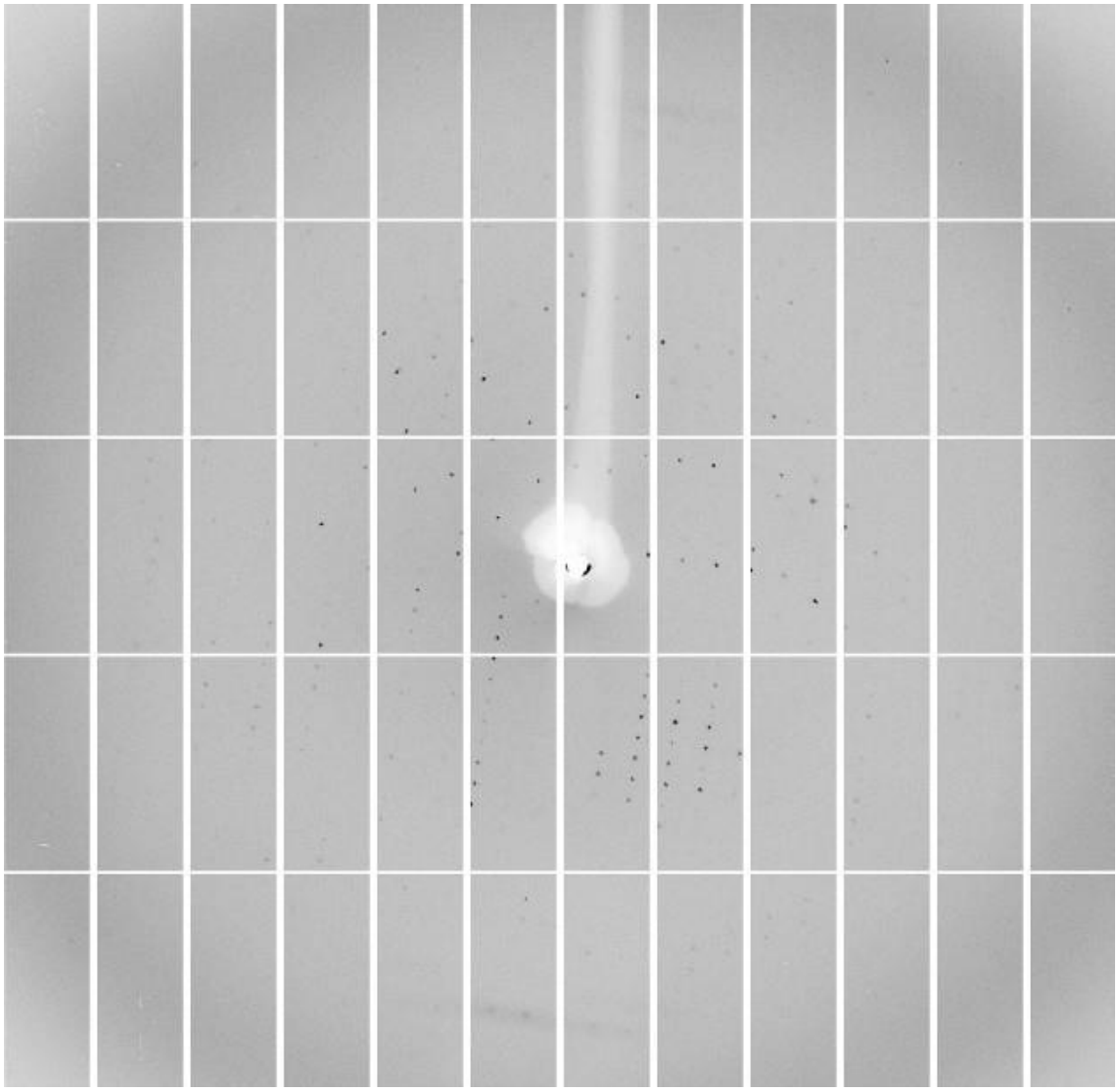

A1.6. Diffraction pattern obtained from diffraction of a cubic HRG crystal.

Data Collection	HRG – cube
Beamline	Diamond I24
Wavelength (Å)	0.99
Space group	F 2 3
Cell dimensions (c), (°)	172.6 172.6, 172.6 90, 90, 90
Resolution (Å)	52.0 – 5.05
(high resolution)	(5.53 – 5.05)
R_{merge}	11.2 (26.5)
I / σ (I)	2.9 (2.2)
Completeness (%)	66.2 (66.2)
Average redundancy	1.4 (1.4)

A1.7. Crystallography data for a cubic HRG crystal.

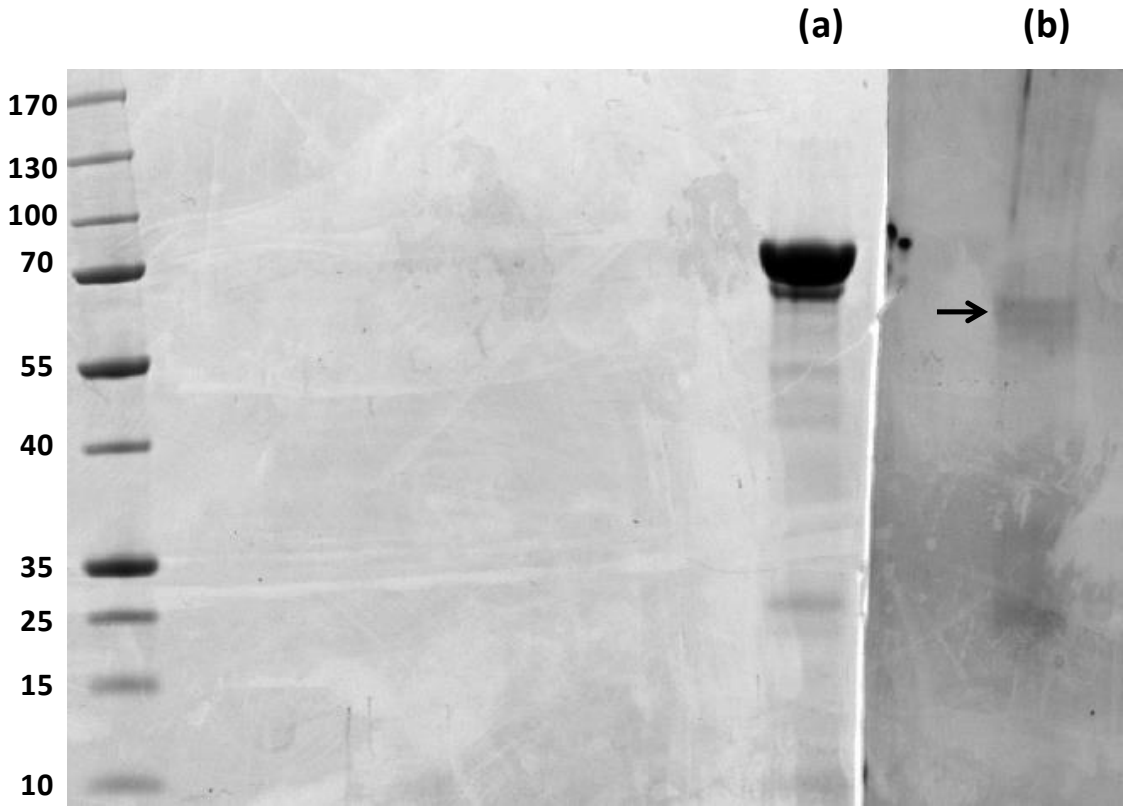

A.1.8. SDS-PAGE analysis of cubic crystals. (a) HRG sample from solution, visualised with coomassie stain. (b) Cubic crystals, after washing in mother liquor, visualised with silver stain. It appears that this morphology of crystal could contain a significant proportion of the protein, as indicated by the arrow.

Appendix 2

The supporting material provided in this section relates to Chapter 3, the investigations into Zn^{2+} and heparin binding to HRG and implications for thrombin activation. This includes raw data of all of the ITC experiments performed, as well as additional experiments as described in the main text (unless otherwise stated).

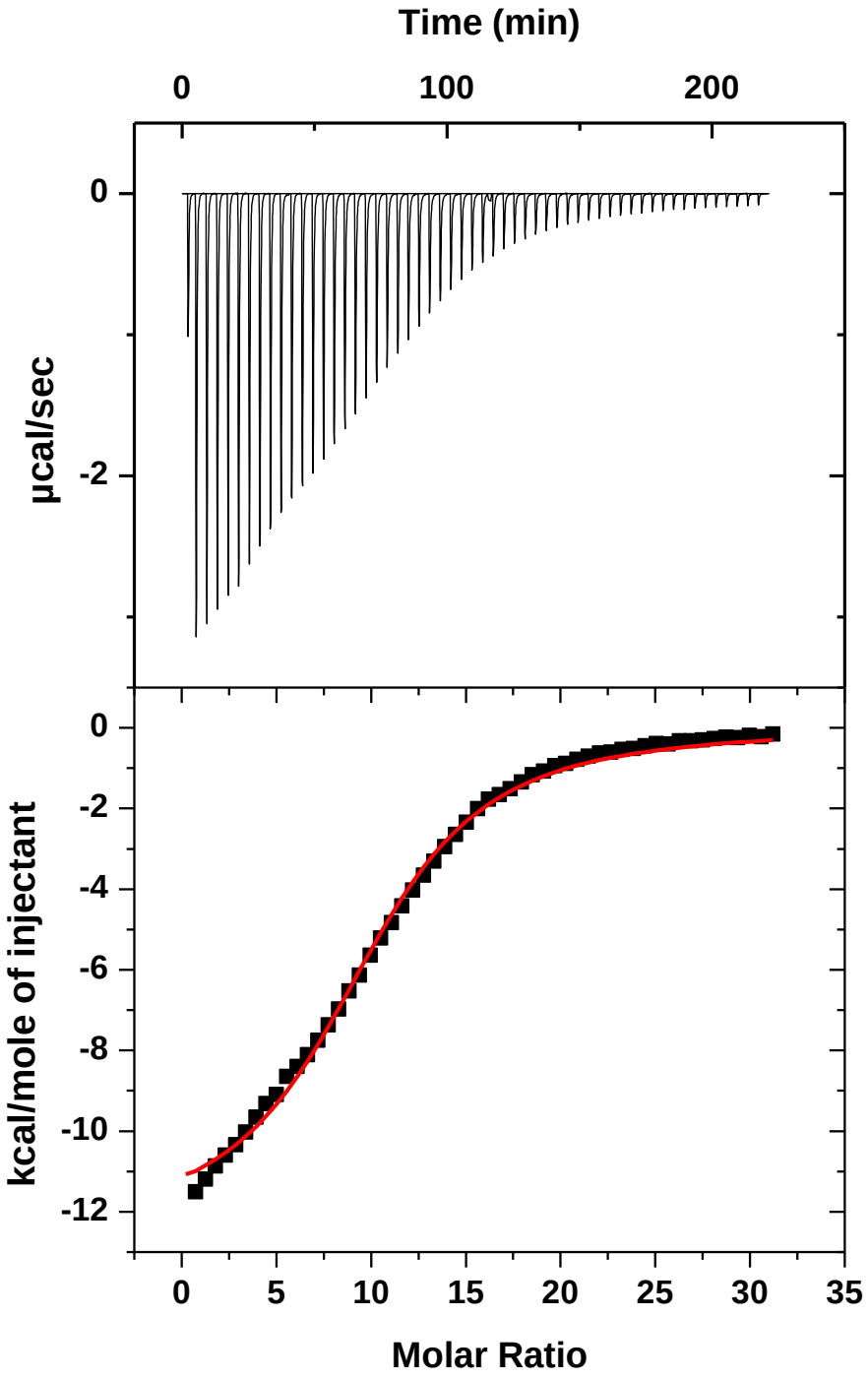

A2.1. ITC data for human HRG titrated with Zn^{2+}.

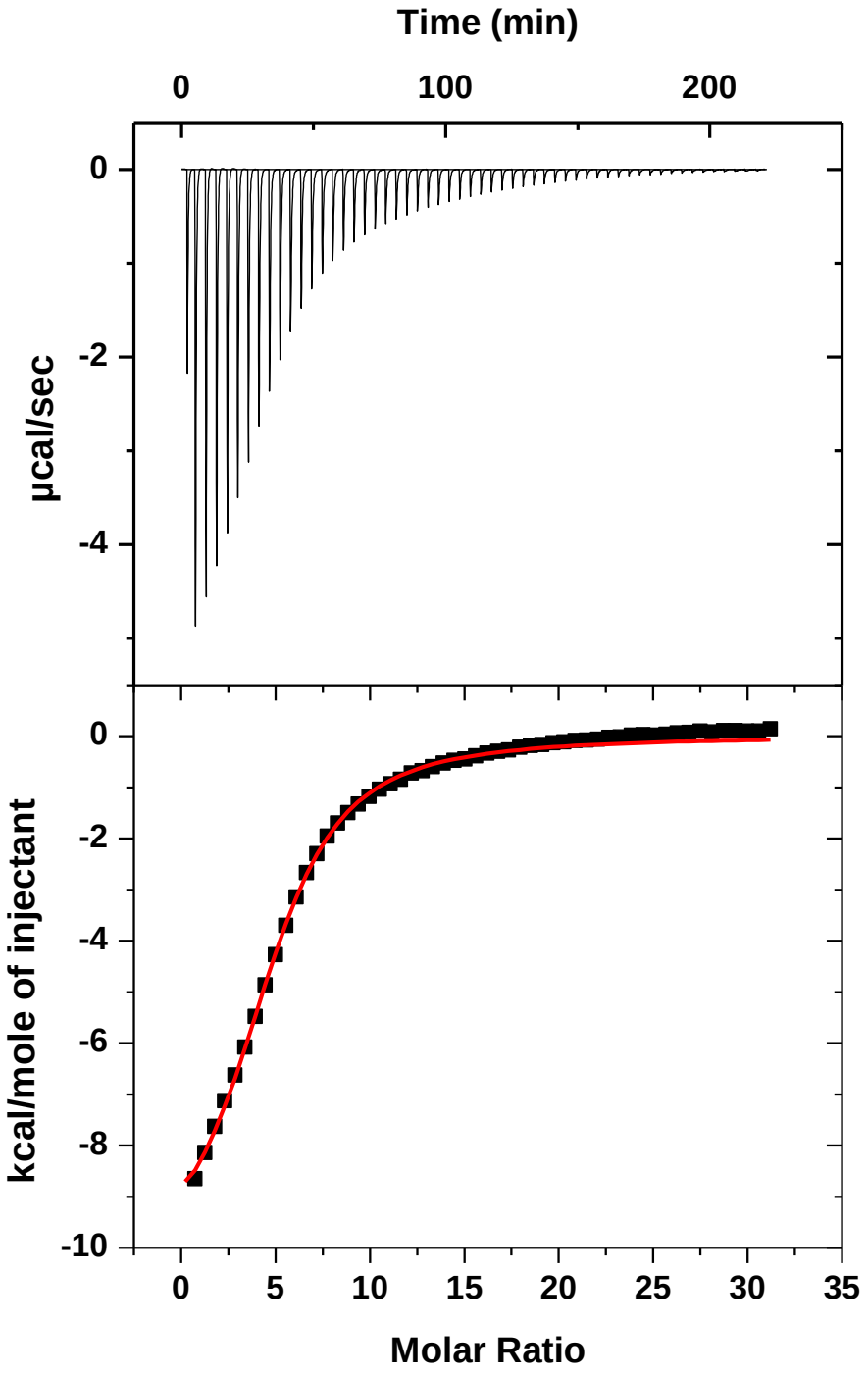

A2.2. ITC data for human HRG titrated with Zn^{2+} in a low ionic strength buffer.

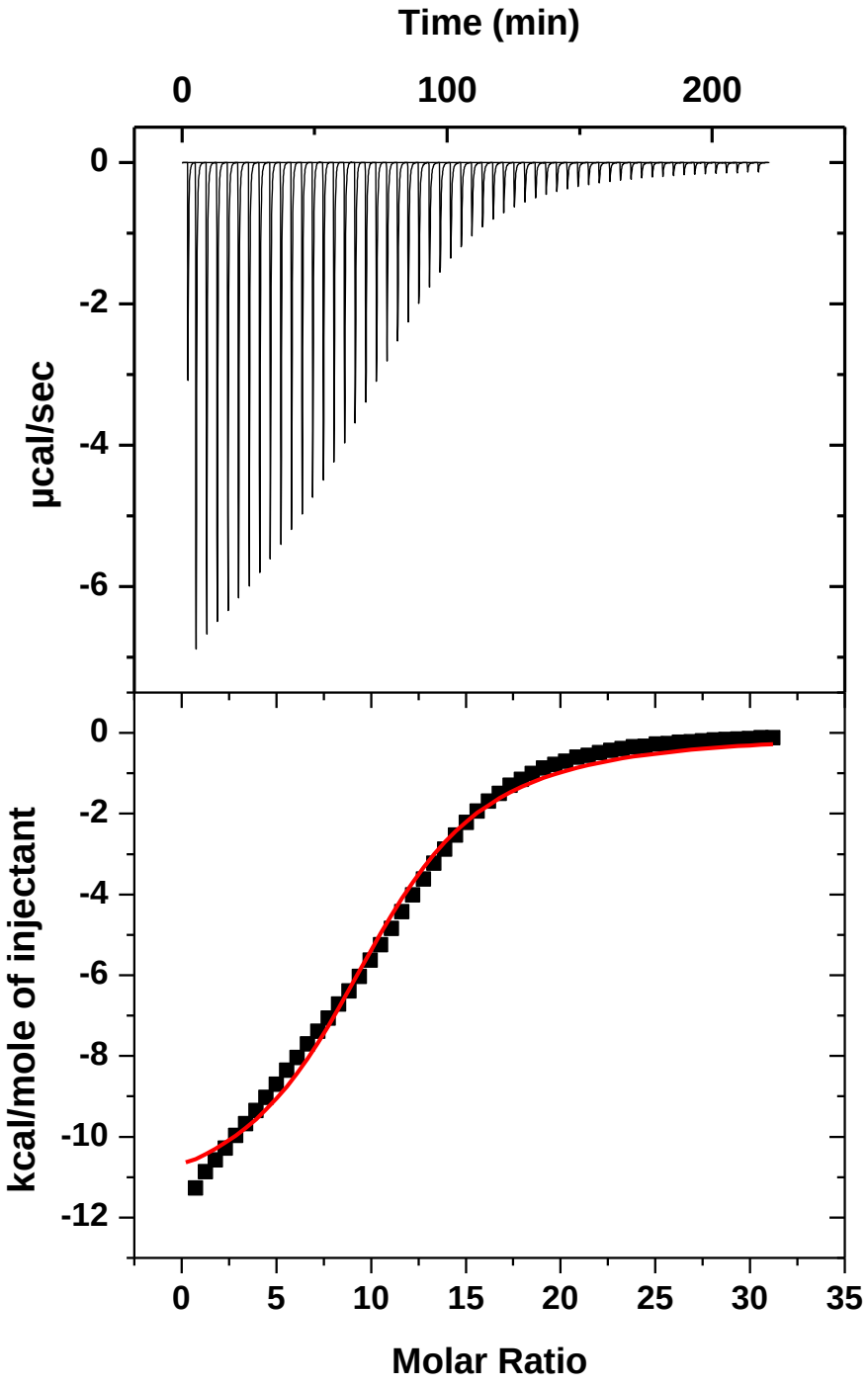

A2.3. ITC data for rabbit HRG titrated with Zn^{2+}.

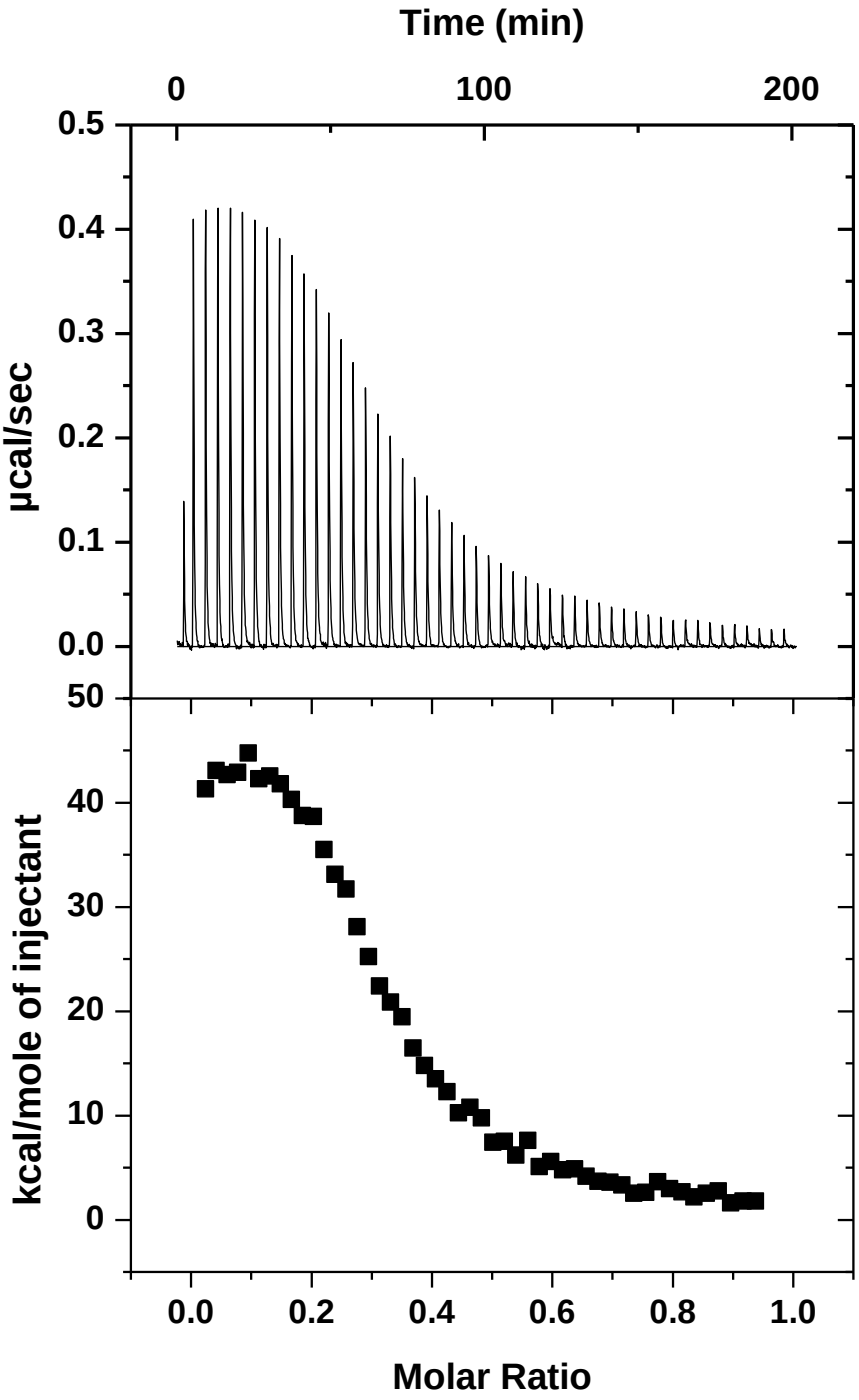

A2.4. ITC data for human HRG titrated with heparin.

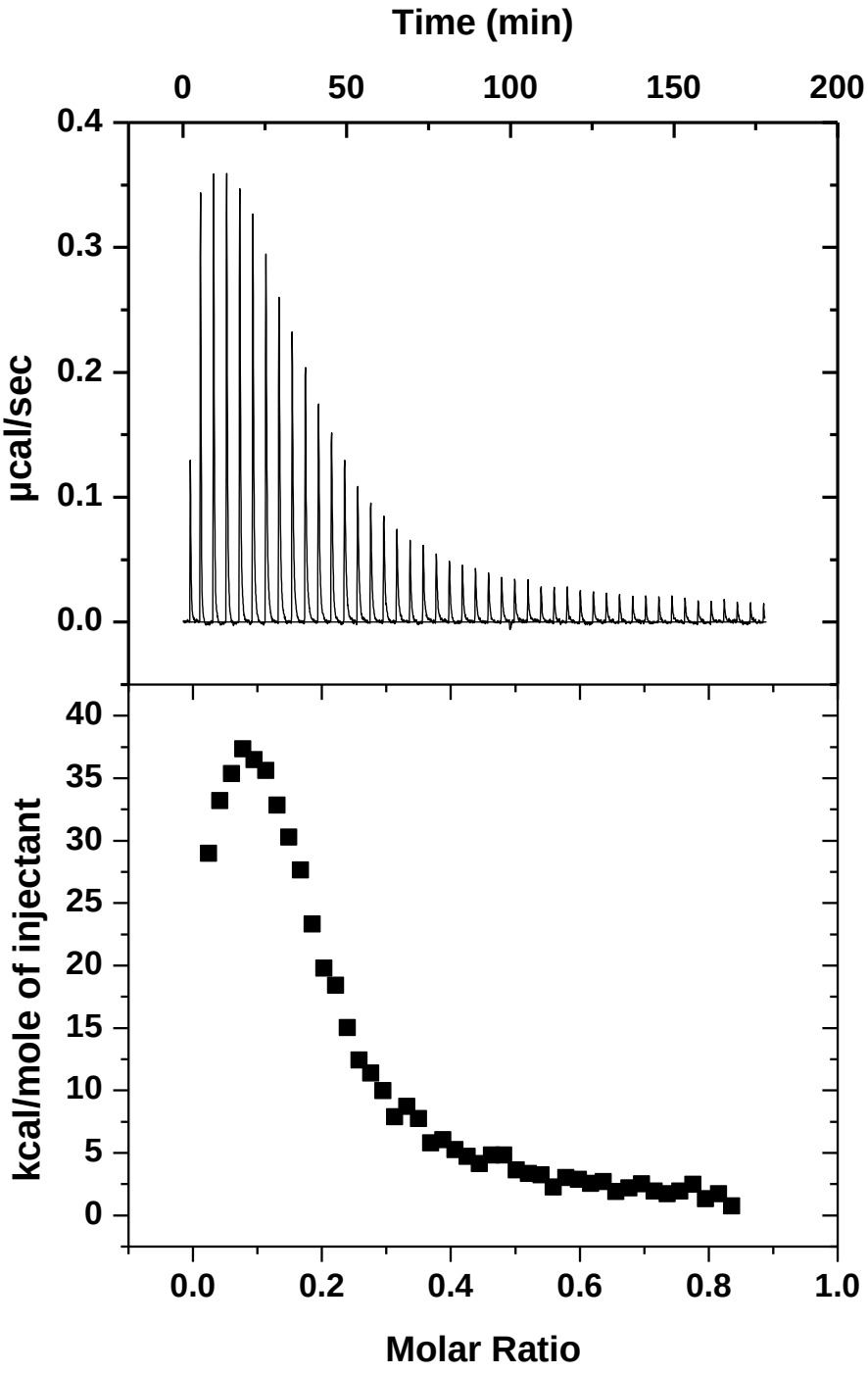

A2.5. ITC data for human HRG titrated with heparin in the presence of 1 µM Zn^{2+}.

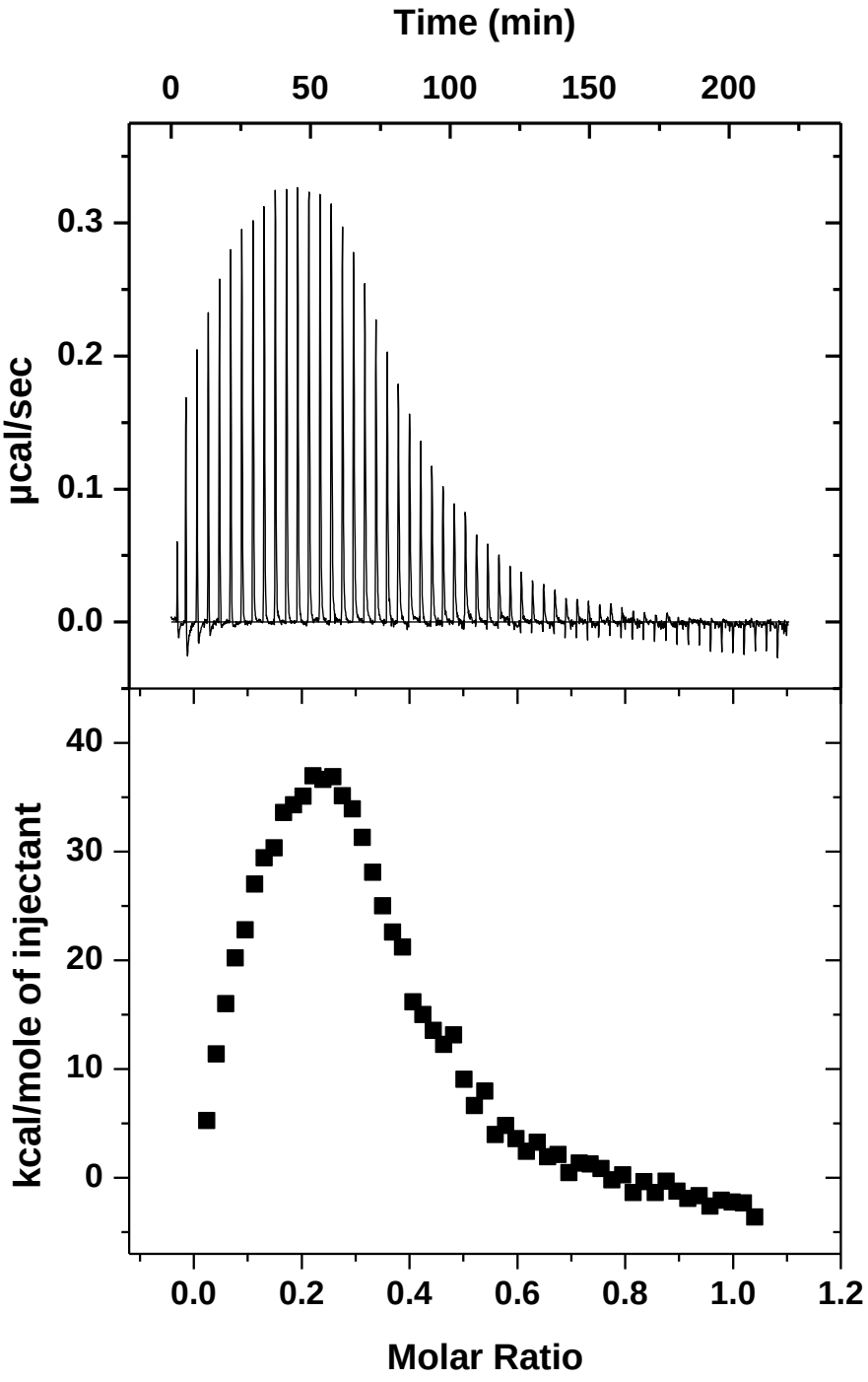

A2.6. ITC data for human HRG titrated with heparin in the presence of 5 µM Zn^{2+}.

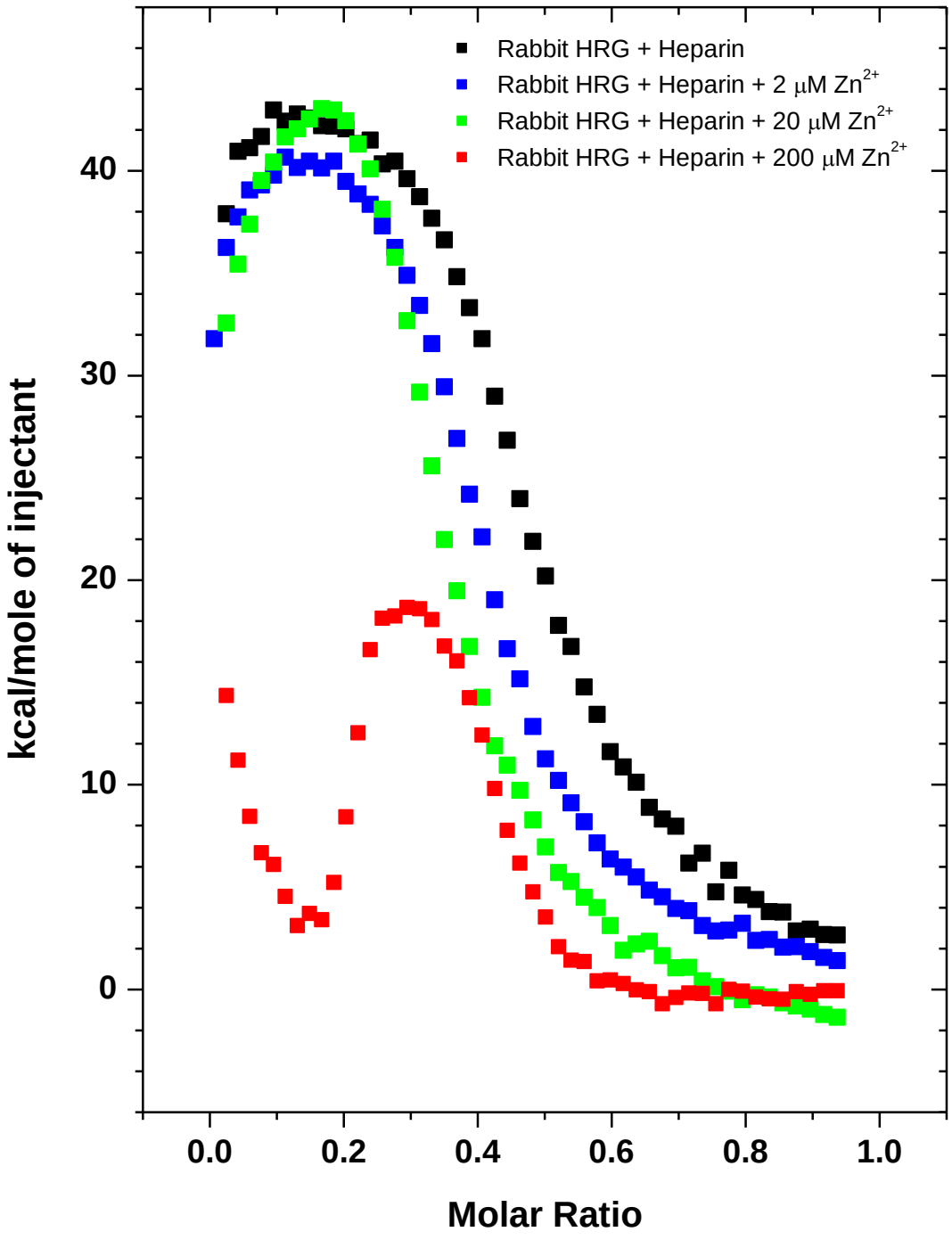

A2.7. ITC data for rabbit HRG (20 μM) titrated with unfractionated heparin (100 μM, average mass of 15 kDa), at increasing concentrations of Zn^{2+}.

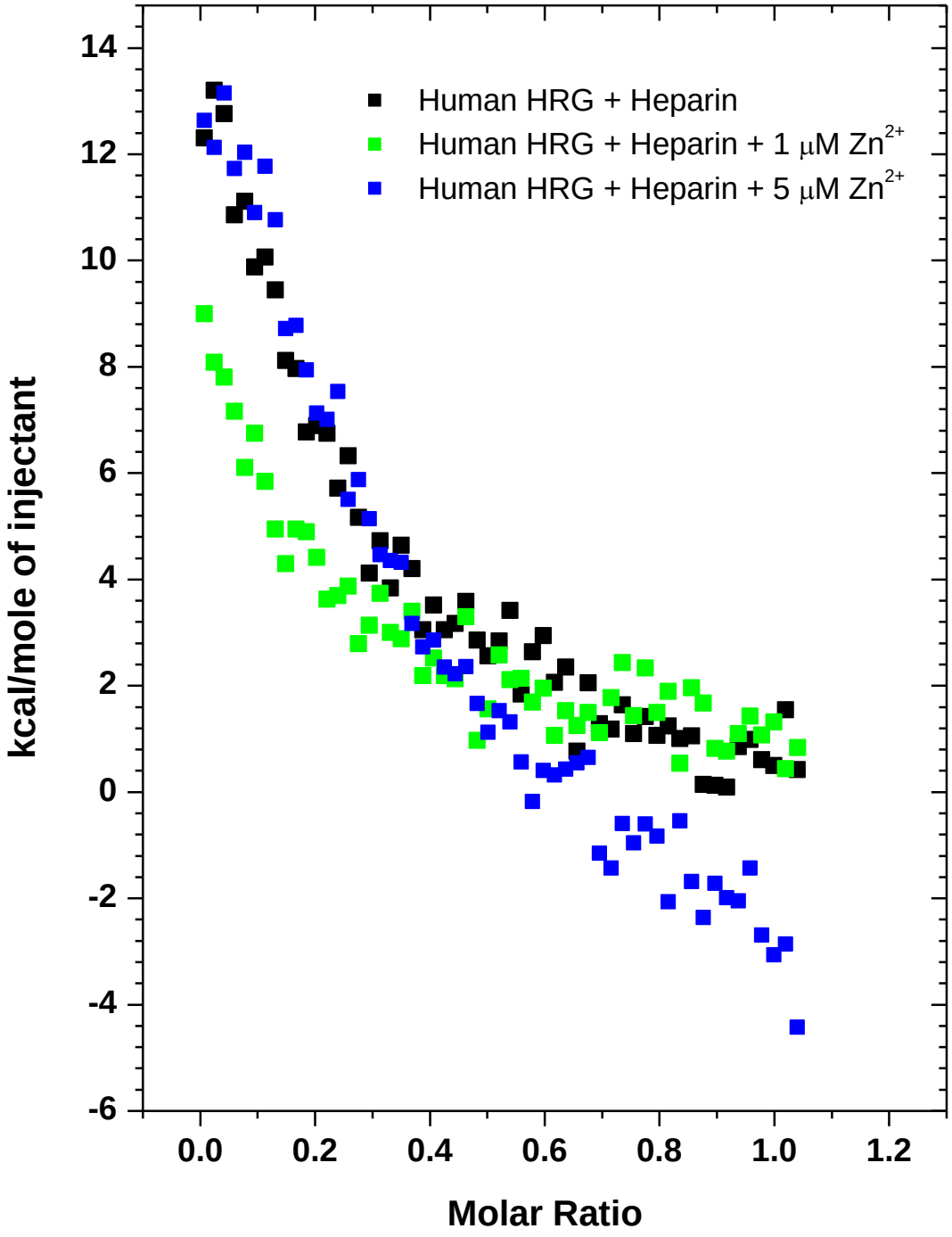

A2.8. ITC data for human HRG titrated with unfractionated heparin at increasing concentrations of Zn^{2+}. The experiment was conducted in 50 mM tris, 140 mM NaCl at pH 7.4.

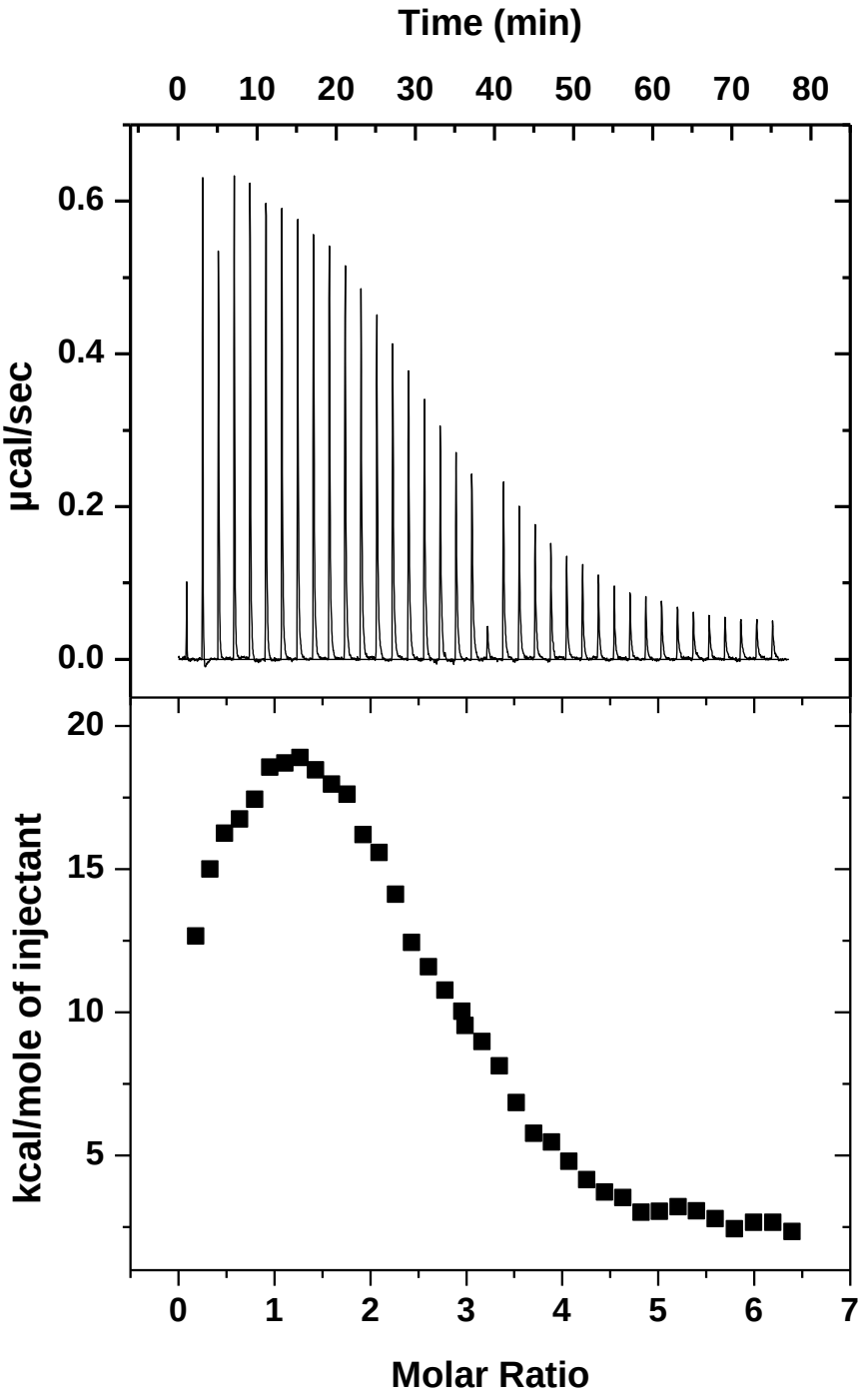

A2.9. ITC data for human HRG titrated with low molecular weight heparin. Consecutive experiments were combined using ConCat32.

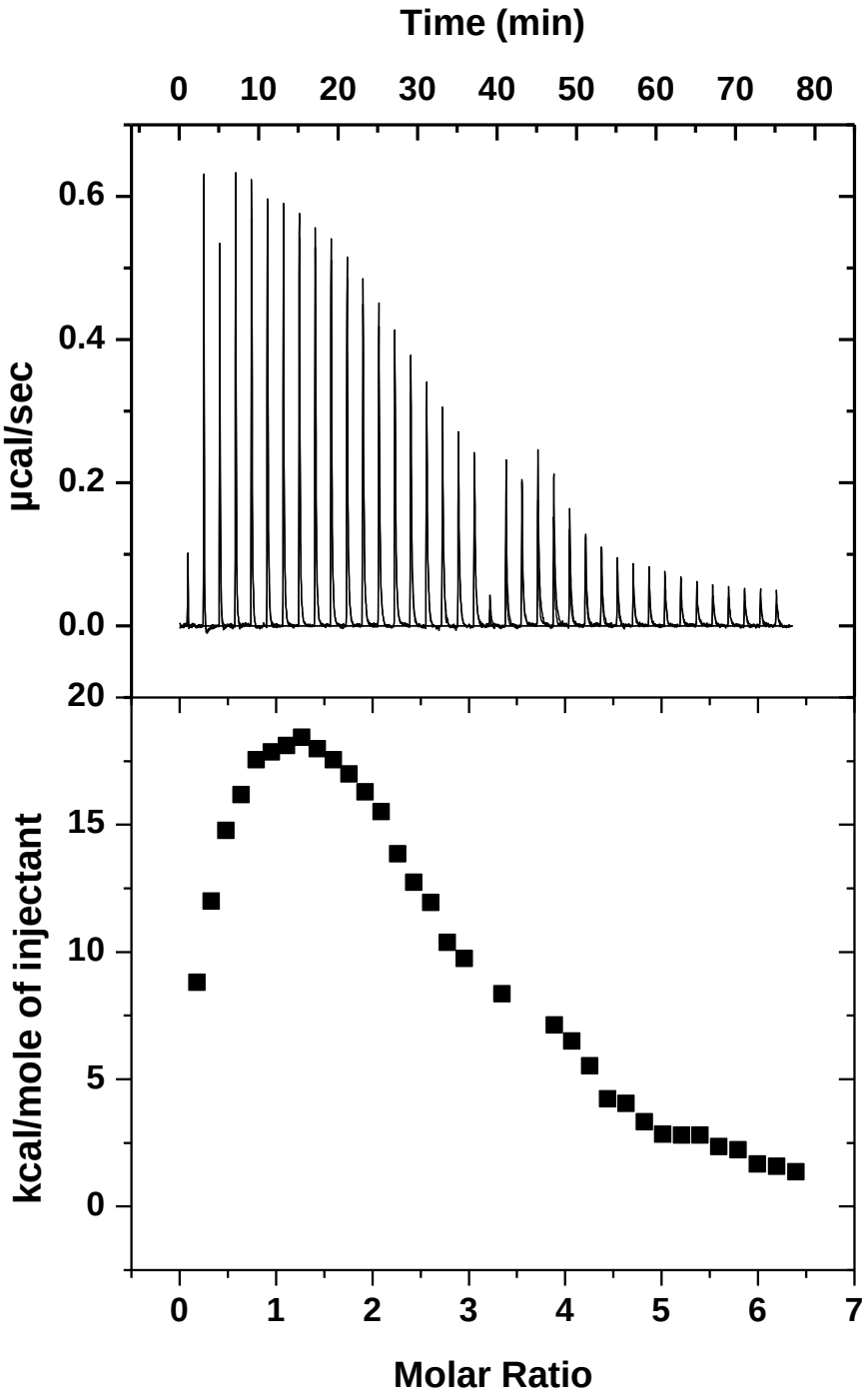

A2.10. ITC data for human HRG titrated with low molecular weight heparin in the presence of 1 µM Zn^{2+}. Consecutive experiments were combined using ConCat32.

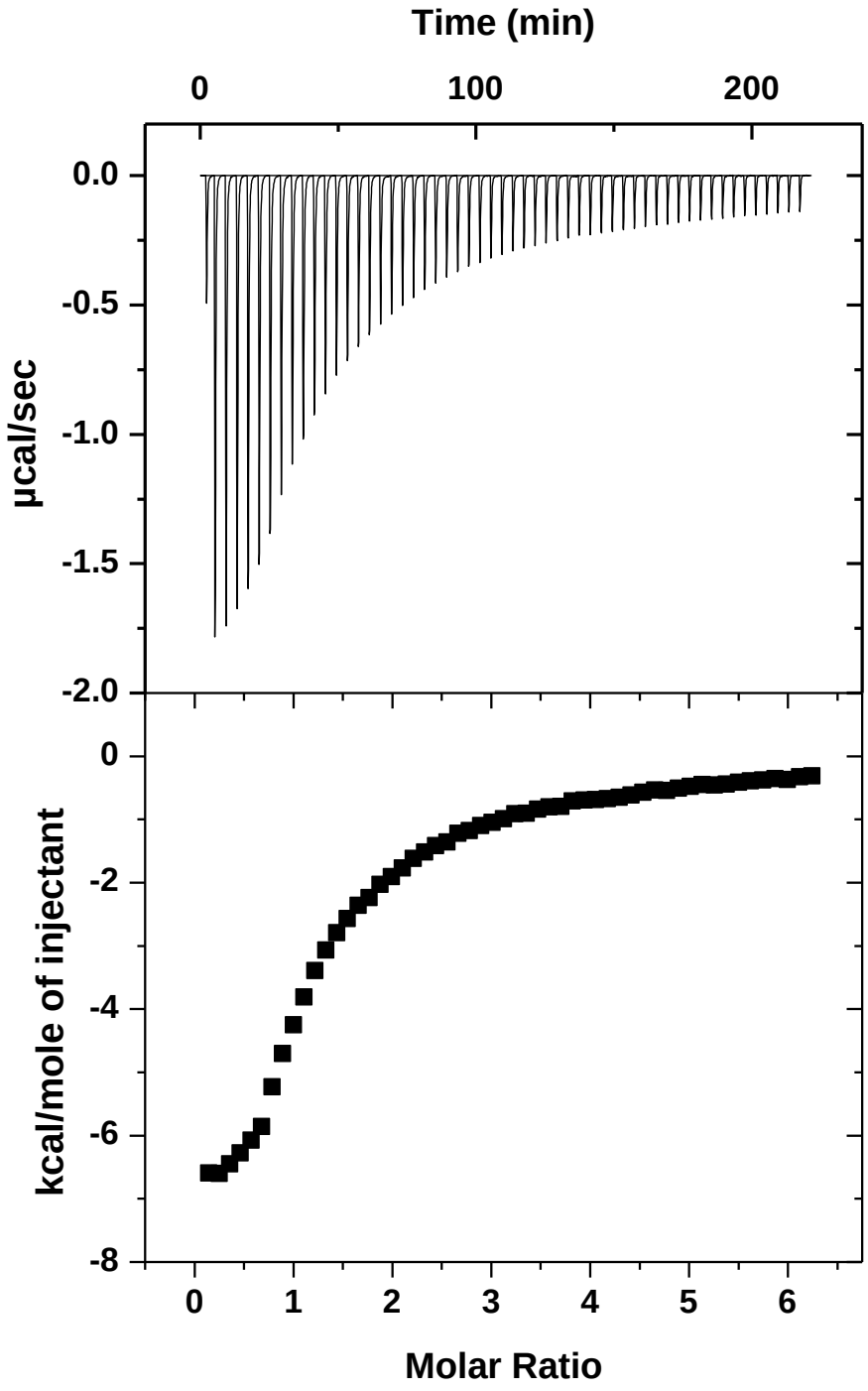

A2.11. ITC data for HSA titrated with Zn^{2+}.

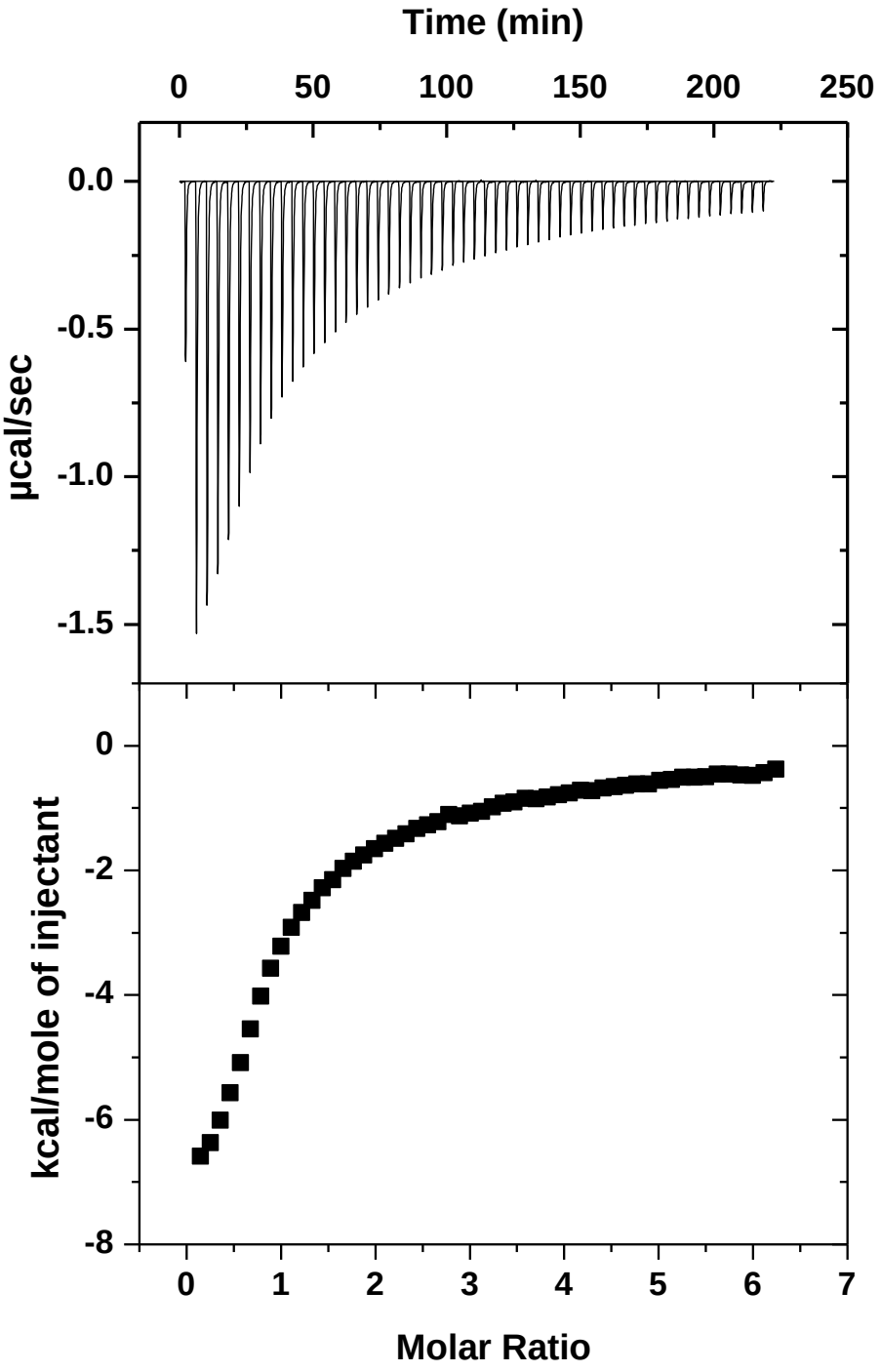

A2.12. ITC data for HSA loaded with 1 molar equivalent of myristic acid, titrated with Zn^{2+}.

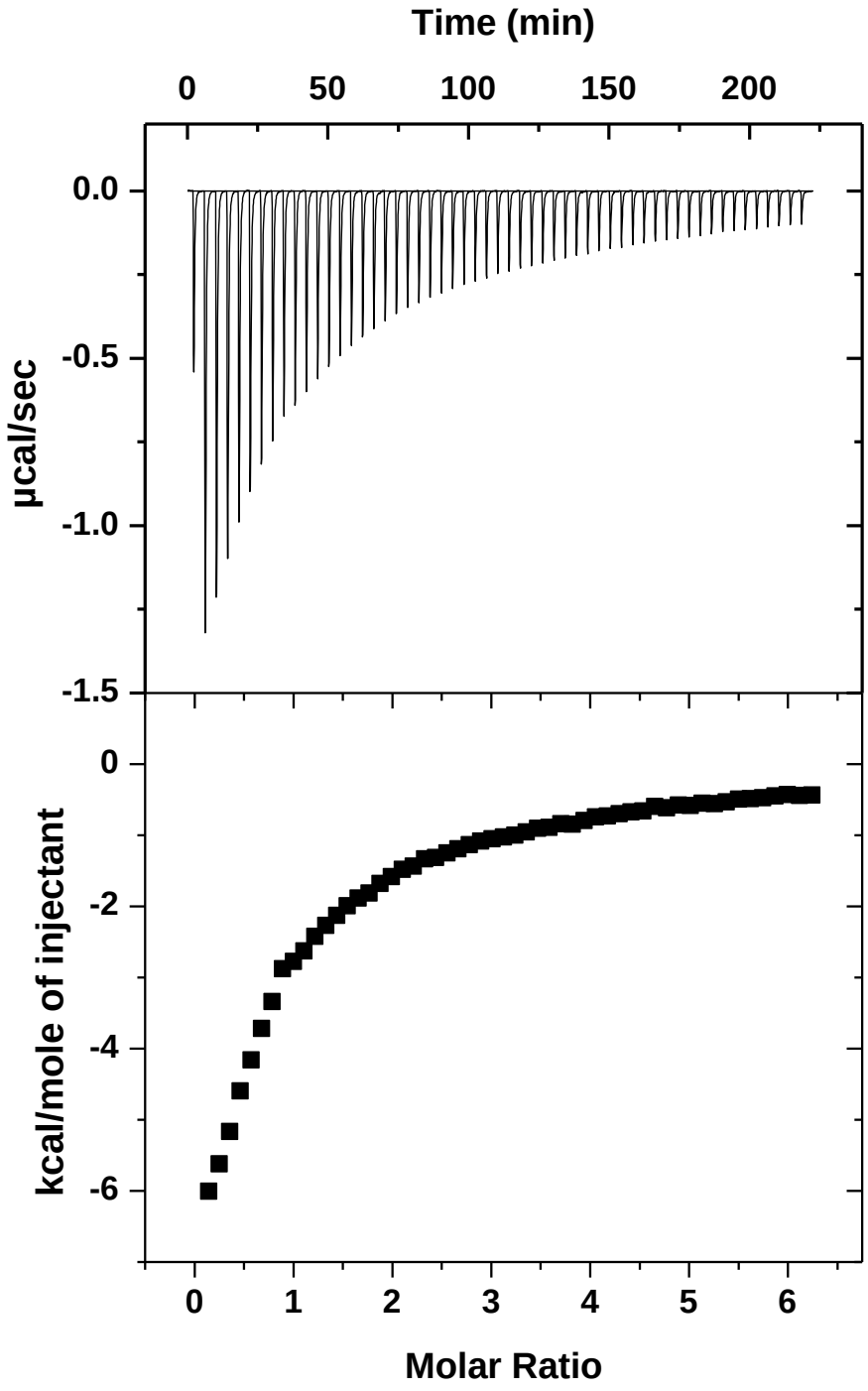

A2.13. ITC data for HSA loaded with 2 molar equivalent of myristic acid, titrated with Zn^{2+}.

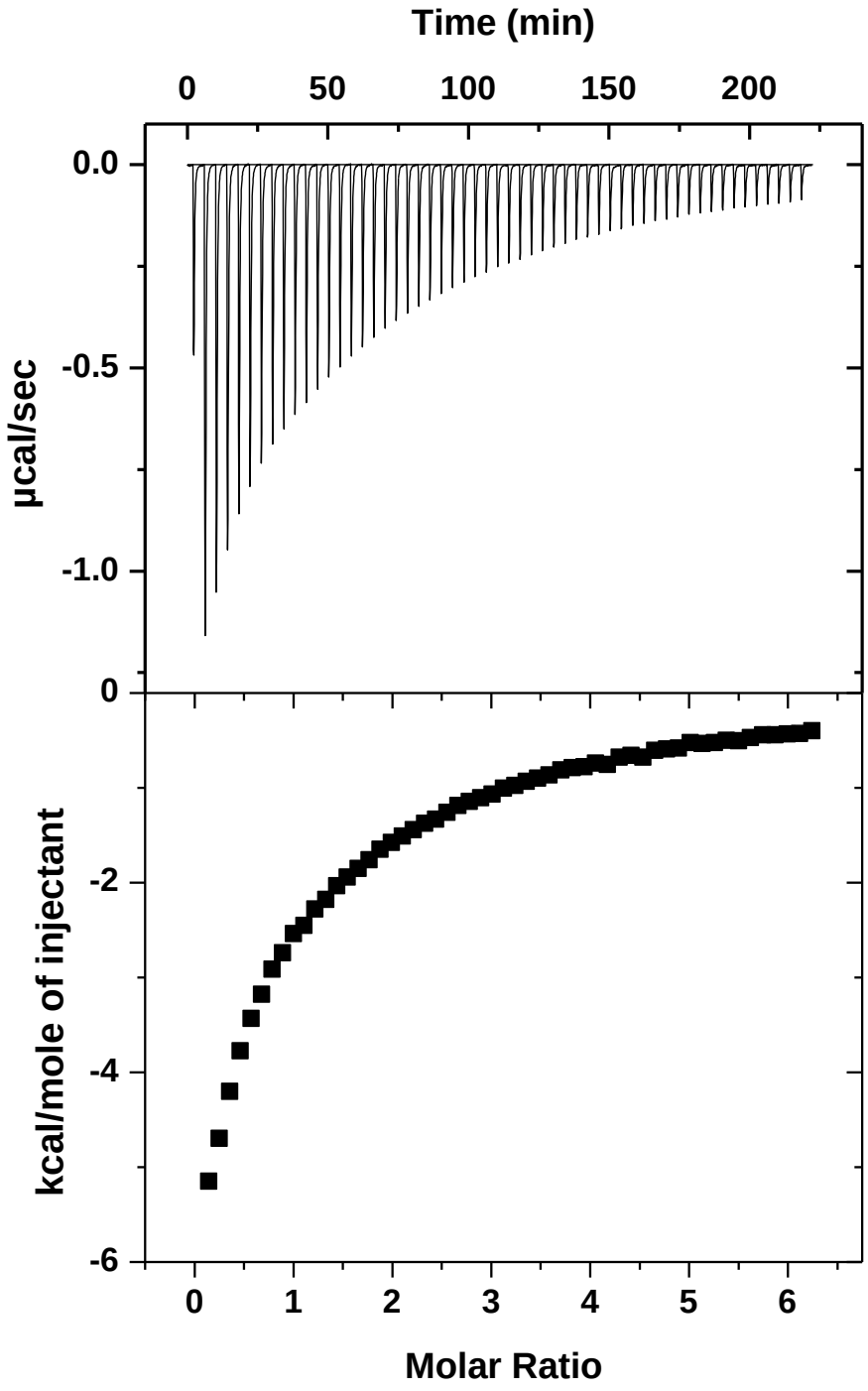

A2.14. ITC data for HSA loaded with 3 molar equivalent of myristic acid, titrated with Zn^{2+}.

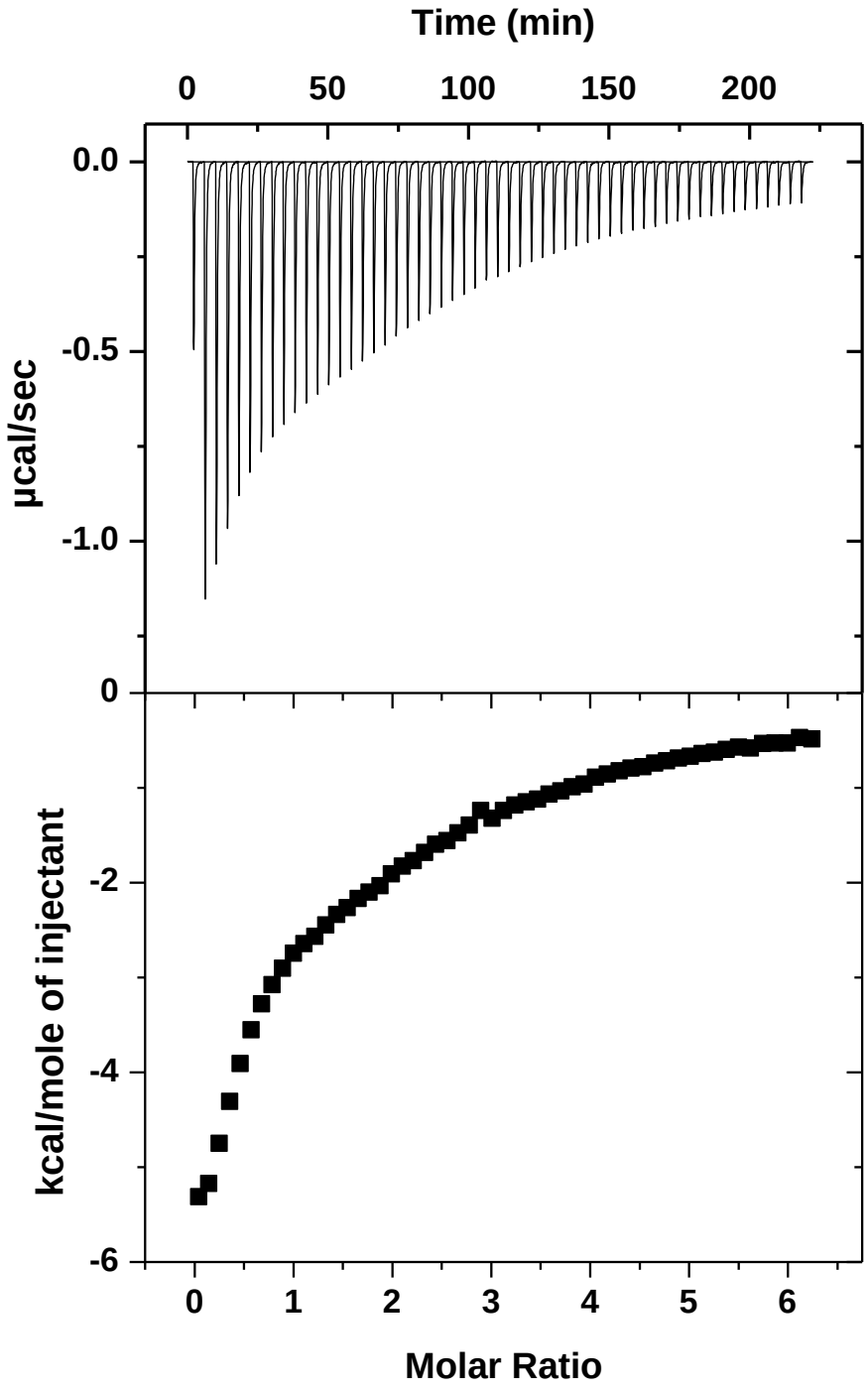

A2.15. ITC data for HSA loaded with 4 molar equivalent of myristic acid, titrated with Zn^{2+}.

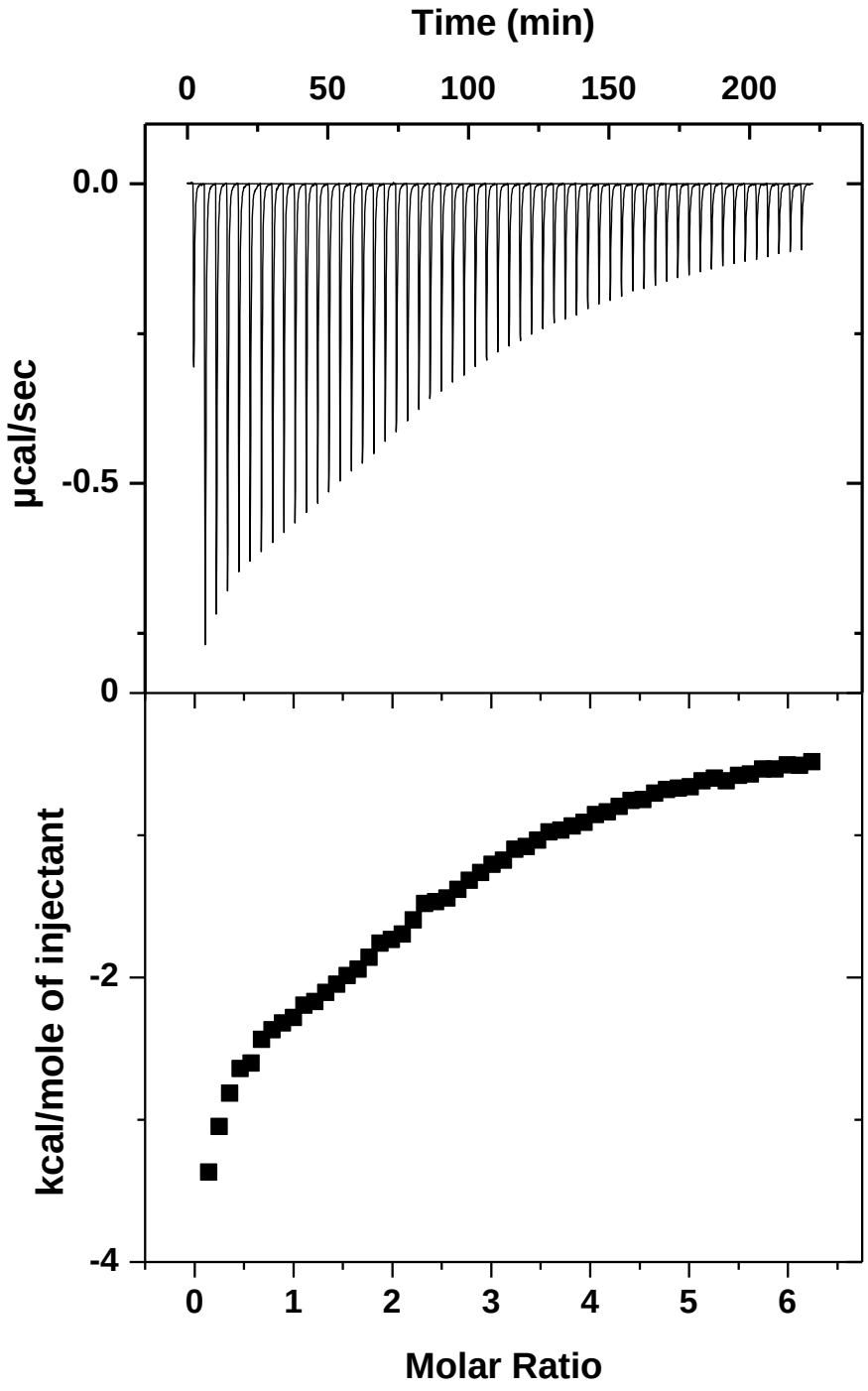

A2.16. ITC data for HSA loaded with 5 molar equivalent of myristic acid, titrated with Zn^{2+}.

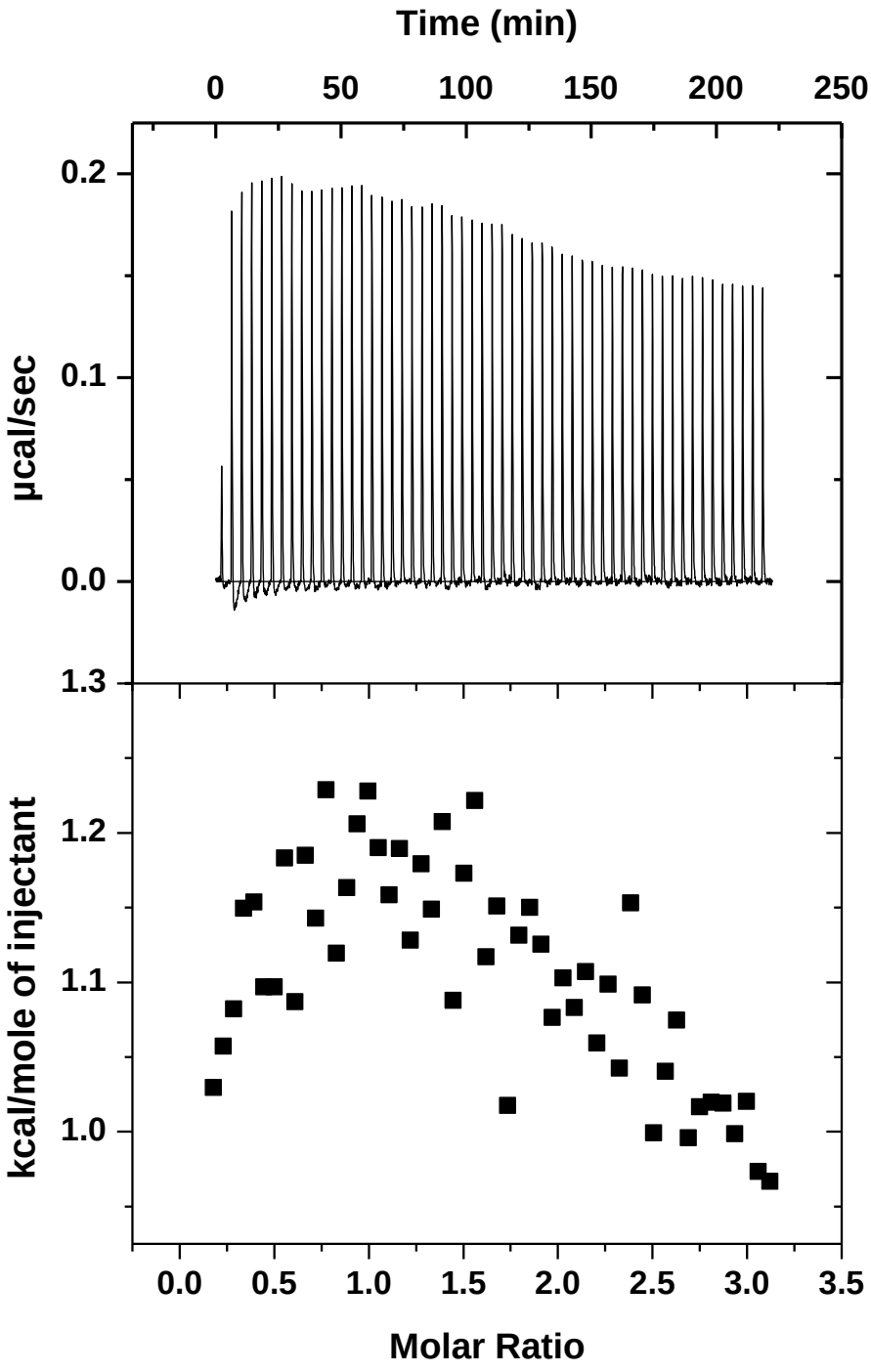

A2.17. ITC data for heparin (50 µM) titrated with Zn^{2+} (750 µM), using the standard conditions described in text.

Appendix 3

The supporting material provided in this section relates to Chapter 4, the identification of novel metal binding sites on albumin. This includes raw data of the ITC experiments performed (as described in the main text, unless otherwise stated) and tabulates primers used during the cloning of albumin.

	Primer name	Sequence
Expression Primers	HSAexp Fwd1	5'-gcatctcgagaaaagagatgcacaagagtgaggttgc-3'
	HSAexp Rev1	5'-cccgcggccgcttacttctcgaattgtgggtggctccataagcctaaggcagcttgacttgc-3'
	HRGexp Fwd1	5'-gcatctcgagaaaagagtgagtcccactgactgcag-3'
	HRGexp Rev1	5'-cccgcggccgcttacttctcgaattgtgggtggctccattttggaaatgtatgtgtaaaaaacatggaaacttg-3'
Mutation Primers	H9A fwd2	5'-gatgcacacaagagtgaggttgctgctcggtttaaagatttgggagaag-3'
	H9A rev2	5'-cttctcccaaatctttaaaccgagcagcaacctcactcttgtgtgcatc-3'
	D256A Fwd1	5'-gatctgcttgaatgtgctgatgccagggcggaccttgccaagta-3'
	D256A Rev1	5'-tacttggcaaggtccgccctggcatcagcacattcaagcagatc-3'
	H288A Fwd1	5'-gaaaaacctctgttggaaaaatccgcctgcattgccgaagtggaaaatg-3'
	H288A Rev1	5'-cattttccacttcggcaatgcaggcggatttttccaacagaggtttttc-3'
Sequence Primers	pKLAC2 seq fwd	5'-gaagaagccttgattgga-3'
	pKLAC2 seq rev	5'-tcggcactaataaccgttt-3'
	HSA seq1	5'-gaggttgatgtgatgtgc-3'
	HSA seq2	5'-cctctgttggaaaaatcc-3'
	HSA seq3	5'-gttatgtgtgttgcatgag-3'
	HRG seq1	5'-cttgagaagtacaaagaggag-3'
	HRG seq2	5'-cctgctcaagttgtcaac-3'
K. Lactis Integration Primers	Integration Primer 1	5'-acacacgtaaacgcgctcggt-3'
	Intergation Primer 2	5'-atcatccttgtcagcgaaagc-3'
	Integration Primer 3	5'-acctgaagatagagcttctaa-3'

A3.1. Primers used during the expression of albumin in *K. Lactis*.

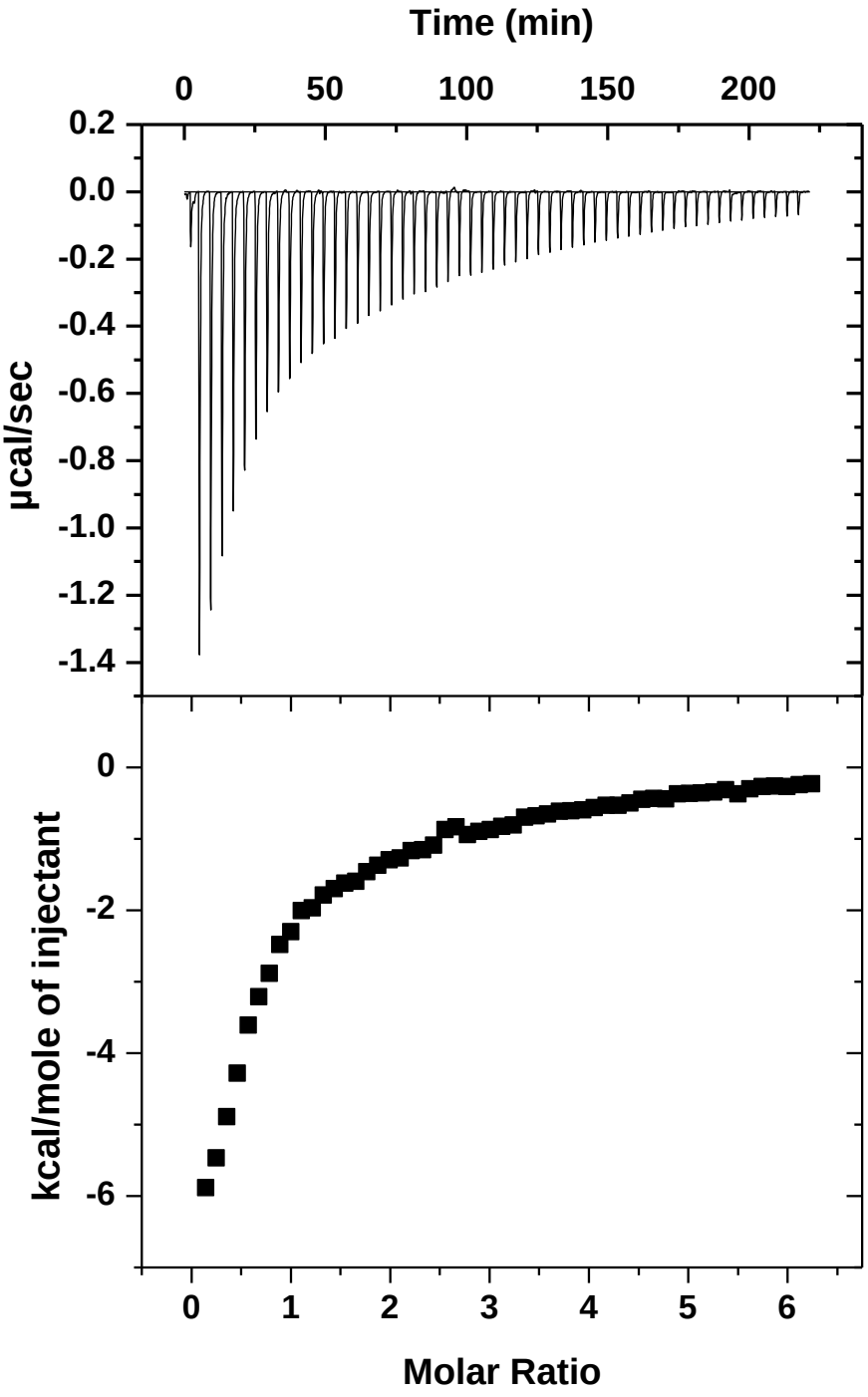

A3.2. ITC data forH9A titrated with Zn^{2+}.

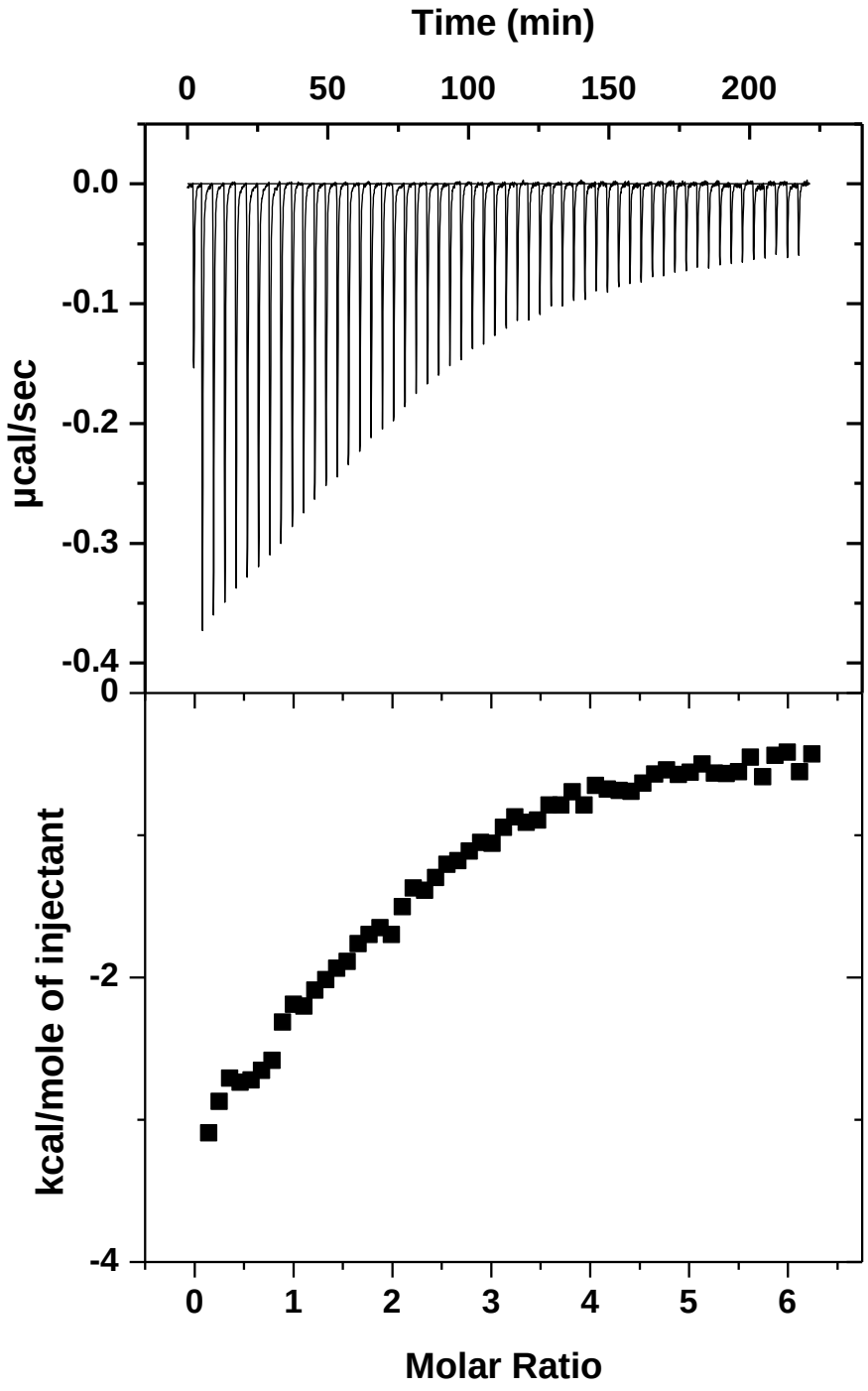

A3.3. ITC data for H67A titrated with Zn^{2+}.

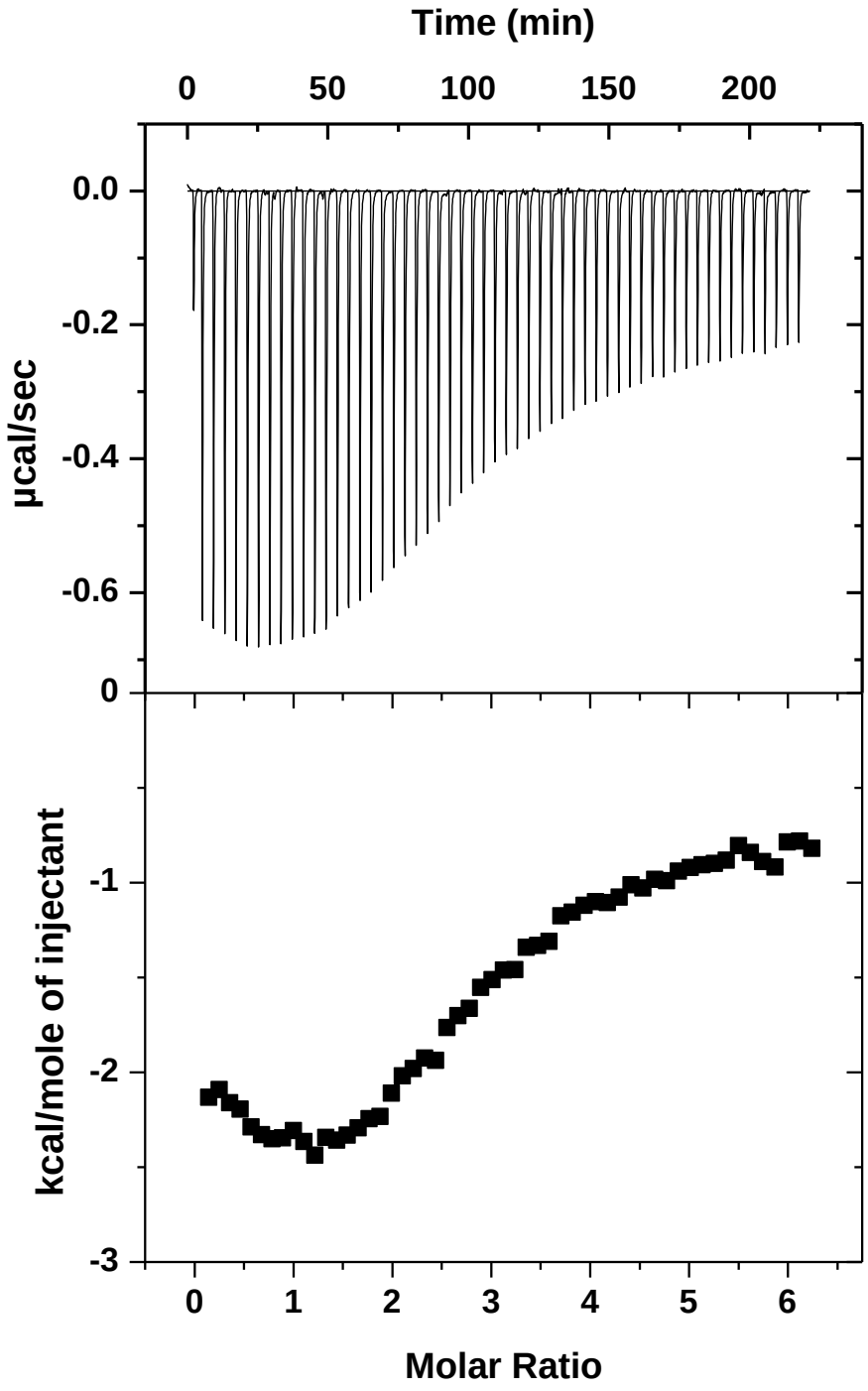

A3.4. ITC data for E252A titrated with Zn^{2+}.

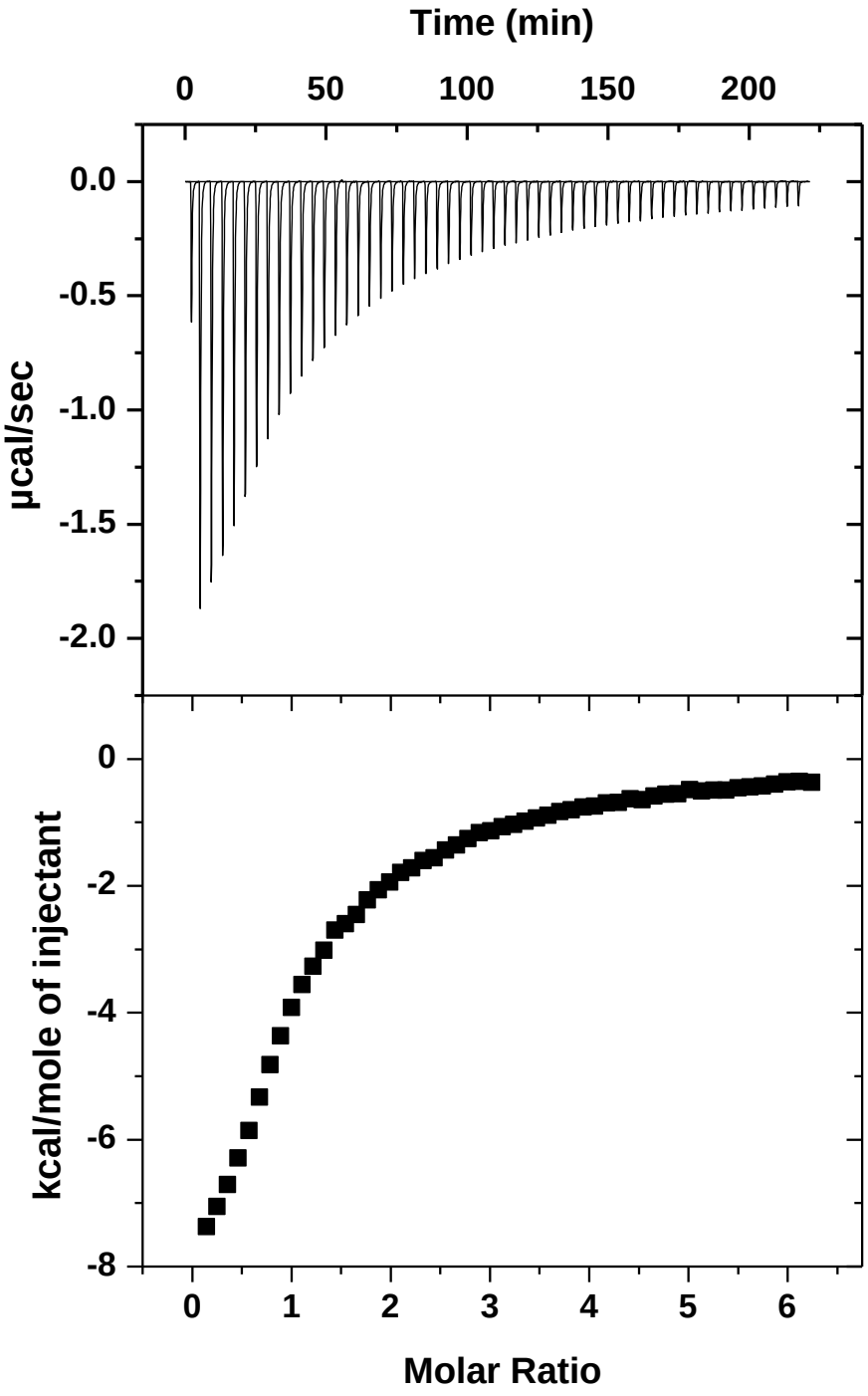

A3.5. ITC data for D255A titrated with Zn^{2+}.

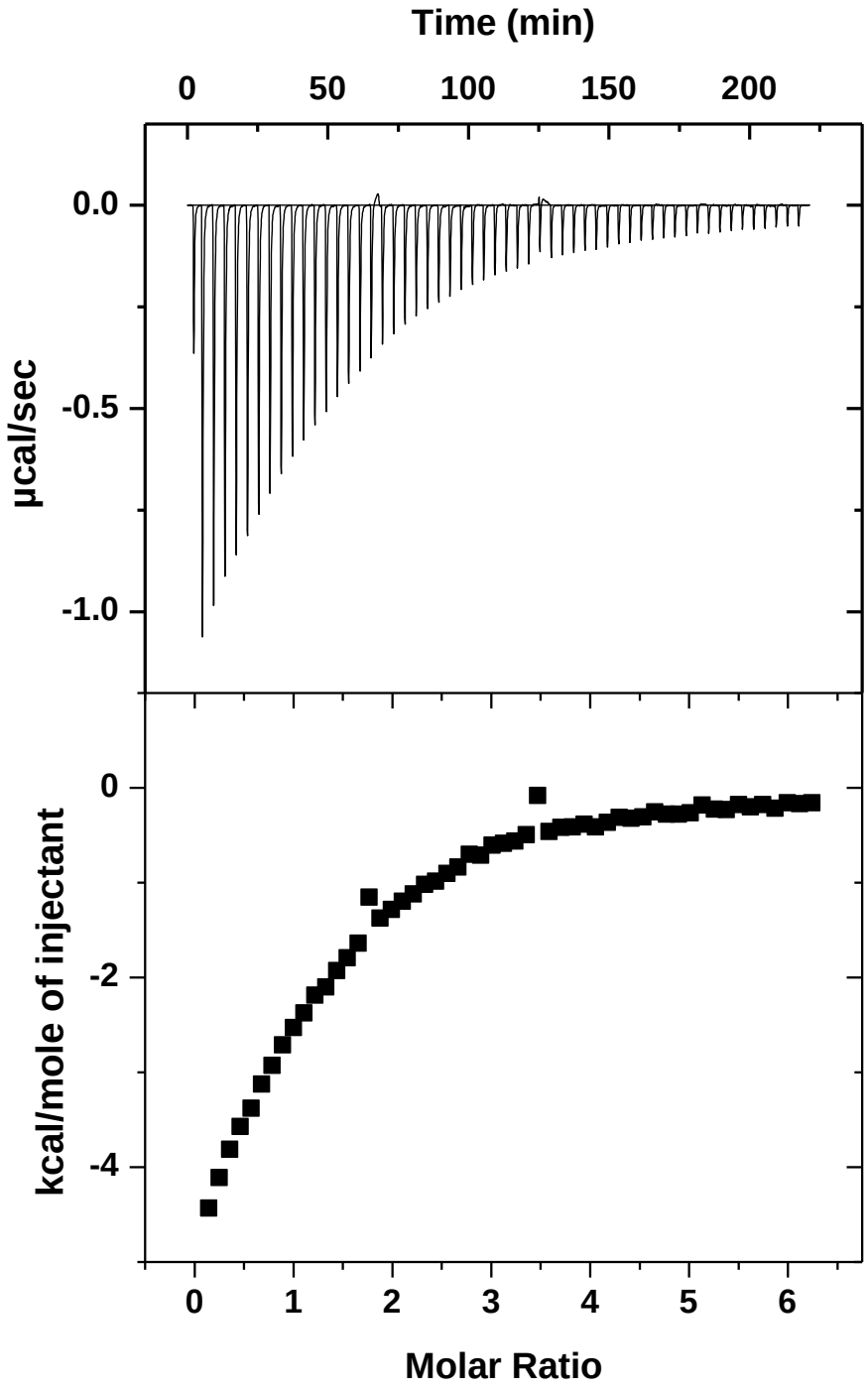

A3.6. ITC data for D256A titrated with Zn^{2+}.

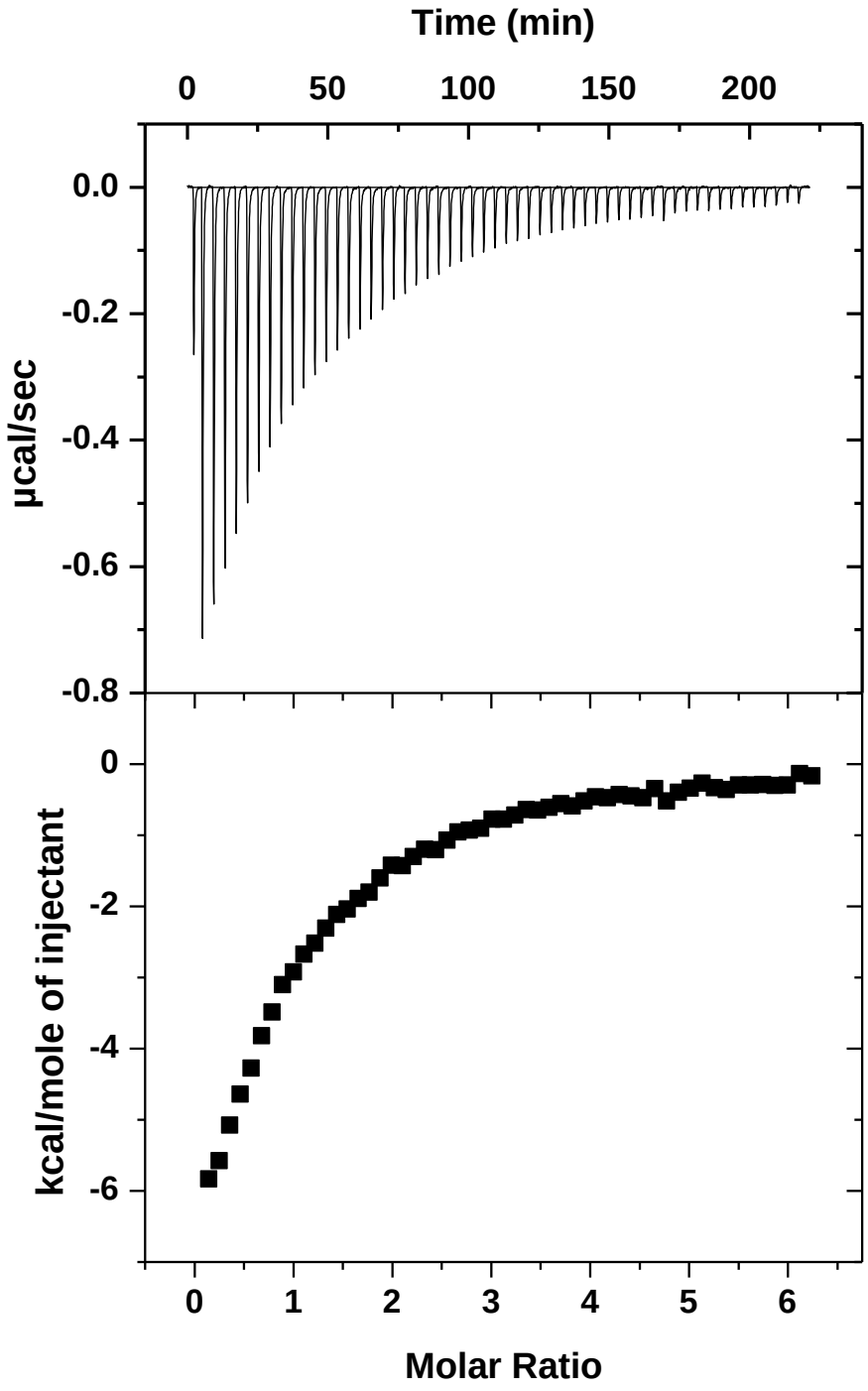

A3.7. ITC data for H288A titrated with Zn^{2+}.

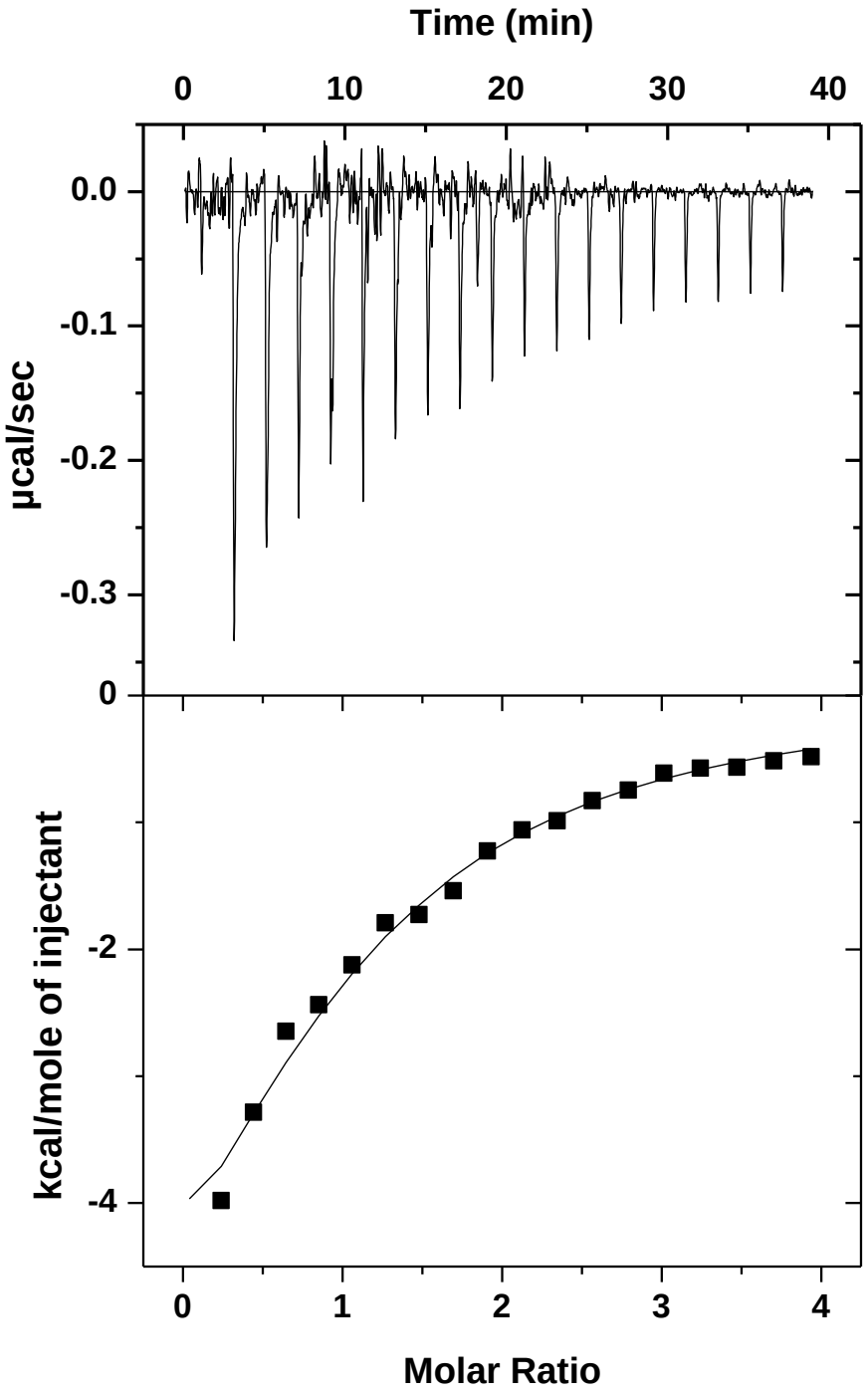

A3.8. ITC data for AFP titrated with Zn^{2+}.

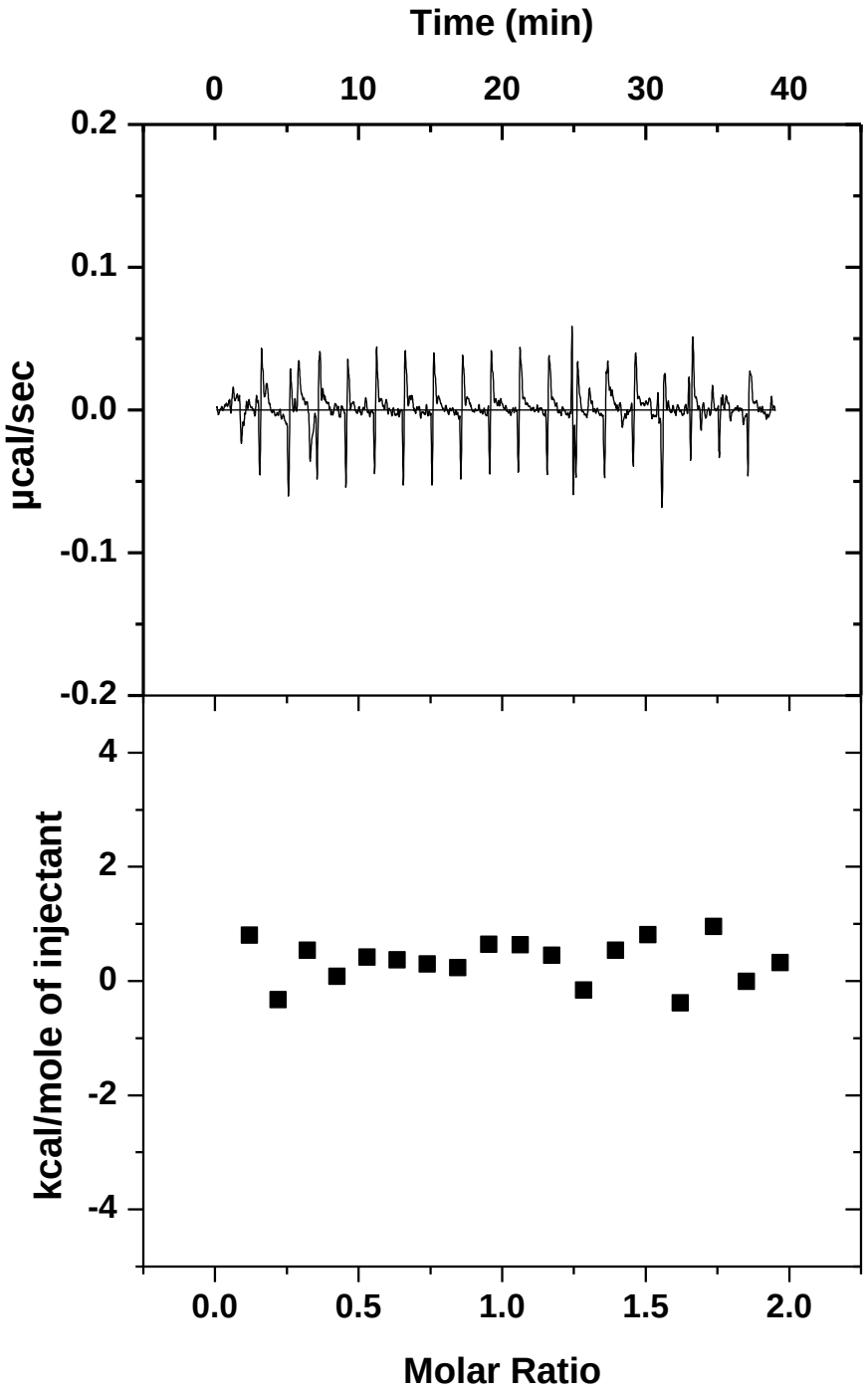

A3.9. ITC data for AFP titrated with estradiol.

Appendix 4

This section provides sample chromatograms for all protiens purified during this project.

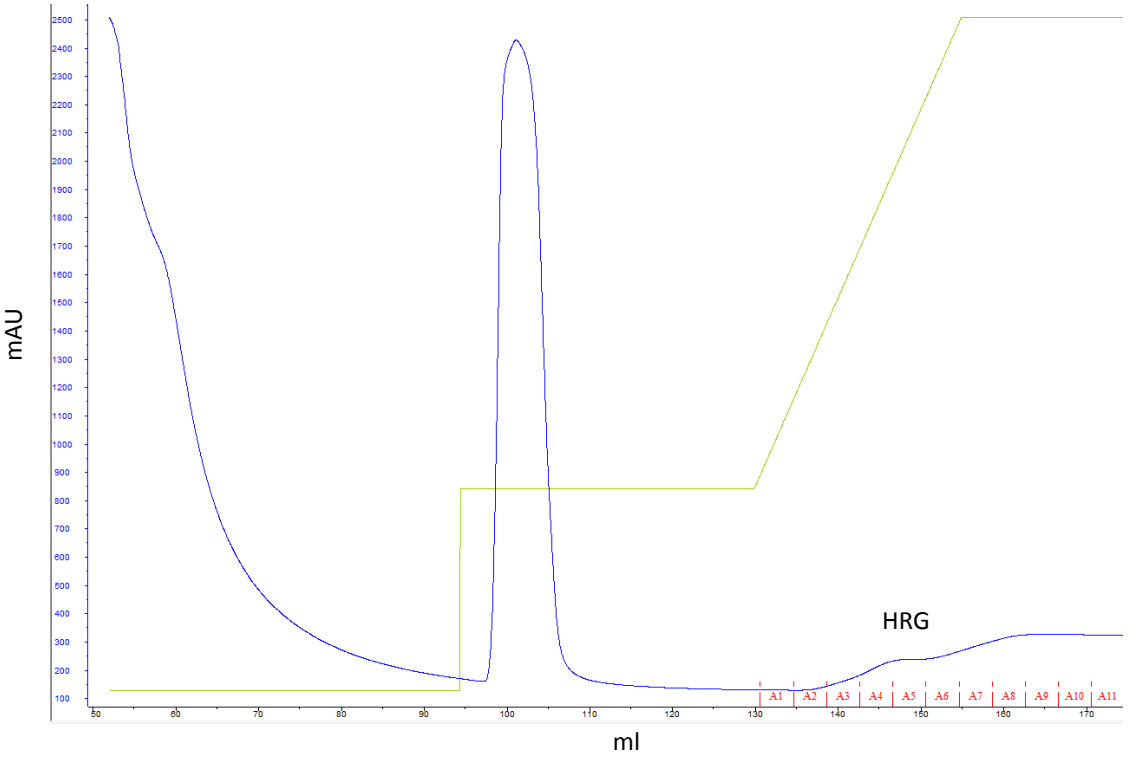

A4.1. Purification chromatogram for human HRG following nickel affinity column.

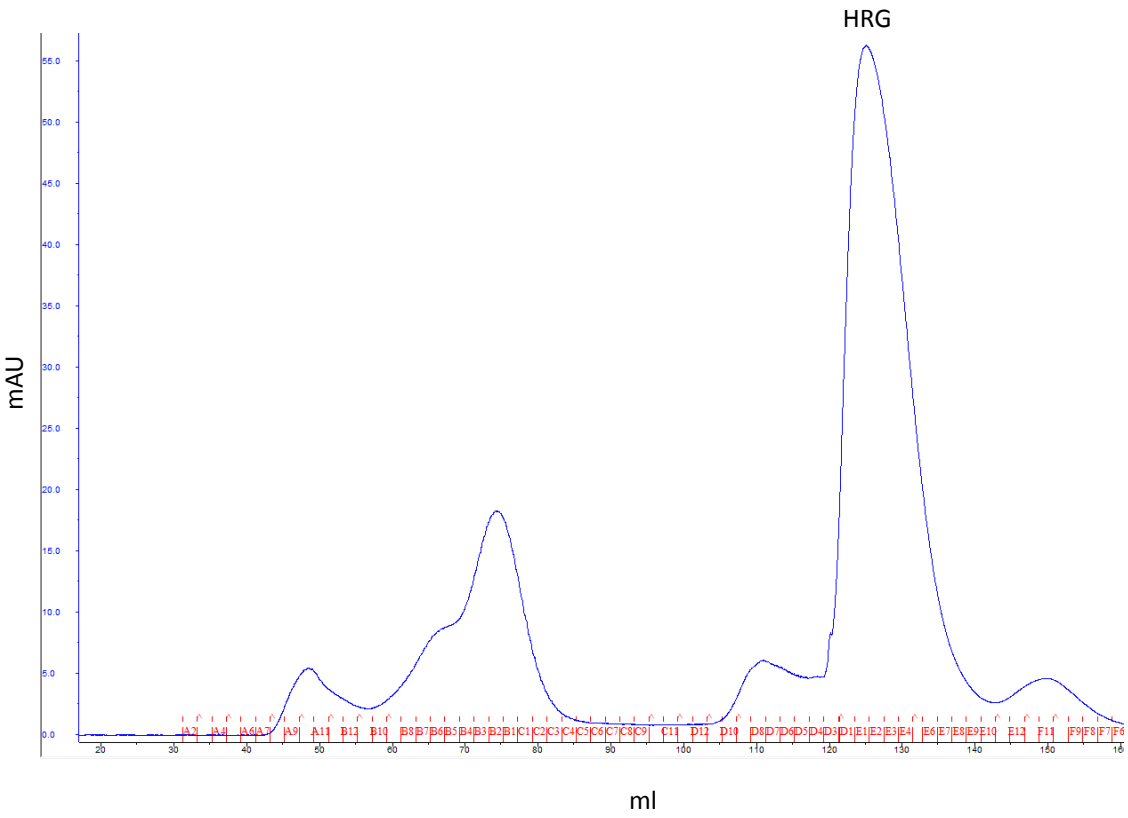

A4.2. Purification chromatogram for human HRG following size exclusion column.

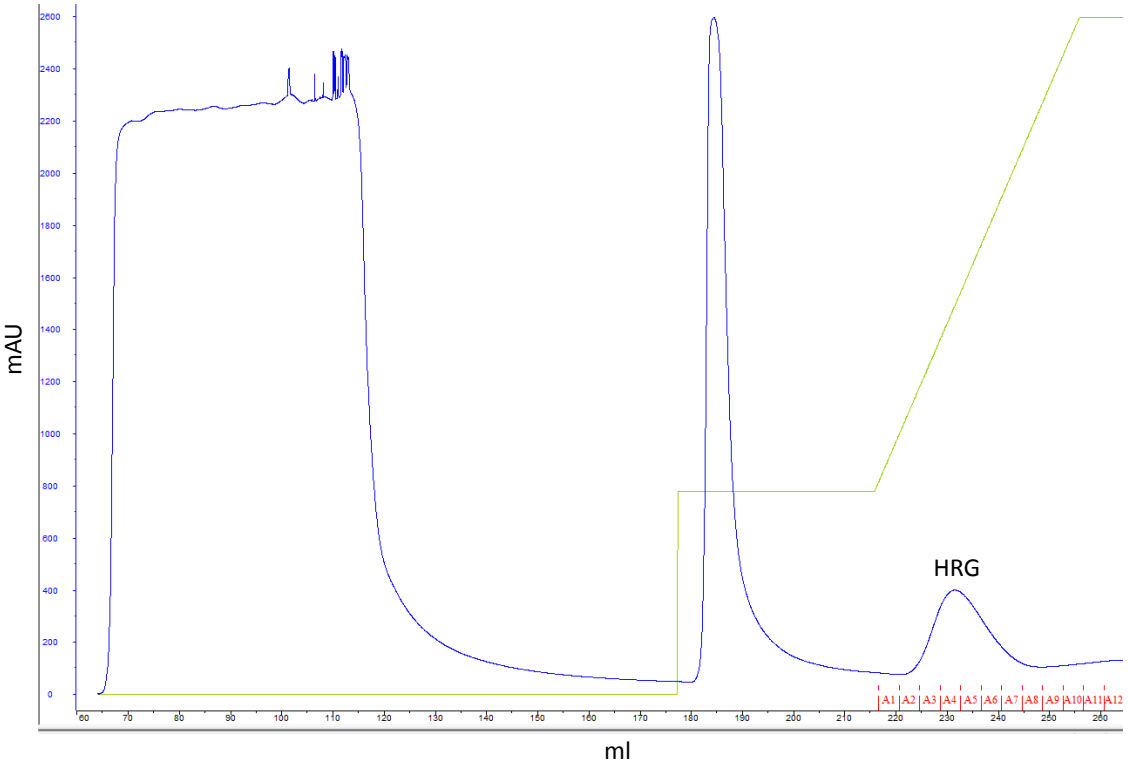

A4.3. Purification chromatogram for rabbit HRG following nickel affinity column.

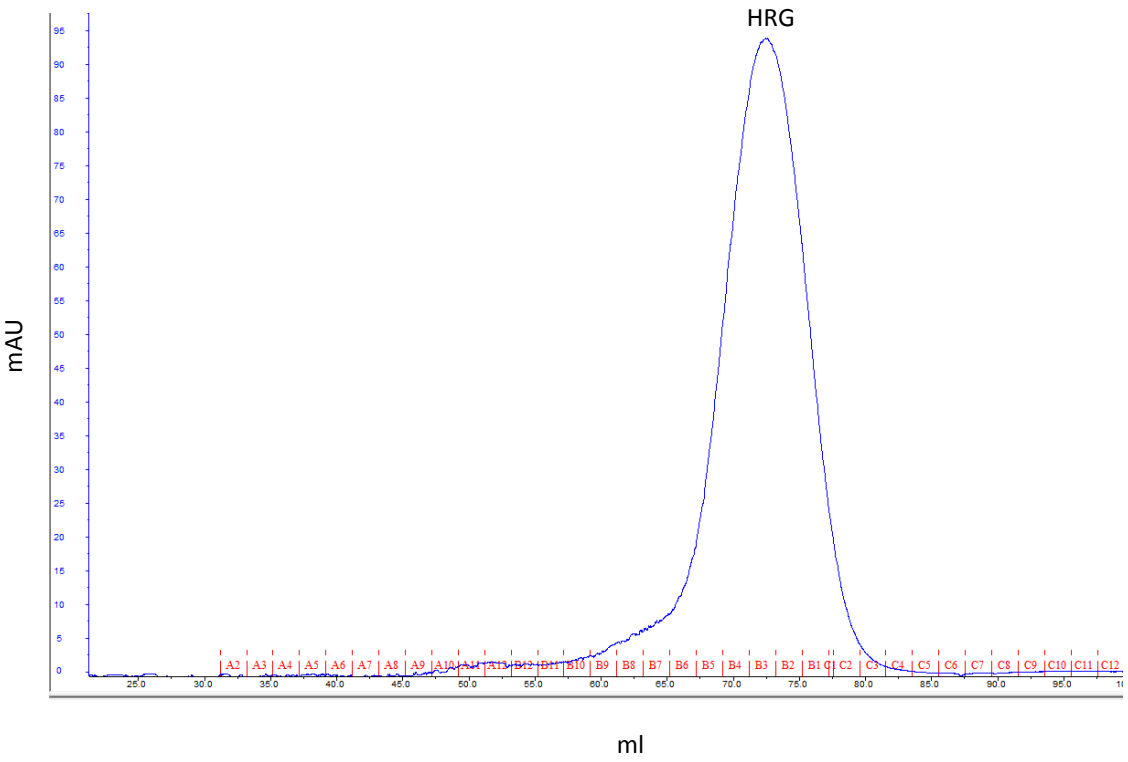

A4.4. Purification chromatogram for rabbit HRG following size exclusion column.

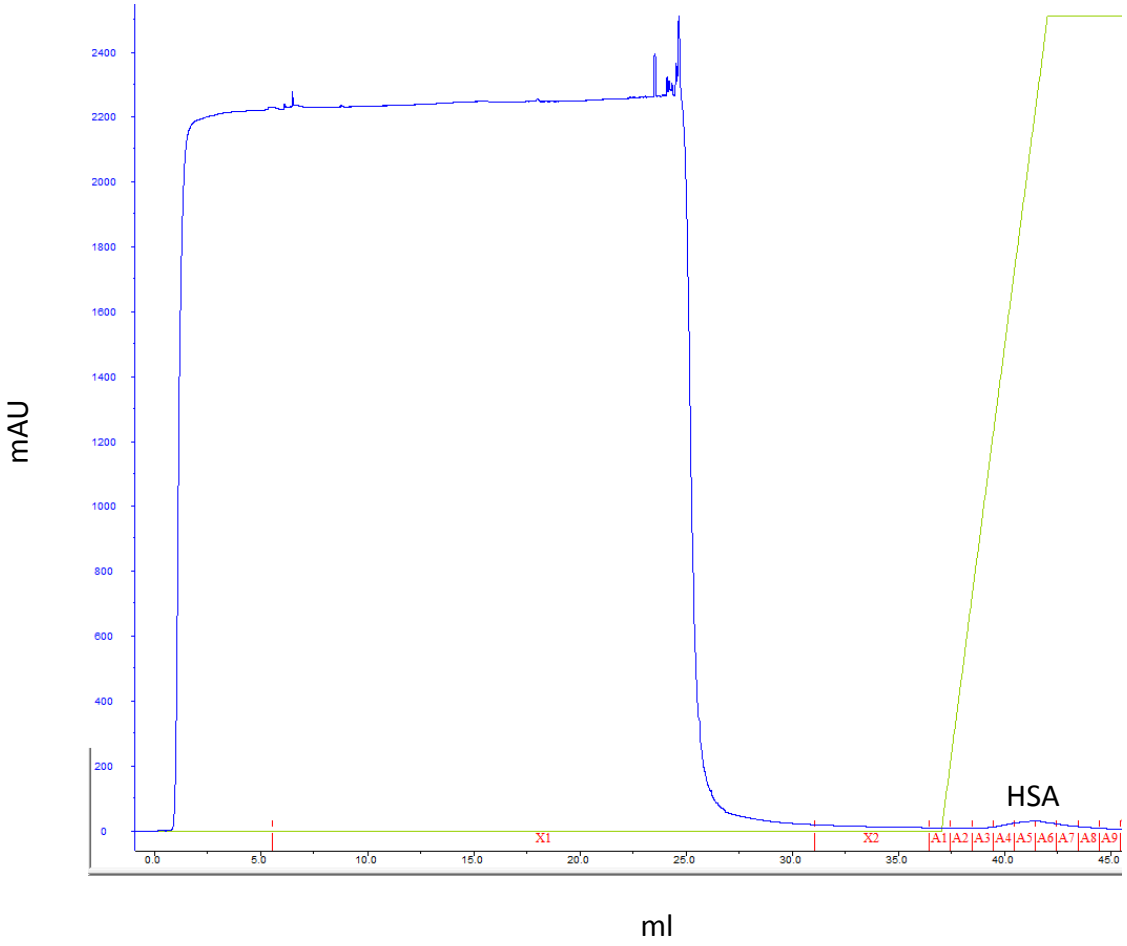

A4.5. Purification chromatogram for recombinant HSA following Blue Sepharose column.

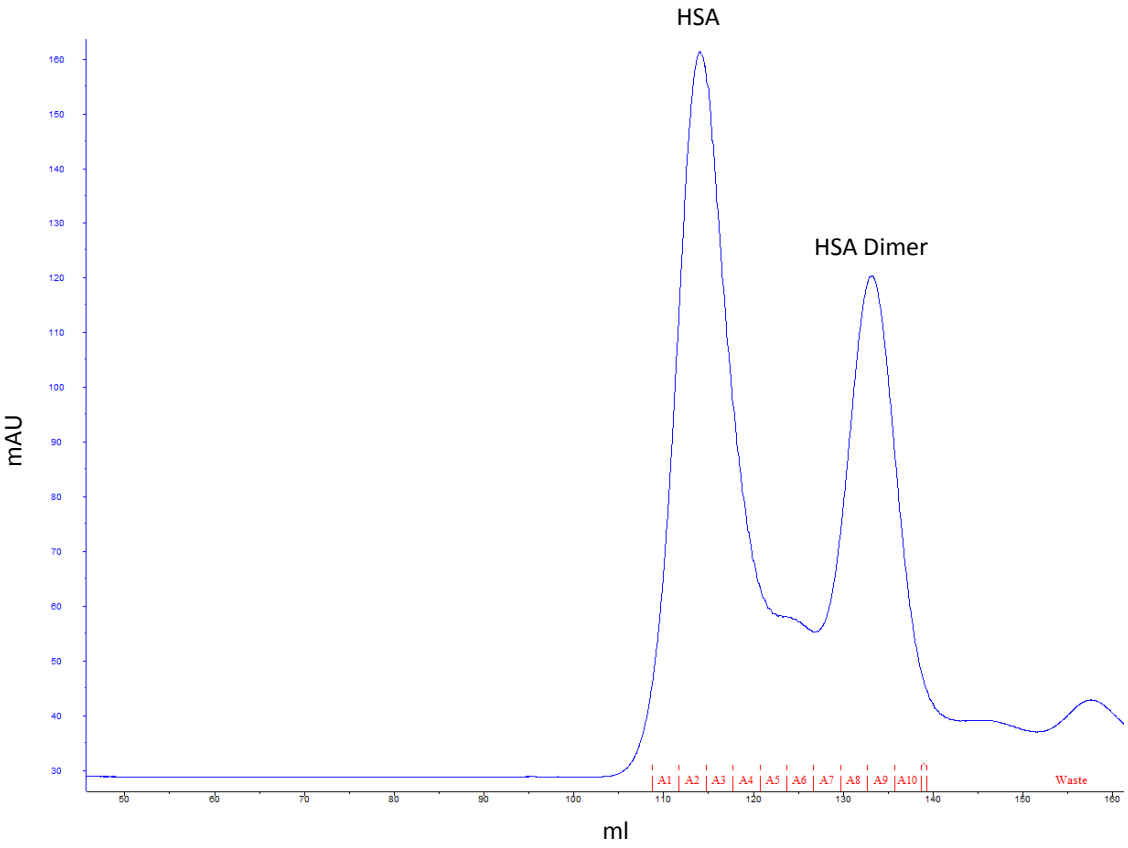

A4.6. Purification chromatogram for recombinant HSA following size exclusion column.

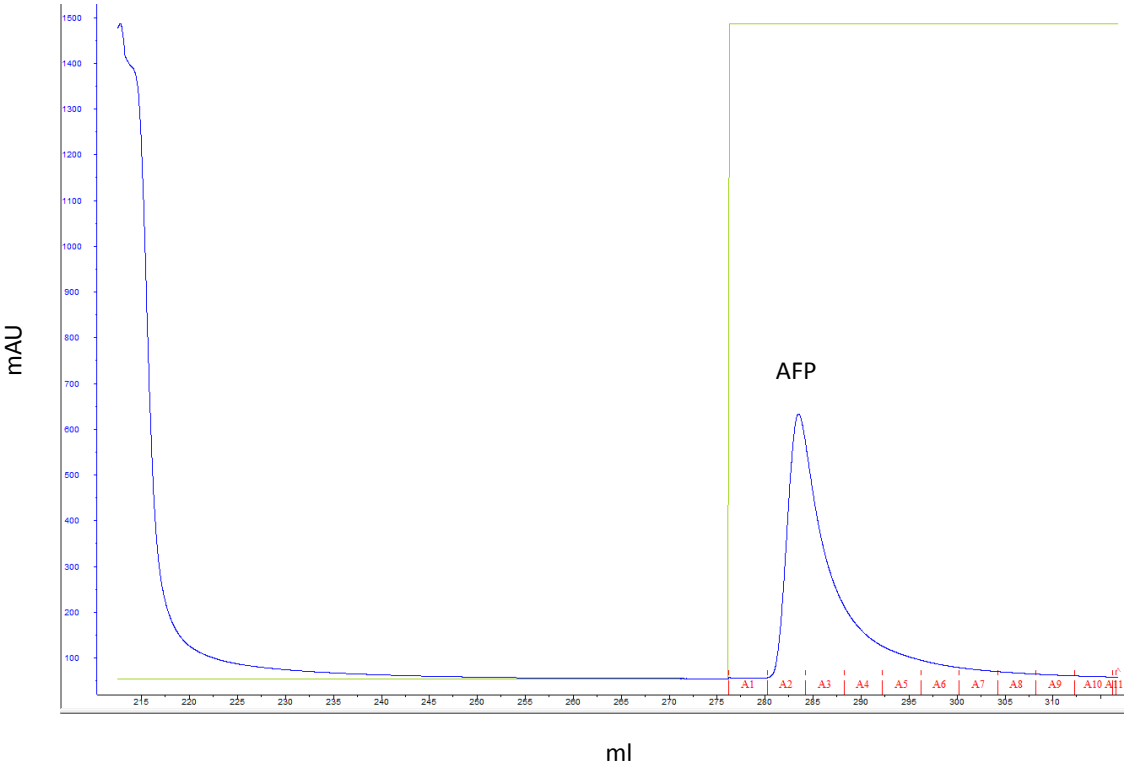

A4.7. Purification chromatogram for recombinant AFP following copper affinity column.